Assemblage couche-par-couche de nano-composites bio-inspirés

Rémi Merindol

▶ To cite this version:

HAL Id: tel-01126885

https://tel.archives-ouvertes.fr/tel-01126885

Submitted on 6 Mar 2015

UNIVERSITÉ DE STRASBOURG

ÉCOLE DOCTORALE de Physique et de Chimie-Physique

Institut Charles Sadron (UPR22-CNRS)

THÈSE présentée par :

Rémi Mérindol

Soutenue le : **22 Septembre 2014**

pour obtenir le grade de : **Docteur de l'université de Strasbourg**

Discipline/ Spécialité : Chimie-Physique

Layer-by-layer assembly of strong bio-inspired nanocomposites

THÈSE dirigée par :
M. FELIX Olivier   Chargé de Recherche, université de Strasbourg
M. DECHER Gero   Professeur, université de Strasbourg

RAPPORTEURS :
M. WAGBERG Lars   Professeur, KTH Royal institute of technology
M. STUDART André   Professeur, ETH Zürich

AUTRES MEMBRES DU JURY :
Mme DE COLA Luisa   Professeur, université de Strasbourg
Mme SCHONHOFF Monika   Professeur, Westfälische Wilhelms-universität Munster

Acknowledgments

The work of this dissertation was carried out at the Institut Charles Sadron (ICS) in Strasbourg, France.

First, I would like to express my sincere gratitude to Professor Gero Decher and Doctor Olivier Félix, my PhD advisors, for their support, advices, kindness and optimism during my doctoral research. Thank you for the freedom you gave me on the project management, for letting me supervise several master students and for letting me enroll in teaching assistantship.

I would like to express my gratitude Professor Lars Wågberg, Professor André Studart, Professor Luisa De Cola and Professor Monika Shönhoff for having accepted to act as referees for my thesis work and for the interesting discussion during the defense and for their comments.

I would like to thanks Professor Christian Gauthier for letting me perform the mechanical characterization of the film in his lab and I am grateful to Damien Favier, Thierry Roland and Leandro Jacomine for their help and advices with the mechanical characterization of the films. I am grateful to Mathias Pauly for his advices on fibrilar nano-composites, in particular with the characterization of orientation. I would like to thanks Christophe Contal for teaching me AFM and letting me use the equipment in autonomy. I would also like to thanks Professor Valerie Keller for the XPS measurements, Cedric Leuvrey of the SEM images and Gerard Strub for his help restarting the dipping robot.

I would like to thanks the Ministère de l'Enseignement Supérieur et de la Recherche for the financial support. I would also like to thanks Ulrich Soling and SüdChemie (now Clariant) for the financial support and for providing the clays and Inventia for providing the microfibrillated cellulose.

A special thanks to Seydina Diabang and Charly Ou, the two master student I supervised, for their great work.

I would like to thank everyone that helped me with move forward with administrative task along this PhD Paule Vannson, Katia Bruzzone, Magalie Meyer, Annette Winter and Leyla Ermis.

I dedicate this work to my family.

Table of contents

List of abbreviations

AFM   Atomic Force Microscopy

CNT   Carbon NanoTubes

DLS   Dynamic Light Scattering

DNA   DeoxyriboNucleic acid

LB   Langmuir-Blodgett

LbL   Layer-by-Layer

MFC   MicroFibrillated Cellulose

Milli-Q   Ultrapure Millipore water

OTS   Octadecyltrichlorosilane

PAH   Poly(Allylamine Hydrochloride)

PDDA   Poly(DiallylDimethyl Amonium chloride)

PDMS   Poly(DiMethylSiloxane)

PEI   Poly(EthyleneImine)

PMEMA   Poly(Methyl vinyl Ether-alt-Maleic Anhydride)

PVAl   Poly(Vinyl Alcohol)

PVAm   Polyvinylamine

QCM   Qartz Crystal Microbalance

RH   Relative Humidity

RMS   Root Mean Square

THF   TetraHydroFuran

XPS   X-ray Photoelectron Spectroscopy

Assemblage couche-par-couche de composites bio-inspirés

Résumé de Thèse en Français

(Summary of the Thesis in French)

Les composites naturels sont à la fois polyvalents et très performants (résistant, auto-réparant, tenace, léger, …). Ces matériaux sont composés de renforts rigides (souvent fragiles) liés ensembles par une matrice molle et ductile. La structuration à l'échelle micro- et nanoscopique donne à ces composites une résistance et une ténacité plusieurs fois supérieures à celles de leurs éléments constitutifs. En comparaison les matériaux synthétiques ont des structures bien moins contrôlées, ce qui limite leurs performances. L'objectif de ces travaux est la fabrication de nano-composites polyvalents et performants s'inspirant des principes identifiés dans les matériaux biologiques. L'assemblage couche-par-couche permet un contrôle nanométrique de la composition et de l'architecture de films minces. En utilisant cette technique nous avons fabriqué d'une part des composites lamellaires combinant des nano-plaquettes d'argiles et des silicones imitant la structure de la nacre et d'autre part des composites fibrillaires à partir de cellulose dont la structure est inspirée du bois. Ces deux types de structures, renforcés par des nano-plaquettes ou des nano-fibres, sont à la fois transparents et extrêmement résistants, certains films ont même des propriétés d'auto-réparation. Cette thèse décrit la préparation et la caractérisation de ces composites aux propriétés multiples. Nous montreront aussi comment il est possible grâce à la technique couche-par-couche de contrôler l'architecture de ces films bio-inspirés et donc leurs propriétés mécaniques.

Des matériaux biologiques aux matériaux bio-inspirés

Les matériaux structurels biologiques comme la nacre ou le bois sont à la fois légers, résistants, résilients et auto-réparants. Alors que ces matériaux sont composés d'éléments aux propriétés mécaniques limitées, soit mous (polymères amorphes, petites molécules), soit fragiles (minéraux, polymères cristallins), l'organisation à l'échelle nano- et microscopique de ces briques élémentaires aux propriétés mécaniques très contrastées conduit à des composites aux propriétés exceptionnels. Dans la nacre, par exemple, l'empilement compact de plaquettes inorganiques liées entre elles par un polymère mou conduit à une résilience près de cent fois supérieure à celle de ses constituants. Dans le bois l'organisation des fibrilles de cellulose est déterminée par la nature des sollicitations exercées sur la plante. Les fibres sont inclinées pour donner de la flexibilité aux jeunes arbres et alignées verticalement dans les troncs des vieux arbres pour soutenir le poids des branches et des feuilles.[1] Des exemples d'organisation de matériaux naturels sont présentés dans la Figure 1. La Figure 1A montre un schéma de la structure de la paroi cellulaire du bois qui souligne l'importance de l'organisation des microfibres dans la structure du bois. A l'extérieur les fibres orientées aléatoirement permettent un contact résilient et efficace avec les autres parois cellulaires, tandis que l'alignement dans les couches internes rend la structure résistante, et enfin le vide central rend ces matériaux légers. Dans la Figure 1C on observe la tortuosité d'une fissure dans la nacre qui montre comment l'arrangement lamellaire des plaquettes minérales permet de dévier la propagation des fissures en augmentant de ce fait grandement la ténacité du matériau. La grande proportion de phase minérale dans la nacre (>90%) permet de conserver une forte résistance à la déformation, mais au contraire du carbonate de calcium constituant la phase minérale la nacre n'est pas fragile. Dans ces deux structures l'arrangement des nano-renforts, sous forme de fibrilles dans le bois ou de plaquettes dans la nacre, permet de nouvelles combinaisons de propriétés mécaniques : côté bois légèreté et flexibilité, côté nacre ténacité et résistance à la déformation.
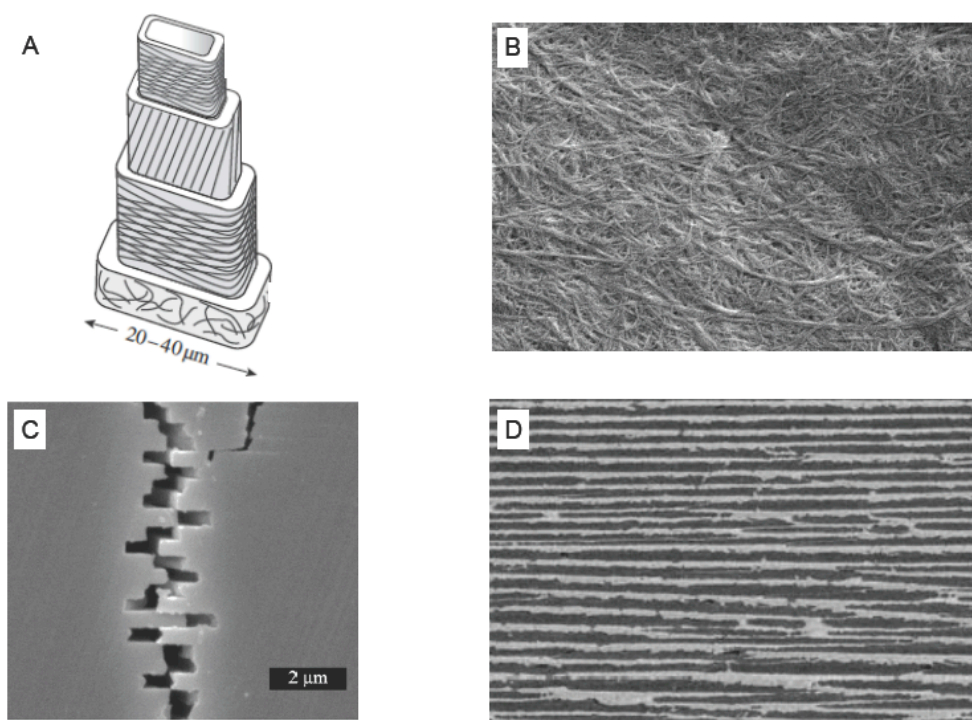
Figure 1. Matériaux structuraux biologiques et bio-inspirés. (A) Représentation schématique de la structure de la paroi cellulaire du bois. (B) Nano-papier préparé à partir de nano-fibrilles de cellulose.[2]. (C) Fissure dans de la nacre montrant les plaquettes de carbonate de calcium imbriquées les unes dans les autres. (D) Organisation lamellaire d'un composite à base d'époxyde et d'alumine structurée par congélation d'une solution de colloïdes. [3]

Beaucoup de nano-renforts et de polymères disponibles pour la fabrication de composites artificiels ont des propriétés mécaniques supérieures à celles des composants naturels, cependant leurs assemblages en composites aussi performants que leurs homologues naturels restent un challenge. Par exemple l'incorporation de grandes quantités de nano-renforts dans une matrice polymère conduit à l'apparition de micro inhomogénéités par démixtion et à des matériaux fragiles. De même l'orientation précise de renforts lamellaires ou fibrillaires en masse, nécessaire à l'obtention de composites performants reste difficile. De manière générale le manque de contrôle à l'échelle micro- et nanoscopique diminue l'efficacité structurale des composites synthétiques.

L'objectif de la biomimétique est de s'inspirer des stratégies identifiées dans les matériaux naturels pour produire des composites synthétiques plus performants. De nombreux groupes travaillent sur la production de composites résistants et résilients imitant la structure de la nacre. La difficulté réside dans le contrôle de

l'architecture de ces matériaux. L'exemple dans la Figure 1D montre un composite lamellaire fabriqué par congélation d'une solution de particules d'alumine. Les cristaux de glaces grandissent sous forme de lamelles (suite à un gradient de température) et confinent les particules inorganiques sous forme de plaquettes par démixtion. Après lyophilisation de la glace, et frittage des particules d'alumine, il est possible de remplir les interstices de polymères pour conduire au composite. La ténacité de ce type de composites dont la structure est inspirée de celle de la nacre est dix fois supérieure à celle d'un matériaux de composition identique sans structuration.[3] L'exemple dans la Figure 1B montre un film préparé par filtration d'une solution de nano-fibrilles de cellulose. La structure de ces films est similaire à celle du papier. Cependant, comme les fibrilles utilisés sont nanométriques (et non micrométriques comme dans le papier traditionnel), les interactions dans le matériau sont beaucoup plus nombreuses et mieux réparties. Bien que moins complexes que le bois ces films ont une résistance et une résilience exceptionnelle pour des polymères.[2] Les exemples présentés ci-dessus ne sont qu'un aperçu des avancées technologiques s'inspirant de la nature et beaucoup reste à découvrir.

L'assemblage couche-par-couche

Le contrôle précis de l'architecture est l'étape clé pour la préparation de matériaux bio-inspirés performants. Développé par Gero Decher dans les années 90, l'assemblage couche-par-couche (abrégé LbL pour «Layer-by-Layer» en anglais) est facile d'utilisation, écologique et permet de contrôler à l'échelle nanométrique la composition et la structure de films supportés.[4] Largement utilisé pour la construction de films de polyélectrolytes, la technique LbL a été rapidement adaptée à de nombreux autres nano-objets: colloïdes (quantum-dots 0D, nano-fibrilles 1D, nano-plaquettes 2D), protéines, cellules vivantes, ADN, polymères non chargés, petites molécules, …). Le principe simplifié de la technique LbL est présentée dans la Figure 2A en prenant pour exemple un couple de polyélectrolytes. Un substrat chargé positivement est mis en contact avec une solution de polyanion qui s'adsorbe à sa surface (interactions électrostatiques) conduisant à une inversion de la charge de surface. De fait cette étape est autolimitée car après inversion de la charge de surface les polyanions ne s'adsorbent plus. Le substrat est ensuite rincé pour enlever l'excès de

polyélectrolytes faiblement adsorbés, avant d'être mis en contact avec une solution de polycation. Ces derniers s'adsorbent à leur tour sur le support, et la charge de la surface redevient positive. Après rinçage on peut donc répéter le procédé pour déposer une nouvelle paire de couche et ainsi de suite jusqu'à obtenir l'architecture désirée. En première approche ce sont les multiples interactions électrostatiques entres les différents objets qui maintiennent la structure du film. Les détails des mécanismes dirigeant l'assemblage, la structure et la stabilité des films couche-par-couche sont cependant plus complexes, et toujours en cours d'investigation. Au delà de la diversité des objets pouvant être introduits dans les dépôts couche-par-couches, c'est la facilité d'utilisation qui fait la force de cette technique. La Figure 2B présente le matériel nécessaire pour préparer un dépôt couche-par-couche par trempage. D'autres méthodes comme la pulvérisation ou le spin-coating permettent d'accélérer le procédé de dépôt. Il est enfin possible d'incorporer plus de deux composés dans un même film et de contrôler l'architecture du film de manière arbitraire en choisissant la séquence de déposition.
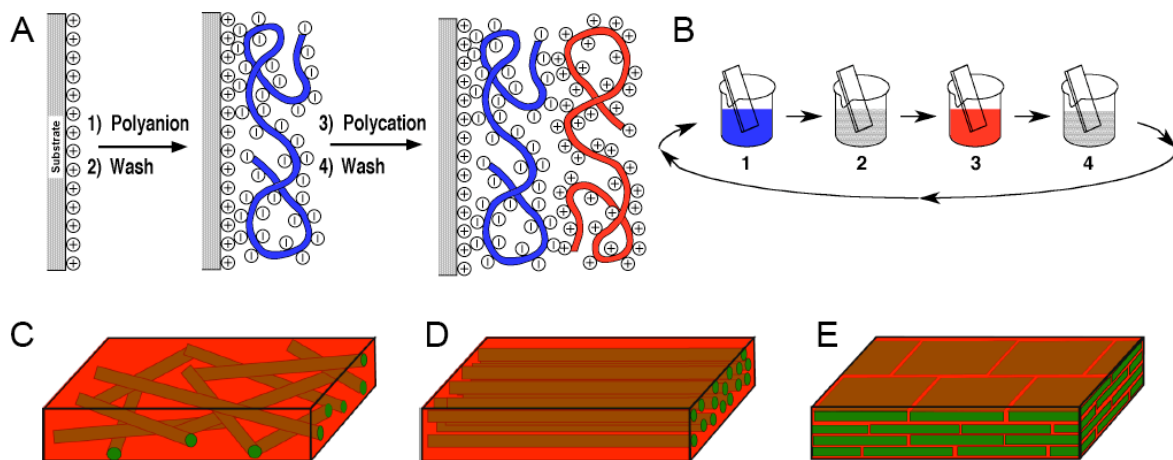
Figure 2. (A) Principe de la technique couche-par-couche. (B) Montage expérimental pour un dépôt couche-par-couche effectué par trempage. (C, D, E) Représentation schématique des films que nous allons préparer : (C) nano-composite à base de fibrilles orientées aléatoirement dans le plan, (D) nano-composite à base de fibrilles orientées dans une seule direction, (E) nano-composite lamellaire à base de plaquettes orientées dans le plan.

Le contrôle de l'architecture des films composites assemblés par la technique LbL est un avantage clé pour la fabrication de matériaux bio-inspirés performants. Des

films s'inspirant de la nacre, combinant des argiles et du poly(vinylalcohol) ont déjà été assemblés par LbL.[5] Ils sont transparents et leurs propriétés mécaniques sont exceptionnelles, avec un module d'Young atteignant 100 GPa et une résistance à la rupture de 400 Mpa. Ces films ont cependant une déformation à la cassure de l'ordre de 0.4 % et restent donc fragiles contrairement aux matériaux naturels qui sont bien plus tenaces. Pour obtenir des matériaux à la fois résistants et tenaces l'un des objectifs de cette thèse a été d'introduire des couches de poly(dimethylsiloxane) (un polymère extrêmement mou) dans ces films. La modulation de la quantité d'argile incorporée dans le film devrait permettre de contrôler de manière précise le module d'Young des films préparés et d'obtenir une fracture ductile (après la déformation plastique) nécessaire à l'obtention d'un file tenace. La technique LbL a aussi été utilisée pour fabriquer des matériaux inspiré du bois à partir de microfibrilles de cellulose.[6] Cependant, les propriétés mécaniques de ces composites sont bien en dessous des performances attendues pour des matériaux à base de microfibrilles de cellulose.[2] En étudiant de nouveaux polymères et en contrôlant le dépôt, nous avons montré qu'il était possible d'obtenir de nouveaux composites très performants par LbL.

Pour les films à base de plaquettes d'argile (nanorenforts 2-D) l'utilisation de la technique de trempage permet d'obtenir des films lamellaires orientés dans le plan (Figure 2E). Pour les films à base de microfibrilles de cellulose (nanorenforts 1-D) cette même technique conduit à des films orientés aléatoirement dans le plan, or dans le bois c'est l'orientation des fibrilles qui apporte les performances mécaniques. Nous avons donc utilisé les forces de cisaillement induites lors de l'assemblage LbL par spin-coating pour fabriquer des films orientés encore plus résistants que les précédents.

Films inspirés de la nacre, combinant argiles et silicones

Les argiles sont un groupe de minéraux naturels composés d'un empilement de plaquettes mono-cristallines épaisses de quelques nanomètres et larges de plusieurs centaines de nanomètres. En présence d'eau les forces électrostatiques qui maintiennent la structure sont écrantées et les plaquettes se dispersent pour former une solution colloïdale. Les charges négatives présentes à la surface de ces plaquettes permettent cependant de les assembler en utilisant la technique

LbL en les combinant avec un polycation. En premier lieu, nous avons étudié l'assemblage d'argile avec des polycations forts (chlorure de poly(dimethyldiallylamonium)) et des polycations faibles (poly(vinylamine)) et nous avons montré que la vitesse de croissance était fonction de la densité de charge du polycation utilisé, de la nature et de la pureté des argiles. Nous avons ensuite étudié l'influence du séchage sur le régime de croissance des films multicouches à base d'argiles. Nous avons observé des phénomènes d'hystérésis lors du séchage et de l'hydratation des films qui induisent la transition d'une croissance linéaire vers une croissance exponentielle en l'absence de séchage.

Ensuite, nous avons construits des films multicouches combinant des argiles et du poly(dimethylsiloxane) (PDMS). Pour cela nous avons fait réagir un poly(anhydride) avec un PDMS fonctionnalisé par des amines en bout de chaine. Les groupes réactifs disponibles du poly(anhydride) réagissent ensuite avec la poly(vinylamine), ce qui permet d'assurer la cohésion entre le PDMS et les argiles (Figure 3A, 3C).
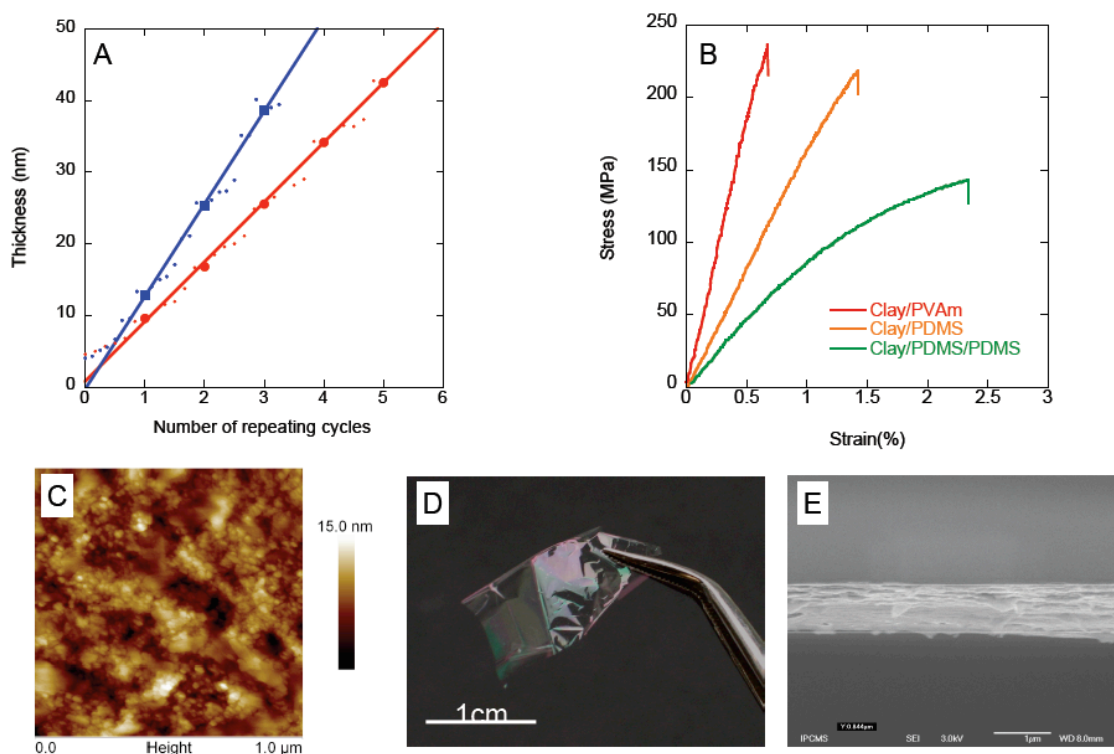
Figure 3 : (A) Croissance de films constitués d'argiles et de PDMS suivie par ellipsométrie. (B) Courbes de traction obtenues en fonction de la composition des films. (C) Image AFM de la surface d'un film multicouche après dépôt d'argiles. (D) Photo d'un film auto-supporté de 800nm d'épaisseur. (E) Image MEB d'une coupe transversale d'un film multicouche à base d'argiles.

La construction de films épais auto-supportés (~1 μm), nécessaire pour les mesures de propriétés mécaniques, a été effectuée en utilisant un robot de trempage automatisé remis en état de marche au cours de la thèse. Ces films sont transparents (Figure 3D) et présentent une architecture similaire à celle de la nacre (Figure 3E). Nous avons ensuite mesuré les propriétés mécaniques de ces films et montré qu'il était possible de faire varier le module d'Young entre 45 et 10 GPa en modifiant la composition des films (Figure 3B). Les contraintes à la cassure (130-230 MPa) et les modules obtenus pour les films composés uniquement d'argiles et de polymères sont comparables à ceux de certains alliages à base de magnésium, tout en étant légers et transparents. La ténacité des films varie aussi avec leur composition. Cependant même dans les films contenant le plus de PDMS la déformation plastique est limitée, ce qui empêche la fabrication de films tenaces. Il serait intéressant de continuer ces travaux en changeant la taille des particules d'argile incorporées dans ces multicouches ou les caractéristiques mécaniques de

la matrice polymère pour augmenter la déformation plastique de ces matériaux et améliorer leurs ténacités.

En effet, différentes particules de différentes formes et de différentes structures conduisent à des propriétés mécaniques différentes. A l'échelle nanométrique il reste beaucoup à découvrir sur les relations entres la formes des renforts et les propriétés mécaniques du composite. La suite de la thèse concerne l'étude de nano-composites renforcés par des nanoparticules unidimensionnelles, les microfibrilles de cellulose.

Films inspirés du bois, combinant microfibrilles de cellulose et poly(vinylamine)

Les microfibrilles de celluloses sont les briques élémentaires qui donnent au bois sa structure et sa résistance mécanique. Elles ont un diamètre d'une vingtaine de nanomètres et une longueur qui peut atteindre quelques microns. Elles sont obtenues à partir des macrofibres présentes dans le bois par homogénéisation à haute pression et traitement chimique. La fonctionnalisation de la surface des microfibrilles par des groupements carboxylates permet d'obtenir des solutions colloïdales stables dans l'eau et d'incorporer ces microfibrilles dans des films multicouches via la technique LBL. Dans un premier temps, nous nous sommes intéressés à la construction de films contenant des microfibrilles de cellulose et de la poly(vinylamine) et nous avons étudié l'influence du pH de la solution de poly(vinylamine) sur la construction et la composition de ces films par trempage (Figure 4 A). Nous nous sommes ensuite intéressés à la structure de ces films et à leurs propriétés mécaniques en fonction du pH de construction (Figure 4 B). Finalement, nous avons étudié les variations de la résistance mécanique des films en fonction de l'humidité. Les propriétés mécaniques obtenues sont supérieures à celles du bois et comparables à celles des meilleurs composites à base de microfibrilles de cellulose. Ces films sont transparents, et certains (construits à pH élevé) s'auto-réparent en présence d'eau.
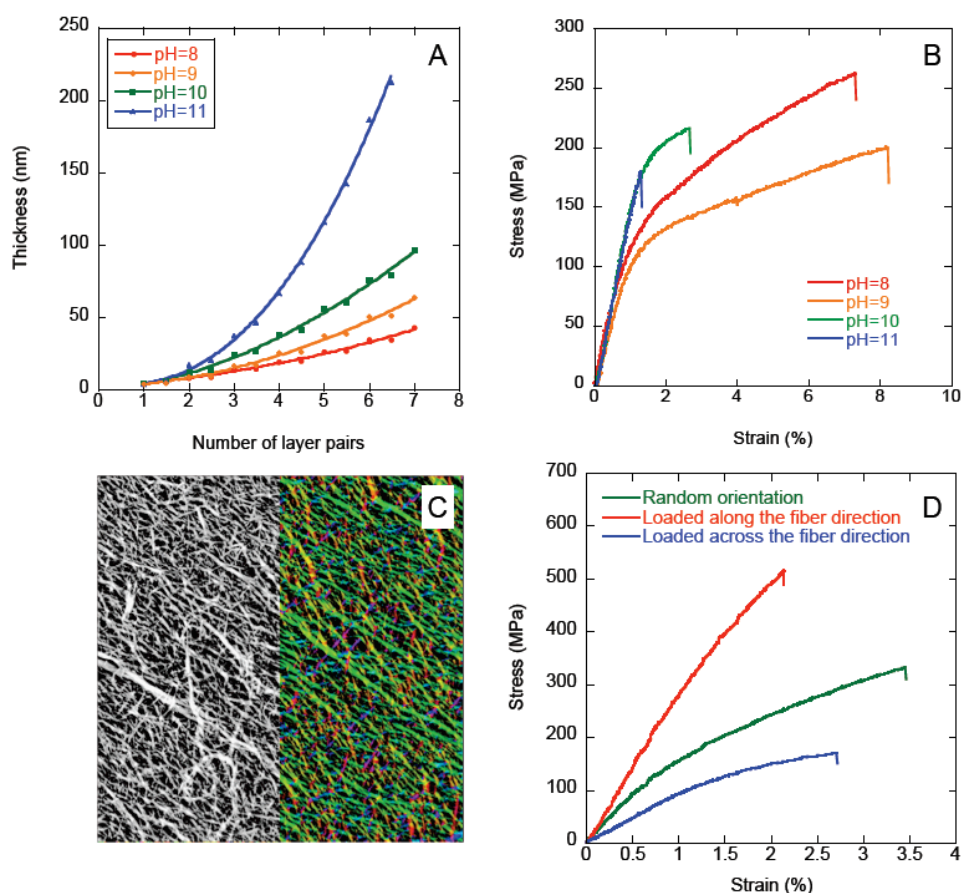
Figure 4 : (A) Croissance de films constitués de microfibrilles de cellulose et de poly(vinylamine) à différents pH suivie par ellipsométrie. (B) Courbes de traction obtenues en fonction du pH de construction. (C) Image AFM d'une couche de microfibrilles de cellulose orientée (à gauche); Traitement d'image permettant la visualisation et la quantification de l'orientation (à droite). (D) Propriété mécaniques des films en fonction de l'orientation et de la direction de sollicitation.

La dernière partie de la thèse concerne l'orientation des microfibrilles de cellulose dans les films multicouches en remplaçant le dépôt par trempage par un dépôt par spin-coating. Les films obtenus par cette technique présentent une orientation radiale des microfibrilles de cellulose. Nous avons caractérisé l'orientation des microfibrilles dans le matériau en combinant de l'imagerie AFM et un programme de caractérisation de l'orientation (Orientation J plug-in pour Image J) (Figure 4C). La résistance mécanique des films dans le sens des fibres est nettement supérieure à celle de films non orientés qui est elle même supérieure à celle des films dans le sens perpendiculaire aux fibres (Figure 4D). Avec une résistance mécanique de plus de 500MPa et un module de 30GPa ces films sont

comparables à des matériaux tels que des alliages d'aluminium ou certaines gammes de Kevlar®.

Les perspectives de ces travaux sont nombreuses; la combinaison de microfibres de cellulose et de particules d'argile pourrait par exemple conduire à de nouveaux matériaux encore plus résistant. Il pourrait aussi être intéressant d'assembler des films où l'orientation des fibres de cellulose varie dans l'épaisseur des films.

Lors de cette thèse, nous avons été amenés à remettre en marche un robot de trempage et à adapter les équipements de mesures mécaniques à l'étude de films micrométriques. Une fois ces outils opérationnels, nous avons pu préparer et caractériser des films inspirés de la nacre ou du bois en jouant sur divers paramètres (forme des renforts, nature des composants, architecture, méthode de dépôt, pH, ...). Ces nouveaux composites nano-renforcés présentent de multiples propriétés intéressantes, résistance mécanique, transparence, résilience ou encore auto-réparation. Au delà des premiers résultats obtenus ces travaux ouvrent les portes vers une meilleur compréhension des mécanismes gouvernant les propriétés mécaniques des nano-composites et donc vers la découverte de matériaux possédant de nouvelles combinaisons de propriétés mécaniques.

<div align="center">*</div>

1.   Lichtenegger, H.; Reiterer, A.; Stanzl-Tschegg, S. E.; Fratzl, P., Variation of cellulose microfibril angles in softwoods and hardwoods - A possible strategy of mechanical optimization. *Journal of Structural Biology* **1999,** *128* (3), 257-269.

2.   Henriksson, M.; Berglund, L. A.; Isaksson, P.; Lindstrom, T.; Nishino, T., Cellulose nanopaper structures of high toughness. *Biomacromolecules* **2008,** *9* (6), 1579-1585.

3.   Munch, E.; Launey, M. E.; Alsem, D. H.; Saiz, E.; Tomsia, A. P.; Ritchie, R. O., Tough, Bio-Inspired Hybrid Materials. *Science* **2008,** *322* (5907), 1516-1520.

4.   Decher, G., Fuzzy nanoassemblies: Toward layered polymeric multicomposites. *Science* **1997,** *277* (5330), 1232-1237.

5.   Podsiadlo, P.; Kaushik, A. K.; Arruda, E. M.; Waas, A. M.; Shim, B. S.; Xu, J.; Nandivada, H.; Pumplin, B. G.; Lahann, J.; Ramamoorthy, A.; Kotov, N. A., Ultrastrong and stiff layered polymer nanocomposites. *Science* **2007,** *318* (5847), 80-83.

6.   Karabulut, E.; Wagberg, L., Design and characterization of cellulose nanofibril-based freestanding films prepared by layer-by-layer deposition technique. *Soft Matter* **2011,** *7* (7), 3467-3474.

Introduction

Biological structural materials possess fascinating combinations of properties such as lightweight, strength, shock resistance and self-healing. These materials are based on a limited number of compounds, which are either mechanically weak (amorphous polymers, small molecules) or fragile (minerals, crystalline polymers). In biological composites the combination of such materials with contrasting mechanical properties and the optimization of their micro- and nano-scale structures brings exceptional performance. For example the precise stacking of mineral platelets connected by soft polymers provides nacre or bones with a toughness orders of magnitudes above that of their individual components.[1] In wood the mechanical performances are brought about by the organization of the cellulose fibers, tilted fibers for flexibility in young trunks and vertical fibers for stiffness and compressive strength in older trunks as the weight of branches and leaves increases.[2] Generally speaking the structure-property strategies evolved in biological materials are remarkably efficient.[3]

In comparison, the structural efficiency of synthetic composites is limited. Although the reinforcing particles in current structural composites have intrinsic mechanical properties above that of biological ones, their organization into mechanically efficient materials is still a challenge. Phase separation hinders the production of composites with homogeneous structure and large particle contents. The lack of micro- and nano-scale control over the architecture of man-made composites undermines their mechanical efficiency. The objective of bio-mimetism is to identify and use existing successful concepts responsible for the mechanical properties of biological materials in order to minimize learning cycle in the design of new materials, especially composites.

The conception of new bio-inspired composites requires a detailed understanding of biological and man-made materials. The first chapter of this thesis introduces the reader to the diversity of biological materials and provides notions on the properties and the mechanical characterization of common structural materials. Focusing on nacre, bone and wood we will then discuss the structure-property

relationships in biological composites. Finally we will review how these concepts have been applied in state-of-the-art bio-inspired composites.

The control of the nano- and micro-scale architecture is the bottleneck for the preparation of bio-inspired materials with good performance. Layer-by-layer (LbL) assembly is a cheap and environment friendly technique that offers a one dimensional nano-scale control over the structure and composition of thin films (also called multilayers).[4] It has been used to prepare nacre-inspired multilayers from clay nano-sheets and poly(vinyl alcohol) with strength as high as 400 MPa.[5] The contribution of layer-by-layer assembly to the preparation of platelets and fibrils containing multilayers is reviewed with focus on the mechanical properties of such composites.

The goal of this thesis was to take inspiration from nature and implement some concepts in mechanically resistant layer-by-layer assembled films. More precisely, our objective was to control through the conditions of LbL-assembly, the composition and the structure of the films prepared in order to investigate the structure-property relationships in such materials. Two concepts have been driving our work; the reinforcement of a soft polymer matrix by well organized anisotropic nano-particles and the prevention of crack propagation through the optimization of structural parameters. This work consists in the application of these concepts in nacre-inspired clay-based multilayers and wood-inspired fibril-based multilayers.

In depth investigation of the parameters controlling the assembly of clay-based multilayer provided resources to optimize the construction of nacre-inspired films. The best nacre-inspired layer-by-layer assembled films reported reached high strength (400 MPa) but their strain at break was limited (0.4%) making these films brittle.[5] Our strategy was to combine clay with poly(dimethylsiloxane), an extremely soft polymer. We have shown that it was possible to build multilayers with clay and poly(dimethylsiloxane) derivatives and to control their mechanical properties by simple variation of the constituents and film architecture.

For the preparation of wood-inspired structures we used microfibrillated cellulose, a promising class of nano-fibers extracted from wood. The composition of the LbL-assembled films was controlled by adjusting the pH of the solutions during deposition. We evaluated the influence of this parameter on the mechanical properties of the films. We also used water to plasticize the multilayers and

identified some experimental conditions where the film show self-repairing properties. Finally, we prepared and characterized oriented microfibrillated cellulose composites exhibiting record strength (490 MPa) as compared to natural wood[8] and previously reported layer-by-layer assembled films.

1 Biological and bio-inspired structural materials

1.1 Diversity and limits of biological materials as source of inspiration

Through evolution nature has selected a wide variety of function-specific multi-property materials. A single material can provide shape, nutriment transport, resistance and movements. These materials can in addition be self-healing and their colors serves as camouflage, mating signal or uv-protection. The diversity of structures and properties found in nature is colossal, yet some man made materials have unique features that are not found in biological materials.

Nature is especially good at making polymers, silk for example has a toughness surpassing that of steel.[9] While a few DNA molecules store the information necessary to build a new living species from scratch. Industrial production of some regular polymer such as poly(cis-isoprene) is still challenging but it can easily be extracted from the latex secreted by *Hevea Brasiliensis*. Tires, gloves or balloons are still made of reticulated natural rubber that offers excellent elasticity, hydrophobicity and barrier properties. Nature also makes actuators, and motion mechanism. The flagellar motor of bacteria is a beautiful example of micro-propulsion.[10] In eukaryote cells actin filaments and microtubules enable the diversity of motion that we know in the animal kingdom.[11] Many photonic structures are found in nature,[12] structural color in butterfly wings are effective intra and inter

species communication signals, and the micro lens array on the back of brittle star allows them to change colors.

Figure 5. Biological materials (A) Structure of DNA (deoxyribo-nucleic acid) (B) A butterfly (Genus Morpho) showing structural color. (C) Extraction of latex from *Hevea Brasiliensis.*

But nature lacks some properties needed for engineering applications. Magnetism for example, even if some organisms can sense and orient according to earth magnetic field[13] their level of sophistication is low compared to man made structures (hard drive or loud speakers). Another property missing to biological materials is electrical conductivity. Relying mostly on polymers and ceramic, nature can only produce materials with low conductivity. Even the nervous system based on the propagation of electrical signals relies on electrolyte solutions rather than conductive materials. At last, maybe the major drawback of natural materials is their shaping, as resistant and perfect as they can be, their shape and structure are defined by their function and can hardly be altered. The wings of butterflies are not meters wide, and nacre cannot be grown as car parts or bricks where its exceptional strength and toughness are needed.

Producing material that suits human needs in terms of shape, size and properties using the design principle found in natural materials is the aim of bio-mimicry. A very exiting field of material science that already found several everyday applications and where a lot is left to discover

For hundreds of years humans have taken ideas from their environments to create new objects, new techniques, and new theories. Romans were fighting in turtle like formation, Newton formulated his theory about gravity from the fall of an apple, and we travel in bird shaped planes. Our environment has always been a source of inspiration, conscious or unconscious. However there was a turn in the recent

years with the systematic investigation of the design principle of natural structures in order to mimic them and produce bio-inspired objects.

The resemblance of the Gherkin tower (Former 30 St Mary axe) in London with a deep sea-sponge (Figure 6 A and B) may be accidental[14] but it is nevertheless remarkable. Both share a tubular structure reinforced along four axes (horizontal, vertical and two spiraling diagonals) bringing high mechanical resistance with limited amount of structural material. The sponge needs water flowing through its structure to filtrate nutriments while the "Gherkin" uses its open structure to allow ventilation and save energy.
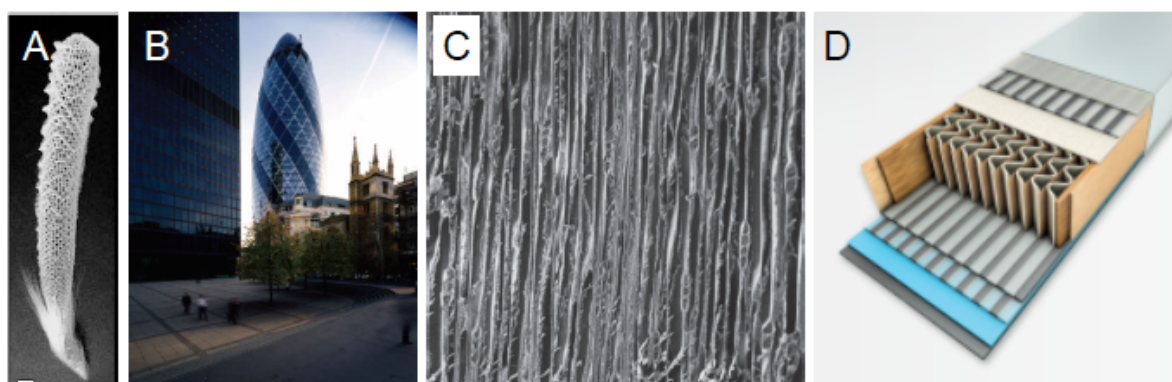
Figure 6. Comparison of biological and man-made structures. (A) Photograph of a deep sea-sponge (see also Figure 11 A).[15] (B) Photograph of the "Gherkin" a building located in London.[14] (C) SEM image showing the longitudinal micro-structure of cedar wood (see also Figure 15 D). (D) Schematic representation of the core structure of Nordic skis (taken from www.fischersports.com).

There are also plenty of examples of bio-inspired structures in sports and high technology. Nordic skis for example have a structure that combines principles found in wood and porcupine quills (Figure 12 and Figure 6 C and D). The hard outer skin with a cellular filling, found in porcupine quills, brings lightweight and bending resistance. On the wood side the vertical alignment of the cells in the ski provides enough compressive strength to hold the weight of the skier.

Velcro scratch, present on shoes and clothes, owes a lot to the tiny hooks found on the surface of cocklebur's fruits. These fruits stick to the fur of animals upon contact, travel with the animal and are seeded far from the mother plant when the animal scratches itself. In the same way that Velcro fasten upon pressure and detach upon pulling.[16] Following these successes on the macroscopic scale, the

current research is focusing on mimicking biological structures at the micro and nano-level.

Among biological structures, the ones providing structure and protection to plants and animals are especially interesting. Wood, nacre and bone are strong, tough and light a combination of properties sought after in engineering composites. While the elementary bricks that compose them are either weak or brittle, their organization takes the best of each to produce a material that is both strong and tough. The translation of nature's design principles in man-made nano-composites is promising, yet the description of structure-properties relationships in biologic and bio-inspired materials requires notions of mechanics of material.

1.2   Mechanics of materials

This section introduces the basic concepts for the mechanical characterization and description of structural materials such as polymers, ceramics, and metals.

1.2.1   Stress-strain tests

Stress strain tests, or tensile tests, consist of recording the force needed to deform a sample at a constant strain rate up to rupture (Figure 7).
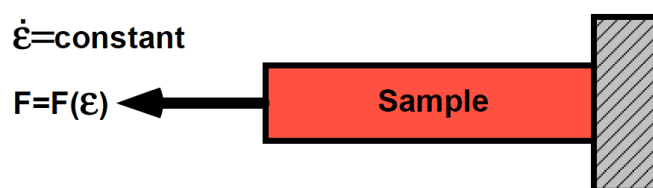
Figure 7. Schematic representation of stress-strain tests. The sample is pulled at a constant speed and the applied force (F) is recorded as function of the strain (ε).

These tests are the most popular mechanical characterization technique for studying structural materials.[17] They are easy to set up and intuitive, if one wants to know how resistant is a material one simply pulls on it. Tensile tests only probe the macroscopic behavior of the material under tension, however the macroscopic

properties of the material depends on its nano- and microscale structure. Other tests can complete the description of the mechanical behavior of the material:

- Dynamic mechanical analysis gives information about the dependence of the mechanical properties to the solicitation speed.

- Compression, shear, or flexion tests correspond to different types of solicitation of the material.

- Nano-indentation and AFM directly probe the properties of the material at the micro or nano-scale.

Many other mechanical tests exist, but often they probe properties for specific applications. In this manuscript, we will focus on stress-strain tests to allow easy comparison between different materials.

In tensile tests the force needed to deform a sample depends on its size, and more precisely on its cross section (A), while the distance of deformation (L-L_0) depends on the initial length (L_0) of the sample. Considering the stress (σ) instead of the load (F) and the strain (ε) instead of the distance of deformation allow to get rid of these geometrical constrains.

$$\sigma = \frac{F}{A} \qquad \text{Equation 1}$$

$$\varepsilon = \frac{(L - L_0)}{L_0} \qquad \text{Equation 2}$$

This way stress and strain measured are representative of the material properties and independent of the sample size, which makes comparison between different samples possible.

The quantitative treatment of tensile test data yields a curve were the stress recorded is plotted as function of the strain applied on the sample. Typically three properties can be obtained from this curve:

- The Young's modulus (E) is slope at the origin of the stress-strain curve, it corresponds to the property of the the material to resist to deformation.

- The stress at breaks (σ_{max}) that corresponds to the strength of the material.

- The strain at breaks (ε_{max}) that corresponds to the maximum strain the material can handle.

In a more detailed interpretation the tensile test curve (Figure 8) is divided into three parts.[17] The first part corresponds to the elastic regime at low strain (in red) where the stress is proportional to the deformation of the material. The elastic deformation is reversible, meaning that the material relaxes back to its original shape if the load applied to the material is removed. The last part is the plastic regime at high strain where the material deforms with only a small increase of the strain. Plastic deformation corresponds to a failure of the material structure it is therefore irreversible. Between these two regimes, the yield point corresponds to the transition from elastic to plastic behavior.
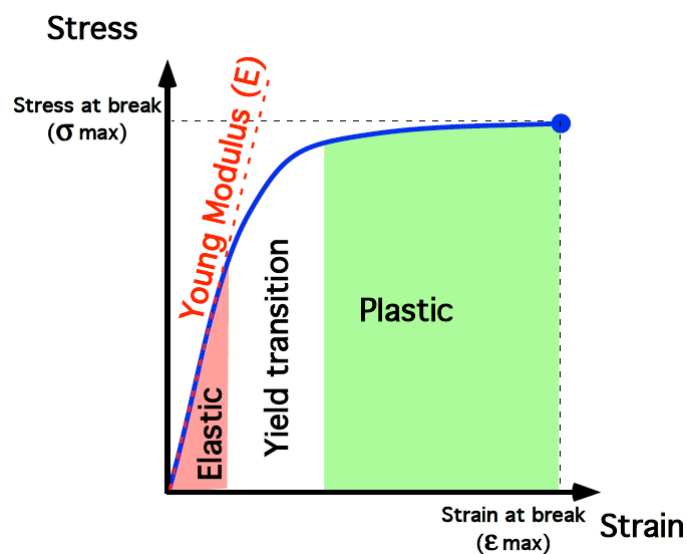
Figure 8. Schematic representation of a stress strain curve.

The area under the curve (red, white and green) corresponds to the total energy needed to break the material. The energy stored in the elastic deformation of the material will be released after breaking, while the energy associated with the plastic deformation is dissipated or absorbed by the material.

There is a multitude of materials with various mechanical properties. This single curve is only a simple example used to illustrate the general terms. The next section will present material properties that can be extracted from the shape of a given stress-strain curve.

1.2.2   Brittle, soft, or tough

The choice of a structural material with given mechanical properties provides its mechanical resistance and shape to an object. Their core characteristics are,

therefore, their strength (the maximal load they can handle before breaking), their toughness (the maximal energy they can handle before breaking) and their ability to resist deformation (Young's Modulus). There is no good or bad material, the property of an object must always be in equation with an application. A rubber knife and a stone pillow are equally useless. Three of the most important types of material behavior are presented Figure 9.
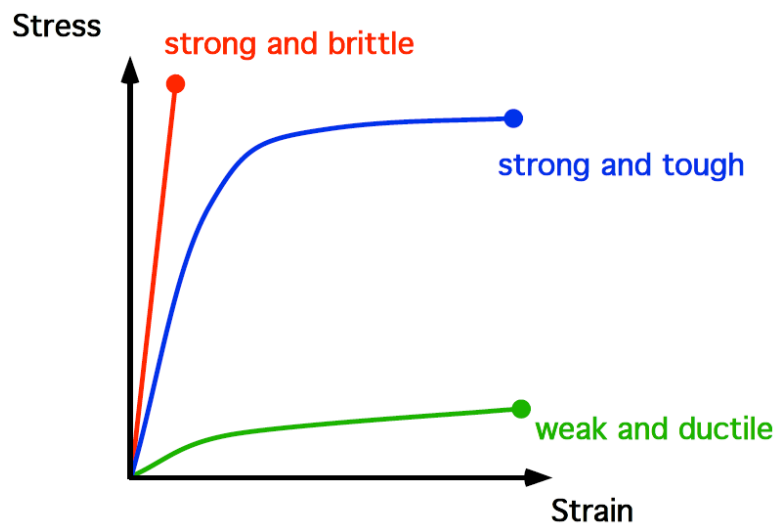
Figure 9. Three types of stress-strain curves.

Strong and brittle materials (red curve) deform elastically and have a high Young's modulus (e.g. glass). This type of material resists well to deformation, but as the area under the curve is limited, such materials is very sensitive to shocks and break easily. They are also sensitive to flaws because they don't dissipate energy (purely elastic). If a pre-cracked material is deformed, the energy accumulates near the crack and when the material fails the energy released leads to a fast development of the crack and premature breaking of the material. These materials exhibit better performance in compression than in tension and need protection against shocks for better performance.

At the other end of the range, weak and ductile materials (green curve) have a small elastic and a large plastic regime (e.g. dough). These materials are easy to deform and nearly insensible to flaws and shocks. As their structure is irreversibly modified upon solicitation, they find few applications as structural components.

Strong and tough materials (blue curve) combine a high Young's modulus with a plastic deformation (*e.g.* steel). These materials resist well to deformation and

shocks while being nearly insensitive to flaws and defects. They are good candidates for demanding structural applications.

To finish, elastomeric materials (not represented in Figure 9) combine a large elastic regime with a low Young's Modulus (e.g. rubber). They are easy to deform and do not break upon shocks but they can be sensitive to flaws. They are used for objects subject to large reversible deformation.

The material selection for the design of an object is a delicate task. In order to visualize the properties of material and facilitate the material selection engineer usually use properties maps of materials, also called Ashby plots.[18]

1.2.3   Mapping material properties

There are three main classes of homogeneous structural material: polymers, metals and ceramics. Some mechanical properties of the three class of material have been presented Figure 10.[18-20] The strength values reported for polymers and metals correspond to yield strengths, which are the stress at the end of the elastic deformation; they are typically lower than the maximal stress for materials with a plastic deformation. For ceramics the modulus of rupture reported corresponds to the maximal bending stress that a beam of material can handle. For ceramics it is typically higher than the tensile strength and lower than the compressive strength.

Polymers usually have Young's moduli below 10 GPa and a maximal strength below 200 MPa (with some exceptions like polyaramides whose Young's modulus and strength reach 130 GPa and 3000 MPa respectively). Their mechanical behavior range from liquid to brittle solids, and a single polymer often switches from brittle at low temperature to elastomeric or tough at higher temperatures (and ductile or liquid at even higher temperatures). They are light compared to the other classes of structural material (density between 0.5 and 2.5) and generally easy to shape as they melt below 300 °C (extrusion, injection molding, coating or thermoforming) but they are sensitive to environmental conditions (UV, solvents, heat) and loose their mechanical properties with time.[19]

Metals have Young's moduli between 30 and 300 GPa, and maximal strengths between 200 and 3000 MPa. They are generally tough but their high density (between 2 and 20) makes them undesirable for lightweight applications. Naturally occurring as oxides, they need to be reduced at high temperature before being

shaped using high mechanical strength (rolling, embossing) or high temperatures (extrusion, casting), which makes them generally expensive. It is the class of materials with the highest electric and thermal conductivities but they tend to corrode for example in the presence of water.[19]
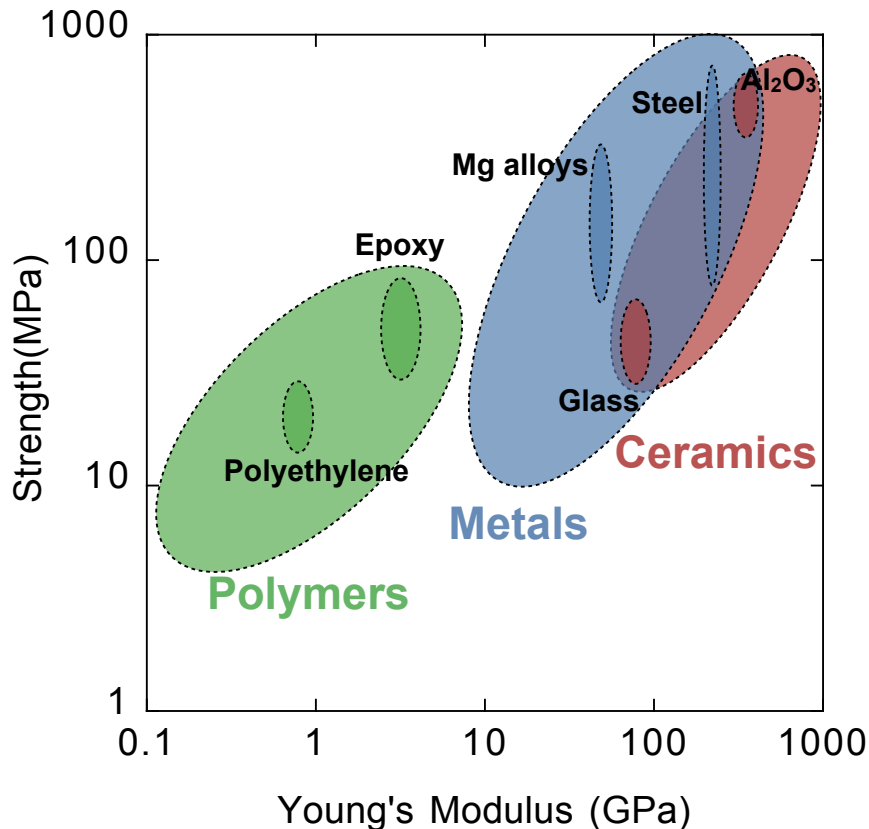
Figure 10. Ashby plot showing the strength and Young's modulus of polymers (yield strength), metals (yield strength) and ceramics (modulus of rupture) at ambient conditions.[18]

Ceramics combine high Young's modulus between 100 and 600 GPa (up to 1000 GPa for diamond), with high compressive strength from 1000 to 10000 MPa. But their brittle behavior limits their strength in traction (and the modulus of rupture plotted above) to a tenth of the compressive value. With a melting point above 1500-2000 °C, they are extremely difficult to shape, but they keep their mechanical properties even at very high temperature. Ceramics are generally insensitive to environmental conditions (UV, solvents, temperature) and can be used as electric or thermal insulators.

1.2.4   Composite materials

Some combinations of properties are difficult to obtain from a single material, for example lightweight and toughness or conductivity and transparency. Nature and humans solved this problem with composites. In composites two or more materials are combined to reach a specific set of properties that could not be obtained otherwise (at least not at similar costs). Some examples can be found in everyday life, reinforced concrete combines the compression resistance from concrete and the tensile strength from steel. While in aeronautics carbon fiber composites are light, strong and tough.[19]

The history of man-made composites started with Egyptians where straw was mixed with clay to improve the resistance of bricks. Since then composites science improved and diversified, but natural materials are still far ahead. From wood to bones and shells, the degree of precision and level of sophistication achieved by nature is mesmerizing.

1.3   Biological materials

Nature produces materials in restricted conditions (aqueous medium and room temperature), using only a limited set of elements (hydrogen, oxygen, cabon, nitrogen, sulfur, phosphorus, and calcium). Nevertheless, these materials have shock resistance, flexibility, or strength beyond expectations. In this section we will discuss the mechanisms that give natural nano- and micro-composites their exceptional mechanical properties.

1.3.1   Efficient functional structures in nature

Famous for the beauty and efficiency of its structure, *Euplectella sp,* is a deep-sea sponge. This multicellular animal lives attached to the seabed and filtrates water to feed. It relies on a flexible and resistant skeleton to maintain its open structure in the currents. Several mechanisms bring strength and toughness to its highly open structure.
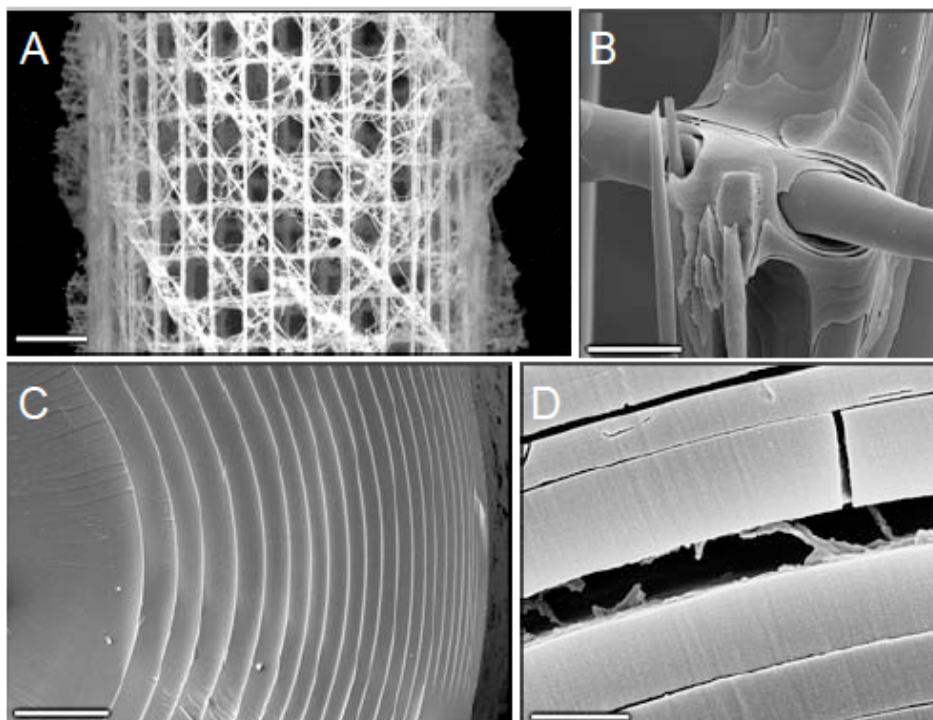
Figure 11. Structure of deep sea sponge _Euplectella sp._[15] (A) Macroscopic image of the cage structure. Scale bar 5 mm. (B) SEM image showing that crossing spicules are cemented with laminated silica layers. Scale bar 25 µm (C) SEM image of a cross section of a spicule. Scale bar 5 µm. (D) SEM image of a fractured spicule showing organic interlayer. Scale bar 1 µm.

At the macroscopic level (Figure 11A) the skeleton consists in a regular network of spicules (silica fibers) oriented vertically, horizontally and in the diagonal of the tubular structure. Each intersection is reinforced by cementation to ensure cohesion (Figure 11B). This arrangement provides resistance in flexion, tension and compression with a minimum amount of material. But the exceptional resistance to shocks comes form the microstructure of the spicules. Composed of concentric microscale layers of silica glued together with nanoscale organic interlayers, they have an excellent damage tolerance and prevent crack propagation. This structure has a fracture toughness twice that of monolithic silica while its modulus is only decreased by 20%.[21] It is amazing how such a small amount of soft mater can improve toughness of the structure by crack deflection and energy dissipation.

Porcupine quills are another beautiful example of precise architecture-function relationships. In combination with their lightweight, these defensive weapons are designed to resist high compressive loads without bending or buckling.
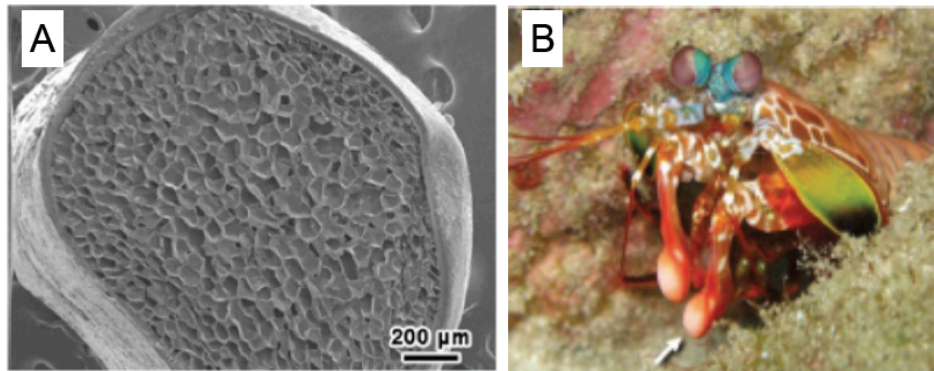
Figure 12. **(A) SEM image of the transversal cut of a porcupine quill (Erethizon).[22] (B) Photograph of a stomatopod. The arrow is pointing its club.[23]**

To make a plain cylinder lighter, one can remove the inner part and turn-it into a tube, but the resistance to bending and buckling is then dramatically decreased. Porcupine quills are filled with a closed-cell foam that maintains lightweight while enhancing the compressive strength (Figure 12A). Yang et al.[24] showed that when the foam is removed from the quills the critical buckling strength is divided by three and the Young's Modulus by two. This is a perfect example of how to minimize mechanical loss upon weight reduction.

The natural material with the highest impact resistance can probably be found in the dactyl clubs of the stomatopod "*Odontodactylus scyllarus*", a tropical shrimp (Figure 12B). It uses these weapons to smash its preys, sea shells or other shrimps, themselves protected by some damage tolerant armors. The architecture of these club described by Weaver et al.[23] combines an outer layer of high modulus, supported by a material whose hardness varies periodically. Their inner structure deflects and stops cracks while the hard outer layer minimize erosion. These clubs are so efficient that when kept in captivity, these shrimps break the glass of the aquarium.

From spider silk, a semi-crystalline elastomer with hard β-sheet linked with softer amorphous segments, to the strong and porous armor of lobsters that consist of an helical arrangement of chitin fibers, the diversity of biological composite is fascinating.[1, 25-28] A common concept in natural composites consist in the precise organization of hard blocks, providing the material with strength, with a soft matrix that prevents cracks propagation and improves the toughness. This concept finds

its best examples in nacre, bones, and wood, which respectively bring shape to mollusks, vertebrae and plants.

1.3.2   Structure and properties of nacre and bone

Nacre and bones are made of small anisotropic particles embedded in a flexible matrix. These two materials have a hierarchic structure that is optimized for toughness.[29-31]
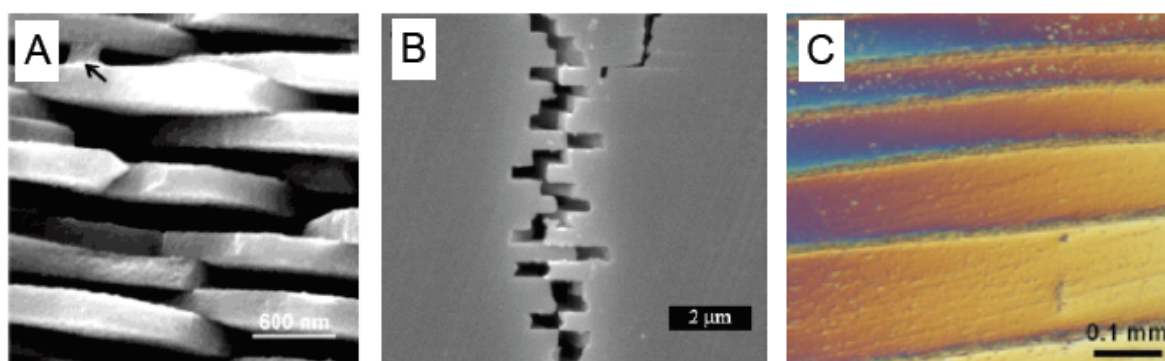
Figure 13. Hierarchical structure of red abalone shell: (A) SEM image showing the organization of calcium carbonate platelets of nacre. An arrow indicates the organic glue bridging them.[32] (B) SEM image of a fractured nacre. (C) Optical micrograph of intermediate meso-layers found in nacre.[33]

Red abalone shell, one of the most studied types of nacre has precise architecture that combines multiple toughening mechanisms. At the micro-scale (Figure 13A), nacre consists of a dense stack of calcium carbonate platelets hold together with organic glue and mineral bridges. The high content of hard inorganic platelets (over 90%) provides nacre with its high Young's modulus and strength. The size of the platelets and the resistance of the glue are such that when nacre starts to fracture, the inter-digitated platelets slide against each other instead of breaking (Figure 13B). In consequence, the material undergoes plastic deformation before fracture, which increases its toughness. At larger scale the meso-layers (Figure 13C) and the multiple platelet-glue interfaces deflect and hinder crack propagation enhancing further the energy needed to break this material. Other toughening mechanisms have been proposed such as interlocking of the platelets,[29] fracture of mineral bridges between platelets and friction associated to platelets roughness.[33] All these

mechanisms are probably contributing to the extreme fracture resistance of this material. Nacre is thousand times tougher than its components.[25]
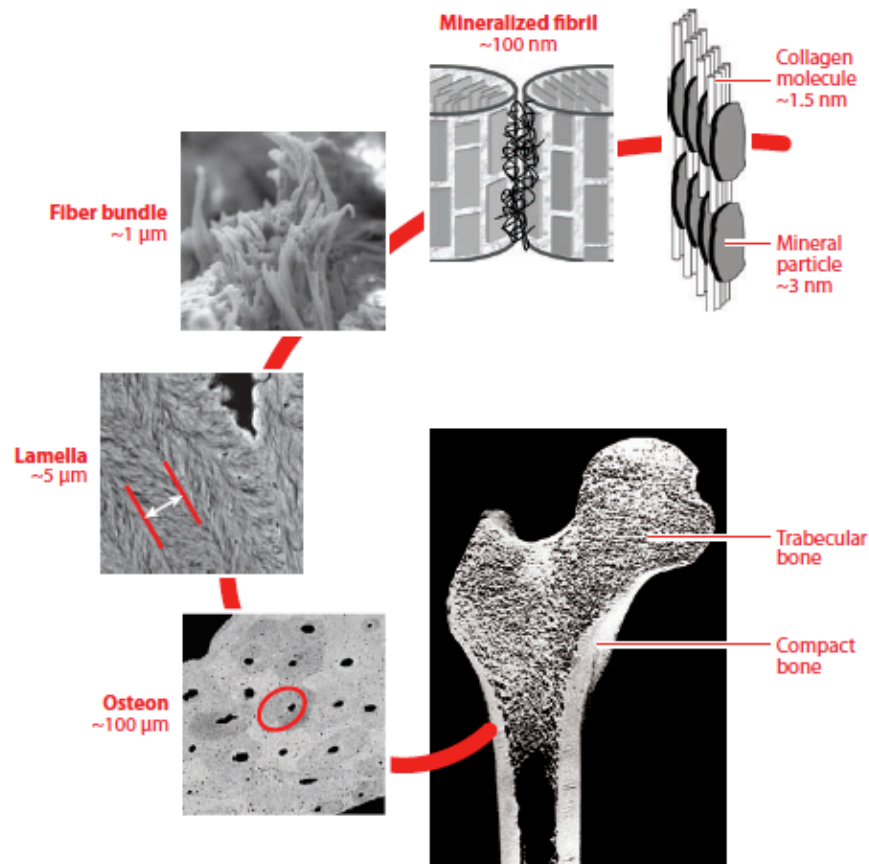
Figure 14. Hierarchical structure of bones.[1]

With a different organization, bone is built according to a similar principle, hard inorganic platelets embedded in a soft polymer matrix. In bone hard hydroxyapatite particles are stacked together with soft collagen (and some other biopolymers). These stacks are assembled in fibrils themselves grouped in bundles. While in nacre the lamellar structure is optimized to resist cracks and out of plane bending, the structure of bones is designed to resist more diverse solicitations such as compression and bending in multiple directions. The bone structure is overall isotropic but specifically reinforced at weak points. Osteons, for example, the holes through which blood brings nutriments to the marrow, create weak points in the structure of bones. These holes are surrounded by lamellae of fiber bundles that prevent crack formation and propagation.[34] This specific reinforcement of weaknesses maximizes the overall strength and shock resistance of bones. Since

each bone is designed to resist specific solicitations their structure is highly variable.

Several mechanisms have been reported to explain the strength and toughness of bone. The size of the inorganic platelets is small enough to be insensitive to flaws and to reach their maximal theoretical strength.[35] The different levels of organization lamellae, bundles and fibers improve crack deflexion by multiplying the interfaces[36] while crack bridging[37] and ductile deformation of collagen dissipate energy. Bones are also self-healing, stress induced micro cracks are continuously repaired preventing weakening of the structure with time.

The precise combination of hard anisotropic platelets and soft polymer brings to bones and nacre their strength and toughness. In wood a similar reinforcement is brought by strong cellulose fibers embedded in a softer polymeric matrix. If the basic principle is the same some specific reinforcement strategies have been developed in this fiber reinforced polymer-polymer nano-composite.

1.3.3 Structure and properties of wood

A large variety of mechanical properties exists in plants, soft tissues in fruits to flexible branches or rigid trunk. Surprisingly only four main components are found in the cell wall of these structures: cellulose, hemicellulose, lignin and pectin. Among these molecules, cellulose has the most interesting mechanical properties (Young's modulus above 100 Gpa and strength probably reaching 1 GPa), while hemicellulose, lignine and pectine behave like regular polymers (Young's modulus around 3 GPa and strength around 50 MPa). The variety of properties found in plants emerges from the organization and structure of their cell walls.[8]

Wood, a material used for thousands of years to build houses, boats and weapons, combines toughness, strength, and lightweight. These properties are still sought after in engineered composites. In the present section, we discuss how its structure controls its mechanical properties.
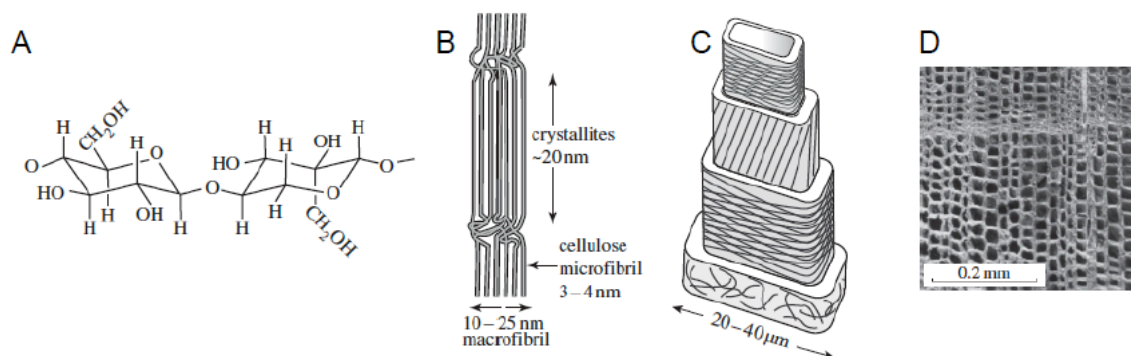
Figure 15. Hierarchical structure of wood. (A) Structure of cellulose. (B) Organisation of cellulose microfibrils in macrofibrils. (C) Structure of the wood cell wall with black lines representing the cellulose macrofibrils. (D) SEM image showing the cross section microstructure of cedar wood.[8]

Wood is mostly composed of cellulose (Figure 15A) that forms long micro-fibrils with alternating crystalline and amorphous parts. The fibrils have a thickness of 3-4 nm and a length that can reach several micrometers. The crystalline parts are composed of 25 chains of cellulose arranged in twisted structure with a diamond cross section.[38] These micro-fibrils form bundles (macro-fibrils) with a diameter around 20 nm (Figure 15B). The cell wall of wood consists of four concentric layers of macro-fibrils bound together by hemi-cellulose (Figure 15C). In each layer cellulose micro-fibrils have a defined organization, the external layer (primary layer) with randomly oriented fibers act as interface with neighboring cells, while the secondary layers (the three internal layers) represents up to 80% of the volume of the cell wall and is responsible for most of the structural properties.

Lichtenegger et al.[39] used micro X-ray diffraction to study the secondary layer. They were the first to prove that cellulose fibrils are oriented in a spiral around the wood cell. Variation of stiffness in the different parts of a tree have been linked to the angle that these fibrils do with the main axis of the wood cell.[2] Large angle leads to more flexible structure while lower angle bring stiffness and compressive strength. The fibers are tilted in young wood to bring flexibility and resistance to shocks and wind. On the contrary, the tilt decreases in older wood because strength and stiffness are required to hold the weight of the increasing number of leaves and branches.

Wood is an anisotropic structure. Wood cells are elongated structures aligned along the main direction of the trunk or branch (Figure 15D and Figure 6C). Cellulose fibers are globally aligned with the direction of the cells (they actually

form slightly tilted helices at the micro-scale). The consequences on the mechanical properties of wood are significant. The tensile strength of wood is up to four times higher along the grain of wood than across. When wood is loaded along the grain cellulose bears the stress providing strength, while across the grain the stress is transferred to the matrix, which breaks easily. For the same reason, woodcutters split wood along the grain direction; in this way cellulose fibers are spread apart while the weak matrix breaks. Splitting wood across the grain direction is difficult because it involves the rupture of many strong cellulose fibers. These properties match the natural function of wood, it needs to resist bending that exert longitudinal stress and compression but rarely stands loads across its structure. In addition the porous structure minimizes weight and allows the transport of water and nutriments. In fibrilar composites such as wood, the most important parameter besides strength and adhesion of the components is organization. The orientation of the reinforcing fibers defines the mechanical properties of the composite. In wood the strength is brought by the strong cellulose fibers while hemicellulose and lignin provide flexibility and toughness.

Wood, bones and nacre achieve superior strength through the precise assembly of hard objects embedded in a softer matrix. The hard objects reinforce the matrix and provide strength to the structure while the soft matrix prevents crack propagation and avoid dramatic failure of the material upon shocks or overloads. The application of such concept in engeneering composite could lead to materials with exceptional mechanical properties, but their conception is often challenging.

1.4   Bio-inspired materials

The preparation of engineering composites combining the intrinsic strength of man made materials with the structural efficiency of biologic composites is a promising topic. Such materials could find many applications where lightweight, strength and toughness are required. Many groups are currently trying to build composites with structures and properties close to those of nacre, bone or wood. Several efficient bio-inspired composites taking the best from natural and artificial design have emerged.

1.4.1   Nacre-inspired artificial structures

The mixture of ceramic nano or micro-particle with polymeric matrix is difficult. Phase separation often prevents proper mixing of the components, resulting in non-homogeneous material with low strength. The preparation of composites with micro and nanocharges is a big field of polymer research.[17, 40] However, in order to produce biomimetic structures close to those of nacre or bone one has to go further and control the orientation of the particles in the material.
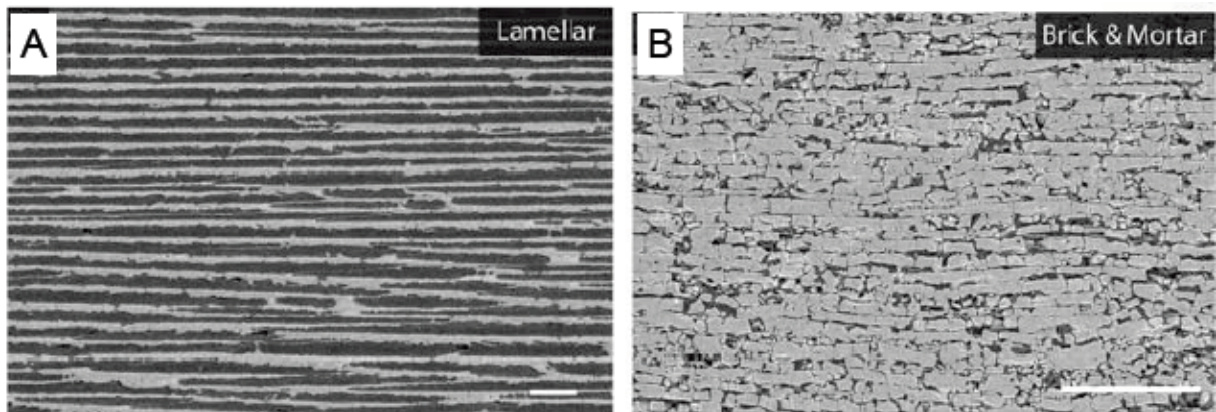
Figure 16. SEM images of biomimetic composites prepared by ice-templating: (A) Lamellar structure (B) Brick and mortar structure. Scale bars represents 100 µm.[41]

Munch and al.[41] used ice-templating to produce oriented ceramic scaffolds that were then impregnated with poly(methylmetacrylate). The structures created in this way (Figure 16) were up to 300 times tougher than their components. One of the key parameters for high mechanical properties was the compatibilisation of the ceramic scaffold with the polymeric matrix using surface grafting. This single step multiplied by two the toughness of the material synthesized. It also appeared that the brick and mortar structure were tougher than lamellar structures. This was explained in a more detailed fashion by Bonderer and al.[42] They developed a sheer-lag model that describes the transition between ductile and fragile fracture of nacre-inspired composites. If the reinforcing platelets have an aspect ratio (s) higher than a critical value (s_c) then they will break before the matrix, leading to a brittle fracture and a small toughness improvement of the material (Figure 17A). This is what happens in the lamellar composite described above. On the other hand if the aspect ratio is below the critical value, the matrix (or the interface) yield

first, leading to a ductile fracture and an enhancement of the toughness (Figure 17B).
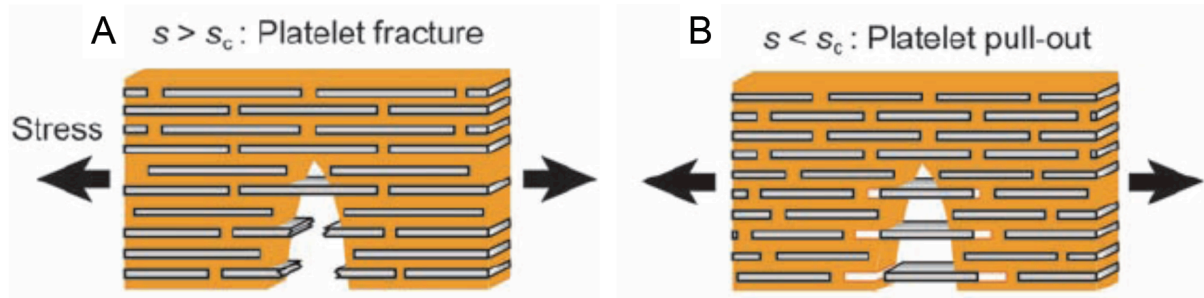
Figure 17. Schematic representation of failure modes in nacre-inspired nano-composites: brittle (A) and ductile (B) fractures.[42]

For strong polymer/platelets interfaces, the critical aspect ratio corresponds to the ratio of the tensile load that the platelets can handle before breaking to the yield shear strength of the matrix. If the interface polymer/platelets is the weakest point then the shear strength of the interface has to be taken into account instead of the yield shear strength of the matrix. This explains why grafting has a lower effect on the lamellar than on the brick and mortar structures previously described,[41] when the platelets fractures an increase of the interface strength has little effect, but its impact can be critical in an interface controlled pull out mode. Based on the principle described in their model they produced composites with strength up to 300 MPa and more than 15% of plastic deformation, which corresponds to a toughness one order of magnitude above those of nacre. They alternated spin-coating of chitosan solution and transfer of alumina platelet from the air-water interface (in a Langmuir-Blodgett like fashion) to produce these hybrid films.

To reach the complexity found in nature, one of the objectives of bio-mimicry is the production of composites with different orientations at different locations. Erb and al.[43] realized a major step in this direction, using a magnetic field to orientate platelets and rods decorated with super-paramagnetic particles.
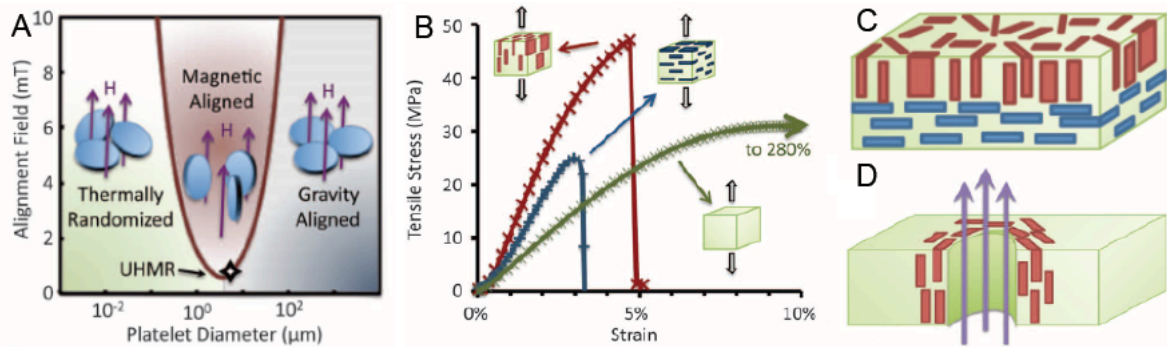
Figure 18. Alignment of inorganic platelets using a magnetic field.[43] (A) Relation between the platelet size and the magnetic field needed for alignment. UHMR stands for Ultra High Magnetic Response where the platelet size minimizes the required magnetic field. (B) Stress-stain tests on composites with various orientation. (C) Composite material with two layers of orthogonally oriented platelets. (D) Hole with reinforced edges, this structure mimics osteons in bones.

As magnetic field can be locally tuned in intensity and direction, this technique allows the production of complex organizations similar to those found in nature. One can for example mimic the reinforcement of osteons in bones[34] (Figure 18D and Figure 14) or reproduce structures found in some seashells with orthogonally oriented platelets that combine hardness with flexural strength (Figure 18C). This technique also enables the production of composites that undergo programmed deformation upon swelling.[44] However, composites prepared by magnetic alignment are not as strong as those prepared by step-wise spin-coating. Many other nacre- or bone-inspired composites have been described with various techniques and material: liquid crystal self assembly of graphene oxyde,[45] vacuum filtration of graphene with different crosslinkers,[46, 47] self-assembly of clay platlets and polyvinylalcohol,[48] step by step spin-coating and Langmuir Blodgett deposition of layered double oxides[49] and layer-by-layer assembly of clay or graphene.[5, 50, 51] The properties and preparation of layer-by-layer assembled nacre-inspired structures will be described later in chapter 2.3.

1.4.2 Wood-inspired artificial structures.

The production of wood inspired structures has been much less advertised than nacre or bones inspired structures. Often so-called wood-inspired structures are also wood-based structures, but most of the fiber micro and nano-composites owe more than they pretend to design principle found in wood.

Aerogels mimic the best wood structure; they have similar cellular structure and combine lightweight with mechanical resistance. Similarly to wood they gain mechanical resistance when their structure contains cellulose fibers.[52] The incorporation of 40% of microfibrillated cellulose in amylopectin aerogel leads to foam whose strength is more than twice that of pure amylopectin aerogel. In addition these materials are less sensitive to atmospheric humidity, making them excellent candidates for bio-based high technology applications.
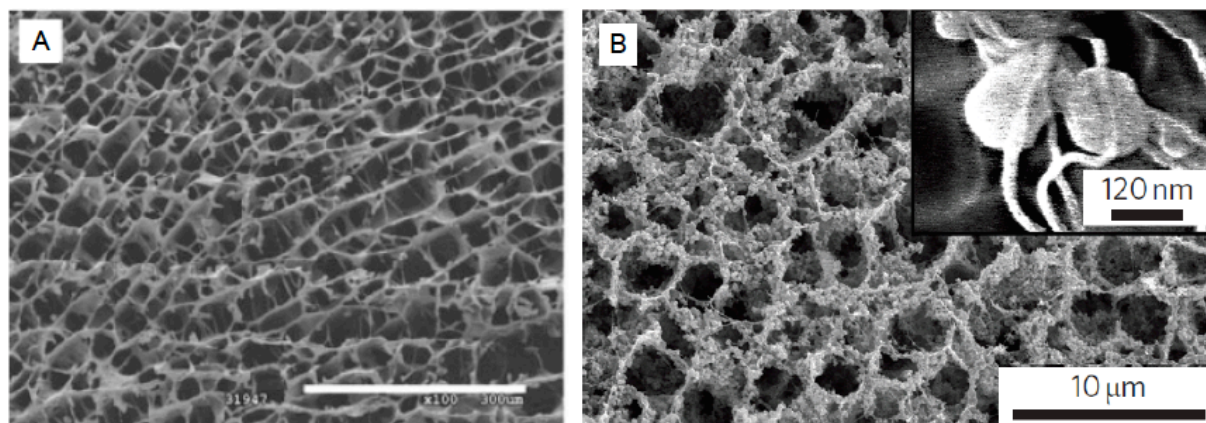
Figure 19. (A) SEM image of the cellular structure of amylopectin aerogel reinforced with 40% of microfibrillated cellulose. Scale bar is 300 µm.[52] (B) SEM image of a microfibrillated cellulose aerogel decorated with cobalt-ferrite nano-particles. Inset: close-up on the nano-particles.[53]

The lack of magnetic or electric properties needed for engineering applications is a recurrent problem in bio-based material. Olsson et al.[53] reported a technique to overcome this problem. Their aerogel (Figure 19B), prepared through precipitation of cobalt-ferrite nano-particles onto previously made cellulose aerogels, can stand deformations up to 80%, absorb 16 times its weight in water and react to magnetic solicitation. They also compressed this aerogels into a strong nano-paper (Young's modulus of 3 GPa) that could be manipulated with magnets. This technique is a key step toward the combination of mechanical strength found in natural materials with exotic man-made properties. Similarly, Agarwal et al.[54] coated cellulose micro-fibers with PDOT-PSS to produce an electrically conductive paper.

The production of strong and tough materials that mimic the structure of wood-cell wall also attracted a lot of interest. Henriksson et al.[7] showed that it was possible to prepare microfibrilated cellulose-based films (so called nanopaper Figure 20) with a strength over 200 MPa and a Young's Modulus up to 13 GPa using vacuum filtration. Their work outlines the importance of a high degree of polymerization of

the cellulose microfibers to improve the toughness and low porosity to maximize the strength and the Young's modulus. A later work[55] showed that a polishing step could make these nanopapers transparent without altering their mechanical properties (Figure 20B).
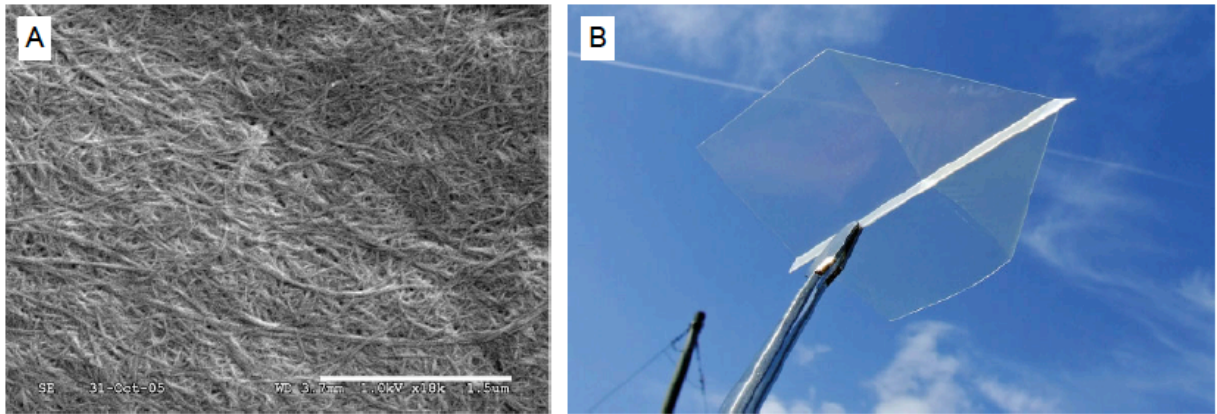
Figure 20. Microfibrillated cellulose-based nanopaper. (A) SEM image of nanopaper prepared by vacuum-filtration.[7] (B) Photograph of a transparent nanopaper.[55]

Structures even closer to wood cell-wall have been prepared by mixing microfibrillated cellulose with hemi-cellulose, another polymer present in wood, using a papermaking technique.[56] These nano-composites have thoughness nearly one order of magnitude higher than bones. The combination of cellulose nanofiber with a softer amylopectine/glycerol matrix in different proportion yield composites with a Young's modulus going from 2 to 13000 MPa.[57] The alignment of microfibrillated cellulose, found in the cell-wall of wood, can be reproduced by drawing wet microfibrillated cellulose gels obtained by filtration.[58] After drying nanopapers made in this way reached strength as high as 400 MPa and a Young's modulus of 33 GPa. The fabrication of hybrid structures that would combine the strength of cellulose with the structure of nacre is also a promising topic.[59-61] Several groups combined cellulose nano-fibers with clay particles to prepare strong films (strength up to 400 MPa[61]), fire retardant coatings[59, 60] and oxygen barrier films.[60, 61]

In nano-composites many strengthening processes can be linked to biological features. Common reinforcing steps in nano-engineering consist in the creation of covalent, electrostatic or hydrogen bonds between nano-particles. This reminds the borate bridges found between the cell-walls of plants.[47] Bridging single wall carbon

nanotubes (Figure 21B) in bundles using an electron beam leads to a 30-fold increase of the bending modulus of such bundles.[62] In a similar way, borate bridges between graphene oxyde layers multiplied by more than two the Young's modulus of graphene oxyde paper obtained by filtration.[47]
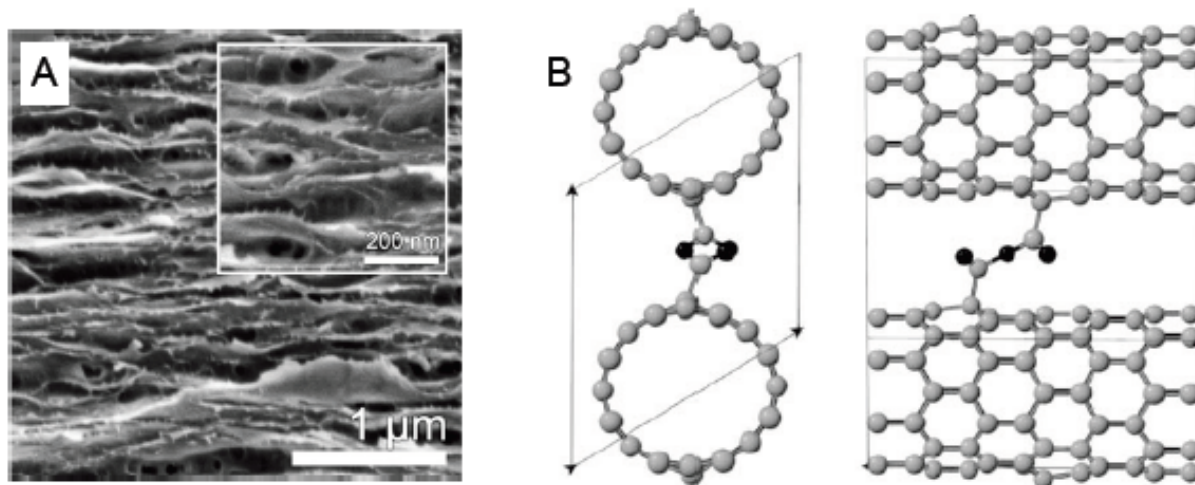
Figure 21. (A) Nacre-inspired architecture based on cellulose nanofibrils.[61]
(B) Bridged cabone nanotubes in bundles with high

To conclude this chapter, Coleman et al.[63] give in their highly cited review the guidelines for the efficient reinforcement of polymer using carbon nanotubes: "These are a large aspect ratio, good dispersion, alignment, and interfacial stress transfer". The reinforcement of cell wall by cellulose fibers illustrates perfectly these rules. Taking lessons from nature or not, improvement of nano-composites efficiency will certainly makes them look closer and closer to biological materials.

2   Multilayer thin films

Multilayered films where hard anisotropic objects (platelets or fibers) are combined with a softer polymer are promising model to understand and optimize the structure-property relationship in bio-inspired composites.[42] The key challenge is the production of macroscopic multilayers with a nano-scale control over their structure and composition.

2.1   Nano-structured materials

The fabrication of nano-structures is an expanding field of material research. This section aims to give overview of current approaches; given the number of experimental procedures developed and in order to maintain a reasonable length this section is not exhaustive.

2.1.1   Top-down versus bottom-up

The techniques to produce nanostructured materials can be split in two groups: top-down and bottom-up approaches. The first group consists of methods where bulk macroscopic materials are shaped with precision tools into nano-structured objects. In the second group, molecules and nano-elements are combined into larger nano-structured objects (Figure 22).

The top-down approaches rely on the controlled physical transformation of a material. For example photolithography relies on light to produce micro-patterns (and sub micro-paterns) on a flat surface. A photosensitive polymer film covered

with a mask is exposed to light. The parts exposed to light crosslink while the protected areas stay unmodified. The pattern is then revealed by dipping into a solvent where only the cross-linked parts remain on the surface.[64] Even if this technique is widely used in micro-fabrication, light diffraction prevents the production of nanometric features. Electron lithography was developed later to reduce diffraction and produce nano-patterns.[65] Recently other techniques have also been developed such as dip-pen lithography that uses a water meniscus formed between an AFM tip and a surface to write with thiols on gold.[66] Soft lithography uses stamps made of polydimetylsiloxane to print on surfaces with polymers, small molecules, colloids or biologic molecules.[67] While all these methods are limited to 2D surfaces, techniques such as two photon lithography or holographic lithography allows to produce three dimensional structures.[68] Top-down techniques can produce structures of almost any shape and the amount of defects is usually low. Their use is however limited by the time needed to prepare the structures, and the difficulty to scale up.
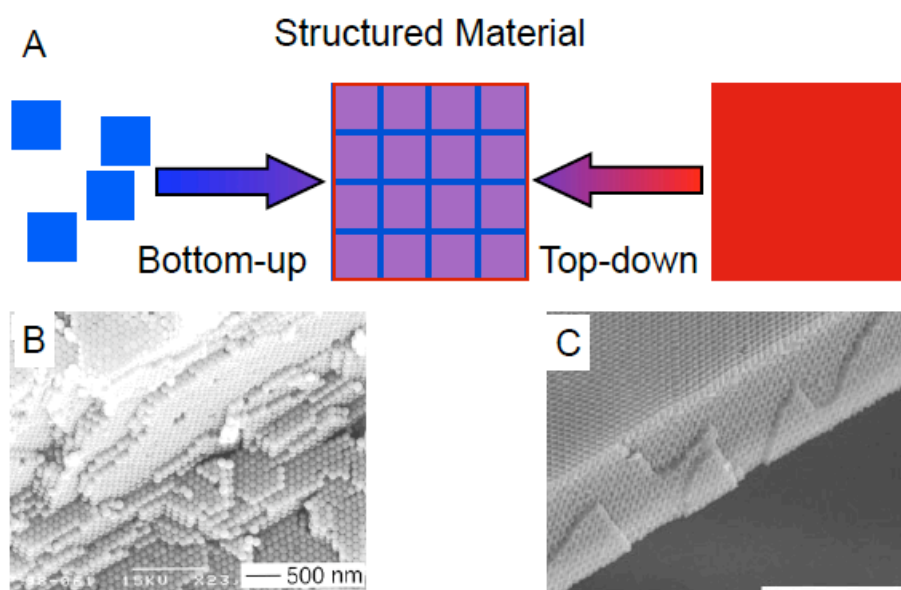
Figure 22. Bottom-up versus top-down approaches. (A) Schematic representation of the two ways toward nanostructured materials. (B) SEM image of a photonic crystal of silica spheres assembled through a bottom-up approach.[69] (C) SEM image of a photonic crystal obtained by holographic lithography, a top-down technique. Scale bar is 10 µm.[70]

Bottom-up techniques use physico-chemical phenomena to combine elementary bricks such as surfactants, polymers or colloids into structured materials. Such techniques are closer to the way biological material are formed.

Many of these techniques have been developed to produce regular nano-structures. For example at high concentration surfactants form highly organized liquid crystal structures. In combination with sol-gel chemistry it is possible to replicate this organization and create mesoporous ceramics.[71] The surfactants can be replaced by blockcopolymers[72, 73] and many kind of metal oxides can be shaped using this technique. Such structures have applications in the fields of heterogeneous catalysis and as molecular sieves for example. Colloidal crystals are another kind of promising structured material for photonic applications. They consist in the 3D organization of colloidal spheres into regular lattice to produces sharp structural colors. Several bottom-up assembly procedures have been reported: sedimentation under a gravitational field, evaporation in the presence of electrostatic repulsion or physical confinement.[74] Such structure find many applications in the domain of photonics. A last example of bottom-up shaping is DNA origami. It has emerged with the recent progress of DNA synthesis and better understanding of DNA folding mechanisms. By using numeric simulation it is possible to engeneer DNA molecule that will spontaneously fold in a given shape due to weak-interactions.[75-77] Molecular self-assembly into nanostructures is not limited to DNA. Supramolecular chemistry also looks at the design of molecules that self-assemble in complex structures.[78, 79] The dynamic and reversible properties of such complex structures could find many applications from drug release in medicine to smart electronics.

The typical structuration size is smaller with bottom-up than top-down techniques (Figure 22B and C) but the equilibrium process at the origin of their structure limits the number of architecture possible. Their main advantages compare to Bottom-up techniques is that they can be easily scaled-up.

Due to their similarity to biological process and ability to produce material on large-scale, bottom-up techniques seem more adapted to the production of bio-inspired structural materials. We have seen in the previous chapter that wood, nacre and bones gain their properties from lamellar arrangement of polymers and ceramics. In the next section we will focus on the bottom-up assembly of thin films that can combine ceramic and polymeric materials.

2.1.2   Surface assisted production of thin films

In order to produce well-organized thin films with a long-range order a support is needed. The surface of the support serves as a template for the macro and micro organization, while physico-chemical interactions are governing the nano-structuration. Atomic layer deposition is widely used for the preparation of thin-films of controlled thickness on surfaces (Figure 23A).[80, 81] It relies on reaction at an interface of gaseous species. Due to the finite number of reactive sites on the surface, the deposition is self-limiting. The sequential atomic layer deposition of co-reactive species allows the preparation of multilayers following the surface morphology. It is possible to prepare ceramic and polymer films but only from monomeric precursors. Indeed, the direct deposition of colloids or polymers is impossible because they cannot be vaporized.
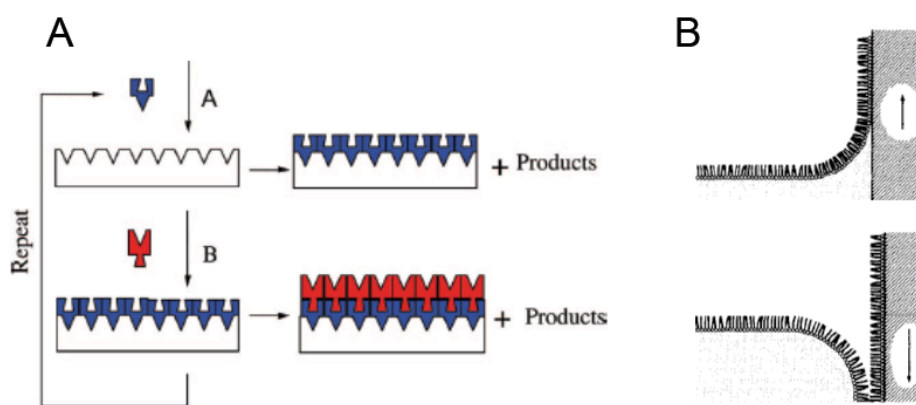
**Figure 23. (A) Schematic representation of the atomic layer deposition.[80]
(B) Schematic representation of the Langmuir-Blodgett technique.[85]**

Colloids or polymer thin films can be prepared by dip-coating, spin-coating or vacuum filtration. These methods are relatively fast and require limited amount of equipments. However the preparation of hybrid nano-materials combining polymers and colloids may face problems of phase separation. In addition these single-step process provide limited control of the organization at the nano-level. The controlled preparation of nano-structured multilayers requires multistep process; this slows down the construction but increase significantly the architecture control. Since several decades, multilayers with precise architecture[82] have been prepared via the so-called Langmuir-Blodgett (LB) method. Discovered by I. Langmuir[83] and further developed by K. Blodgett[84] this technique relies on the

transfer of amphiphilic molecules from the air water interface onto a solid substrate (Figure 23B).

The LB technique is compatible with a limited range of building blocks, the substrate needs to be flat and its size is limited by the size of the trough. In the early nineties Decher and co-workers[86] discovered that oppositely charged macromolecules could be sequentially adsorbed on the surface of solids through electrostatic interactions. Later called layer-by-layer (LbL) assembly, this technique compatible with almost any kind of molecules (colloids, polymers, proteins,...) quickly became a powerful tool for the production of nano-structured multilayers.[4]

2.2   Layer-by-layer assembly

Layer-by-layer (LbL) assembly is a bottom-up approach that leads to nano-organized films. Since its discovery in the nineties,[87] it has kindled widespread interest in the preparation of nano-structured multilayers due to the fact that it combines experimental ease with low cost fabrication and environmental friendliness. This section will provide some background about its principle, parameters and applications.

2.2.1   Principle of the LbL technique

The first reports about electrostatic driven assembly at interfaces was done by R. Iler[88] who sequentially adsorbed oppositely charged colloids on glass slide. These results were overlooked and forgotten for over 20 years[87] before the discovery and development of layer-by-layer assembly by G. Decher.[4]

A simplified notion of the construction of polyelectrolyte multilayers requires two solutions of oppositely charged polyelectrolytes (a polyanion and a polycation) and a solid substrate presenting a surface charge. When a positively charged substrate is dipped into a solution of polyanion, electrostatic attraction causes the polyelectrolyte chains to stick to the substrate leading to a reversal of the surface charge. This adsorption step is self-limiting because once the surface is covered with the polyanion its negative charges exert a repulsive interaction on the chains remaining in solution. The surface is then rinsed to remove the excess of polyanion and the weakly attached chains and dried. A subsequent dipping into a solution of

polycation causes a new adsorption step that corresponds to the complexation of the polycation in solution with the previously adsorbed polyanion. The surface charge of the substrates is reversed and becomes positive. The last rinsing and drying steps complete the process that can be reiterated as many times as necessary to produce a multilayered film (Figure 24).
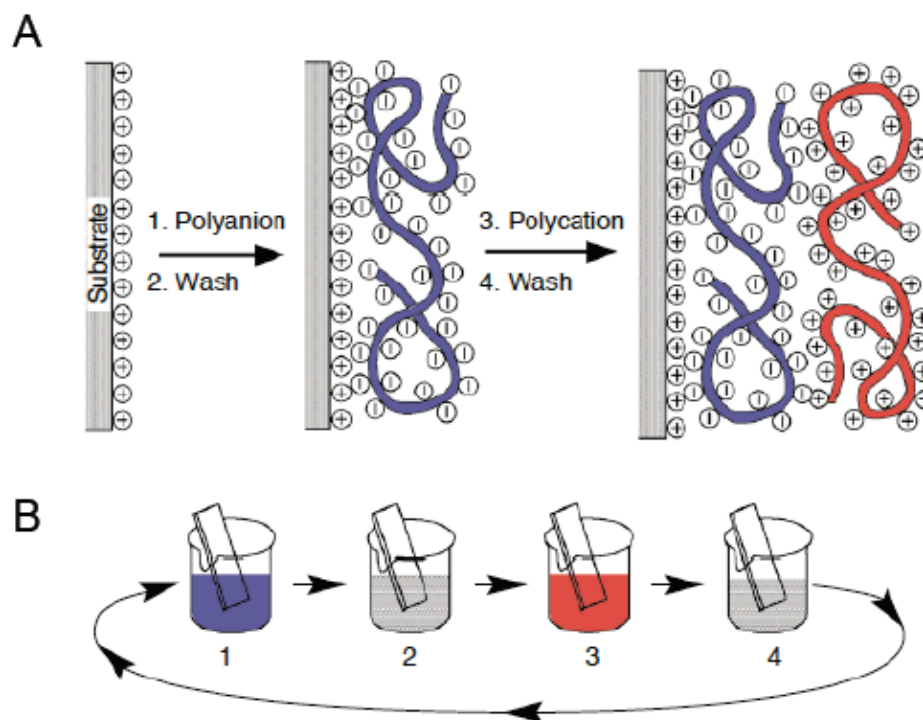
Figure 24. Principle of the layer-by-layer assembly technique. (A) Schematic representation of the alternate adsorption of a polyanion and a polycation on a positively charged substrate. Counter-ions and layer interpenetration are omitted for clarity. (B) Schematic representation of the deposition process.[4]

Several non-trivial physico-chemical phenomena are hiding behind this simplified description. The charge reversal at each adsorption step originates from polyelectrolyte chains that are only partially bounded to the surface. Since polyelectrolytes are large molecules some parts of the chains can remain free even if the rest of the chain is strongly bound to the substrate. The excess of charged groups unbalanced by surface charge are responsible for the charge reversal upon adsorption and allow the deposition of the next layer. The redissolution of the polyelectrolyte complex, which is thermodynamically favorable during the rinsing step, is kinetically frozen by the multiple electrostatic bridges between the polyelectrolyte chains. High temperature (increasing the thermal energy) or high

salt concentration (decrease of electrostatic interaction) could result in redissolution of the film. The organization in the film is not as perfect as represented in Figure 24. Neutron reflectometry studies showed that the film is definitely layered but that each layer is interpenetrated with its neighbors. It was only possible to observe separate layers of deuterated polymers when they were separated by at least three layers of non-deuterated polymers.[4]

In this section, we have discussed the build-up principle of polyelectrolyte multilayers. We will now see how it is possible to tune their growth.

2.2.2   Control of the LbL build-up

The composition and architecture of layer-by-layer assembled films is primarily controlled by the choice of component and deposition sequence. In the absence of diffusion the absorption of a layer of polyelectrolyte depends on its charge and on the charge of the underlayer. In consequence the growth of layer-by-layer assembled film is proportional to the number of deposition step as soon as the influence of the substrate is neglectible (typically after 2-3 layer pairs).[4] This type of build-up is called linear growth and the thickness of the multilayer is defined by the number of repeating cycles. The design of more complex architecture is possible using combination of polyelectrolyte couples. For example with two polyanions A,B and two polycation C,D it is possible to build many architectures: a repeating quadrilayer $[ACBD]_n$, two superposed multilayers $[AC]_n[BD]_m$ or any imaginable variations as long as the alternation of polycation and polyanion is respected. This is a simple and robust way to define and control the structure of a multilayer. The adsorption of each layer is itself controlled by some physico-chemical parameters. Modifying these parameters is another way to control the layer-by-layer assembly.

Polyelectrolytes are sensible to the ionic strength of the solution. At low salt concentration there is a low screening of the charge and the polymer chain is stretched, while as the salt concentration increases the polymer chain approaches more and more a coiled conformation (Figure 25A). During the layer-by-layer assembly the salt also screens the interactions between the substrate and the polymers in solution. Increasing the ionic strength of the polyelectrolyte solutions increases the thickness of each layer deposited and therefore reduce the time necessary to build a multilayer of a given thickness (Figure 25B).[89] Such increase

of the ionic strength also leads to films with more rough surfaces.[90] Ionic strength is one of the major parameters in the growth control during layer-by-layer assembly.
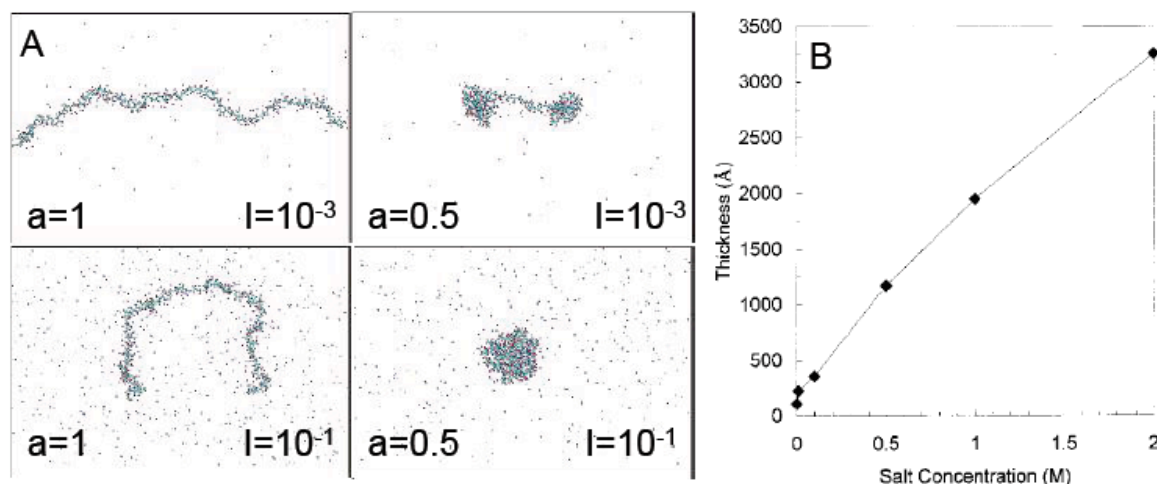
Figure 25. (A) Simulations results of the effect of ionic strength, I, and degree of dissociation, a, on the conformation of polyacrylic acid.[91] (B) Thickness of a film consisting of ten layer pairs of PSS/PDDA built from solutions at various salt (NaCl) concentrations.[89]

When working with weak polyelectrolytes the pH of the solution deposited also plays an important role. The pH of the solution determines the degree of dissociation of the polyelectrolyte that has an effect on the number of charges per molecule and on the shape of the polyelectrolyte in solution (Figure 25A). The consequences of pH modification on the film growth have been studied in several papers.[92-94] In general as the degree of ionization of a polyelectrolyte decreases its incorporation in a polyelectrolyte multilayer increases. Stoichiometry of the polyelectrolyte complexes can explain this effect; when the charge of one of the polymer decreases more molecules are needed to compensate the charge of the underlayer. The detailed effects of the pH on the growth of multilayers are probably more complex, especially when working with two weak polyelectrolyte solutions at different pH.[95]

Deposition time has also an influence on the thickness of each layer.[89] As the deposition time increase the thickness of each layer increase up to a "plateau" corresponding to a complete surface coverage. The deposition time should be long enough to reach this plateau similarly rinsing step should be long enough to ensure desorption of all weakly attached molecules. Short deposition time or insufficient rinsing leads to results hard to reproduce and films with poor quality.[87]
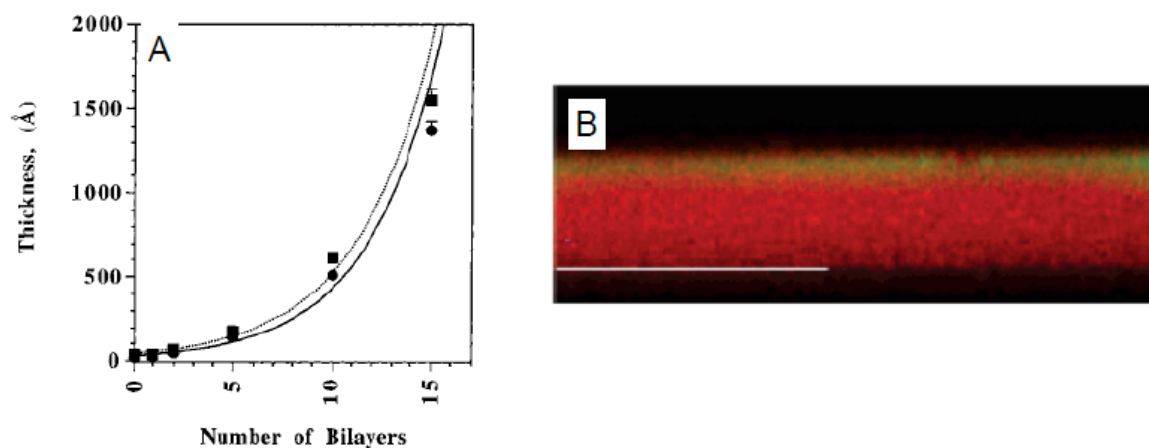
Figure 26. (A) Thickness increase as a function of layer pairs for multilayers consisting of polylysine and alginate followed by ellipsometry.[96] (B) Confocal Laser Scanning microscopy image showing the diffusion behavior of two labeled polylysine with different molecular weight deposited on top of a film of hyaluronic acid and polylysine. The polylysine in red has a molecular weight of 55.000 g/mol, while in green it has a molecular weight of 360.000 g/mol.[97]

In some case the thickness increment for each layer increases with the number of layer pairs (Figure 26). The first reports concerned bio-based polyelectrolytes such as alginate, polylysine or hyaluronic acid,[96, 98] but some synthetic polyelectrolytes have similar behavior.[99] Several experiments looking at the effect of temperature,[99] polyelectrolyte mixtures[100] and molecular weight[97] allowed to clarify its mechanism. Such behavior is related to the diffusion of at least one of the polyelectrolytes in the film (Figure 26B). The polyelectrolyte is stored in the film (that acts as a reservoir) during its deposition and dipping in the complementary polyelectrolyte solution extracts the excess of charges stored in the film, leading to the formation of a thick layer at the surface. The thicker the film is, the more polyelectrolyte can be stored inside and the more polyelectrolyte is deposited at each step. In consequence the speed of growth increases with the number of layer pairs, this type of build up is referred as exponential or super-linear. While linearly growing films have a defined layered structure, films growing super-linearly (or exponentially) are closer to isotropic polyelectrolyte complex. The film growth typically becomes linear after a certain number of layers in consequence the term super-linear is preferred over exponential. This transition is linked to the diffusion speed of the polyelectrolyte in the film. At some point the deposition time is too short compare to the diffusion speed of the polyelectrolyte and the polymer is only stored in the upper region of

the film. Consequently the amount of polyelectrolyte deposited at each step stops increasing and the growth become linear. However, the thickness increase at each step is still higher than for classic linear growth.

Up to now we have explained the growth mechanisms and the factors influencing LbL assembly based on polyelectrolytes. While the mechanisms remain similar the LbL technique is however not limited to polyelectrolytes. In the next part we will see examples of the many other possible building blocks.

2.2.3 Diversity of building blocks and control of the super structure.

Originally developed from polyelectrolytes and bipolar-amphiphile building blocks[86] the layer-by-layer assembly technique has quickly evolved to many other building blocks. Almost any colloid such as silica particles,[88] clays,[101] semiconductor particles[102] or gold[103] can be incorporated in multilayers. This is extremely useful for the preparation of bio-inspired composite combining nano-objects and polymers.
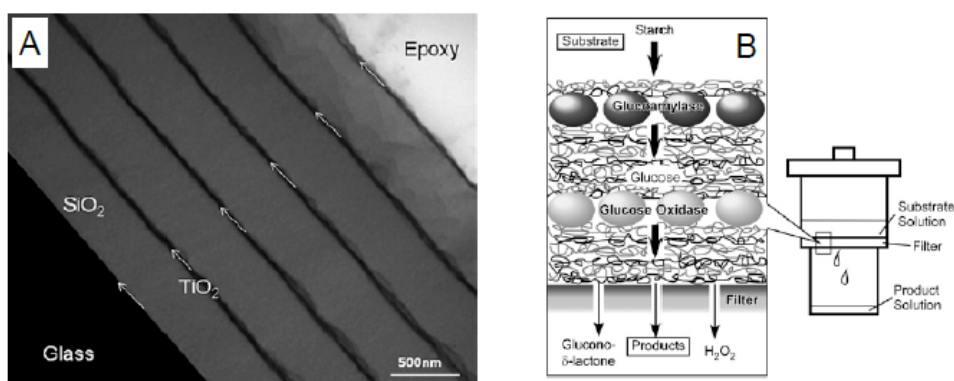
Figure 27. Examples of multilayered architectures produced using LbL assembly. (A) Bragg mirror by combining TiO$_2$ and SiO$_2$ nanoparticles.[106] (B) Sequential transformation of starch in glucose and glucolactone throught a nanoreactor composed of a LbL film containing active enzymes.[107]

It has also been shown that DNA,[104] protein[104] or viruses[105] could be introduced in layer-by-layer assembled films. The possibility to introduce such a variety of components in a single multilayer made this technique popular to study and tune the interaction between surfaces and living organisms. The great strength of layer-

by-layer assembly is that all these features can be mixed and organized at will in the films simply by choosing the deposition sequence.

One can for example mix compounds of high and low refractive index in a well ordered stack to create Bragg mirrors which reflect selective wavelength bands (Figure 27A).[106] Another beautiful example is the assembly of glucose oxydase and glucose amylase in a layered structure on top of a nanofiltration membrane, acting as a nanoreactor. When starch passed throught the supported film it is first hydrolyzed by glucose amylase in glucose which is then converted in gluconolactone and hydrogen peroxide by glucose oxydase in a second step (Figure 27B).[107] The Right enzyme sequence in the film is required to convert starch into the desired products. We have seen that LbL assembly allowed to build thin films with a precise architecture and tunable composition. We will now look at the type of substrates that are compatible.

2.2.4   Diversity of supports

In the laboratory monitoring the layer-by-layer assembly process by conventional characterization techniques (ellipsometry, UV-visible spectroscopy, …) requires the use of specific surfaces (silicon wafers, quartz slides, …) that are most of the time not compatible with final applications. However, a huge advantage of the LbL-approach is that films deposited on different surfaces can be astonishingly similar if prepared at identical deposition conditions. The nature of the support has an influence on the construction of the first layers but typically after two-tree layer pairs the growth of the film only depends on the nature of the building blocks and on the deposition conditions.[108] One can therefore study the construction of the multilayer on model surfaces and then build the multilayer on the desired surface. For example the team of Grunlan efficiently produced fire retardant cotton fabrics by coating textiles with LbL-films made of clays and polyelectrolytes (Figure 28A).[109]
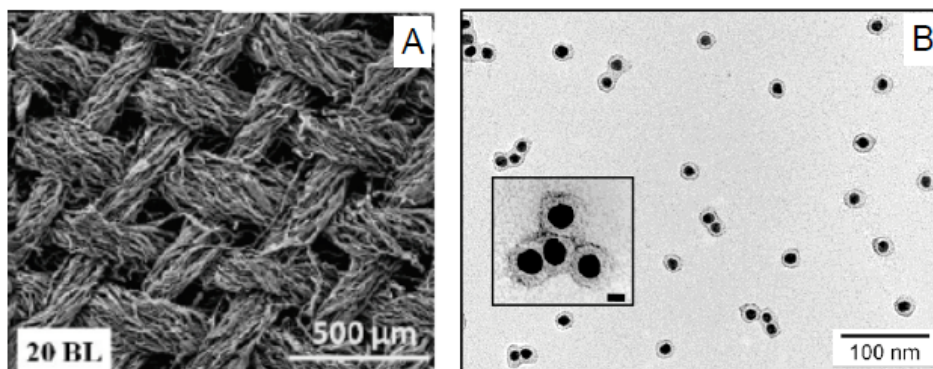
Figure 28. Layer-by-layer assembled films on non-conventionnal substrates. (A) Residues of a cotton fabric coated with montmorillonite after calcinations.[109] (B) 13 nm gold colloids coated with a LbL-film.[110]

The construction of multilayers on irregular surfaces such as fabric (Figure 28A) or micro-channels closely follows the conformation of the substrate.[111] It is even possible to coat microspheres[112] and gold nano-particles (diameter 13 nm) using the LbL technology (Figure 28B).[110]

Layer-by-layer assembly can coat substrates of almost every shape and every size. But the process is time consuming which can be an issue for application purpose and scaling-up.

2.2.5   Speeding-up the layer-by-layer assembly

Layer-by-layer assembly allows the construction of thin films with controlled composition and structure on almost any substrate. However there is an issue with the time required for the film production, the deposition of a single layer by dipping takes from few minutes to hours, which has to be multiplied by the number of layers required for the film production. Shortening the deposition time would allow broader applications and industrial developments. The deposition time is fixed by the free diffusion of species in solution. To reach the adsorption plateau all polyelectrolytes (or colloids) need to diffuse from the bulk to the surface, which requires time. As already mentioned, too short adsorption times result in films of poor quality and hardly reproducible results. In order to decrease the deposition time without giving-up film quality two techniques have been developed: spray-assisted assembly[113] and spin-assisted deposition.[114, 115] Both of these techniques are reducing the diffusion time by increasing the agitation at the solid liquid interface which reduces the time needed for the species to reach the surface.
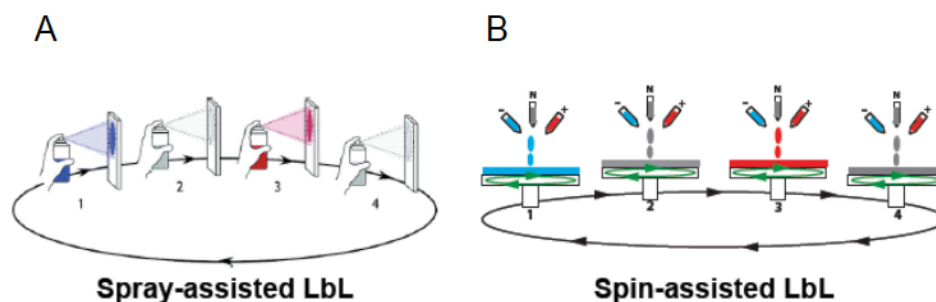
Figure 29. Techniques used for speeding-up the preparation of multilayered thin films. (A) Spray-assisted deposition. (B) Spin assisted deposition.

Spray-assisted deposition consists in the alternated projection of micron-sized droplets of cationic, rinsing, anionic, and rinsing solutions on the substrate (Figure 29B). The liquid at the interface is constantly renewed by the vertical drainage of the solution and the agitation is assured by the random shear forces exerted by the droplets on the liquid film at the surface. Spin-assisted deposition is based on the alternated dropping of the different solutions at the center of a rotating substrate (Figure 29C). In this case, centrifugal force created by the rotating substrate drain the solutions away from the substrate and allows agitation and renewal of the solution at the interface. In both cases the time needed for adsorption of the species and desorption of weakly attached ones are considerably decreased. Only few seconds are needed to prepare a layer pair with each of these techniques, which is over a hundred times faster than dipping.

They also allow to coat large surfaces with low amounts of solutions. Spray-assisted assembly in particular could find industrial application to coat large objects such as cars or window at a reasonable cost. These three deposition techniques have been compared with each other in term of speed of growth and homogeneity of the films.[115, 116] It appears that spin-assisted deposition generally leads to thicker films than dipping which itself produce thicker films than spray-assisted assembly. Both spray and spin assisted methods appeared to lead to smoother films than dipping especially at low deposition times. The dipping method is still widely used for the preparation of multilayer films because it requires little specific equipments and depends on few defined parameters. While spray and spin assisted assembly are good candidates for the preparation of exotic films[117] and for industrial applications.[118]

Layer-by-layer assembly provides a nano-scale control over the structure and composition of multilayers. As such it is a promising technique to assemble nano-composites whose nanostructure mimic that of biological materials.

2.3   Nacre-like multilayers

The production of hybrid nano-composites with layered structure mimicking that of nacre or bones is a promising field of material science. In this part we will discuss contribution of layer-by-layer assembly to the preparation of these nano-composite and focus on the link between structure and properties.

Most nacre-inspired multilayers are based on clays. We will first look at the structure and property of these nano-platelets before discussing their incorporation in LbL assembly finis with the properties of these architectures.

2.3.1   Structure and solution behavior of clays

This chapter is mostly based on chapters of the Handbook of Clay Science.[119]

Clays are naturally occurring materials that have been used by men for millennia to build bricks and pottery. Many types of clays exist: smectites, kaolinites, sepiolites or illites. Montmorillonite (the main component of bentonites) the most widely used type of clay for polymer reinforcement is an alumino-silicate belonging to the smectite group (Figure 30A). Montmorillonite consists of an octahedral layer of aluminum oxide sandwiched between two tetrahedral layers of silicon-oxide (Figure 30C and D). These sandwiches form large platelet-like monocrystals with a constant thickness of 1.1 nm and a diameter between 50 and 1000 nm. The thickness of the platelet is fixed by the structure but the shape is variable and irregular. In their naturally occurring form the platelets are stacked in large piles (Figure 30B) through interactions with cations.

Substitution of aluminum atoms by magnesium atoms in the octahedral layer, or silicon atoms by aluminum atoms in the tetrahedral layer creates a net negative charge in the crystal. This charge is balanced by the presence of counter ions in the interlayer gallery typically sodium or calcium. Because montmorillonites are natural materials their exact composition differs from one batch to another. In the

rest of the thesis the term clay will refer to montmorillonite unless it is mentioned otherwise.
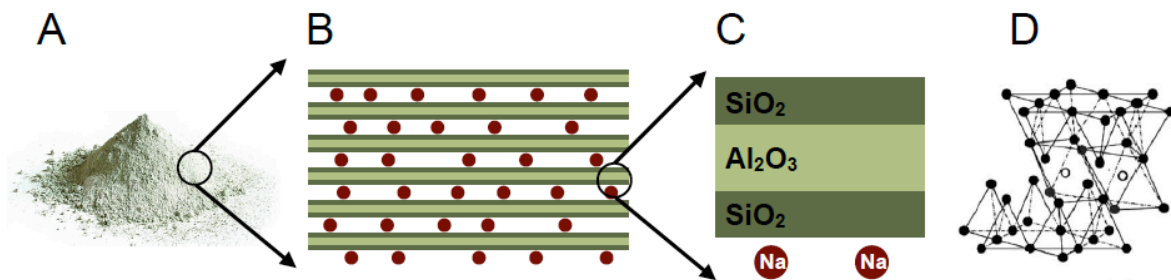
Figure 30. Structure of montmorillonite. The rocks extracted from the mine can be crushed into a thin powder (A) that is composed of stacks (B) clay crystals (C). Crystallographic structure of a clay with oxygen in black and aluminum in white, silicon atoms are not represented.[120]

Water can enter the interlayer gallery, solubilize the ions and separate the individual clay sheets. This process called exfoliation is easier with sodium montmorillonite than with the calcium ones because the bridging between platelets is weaker. Sodium ions are monovalent while calcium ions are bivalent that makes the electrostatic interaction between the counter-ions stronger with calcium than sodium ions. Since naturally occurring montmorillonite presents sodium and calcium ions in the interlayer gallery it is usually necessary to substitute calcium by sodium in order to ensure proper exfoliation. The preparation of clay suspension is done in pure water under agitation; the exfoliation process can take several days. The stability of clay suspension comes from the repulsive interactions between negatively charged clay platelets; it depends on the ionic strength and on the pH of the solution. The addition of salt in the solution screens the repulsive interactions between platelets and causes flocculation as for most colloidal suspensions. Clay suspensions are also unstable at low pH due to the presence of free OH groups on the edge of the clays where the crystalline network finishes. Below a pH of six, these OH groups are protonated and the edges of the clays become positively charged. Since the rest of the clay platelets stays negatively charged they tend to precipitate in a "card house" fashion with edges-surface in contact. Even after agitation for several days clay suspensions can remain turbid because of impurities and unexfoliated particles. A step of sedimentation or centrifugation is then necessary to produce a clear suspension consisting only of exfoliated particles.

The preparation of clear and stable montmorillonite suspensions is necessary to control their incorporation in layer-by-layer assemblies and optimize the properties of such multilayers.

2.3.2   Building films containing clays

Clay platelets bear a net negative charge which makes possible their incorporation in layer-by-layer assembled films. Early after the discovery of LbL, Kleinfeld et al.[101] showed that it was possible to build films of hectorite, a syntetic clay, and permanently charged polycation Poly(diallyldimethylammonium chloride) with a well structured architecture. Later Kotov et al. showed that it was also possible to build films using montmorillonite.[121] Clay containing multilayer prepared by LbL assembly present a high structural order compare to film prepared using other techniques. Minimizing the enthalpy of the system during assembly implies to maximize the interactions between the negative charges on the platelets and the positive charges of the polyelectrolytes. In consequece the clay particles are laying flat on a surface covered with polycation. The multilayers obtained by LbL assembly are so well organized that it is possible to see X-Ray diffraction patterns between the different layers deposited (Figure 31A). The organization of the platelets in the film is also visible on the TEM micrograph (Figure 31B) where the wrinkle, due to the sample preparation, helps to visualize the layered structure of the platelet reinforced multilayer.
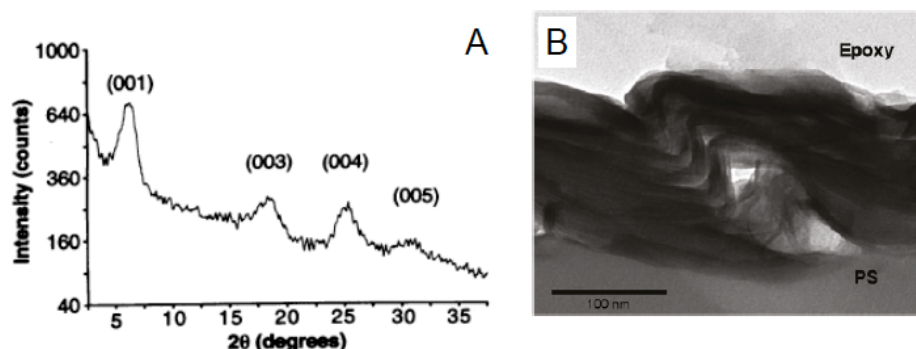
Figure 31. Clay-containing multilayers. (A) X-ray diffractogram of a multilayer showing multiple reflections due to regular basal spacing (1.5 nm).[101] (B) TEM cross-section micrograph of a clay-containing multilayer.[122]

The structure of montmorillonite-containing multilayers can be controlled by the deposition conditions. As expected the nature of the polyelectrolyte changes the

morphology of clay-containing multilayers. For instance poly(dimethyldiallyl-ammonium chloride) led to much denser film than poly(4-vinyl-1-methylpyridinium) bromide.[123] Increasing the concentration of the clay solution increases the speed of growth of the films probably because of a tighter 2D packing and a larger overlap between the platelets.[122] Surprisingly decreasing the deposition time from 300 to 10 seconds did not affect much the growth of the films but the final density of platelet decreased while the roughness of the film increased.[124] It has also been shown that the application of a negative bias on the substrate could promoted the production of smoother films.[121] The absence of intermediate drying step appears to increase the speed of growth of clay containing multilayers[51, 125] but to my knowledge no dedicated research has been done on this topic. To finish it should be noted that the preparation of clay-containing multilayers is not limited to electrostatic interactions. Polyvinylalcohol a non-charged polymer, can be assembled with montmorillonite to form multilayers thanks to hydrogen bonding interactions.[5]

We will now look at the properties provided by the layered structures of clay containing multilayers.

2.3.3 Barrier properties of clay-containing layer-by-layer assembled films.

The dense crystalline structure of clays makes them impermeable to gases. Incorporation of clays in a polymer matrix is commonly used in industry to improve their gaz-barrier properties.[40] In layer-by-layer assembled nano-composites this effect is maximized because all the platelets lay flat on the surface. In order to cross the film a gas needs to find an aperture between each layer of clay, this dramatically increase tortuosity of the gas pathway through the film (Figure 32A). The group of J. Grunlan reported the excellent gas barrier properties of clay containing multilayer.[126] They showed that a film composed of four layers of clays deposited on the surface of poly(ethylene terephthalate) (PET) film was reducing the oxygen transmission rate below the detection limit of the apparatus, this is four orders of magnitude lower than with a polymer coating and two orders of magnitude lower than SiO_X coatings. The barrier properties of such clay-based films where however dramatically decreased in presence of humidity. In a later

work they showed that they could build films from clay and Poly(vinylpyrrolidone) using hydrogen bonding[127] and that the barrier properties of such films where not affected by humidity.
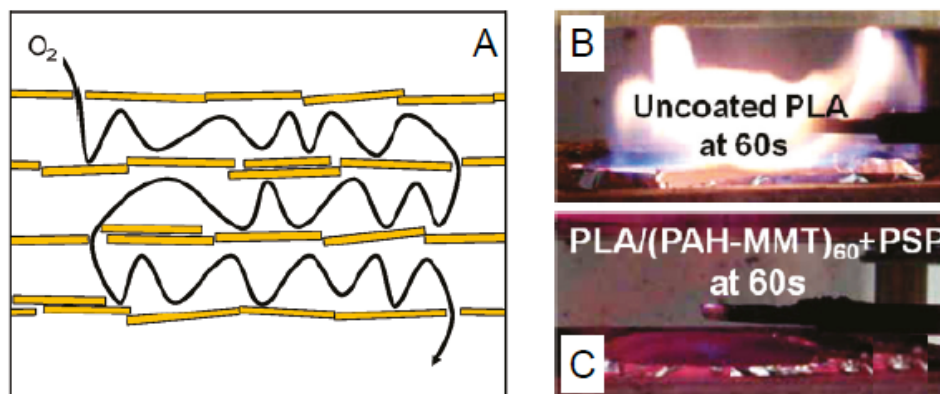
Figure 32. (A) Tortuosity of the gas-pathway through a clay-containing multilayer.[122] (B and C) Behavior after exposition to a flame of an unprotected (B) and clay protected (C) film of Poly(lactic acid) (PLA).[125]

Another property known for bulk composites is the fire-retardancy.[119] This effect is related to the gas barrier properties that prevent the oxygen needed for the combustion to reach the material and the degradation products to escape. Clays are also refractory and show poor thermal conductivity, which further enhance the fire-retardant properties. Coating cotton fabric with montmorillonite multilayers decreased the total heat released and increased the amount of char left after burning[109] because the multilayer prevents a full combustion. The clay coating also maintained the structure of the fabric (Figure 28A). Another group incorporated polyphosphate, a fire retardant agent, into a clay-containing multilayer to form a coating onto a poly(lactic acid) film.[125] The time to ignition of the coated material was multiplied by more than two compare to the uncoated materials (Figure 32B and C). The LbL film also decreased the heat release rate during combustion. To finish one should note that most layer-by-layer assembled clay containing multilayer are transparent.[126, 128, 129] The nano-scale dimension of the clay particles, their exfoliation and proper dispersion in LbL multilayers produce homogeneous film (at the micro-scale) that neither diffuse nor absorb light. The turbidity of the film is a sign of the presence of micro-inhomogeneities such as stacks of clays, cracks or phase separation. The production of homogeneous and transparent film is necessary to obtain optimal properties.

Fire retardant and gas barrier properties will certainly find many applications. Packaging industries demands thin films with barrier properties to conserve aliments while electronic industries need to protect sensitive components from moisture and oxygen. While protecting fabric, foams or films against fire by simple coating would be a cheap way to protect houses against conflagration and save life of numerous people. But all these applications also require mechanical resistance, which might be one of the most interesting features of clay-containing films.

2.3.4   Mechanical properties of clay containing thin films

Composed of aligned mineral platelets glued together by a polymer, the architecture of clay-containing multilayers mimics those of nacre or bones (Figure 33B). The step-by-step incorporation from a solution ensures proper dispersion and alignment of the platelets in the composite while the versatility of LbL assembly enable to chose the soft glue among many kind of polymers. The clay particles are small enough to behave as flawless crystals[35] and reach their theoretical Young's modulus as high as 400 GPa.[130] Similarly to what is observed for biologic materials the platelets are overlapping with each other and the polymer/platelet interactions are strong, thanks to multiple electrostatic interactions or hydrogen bonding. Such materials have a perfect structure to fully transfer the strength of clays to macroscopic films (Figure 33A). The first report of strong nacre-inspired multilayer concerned films consisting of montmorillonite and Poly(diallyldimethylammonium chloride).[51] This material had a strength reaching 130 MPa and a Young's modulus of 10 GPa which respectively approaches to the strength of nacre and the modulus of lamellar bones. The author reported that incorporation of calcium ions in the structure reduced the maximal strain while increasing the maximal stress of the material. The attributed this effect to replacement of polymer clay interactions by direct bridging between clay platelets (Figure 33C). The films were sensitive to humidity. Increasing the relative humidity (RH) from 32% to 92% halved the maximal strength. This result confirmed the electrostatic nature of the interactions in the material.
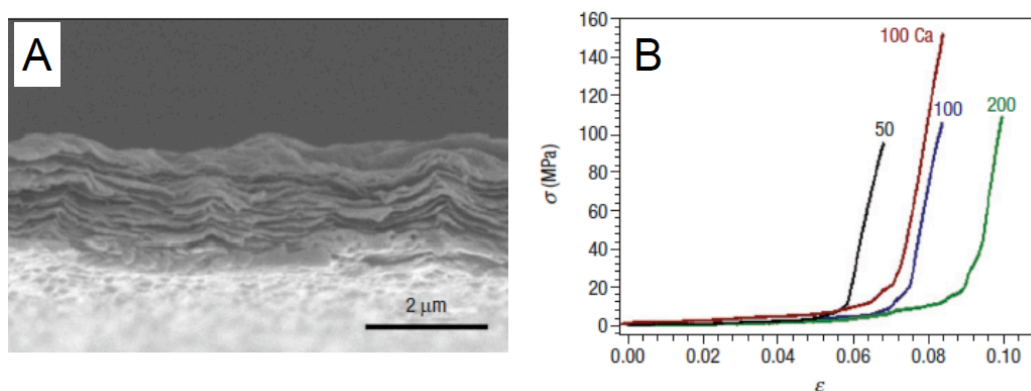
Figure 33. (A) Scanning electron micrograph of a multilayer consisting of hundred layer pairs of clay and polyelectrolyte. (B) Stress-strain curves for multilayers with various numbers of layer pairs. In red, the curve obtained for a film with hundred layer pairs after treatment with calcium ions.[51]

Few years after the first report another multilayer with excellent mechanical properties was discovered.[5] As polyvinylalcohol forms strong hydrogen bonding with clays, the alternated dipping in each solution leads to the formation of well-organized films in the same way that electrostatic interaction does. The strong polymer-clay interaction results from the multiple hydrogen bonds between the silicates groups at the surface of the clay and the hydroxyl group of the polymer. The author also reported that polyvinylalcohol could make covalent bonds with the aluminum atoms appearing on the edges of the clay particles. The strong interfacial bonding and the layered organization explain the superior strength (150 MPa) and Young's modulus (13 GPa) of this material, already surpassing those of films based on electrostatic interactions.[51] The exceptional mechanical properties of these materials are only reached when the film is cross-linked using glutaraldehyde, a bifunctional molecule that can link two OH groups (Figure 34B). A film dipped every ten layer pairs in the cross-linking solution reached strength of 400 MPa and Young's Modulus of 100 GPa (Figure 34A) which is close to materials such as Kevlar or steel. This time the mechanical properties of the multilayer are independent of the humidity because water cannot break covalent bonds. These films are also highly transparent because of the good exfoliation of the nanometric platelets and their homogeneous layered organisation in the film (Figure 34C).
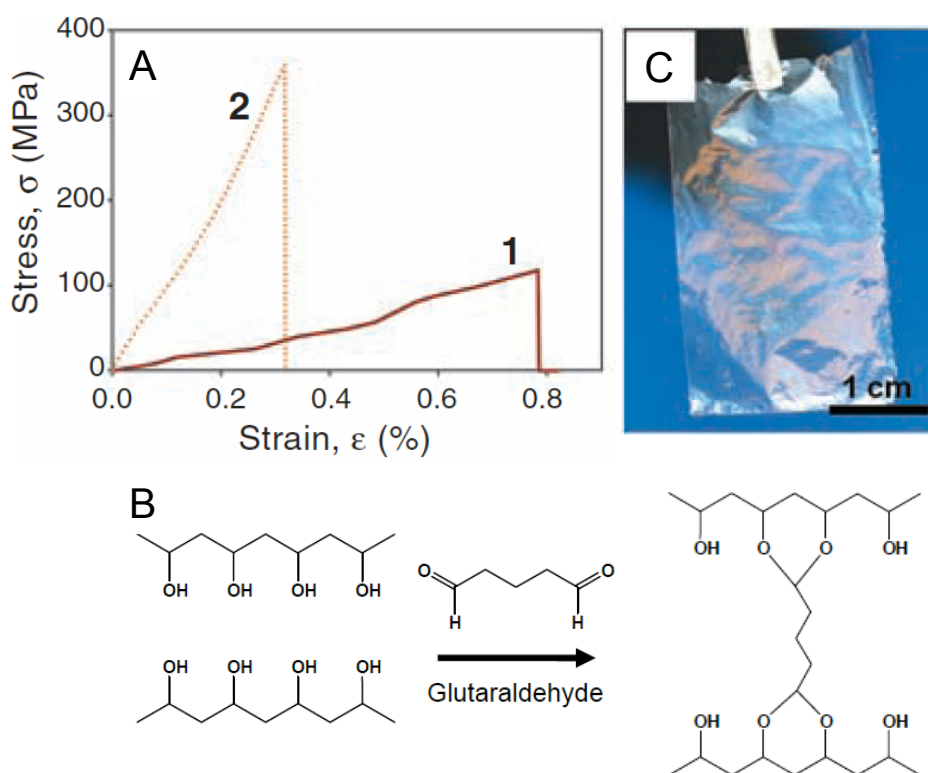
Figure 34. (A) Stress-Strain curves of a Polyvinylalcohol/clay multilayer before (1) and after cross-linking (2). (B) Cross-linking reaction of polyvinylalcohol with glutaraldehyde. (C) Optical photography of a free-standing film composed of 300 layer pairs of montmorillonite and Polyvinylalcohol.[5]

Despite their high strength, these materials are brittle and do not behave like nacre or bones. We have seen in the previous chapter that brittle fracture could be due to a too high aspect ratio of the reinforcing nanoparticles. Using a synthetic clay with a smaller aspect ratio (50 against more than 200 for natural clays) an other group built a layer-by-layer assembled film that could yield and undergo plastic fracture.[131] The mechanical properties obtained where however not comparable with montmorillonite-containing composites since the Young's modulus did not surpass 7 GPa even after cross-linking and the maximal stress hardy reached 150 Mpa. Several other works have looked at the layer-by-layer assembly of strong clay-containing composites. Clays were for example incorporated in exponentially growing films,[132, 133] the preparation time is reduced compare to linearly growing films but the content of platelet and their organization is decreased leading to limited mechanical improvements. An other interesting work combined clays with synthetic mussel glue (the polymer used by mussels to stick to the sea floor),[134] the film produced had strength around 77 MPa before and 200 MPa after cross-linking

with Fe^{3+}. As for natural mussel thread[135] the metalic cross-linking was a key parameter toward strong nano-composites. According to current reports, two parameters are determining the strength of LbL assembled nano-composites the structure of the film (platelet size and layered structure) and the chemical interactions holding the material together.

Montmorillonite is not the only platelet-like colloid that can be incorporated in multilayer; we will now see other materials that bring interesting properties when they are incorporated in LbL-assemblies.

2.3.5   Other nacre-inspired multilayers

Clays are widely available, cheap and easy to process in addition to their excellent mechanical properties. Therefore they have been widely used for the preparation of nacre-inspired structures. But other types of nano-platelets can be incorporated in multilayers. For example layered double hydroxides (LDH) is a large class of synthetic inorganic materials with morphology similar to clays. They shows luminescent, catalytic or magnetic properties[136] depending on their composition. The group of T. Sassaki prepared cobalt-aluminum layered double hydroxide (Figure 35A) and incorporated them in layer-by-layer assembled films using poly(sodium 4-styrenesulphonate) as cationic polyelectrolyte. These films are ferromagnetic and their properties appear to be thickness dependent.[137] An other group presented the fabrication of films combining LDH, montmorillonite and polyvinylalcohol showing that LDH are also capable to form structured multilayer through hydrogen-bonding.[138]
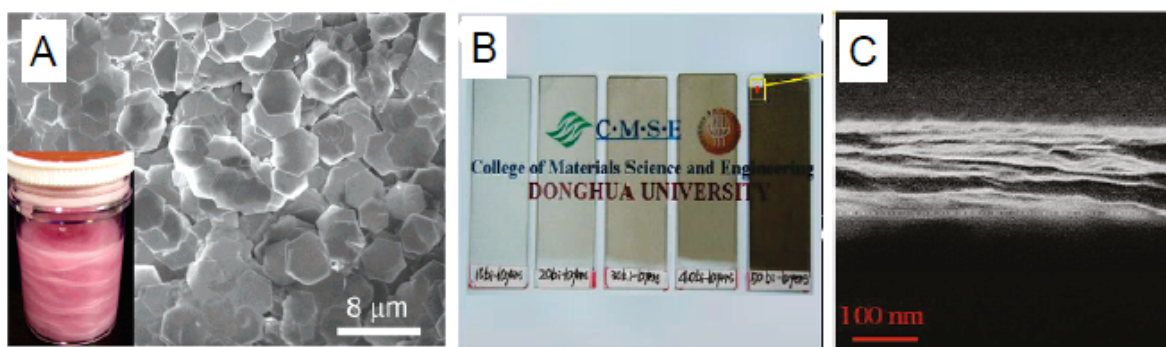
Figure 35. (A) Scanning electron micrograph of Co-Al-CO$_3$ layered double hydroxide platelets showing high homogeneity. Inset: Co-Al-CO$_3$ suspension in water before exfoliation.[137] (B) Optical image of multilayers made of graphene oxyde and polyvinylalcohol with 10, 20, 30, 40, and 50 layer pairs. (C) Scanning electron micrograph of the graphene oxide-based film with 50 layer pairs showing layered structure.[139]

Graphene and graphene oxide are interesting material because of their electrical conductivity and mechanical resistance. Graphene oxide is widely used despite properties lower than those of graphene because it is easier to process.[140] The incorporation of graphene derivatives in multilayered composites is also an attractive topic. Similarly to what was found for clay nano-composites, graphene and graphene oxide improves the mechanical properties of thin films. Assembly of graphene oxide and polyvinylalcohol using the layer-by-layer technique led to a material more than twice harder than pure polyvinylalcohol.[139] In another work the combination of already strong silk fibroin with graphene oxide led to a composite with strength above 130 Mpa and a Young's modulus as high as 140 GPa.[141] Barrier properties similar to those of clay-containing multilayers were reported for graphene-containing multilayers. Built on cotton fabric, such films delayed the combustion and increased the amount of char left.[142] Another work reported that ten layer pairs of poly(ethyleneimine) and graphene oxide could reduce the oxygen transmission rate below detection limits.[143] An advantage point of graphene-containing multilayer compare to clay containing multilayer is their conductive properties. A recent review on graphene-based multilayers[144] presented their applications in field-effect transistors, sensors or super-capacitors. The review also underlines some advantages of the layer-by-layer technique for the production of graphene containing thin films control of the architecture and composition of the film and fine-tuning of the polymer-graphene interactions.

The preparation of nacre-inspired multilayers using the layer-by-layer assembly has found many applications from gas barrier to ultra-strong thin films. Wood-inspired structure (i.e. fibrilar multilayer) are another type of promising nanocomposites. In the next chapter we will discuss the contribution of LbL assembly to the preparation of such structures.

2.4 Wood-like multilayers

For the preparation of wood-inspired nanocoposites we will focus on the use of microfibrillated cellulose, the elementary fibrils that give strength to wood structures. Their extraction from plants and assembly in multilayer will be discussed. We will then review the properties of LbL films containing such fibrils before looking at the properties of other fiber reinforced multilayers.

2.4.1 Microfibrillated cellulose (MFC)

Cellulose is the main component of most of the vegetal kingdom; therefore it is the most widely available polymer. We have seen in the previous section that wood consists of thin fibrils of cellulose bound together by hemicellulose and lignin.[8] In the paper industry wood is transformed into micron-sized fibers by chemical or mechanical treatment. Fibers obtained in this way are much bigger than wood elementary micro fibrils but their size can be reduced to a diameter between five and fifty nanometers and a length of several microns using high-pressure homogenization.[145, 146] Microfibrillated cellulose produced in this way, still consists of several individual cellulose fibrils linked together but its functionalisable surface, large aspect ratio and high specific surface makes it a excellent candidate for the preparation of artificial wood structures.[146, 147]

There exist other forms of commercial cellulose fibrils. An acidic treatment of the fibers dissolves their non-crystalline parts leading to cellulose nano-whiskers. With a similar diameter these rods have shorter length comprised between 100 and 250 nm. Cellulose nano-whiskers can also be directly extracted from algae and tunicate their length can then reach several micrometers. Some bacteria produce cellulose directly from sugars, called bacterial-cellulose. This material forms networks of fibers with diameters ranging from 20 to 100 nm.[145, 147]

Figure 36. Microfibrillated cellulose. (A) Wood pulp recovered after high pressure homogenization of wood.[146] **(B) Solution of MFC (1.9 g/L) obtained after dilution of the pulp, ultrasonication and centrifugation. (C) TEM images of the MFC from solution described in (B). The scale bar is 500 nm.**[148]

Using chemical treatment it is possible to functionalize the surface of microfibrillated cellulose with charged groups. Negatively charged cellulose fibers are prepared by sulfite or TEMPO treatments. When they are applied to the starting wood pulp these treatments induce charge repulsion between the fibrils and strongly reduce the energy needed to produce microfibrillated cellulose.[145]

After surface fonctionalization and high pressure homogenization a gel is obtained (Figure 36A). This gel can be diluted, sonicated and centrifugated to obtain clear and stable solutions of microfibrillated cellulose necessary for the layer-by-layer assembly (Figure 36B).[148] The clear solutions are characteristic of suspension of sub-micron particles that do not scatter light. The suspension of microfibrillated cellulose in water is at a fragile equilibrium. Increase of the ionic-strength of the solution or decrease of the pH reduces the electrostatic repulsion between cellulose fibers and leads to gelation of the MFC suspension.[149] In consequence these suspensions are typically used without modification.

The preparation of films from a suspension of microfibrillated cellulose can be done by vacuum filtration or simple drying. The control over the film architecture using such process is however limited. Layer-by-layer assembly offers a superior control over the nano-structure and composition of MFC containing films.

2.4.2 Layer-by-layer assembly of microfibrillated cellulose thin films.

Suspensions of negatively charged cellulose fibers have been used to build films using the layer-by-layer assembly technique. Wågberg et al. showed that it was possible to build LbL films with several polycations,[148] namely poly(ethylenimine) (PEI), poly(allylamine hydrochloride) (PAH) and Poly(diallyldimethylammonium chloride) (PDDA) (Figure 37A). They observed that PEI led to thicker films than PAH or PDDA. After addition of salt to the solution of PAH or PDDA the speed of growth of these systems were comparable to the PEI/MFC system.
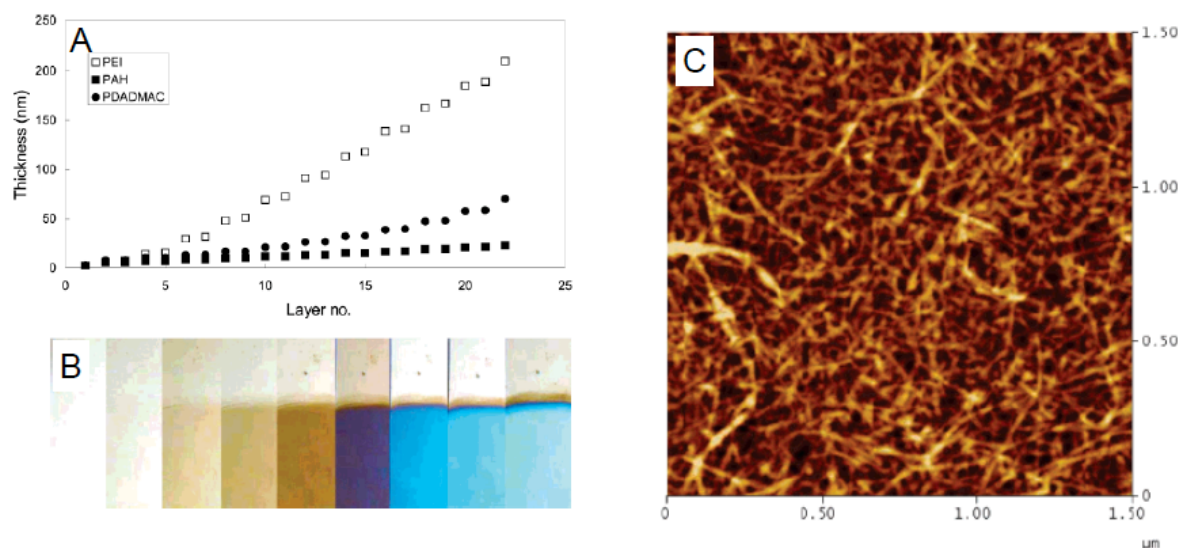
Figure 37. (A) Growth of polyelectrolyte multilayers made of MFC and several polyelectrolytes. (B) Evolution of the interference color of PEI/MFC films from one to nine layer pairs (left-right). (C) AFM image of one layer pair of PEI and MFC on silicon wafer.[148]

Addition of salt to the MFC solution had the opposite effect.[150] The construction of PEI/MFC multilayer was reduced by two upon addition of 10 mM of sodium chloride in the solution probably due to the destabilization of the solution. The same article also reported that increasing the pH of the PEI solution from six to ten led to an increase of the mass of PEI and MFC in the film. The mass of component adsorbed in the film was followed using Quartz Crystal Microbalance (QCM) while the thickness and refractive index were followed by interferometry, both techniques gives consistent results. The combination of QCM with dual polarization interferometry allows calculating the amount of water trapped in the film. For

PEI/MFC films the water content was close to 50%. These articles reported a steady growth of films based on anionic microfibrillted cellulose with uniform coverage of the surface both at the macroscopic and microscopic levels (Figure 37B and C). Positively charged microfibrilated cellulose was produced by chemical fuctionalisation of microfibrils with quaternary ammonium groups. Such fibers were used in combination with anionic microfibrilated cellulose to produce pure cellulose LbL assembled multilayers.[151] The growth reported for pure cellulose assemblies was slower than for films containing PEI and the water content higher. The possibility to build films with more exotic polyelectrolytes such as thermo-responsive polymers[152] comforts microfibrillated cellulose as efficient new building block for the fabrication of layer-by-layer assembled films toward specific applications.

2.4.3   Properties of MFC-containing thin films.

Polyelectrolytes can efficiently glue cellulose fibers together just as lignin in wood. Building polyelectrolyte multilayers on paper fibers improved the adhesion between the fibers in the resulting paper and nearly doubled its strength.[153] Polyelectrolytes multilayers are known to change the adhesive properties of the surfaces on which they are built.[154] It has been shown that the work of adhesion (energy) needed to separate surface coated with PEI and MFC was higher than for surface coated with cationic and anionic MFCs.[151] This is certainly due to the strong adhesion of PEI to many surfaces including MFC fibers. Such example underlines the importance of the polymeric binder to the production of mechanically strong cellulose containing films. Dopamine is a functional sub-unit found in the glue produced by mussels to stick to the rocks; when combined with iron ions (Fe^{3+}) it cross-links and adheres to many surfaces. MFCs functionalized with dopamine where used in combination with PEI to build multilayers whose wet adhesion increased by a factor of three in the presence of Fe^{3+}.[155] Microfibrillated cellulose is also used to improve barrier properties, mainly in the domain of bio-based and biodegradable polymers. The construction of twenty layer pairs of PEI and MFC on poly(lactic acid) films reduced the oxygen permeation rate by a factor of three without modifying the transparency of the film.[156] At fifty layer pairs the transparency slightly decrease (Figure 38A) but the oxygen permeation rate is more than fifteen times lower than without a coating.
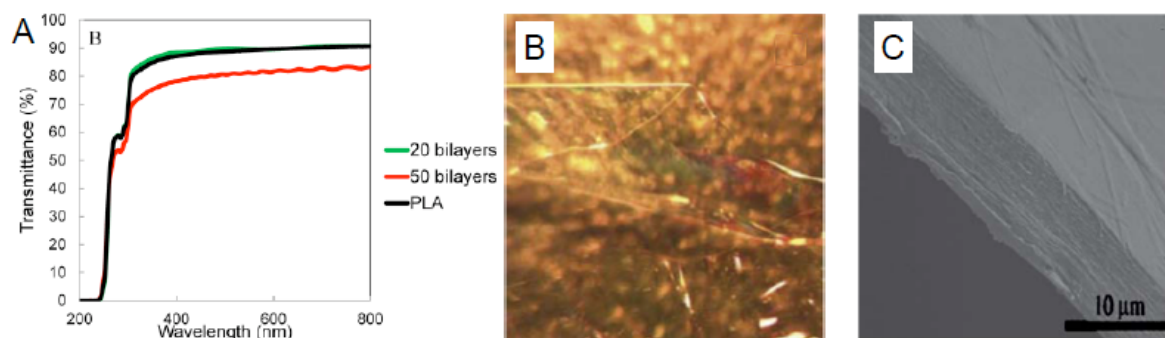
Figure 38. (A) Transmittances of poly(lactic acid) films coated with 20 and 50 layer pairs of PEI/MFC compared to a uncoated one.[156] (B) Optical micrograph of a micron thick PEI/MFC free-standing film. (C) FE-SEM micrograph of a film consisting of 150 layer pairs of PEI/MFC.[6]

Films combining high strength from cellulose fibers and transparency were fabricated using the PEI/MFC system.[6] Such films where three times as strong as solvent cast MFC films. They were transparent (Figure 38B) and presented a structure somehow similar to the wood cell wall with an in-plane random orientation of strong fibers glued together by a soft polymer (Figure 38C). Sub-micron MFC films where also characterized using buckling mechanics, a technique that is described in chapter 2.5.2. The Young's modulus of such film decreased upon hydration, from 17 GPa at 0% RH (Relative Humidity) to 1.2 GPa at 50% RH.[157] The incorporation of silica particles doubled the Young's modulus of such multilayers at 50% RH.[158]

We have seen that microfibrillated cellulose is an interesting building block for the production of strong and transparent films. We will now look at the properties of multilayers incorporating other types of fibrils.

2.4.4 Other wood-inspired multilayers.

With nano-scale diameter and micro-scale diameter carbon nano-tubes (CNTs) and microfibrillated cellulose have a similar geometries (Figure 39). With their record mechanical properties of CNTs are also excellent candidates as reinforcing fibers for composites. When incorporated in polyelectrolyte multilayers CNTs improved the strength of the films by one order of magnitude reaching 150 MPa.[159] A review on carbon nanotube-containing multilayers summarizes their interesting mechanical and electrical properties that can be applied in many domains from sensor to fuel cell applications.[160] Fibrillar nano-composites with a catalytic activity

can also be assembled using for example titanium oxide nanotubes.[161] Recently the preparation of multilayers from aramide fibers suspended in water atracted interest as new building block for the preparation strong LbL assembled thin films.[162]
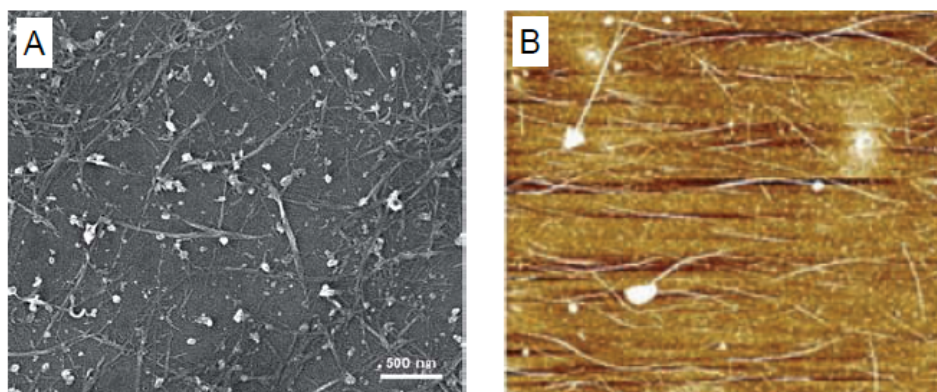
Figure 39. Scanning electron micrograph of a layer-by-layer assembled film containing carbon nanotubes with random in-plane orientation.[163] Atomic force microscopy image of carbon nanotubes oriented on a surface by spin coating. Image width 10 μm.[164]

Building an architecture similar to the one of wood cell wall requires control of the in-plane orientation of the nano-fibers during construction. Several methods have been presented for this purpose. The combination of layer-by-layer deposition with combing using high pressure tangential air-flow led to the formation of oriented carbon nanotube layers.[165] Apart from the layer-by-layer technology several methods have been used to align fibrillar structures using a shear flow in micro-fluidic circuits[166] or a radial shear created by centrifugal forces in spin coating (Figure 39B).[164] Other groups used liquid crystals as template[167] or the decoration with iron nano-particles combined with magnetic field[168] to orient carbon nanotubes in thin films. Aligned fibrillar multilayers prepared using a combination of layer-by-layer assembly and an orientation procedure would probably have interesting mechanical properties, yet the characterization of such films is not an easy task.

2.5   Mechanical characterization of thin films

Testing the mechanical properties of supported micrometric films is a difficult task. Indeed, direct tensile testing is impossible because the resistance of the support masks the properties of the film that was deposited on it. Production of free-

standing multilayers appears as the easiest way to access to their mechanical properties. Self-supported structures can be characterized using classic mechanical tests but it requires dexterity and precise apparatus. Some methods developed recently can directly probe the mechanical properties of supported films but they have their own limitations.

2.5.1 Free-standing films

In principle, the production of free-standing multilayers is difficult because the film strongly adheres to the substrate mainly with electrostatic or hydrogen interactions. Taking inspiration from the preparation of hollow capsules (Figure 40A)[112] the first free-standing films were released from a sacrificial substrate. Mamedov and Kotov built a multilayer on cellulose acetate which was dissolved in acetone afterward[169] but other combinations of polymers and solvents can be used as sacrificial layers.[170] Polyelectrolyte multilayers dissolving upon pH increase have also been used to produce free-standing multilayers.[171] A last technique consists in the dissolution of the silicon oxide layer at the surface of glass slides and silicon wafers with hydrofluoric acid to release the film.[5] This method does not require any substrate preparation but the use of fluoridric acid is dangerous and might induce chemical modifications of the film structure.

To avoid the use of sacrificial layers and harsh releasing conditions some groups developed alternative approaches. Skipping the drying steps during the layer-by-layer assembly allows to produce multilayers spanning across 100 µm wide gaps on TEM grids (Figure 40B).[172] While some stimuli-responsive films generate enough stress as they swell to spontaneously detach from their substrate.[173]
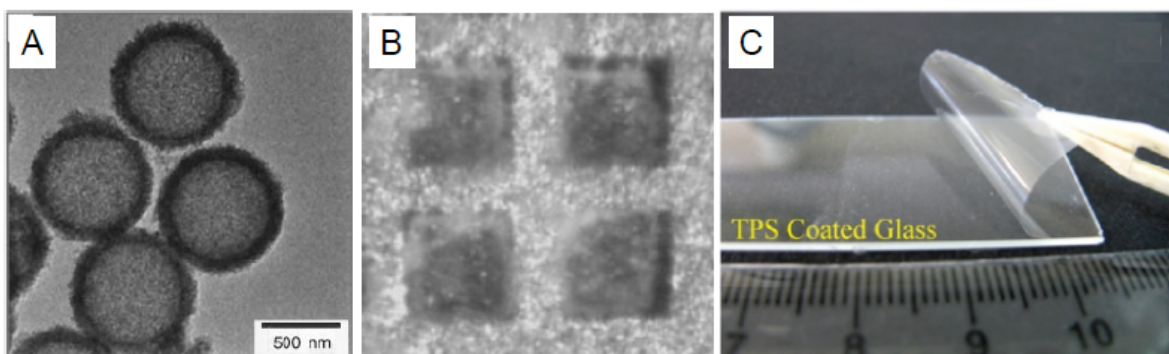
Figure 40. (A) Hollow ceramic capsules prepared by calcination of LbL coated polystyrene colloids.[112] (B) LbL film directly build across the 100 μm wide gaps of a TEM grid.[172] (C) Detachment of a thick LBL film from a poorly adhesive glass slide.[131]

A last approach toward the production of free-standing films relies on the mechanical detachment of the multilayer from a weakly adhesive substrate (Figure 40C). Fictionalization of silicon substrates with fluoroalkyl chains produces substrates with hydrophobic surfaces. Layer-by-layer films can still grow on such substrate but they poorly adhere on the surface. This technique was used to produce free-standing films containing clays[131] and micro-fibrillated cellulose.[6] It is easy to set-up and the substrates are reusable. However, it requires films that are resistant enough to handle the mechanical stress during detachment. These techniques can be used to produce free-standing films, it is then possible to characterize their mechanical properties using classic tensile test or to skip the detachment step and perform for example nanoindentation.

2.5.2 Mechanical characterization of thin films

Once the films are detached they can be characterized by tensile tests. Handling the multilayer films requires dexterity because they are extremely fragile and sensitive to airflow. In order to obtain accurate stress at break measurements, the sample needs to have smooth edges it can be difficult to cut such sample in thin multilayers. The sample also needs to be perfectly aligned in the tensile testing system to avoid stress concentration and the low maximal strain of some samples can easily be overestimated due to compliance of the setup. Tensile testing is nevertheless popular for the characterization of thick and resistant multilayers because it allows comparison with bulk materials. Some specific improvements have been developed for the characterization of thin multilayers. In order to record

the true strain (below 1%), Podsiadlo et al. followed the displacement of glass beads electrostatically adhering to the surface of the film using a microscope coupled to a digital camera and a particle tracking software (Figure 41A).[5] While the production of smooth and defect free sample can be done using micromanipulation set-up,[131] these technical difficulties have often pushed the researchers toward different solutions.
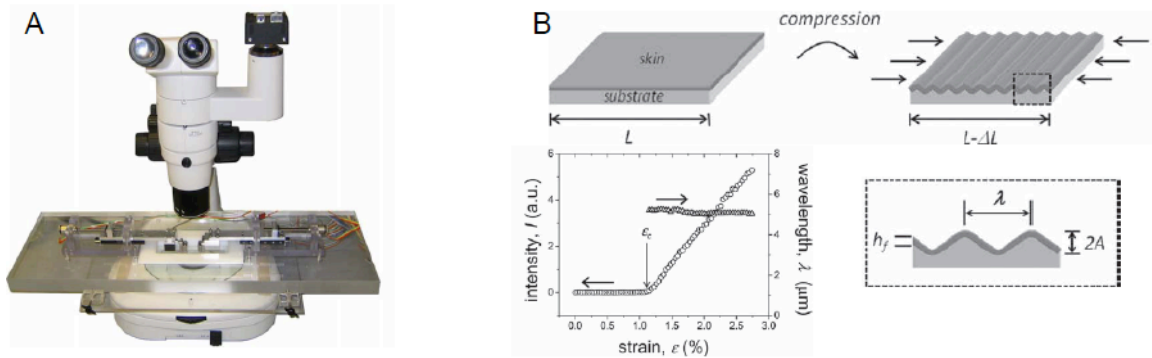
Figure 41. (A) Tensile testing system installed under a microscope for accurate measurement of the true strain.[5] (B) Up : Schematic representation of the wrinkling of a layer pair under compression. Down : Variation of the wrinkling amplitude with the strain while the wavelength stays constant.[174]

An elegant method to calculate the Young's modulus of supported thin film called "buckling" was developed by Nolte.[174] When a rigid film supported by a soft substrate is compressed the surface wrinkles (Figure 41B). In mechanical engineering knew this was known for a long time but most of the research was focusing on ways to avoid it rather than its uses as characterization technique. The periodicity of the wrinkles at the surface depends on the thickness of the film, on the relative plane-strain modulus of the film and on the properties of the support, while the percentage of compression of the sample only impacts the amplitude of the wrinkles and not their periodicity (Figure 41B). Knowing the thickness of the film and the characteristics of the support the film modulus can be directly recovered from the wavelength of the wrinkles. This method has been used to determine the modulus of multilayer under various humidity conditions[175] and the mechanical properties of multilayers containing microfibrillated cellulose.[157, 158] Most of the results obtained by buckling are in agreement with those obtained by

tensile testing, however the conversion from the plate-strain modulus to the Young's Modulus becomes complex if the material is not isotropic.[176]

Nano-indentation has also been used to characterize mechanical properties of multilayers.[125, 139] Such measurement can be done directly on supported films and do not require any pretreatment. However, if the film is not thick enough the mechanical properties measured are over estimated because the nano-indenter measure at the same time the film and the substrate (harder).[177] This technique is nevertheless useful to compare films of similar thickness deposited on similar surfaces. A last method commonly used to measure the mechanical properties of LbL films is Atomic Force Microscopy (AFM).[178, 179] This technique is also limited to the comparison of similar samples and should be performed with similar apparatus. The modulus measured depends strongly on the shape and quality of the tip used, on the model used to describe the interactions (hard or soft contact, indentation) and on the experimental conditions (force applied). A last limitation of buckling, nano-indentation and AFM measurements is that none of them can give informations about the rupture properties of the film.

Many characterization techniques have been developed to probe the mechanical properties of thin films. The preparation of free-standing multilayers and tensile characterization is a difficult task but it gives access to mechanical properties that difficult to obtain otherwise and rely on very robust models.

Layer-by-layer assembly is a powerful bottom-up approaches to the fabrication of layered thin films. Its low cost and experimental ease have made it very popular for the production of nano-composites. We have seen some of its application toward the production of wood and nacre-inspired multilayers. The preparation of strong LbL assembled composites was the main goal of this work. Prior to discussing the results obtained in the last three years we will describe the preparation procedures and characterization techniques used.

3 Material and methods

3.1 Materials and solution preparation

3.1.1 Materials

Montmorillonite clays were provided free of charge by Clariant® (Clariant Produkte GmbH, Moosburg, Germany) as ground clay powders. Clays from different origins and pretreatments were used:

- EXM 1289 is a natural montmorillonite with calcium and sodium counter-ions. It has a cation exchange capacity of 113 meq/100g (medium charge).

- EXM 1246 has the same origin as EXM 1289 but calcium ions in the structure were exchanged by sodium ions.

- EXM 2039 has similar origin as EXM 1289 and EXM1246. In addition to the exchange of calcium ions by sodium ions this clay undergoes an additional phosphate treatment in order to improve exfoliation.

- EXM0242 is a natural montmorillonite with a cation exchange capacity of 99 meq/100 g.

EXM1743 is a natural montmorillonite with a cation exchange capacity of 66 meq/100 g.

Microfibrillated cellulose (MFC) was obtained from Innventia AB (Stockholm, Sweden) as a pulp containing 2.5% of fibers in water.

Poly(vinyl amine) (trade name LUPAMIN 9095, PVAm, 20% in Water, $\overline{M_w}$ ≈ 340,000 g/mol, more than 90% hydrolysed) was freely provided by BASF.

Poly(dimethyldiallylammonium chloride) (PDDA 20% in water, $\overline{M_w}$ ≈ 100,000-200,000 g/mol), low molecular weight [bis(3-aminopropyl)]-terminated-poly(dimethylsiloxane) (PDMS-2500, $\overline{M_w}$ ≈ 2,500 g/mol), high molecular weight [bis(3-aminopropyl)]-terminated-poly(dimethylsiloxane) (PDMS-27000, $\overline{M_w}$ ≈ 27,000 g/mol, polydispersity index = 2.7), poly(methyl vinyl ether-*alt*-maleic anhydride) (PMEMA, $\overline{M_w}$ ≈ 210,000 g/mol) and poly(vinyl alcohol) (trade name Moviol 10-98, PVAl, $\overline{M_w}$ ≈ 61,000 g/mol, 98% of hydrolysis) were purchased from Aldrich (Lyon, France).

Octadecyltrichlorosilane (OTS, > 97%) was purchased from Acros-Organics (Illkirch, France). Toluene (> 99.9%) was obtained from VWR Chemical (Strasbourg, France). Ethanol absolute anhydrous (> 99.9%) was obtained from Carlos Erba Reagents (Peypin, France).

Sodium hydroxide pellets (> 97%) were purchased from Sigma-Aldrich (Lyon, France).

Ultrapure water (Milli-Q water) with a resistivity of 18.2 MΩ was obtained by purification with the Milli-Q Gradient System from Millipore (Molsheim, France). The water was used directly after production.

Silicon wafers (200 mm and 50 mm in diameter) were purchased from Wafernet Inc. (San José, CA) and cut in 1 x 4 cm for build-up characterization and 3 x 10 cm for thick film preparation. For spin-assisted deposition the 50 mm diameter wafers were used directly.

All chemicals were used as purchased unless otherwise specified.

3.1.2   Preparation of clay suspensions

For the production of thick films the clay (EXM 2039) was suspended at 10 g/L in Milli-Q water for 3 days under magnetic stirring. The suspension was then centrifuged for 3 hours at 5,000 rpm ie 1,000 g (centrifuge 4K10 with Rotor Nr 12254 from Sigma, Lyon, France). The resulting supernatant was used without further dilution (about 4.5 g/L from dry mass).

For the other experiments the clay powders were suspended in Milli-Q water by stirring 5 g of clay in 1 L of water for 3 days. The effect of sedimentation and centrifugation was studied directly on these suspensions.

The preliminary studies about the nature of the polyelectrolyte, pH of the solution and intermediate drying steps were carried out on clay suspensions centrifuged for 1 hour at 10,000 g. The concentration of clay in the supernatant was estimated by drying a precise volume of suspention in a beaker of known weight. The concentration of the initial solution was then adjusted with Milli-Q water to obtain solutions at 1 g/L.

3.1.3   Preparation of MFC suspensions

The pulp provided by Innventia AB (Stockholm, Sweden) was dispersed in Milli-Q water to obtain a suspension at 2 g/L and sonicated with a tip sonicator (Vibra cell 75042 from Bioblock Scientific, Illkirch, France) for one hour at 20% of amplitude. The suspension was then centrifuged for 3 hours at 5,000 rpm (centrifuge 4K10 with Rotor Nr 12254 from Sigma, Lyon, France), and the resulting supernatant was used as deposition solution after filtration on cotton wool. Typical MFC concentration was in the range of 0.9 g/L as determined from dry mass measurements.

3.1.4   Preparation of polymer solutions

Poly(vinyl amine) and poly(dimethyldiallylammonium chloride) were diluted in Milli-Q water to obtain solutions at 1 g/L. The pH of the poly(vinyl amine) solution was then adjusted using a solution of sodium hydroxide at 0.5 M in Milli-Q water.

Low and high [bis(3-aminopropyl)] terminated poly(dimethylsiloxane) were diluted in toluene to obtain solutions at 5 or 50 g/L.

Poly(methyl vinyl ether-*alt*-maleic anhydride) was diluted in tetrahydrofuran to obtain solutions at 1, 5 or 50 g/L. The solutions were filtered on paper filter before use to remove small aggregates present in solution.

Poly(vinyl alcohol) was dissolved in Milli-Q water to obtain solutions at 5 g/L. To fully dissolve the poly(vinyl alcohol) it was necessary to heat the mixture to about 80 ºC. Insoluble aggregates were removed by filtration on paper filter.

3.2   Sample preparation

3.2.1   Substrate cleaning

The silicon wafer slides were cleaned using ethanol (10 min in ultrasound bath) and Milli-Q water (10 min in ultrasound bath) and dried using compressed air flow. Clean silicon wafers were activated for 3 min in a Plasma Cleaner (Harrick Plasma, Ithaca, NY) on medium intensity.

The QCM-D sensors were rinsed with Milli-Q water, dried with compressed air and treated with UV-Ozone for 15 min in Uv-Ozone cleaner (UV/Ozone ProCleaner BioForce Nanoscience, Inc., Ames, IA).

3.2.2   Hydrophobic substrates

The activated silicon wafers were dipped in a freshly prepared solution of octadecyltrichlorosilane 0.1% in toluene for one hour. Then the modified substrates were rinsed with fresh toluene, ethanol and Milli-Q water and finally rubbed with dust free cloth (Ko-ton, Chicopee Europe, AA Cuijk, The Netherlands). After surface modification, the thickness typically increased from 1.8 nm for activated silicon wafer to 4.5 nm from ellipsometry measurements.

3.2.3   Dip-assisted LbL assembly

Unless otherwise specified the time and process was the following. The substrate was dipped for 5 min in a given suspension (polymer, clay or MFC) followed by three rinsing steps of 1 min in the pure solvent (Milli-Q water, toluene or THF) of the suspension deposited. The substrate was then dried with compressed air and the thickness of the film was measured by ellipsometry. Similar process was applied for the deposition each component.

The consecutive repetition of these steps leads to the preparation of a multilayer. For films made of two oppositely charged polyelectrolytes the repeating cycle consisting of two deposition steps is called a layer pairs. For more complex architectures (e.g. with clay and poly(dimethylsiloxane)) the repeating cycle could

consist of up to 8 adsorption steps. The procedure was the same for covalent-LbL with amine and maleic anhydrid groups.

Preparation of thick multilayers was performed using a home made dipping robot, consisting of three motorized arms (x,y,z directions), a drying station, an interface from ISEL (Houdan, France) and a Labview program. The deposition was done according to the procedure described above without ellipsometry measurements.

It is usual to deposit poly(ethylene imine) (PEI) as adhesive layer on the substrate before construction of any multilayer. In our case the use of poly(vinyl amine) made possible to build most of the films without a first layer of PEI.

3.2.4   Spin-assisted LbL assembly

A spin coater (model WS-50H7-8NPP/A8/AR, Laurell Technology Corporation, North Wales, PA) was used to prepare spin-assisted multilayers. The rotating speed was defined and kept constant during the entire build-up. Typically ten drops (0.3 ml) of a given solution were deposited on the center of the rotating substrate at a rate of about one drop per second. The substrate was rinsed immediately after with 1 mL of milli-Q water and left rotating until dry. The oppositely charged solution is then deposited in a similar way. The process was repeated to reach the desired thickness or layer number.

3.2.5   Spray-assisted LbL assembly

Spray-assisted assembly was carried out using AIRBOY bottles to spray a given solution against a vertically mounted substrate. The first component to deposit was sprayed for five seconds. The functionalized substrate was then rinsed with Milli-Q water for five seconds in order to remove the weakly absorbed material. The substrate was then dried with compressed air before deposition of the oppositely charged compound according to the same procedure. The process was repeated to reach the desired thickness or layer number.

3.2.6   LbL assembly in QCM cell

After cleaning with UV-Ozone the quartz crystal was introduced in the measurement cell, rinsed and equilibrated in Milli-Q water before any deposition.

Typically 600 µl of the solution was injected in the QCM cell at 300 µl/min. The solution was left in contact with the quartz crystal until an adsorption plateau was reached and then we rinsed with Milli-Q Water. The next deposition was performed without intermediate drying. At least two injections of the component solution and three rinsing with Milli-Q water were carried out at each step.

3.3 Imaging

3.3.1 Optical photography

Imaging reflecting surface is a difficult task because it is difficult to focus on the surface and also because its aspect depends on the background. The camera was mounted on a tripod and the focus was set manually beforehand. Two different set-ups were used: one to take images from the light reflected by the sample and one to take image from the light diffused by the sample.

In order to take an image of the light reflected (interference colors) the sample is placed face up and the camera is positioned so that it sees the lightning softbox through the sample (that acts as a mirror) (Figure 42A). To image the light diffused by the sample, a black cardboard is placed on the path of the light in order to prevent direct reflection toward the camera. There is still light coming on the sample from the side but the camera only sees the part diffused by the sample itself (Figure 42B).
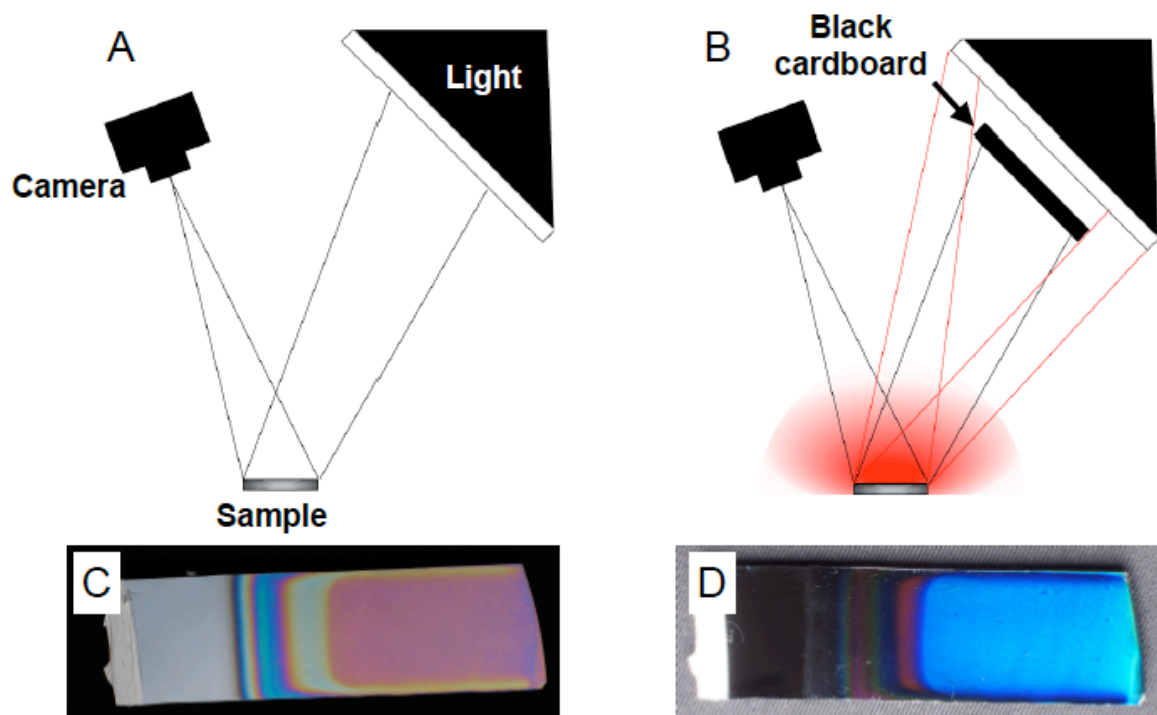
Figure 42. Schematic representation of the set-up used for taking pictures of the light reflected by the sample (A) and diffused by the sample (B). Optical images of the light reflected (C) and diffused (D) by a [PMEMA/PDMS$_{2500}$]$_{80}$ film.

Reflection pictures show the interference colors at the surface of the sample (Figure 42C). Diffusion pictures outline the macroscopic defects in the film and reveal microscopic inhomogeneities responsible for light diffusion (Figure 42D). These two observation modes correspond to what is found in optical microscopy under the names bright field (reflection) and dark field (diffusion).

Optical photographs of the samples were taken using a canon Power Shot G5 under illumination with a FotoQuantum Studiomax daylight Kit 600/600. The white balance of the camera was set manually from the picture of a white paper. The pictures of non-reflecting objects were taken with the reflection set-up without adjustment.

3.3.2   Atomic Force Microscopy (AFM)

Atomic force microscopy (AFM) was discovered in 1986 by Binning and coworkers[180] based on their studies on Scanning Tunneling Microscopy (STM) discovered in 1981. The resolution of AFM is in the order of 3 nm in the horizontal scale and below 1 Å in the vertical scale. It is possible to image the topography of

the surface of samples that are not conductive (while STM is limited to conductive sample) in room environment but also in liquid medium or vacuum.

AFM is based on the measurement of the force applied on a nanometric tip placed near the surface of the sample (Figure 43).[181] The tip scans the surface using a piezoelectric scanner with a nanometric control of its displacement. The cantilever acts as a small spring and its deflection corresponds to the variation of height of tip. The deflection of the cantilever is measured by reflecting a laser on its extremity toward a four quadrant photodiode. The displacement of the laser on the photodiode is therefore related to movement of the tip that moves along the surface. By measuring the variation of light intensity on the split photodiode it is possible to image the topography of the substrate. Usually a piezoelectric scanner coupled to a feed-back electronic loop adjusts the distance between the sample and the tip in real time.
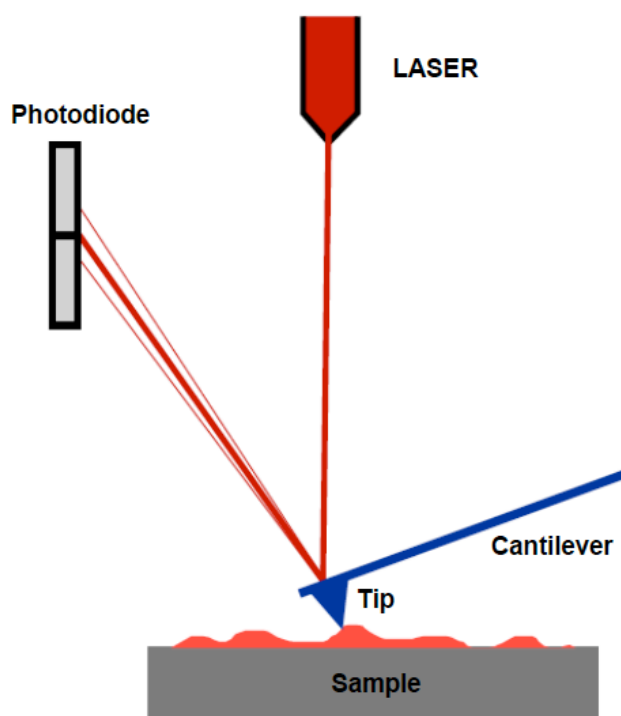
Figure 43. Schematic representation of the principle of an Atomic Force Microscope (AFM).

There have been many developments of AFM microscope in order to image the topography of materials but also to measure the friction of the tip with the surface

or the modulus of the material. We will only discuss here the contact and tapping modes.
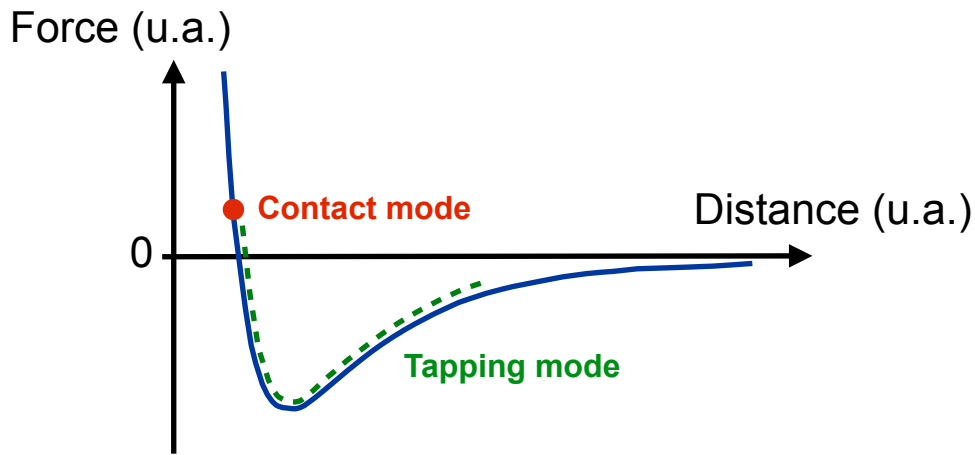
Figure 44. Lennard-Jones potential describing the tip-substrate interactions. Positions of the contact and tapping AFM modes on the potential.

The first mode that was developed was the contact mode. In this set-up the tip is close enough of the surface to feel the repulsive potential from the surface. If the substrate gets closer to the tip the force applied on the cantilever will be higher and it will bend upward to compensate. If the substrate gets further from the tip, the force applied on the cantilever will decrease and it will relax to maintain the contact with the surface. This is the simplest mode and the displacements of the laser are directly related to the topography of the substrate.

The force constantly applied on the substrate in contact mode can damage fragile samples such as polymers. To image fragile materials and to avoid tip contamination it is common to image the sample using the tapping mode or intermittent contact mode. In this mode the cantilever is oscillating near its resonance frequency. In this case the laser is constantly oscillating on the photodiode and it is the amplitude of the oscillation that are recorded. When the cantilever gets closer to the surface the repulsive wall damps the oscillations of the cantilever, when it gets further the oscillations increase. The variations of the amplitude of oscillation measured on the photodiode are representative of the topography of the substrate. Due to the short contact time and low forces applied on the sample it is possible to limit the destruction of soft samples and

contamination of the tip. The typical interactions between the tip and the surface in tapping and contact modes are represented Figure 44.

The AFM images presented here were performed in tapping mode on an AFM Multimode from Bruker Nano Surface (Palaiseau, France) with the controller Nanoscope IV from Veeco (Mannheim, Germany) and non coated silicon cantilevers (resonance frequency 300 kHz, resonance constant of 40 N/m, and radius below 10 nm). Phase and height modes were recorded simultaneously using a constant scan rate of 1.3 Hz with a resolution of 512 x 512 pixels. The samples were fixed on metallic supports with either cyanoacrylate glue for large samples or microscopy tape for small substrates.

To measure the edge profile of thick multilayers a small piece of the freestanding films was cut and transferred on an activated silicon wafer. The transfer was done with the help of a drop of water on which the film is initially deposited. After drying it with compressed air the film laid flat on the surface. The measurement was then performed as described previously.

3.3.3 Scanning Electron Microscopy (SEM)

Scanning Electron Microscopy (SEM) consists in scanning the surface of a sample with a focused beam of electrons and detecting the electrons re-emitted.[182] It is possible to produce parallel and thin (in the range of few nanometers) beams of electrons that providea resolution typically below 5 nm and a large depth of field. Under the electron beam several kinds of electrons are re-emitted (primary, secondary, back scattered, low-energy…). It is possible to sort these different electrons depending on their energy and to obtain information about the morphology and composition of the substrate. We mostly worked with secondary electron detectors that provide topologic information. Most SEM requires high vacuum and conductive substrates. In order to image non-conductive substrates it is common to sputter a thin layer on conductive material (gold, carbon, platinum…) on the sample.
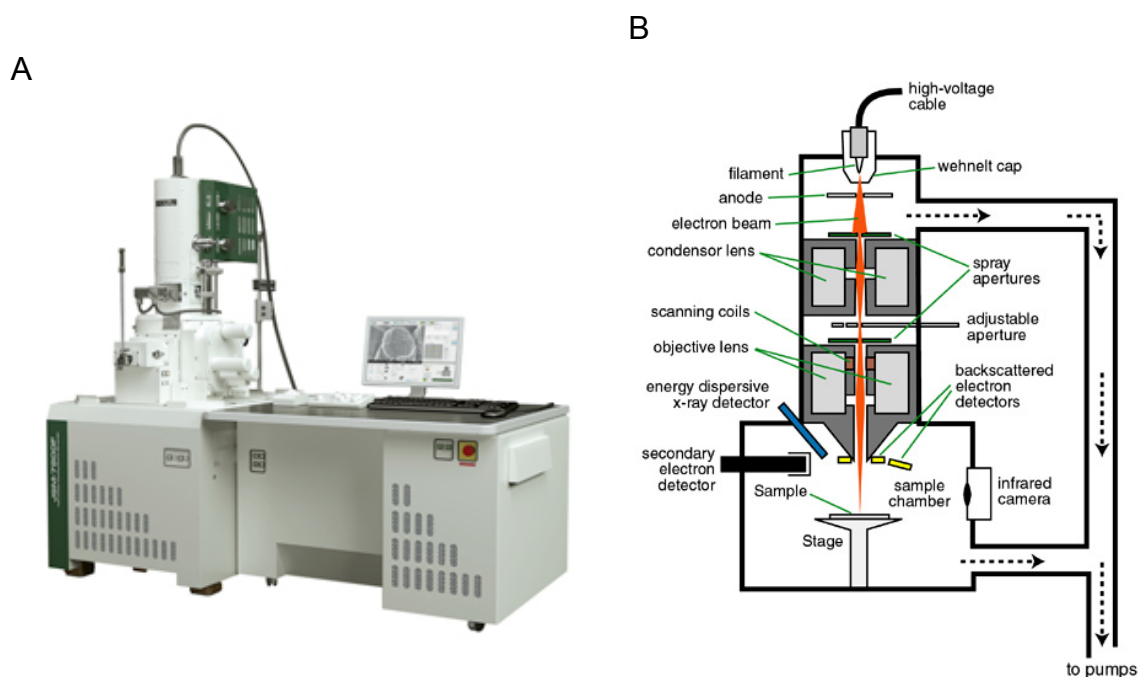
Figure 45. (A) Image of SEM from JEOL (www.jeol.com). (B) SEM overview.

Films were observed with a scanning electron microscope (JEOL 6700, JEOL SAS, Croissy-sur-Seine, France) equipped with a field emission gun (SEM-FEG) at an accelerating voltage of 3 KV. The imaging was carried out with the detector collecting secondary electrons. Before imaging the multilayer films were notched and carefully torn with tweezers in order to obtain sharp edges. Samples were glued vertically with carbon tape and about 5 nm of conductive carbon were evaporated on the surface before imaging.

3.3.4   Orientation analysis

OrientationJ is a plug-in developed for ImageJ by the group of biomedical imaging at the École Polytechnique Fédérale de Lausanne (EPFL).[183] This plug-in provides a visual image and quantification of the direction and degree of orientation from a black and white image (Figure 46).

The software defines a structure tensor for each pixel of the image that is representative of the partial derivative of the grey value of the image along the x and y directions. From this it is possible to calculate the direction of highest gradient of grey on each pixel. The direction of orientation is normal to this gradient and corresponds to the direction of the largest eigenvector of the tensor. A more

complete description of the mathematics behind the algorithm is described in the article of R. Rezakhniha *et al..*[183]
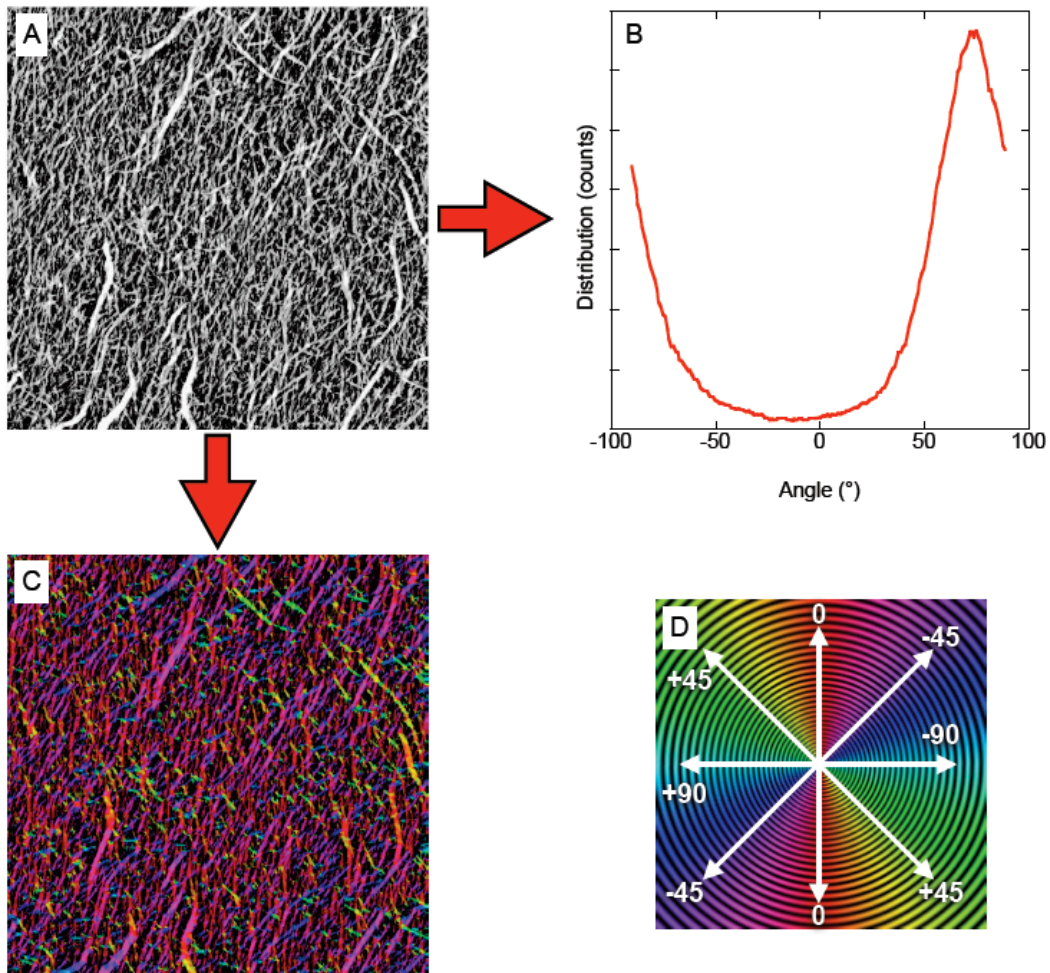
Figure 46. Treatment of a black and white AFM image (A) with OrientationJ leads to a distribution of orientation (B) and to a colorized image (C) where each color represents a direction (D).

During calculation several parameters need to be adjusted. The Gaussian window corresponds to the distance in pixel over which the grey value gradient is averaged. If the Gaussian window is too small the noise can interfere, while if it is too big small objects will not be considered. The energy is equal to the trace of the tensor matrix. The larger the energy is the less isotropic the image is close to a given pixel. It is possible to fix a minimum energy level for the calculation in order to only measure pixels that are clearly oriented. The coherency parameter is equal to the ratio between the difference and the sum of the extrema eigenvalues of the tensor. The higher the coherency is the less isotropic is the material. It is also

possible to fix a minimum coherency level for the calculation in order to remove isotropic pixels from the analysis.

The AFM images were flattened before analysis and the grey scale was typically set to 15 nm (for one layer pair of PVAm/MFC on silicon wafer) in order to visualize most of the fibers.

For our calculations we used a Gaussian window of 1 pixel because it is the diameter of the smallest fibers. We set the minimum energy and coherency values to 1% where only isotropic areas are excluded.

Drift of the sample during imaging causes an artificial orientation because the objects are moving during the scanning process. This general concern for AFM imaging is more critical when it comes to orientation analysis. We avoided office tape for fixing the sample and replaced it with SEM tape that has shorter relaxation time and does not create drift. We also avoided any large displacement of the piezoelectric platform as it is known to create drifts afterward. When there was a doubt about an image a second scan in the opposite direction was performed and the two images were compared. If there is a drift then the two images will give different orientation distributions.

3.4   Mechanical tests

3.4.1   Sample preparation

Handling and testing the mechanical properties of micrometric thin film is difficult because films tend to fly away. It is also necessary to obtain smooth edges since the presence of irregularities on the edges of the sample leads to premature breaking of the material (due to strain concentration).

In order to manipulate samples easily and to place them properly in the tensile testing machine we used a paper support. Before the test the support holds the strip of film, prevents that an external stress destroys the sample and enable manipulation without tweezers. The paper was cut before testing and did not influence the mechanical characterization.

The LbL films were cut using a scalpel blade (regularly changed to prevent tearing off the film). Typically stripes (~1.5 mm wide and 15 mm long) were cut directly

from the silicon wafer. Each stripe was then suspended, with double faced tape, on a U-shaped support (Figure 47A) consisting of a 25 x 20 mm piece of paper with a 5 x 10 mm gap in the middle.
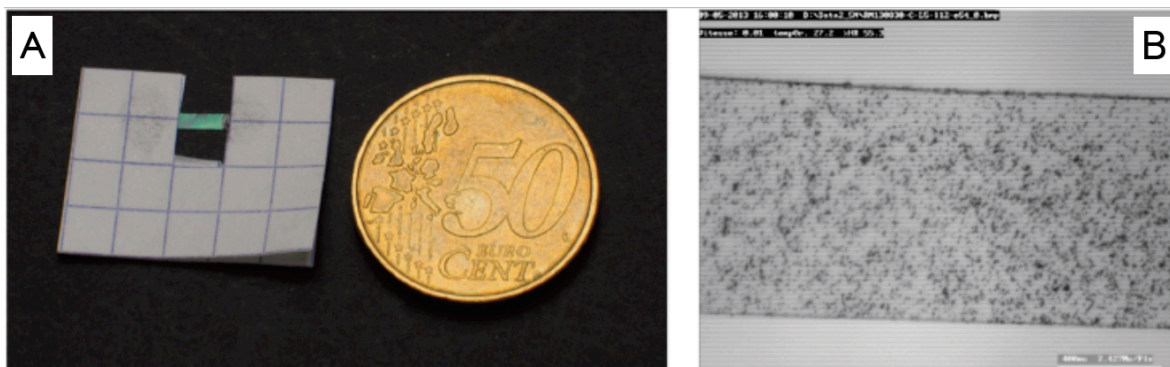
Figure 47. (A) Optical photograph of a piece of film in its U-shaped support. (B) Typical pattern observed after flicking dry toner powder on top of the film.

In order to measure the deformation of the sample during tensile testing we also needed to create a pattern on the film. It is possible to spray paint to create patterns, but the thickness of the paint layer creates *stress concentration* and leads to premature breaking. We used printer toner because it develops electrostatic charges when rubbed and stick to many surfaces. Electrostatic interactions do not damage the mechanical properties of the film. The color (black) and size of the toner powder led to ideal patterns to monitor the deformation by image correlation (Figure 47B). To create the pattern dry toner was loaded on a brush and flicked on the film from 2 cm distance. The excess was then removed using a gentle blow of compressed air.

3.4.2 Self-repairing experiments

For macroscopic self-repairing experiments a large piece (~20 x 20 mm) is cut in a freshly prepared film. Then, the piece of film was dipped into Milli-Q water and deposited on the initial film on silicon wafer (hydrophobically modified) with a small overlap (0.6 to 2 mm) (Figure 48A). The contact was made between the two upper surfaces of the film in order to prevent interference from the adhesion layer of the film (it however did not seem to make any significant difference when the back side was put in contact with the front side). The repaired film was then gently dried with a flow of compressed air and stripes (~1.5 mm wide) of films were cut with scissors

perpendicularly to the initial cut and prepared as previously described for tensile tests (Figure 48B).
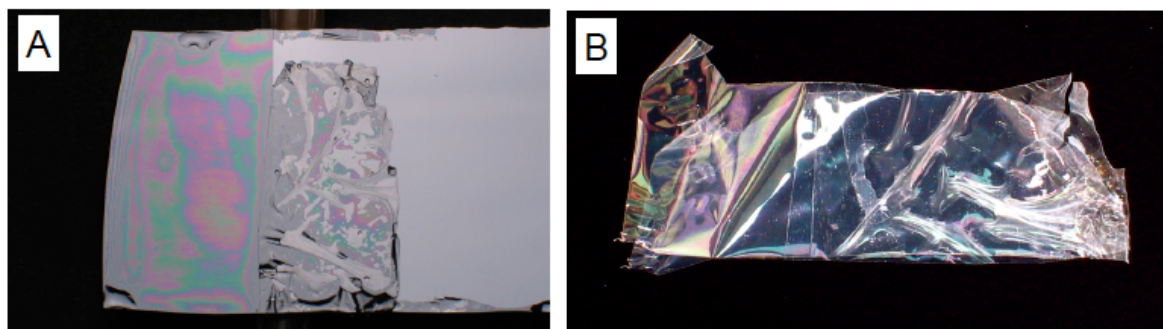
Figure 48. (A) Optical photograph of the superposition of the wet film on top of the initial film. (B) Optical photograph of a piece of film after repairing and prior to mechanical test.

For microscopic self-repairing, a small cross was done on the surface of a film prepared at pH=11 and resting on an activated silicon wafer (hydrophilic). The cross was used as reference point and the AFM image were carried out next to it. After immersion in water for a given time (5 min and 1 hour), the sample was dried with compressed air and imaged at the same position.

3.4.3 Tensile tests

Measuring the mechanical properties of stripes of LbL films with thickness in the range of few micrometers and width of 1.5 nm requires sensitive captors. For a film with a cross section of 2 µm x 1.5 mm and a stress at break of 300 MPa the force needed to break the film is 0.9 N. The traditional tensile testing machines with kilonewton captors were not suitable for these measurements. The use of thicker films would dramatically increase the time needed to prepare the sample while bigger films reduce the number of sample that can be obtained out of a film, and increase the chances that small irregularities strongly decrease the maximal stress. We used a custom made tensile test machine equipped with a 2.5 N load cell to perform the tensile tests (Figure 49A). The film support was taped to the two jaws of the machine and the measurement were performed after cutting the paper support to leave the film as only bridge between the two jaws of the instrument (Figure 49B). The tensile tests were performed at constant strain rate of 0.01

mm/s, at room temperature and the force applied on the film was continuously recorded until rupture of the film occurred.
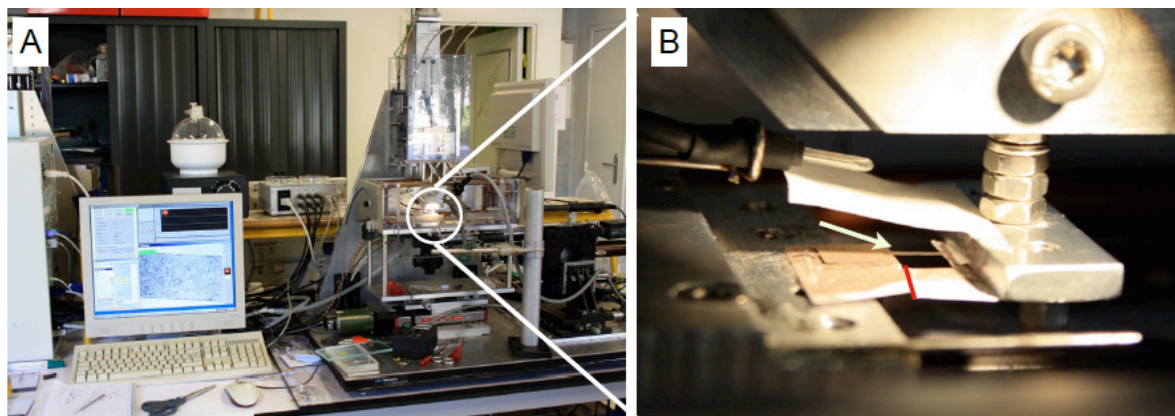
Figure 49. (A) Photography of the tensile experiment set-up. (B) Close-up on the sample set-up in the tensile test machine. The white arrow point to the film and the red line indicates the cut in the sample holder.

A video camera placed below the apparatus recorded a video of the deformation of the sample. White light was projected on white paper above the film light (Figure 49B) to provide a homogeneous white background contrast with the black toner used for patterning. The video was then used for image correlation.

We also needed to control the humidity in order to see the effect of hydration on the mechanical properties. A confined chamber could be mounted around the tensile test machine and a humidity sensor was used to monitor the humidity. Tests run at relative humidity (RH) close to 50% were performed at room conditions (actual relative humidity measured stayed between 45 and 55% and no change of mechanical properties was observed within theses values). All samples were equilibrated at room conditions for at least 24 hours before measurement. Tests run at RH <5% (below the detection limit of the humidity sensor) were carried out in a confined environment under a flow of dry filtered compressed air with an actual RH in the range of 2-3%. All samples were equilibrated before test for at least 24 hours in a dessicator cabinet with freshly activated silica gel. For tests performed in wet conditions (RH~100%) a drop of water was deposited on the upper surface of the film 5 min prior to testing (deposition 30 min prior to testing did not make any significant difference). In these tests the patterning used for the measurement of the deformation was deposited on the lower surface to prevent washing off with water. These films were kept at room conditions before measurement.

3.4.4   Image correlation

The compliance of the machine and the deformation of the tape used to fix the sample are in the same range as the deformation of the sample during the tensile test. Direct measurement of the true strain of the film by the machine was therefore impossible. Therefore, we used digital image correlation[184, 185] to measure the actual deformation of the sample. This technique tracks the displacement of a random grey scale pattern (obtained with the toner) on a sequence of images. The images are subdivided and a correlation algorithm calculates the displacement of each sub-division for every images. Since the displacement is known it is possible to calculate the local deformation of the sample in each subdivision.

In our case a 0.5 Megapixel camera was recording the test at 6 images/second with an image size of 1.86 x 1.40 mm. Typically a sequence of 60 images regularly spaced was extracted from the video and imported into the digital image correlation software, CORRELI^STC. Each image was subdivided into elements of 32 pixels and a reference image for the correlation algorithm was actualized every 5 images. The deformation was then averaged from 81 points (arranged on a 9 x 9 grid) and reported as true strain in the stress-strain curves.
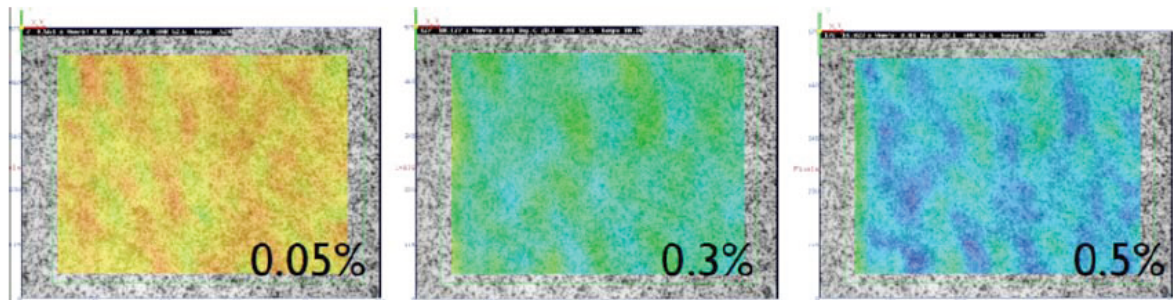
Figure 50. Visual representation of the deformation given by CORRELI^STC after image correlation performed during the measurement. The average values obtained are reported in each image.

It would be possible to obtain a direct measurement of the deformation using cyanoacrylate glue instead of double-faced tape. This would not prevent the compliance of the machine that can distort the measurement. In addition hard glue would create stress concentration if the sample were slightly misaligned. For a 5 millimeters long film breaking at 1% deformation, 50 µm of difference between the

two edges would lead to a rupture of one edge (leading to premature failure of the film) before a complete loading of the film. The soft tape used deforms upon loading and compensate for small misalignments, ensuring even repartition of the stress in the film. This allows to reach maximal stress closer to the actual value of the bulk material.

3.5 Monitoring the multilayer build-up

3.5.1 Ellipsometry

Ellipsometry is a widely used technique for surface analysis based on the measurement of a change of polarization of a light ray reflected by a planar surface.[186] The increasing need of surface characterization with the development of semiconductor industry has greatly improved the use of ellipsometry. This non-destructive technique can measure a large range of thicknesses from nanometers to micrometers. It also relies on equipments robust and easy to manipulate. We will described briefly the principle of the measurement and review its interest and limitation toward the thickness characterization of thin LbL films.

Considering an electromagnetic wave (light) reflecting on a planar surface (Figure 51). The electric field of each wave can be projected on the plane of incidence and on its normal. The reflection of the light on the surface can therefore be represented by two reflection coefficients: one for each component of the electric field r_p and r_s.

$$r_p = \frac{E_{pi}}{E_{pr}} = |r_p|\exp(i\delta_p)$$

Equation 3

$$r_s = \frac{E_{si}}{E_{sr}} = |r_s|\exp(i\delta_s)$$

Equation 4

Where $|r|$ is the modulus of the reflected electromagnetic field and δ its dephasing. The subscript p and s refer to the projection of the electromagnetic wave on the surface place (s) and perpendicular it (p). The subscript i and r refer to the incident (i) and reflected (r) wavelegth.
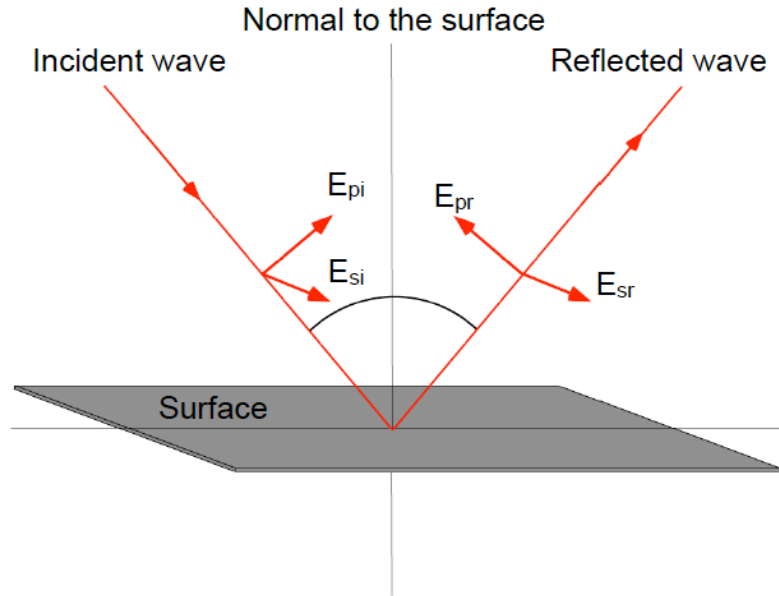
Figure 51. Schematic representation of an electromagnetic wave reflecting on a surface.

In practice the ellipsometer is sensitive to the ratio of these two coefficients.

$$\frac{r_p}{r_s} = \tan(\psi) * \exp(i\Delta)$$

Equation 5

Where $\tan(\psi)$ represents the ratio of the modules ($|r_p|$ and $|r_s|$) and Δ the dephasing induced by the reflection between δ_p and δ_p.

For a flat homogeneous thin film laying on reflecting surface the value of ψ and Δ depend on:

   - the refractive index and thickness of the thin film.

   - the refractive index of the substrate.

   - the angle of incidence and wavelength of the light used.

The user typically search the thickness and refractive index of the film while the wavelength, angle of incidence and refractive index of the substrate are known.

Several types of ellipsometers exist, for instance single wavelength ellipsometer, spectroscopic ellipsometer or variable angle ellipsometer. Simple wavelength ellipsometer is the simplest one, it gives the value of ψ and Δ only for a given incidence angle and wavelength. It can only measure the thickness of a film of known refractive index or measure the refractive index of a film of known thickness.

In addition as both ψ and Δ are 2π periodic the thickness value measured knowing the refractive index are also periodic which can induce errors. Typically our single wavelength ellipsometer had a period of 300 nm with a refractive index of 1.46, meaning that it cannot distinguish similar films of 200 nm and 500 nm.

Spectroscopic ellipsometer and variable angle ellipsometer on the other hand can gives the value the ψ/Δ couple for several wavelengths and several angles respectively. Therefore such equipment can determine at the same time the refractive index and thickness of a film without ambiguity and there is no ambiguity due to the periodicity anymore.

Ellipsometry can also be used to determine the structure of more complex films such as multilayers, rough or inhomogeneous films. Such measurements usually require deep understanding of the underlying physical phenomenon in order to properly model the structure and perform accurate measurements. During this PhD we have used both a single wavelength and spectroscopic ellipsometer. In all cases we modeled our multilayers as flat, homogeneous and transparent film and usually fixed the refractive index. While it may lead to small systematic error this type of measurement prevents that a change in roughness or turbidity distort the measurement. Since the thickness of the individual layers in the multilayers is below the wavelength of light, the refractive index can be assumed constant through the film and does not require modeling. Similarly the objects incorporated in the multilayers are small enough (< 400 nm) to consider the film homogeneous for ellipsometric models. In some cases we needed to perform simultaneous refractive index and thickness measurement on our films, this was always performed for reasonably thick samples (> 500 nm) with a flat surface (homogeneous interference colors). The refractive index found was the same for all the films measured (either with clays, microfibrillated cellulose, poly(dimetylsiloxane) derivatives or poly(vinyl amine)) and was equal to 1.55.

For thin films (up to 300 nm), the thickness measurements were carried out using a PLASMOS SD 2300 operating at a wavelength of 632.8 nm and with an angle of 70°. The refractive index was set at n=1.465. Each data point is an average of 10 measurements at random positions on the wafer. The error bars reported are the standard deviation of these measurements. This procedure leads to slightly inexact absolute thicknesses values. But it allows a quick determination of the thickness

and sufficient precision for the comparison of the buildup and homogeneity of the different films reported.

For thicker films a spectroscopic ellipsometer SENpro (SENTECH Instruments GmbH, Berlin, Germany) was used. The film was modeled as a single layer with a constant refractive index of 1.55. This values was coherent with thicknesses observed by AFM and SEM and did not appear to change with the pH of film deposition. Each thickness recorded is the average of five measurements done along the length of the sample. The error bars reported are the standard deviation of these measurements.

3.5.2   Quartz crystal microbalance (QCM)

Quartz crystal microbalance (QCM) is based on the piezoelectric properties of quartz.[187-189] A piezoelectric material becomes electrically polarized upon mechanical stress and reciprocally deforms under an electric field. In a QCM the quartz crystal is excited by an electric signal at its resonance frequency (Figure 52). A change of the oscillating mass (upon adsorption) will cause a shift of the resonance frequency. While the most sensitive analytic balances reach precision of 0.1 µg, QCM has a sensitivity two orders of magnitude lower, in the range of the nanograms. QCM can be used in liquid medium and monitors in real time the adsorption of polyelectrolytes, colloids or bio-molecules at the surface of a gold-coated crystal. It is a powerful tool to study the build-up of polyelectrolyte multilayers in complement with ellipsometry.
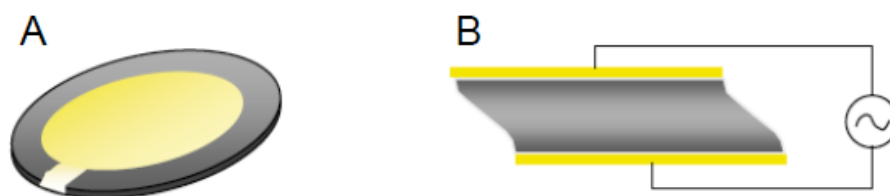
Figure 52. (A) Schematic representation of a gold-coated quartz crystal used in QCM. (B) Schematic representation of the oscillation of the quartz crystal upon excitation. This is a side view of (A) with the gold electrodes in yellow and the quartz crystal in grey. Images have been adapted from a presentation about QCM from Q-Sense AB (Göteborg, Sweden).

The development of the QCM started with the report in 1959 by G. Sauerbrey of the linear relationship between the oscillating mass and resonance frequency of a quartz crystal.[190] The equation is the following:

$$\Delta m = -C \frac{\Delta f}{n}$$

Equation 6

The variation of a resonance frequency (Δf) divided by the harmonic overtone (n) is proportional to the variation of the oscillating mass, where C is a coefficient of proportionality which depends on the geometric parameters of the crystal. In order to apply this relation the mass deposited must stay negligible compared to the mass of the quartz crystal ($\Delta f/f_0 < 5\%$) and the material adsorbed should be rigid. When monitoring the adsorption of soft material (polymer or biologic molecules) from a viscous medium (water) approximation of the Sauerbrey equation should be used.
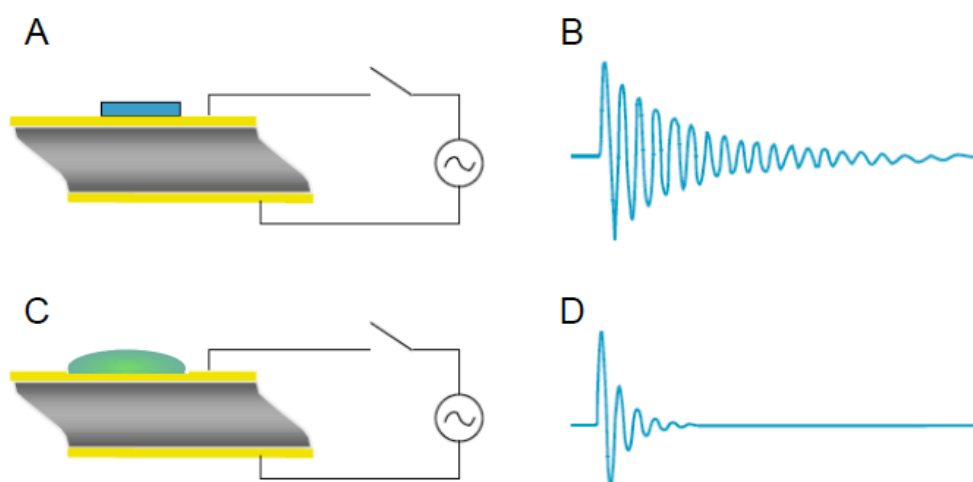
Figure 53. (A) Schematic representation of the quartz crystal after excitation and adsorption of a rigid object. (B) Exponential decay of the oscillations with a low damping observed after adsorption of a rigid object. (C) Schematic representation of the quartz crystal after excitation and adsorption of a soft object. (B) Exponential decay of the oscillations with a high damping. Images have been adapted from a presentation about QCM from Q-Sense AB (Göteborg, Sweden).

Some of the recent QCM monitors at the same time the resonance frequency and the dissipation (this is a measure of the bandwidth of the resonance frequency and it is proportional to the invert of the quality factor). The dissipation is indicative of

the energy loss of the system (due to viscosity of the material deposited and solution, roughness of the deposit…). In QCM the crystal is excited for a short time, the excitation is stopped and the decay of the oscillation is recorded. From this it is possible to calculate the free resonance frequency and the dissipation of the system. The resonance frequency corresponds to the period of the oscillations and the dissipation to the damping speed of the oscillations. If the material adsorbed is rigid the damping is low (Figure 53A and B) and if the material adsorbed is soft the damping is high (Figure 53C and D).

In polyelectrolyte multilayer the amount of water trapped in the film before drying, the softness of the polymers adsorbed and the viscosity of the solution used often leads to a good approximation of the amount of material deposited using Sauerbrey equation. In this work we did not attempt to do these calculations and only considered the frequency and dissipation variations.

QCM-D is a sensitive technique to produce reproducible results. Therefore, many parameters should be controlled during the deposition. The temperature affects the viscosity of water and therefore should be kept constant during the measurement (± 0.05 °C). Changing the composition of a solution also changes its viscosity; therefore the measurement of frequency shift associated to an adsorption of material should always be done in the same medium. In our case the frequency shifts were calculated for films built in Milli-Q water. The choice of the overtone recorded is also crucial. As the overtone increases the sensitivity of the QCM increases (this is visible in the Sauerbrey equation where the overtone is at the denominator) as a counterpart the penetration depth decreases with the overtone. It is usual to use overtones between 3 and 13 for the measurements. In our case we monitored the growth using the fifth harmonic. We also recorded the first harmonic to be able to see some absorption beyond the penetration depth of the fifth harmonic. All measurements were carried out on a QCM-D E4 (Q-Sense AB, Göteborg, Sweden). The precise description of the method for LbL deposition in QCM cell has been described earlier in part 3.2.6.

3.6   Other characterization techniques

3.6.1   Dynamic Light Scattering (DLS)

Dynamic light scattering (DLS) is used to measure the size distribution of small particles in solution.[191] Nanoparticles subject to light undergo elastic scattering (also called Rayleigh scattering), and emit light in all direction (for large particles with dimensions close to the light wavelength and above the emission is not isotropic). DLS consists in shining a laser on a solution to analyse while a photo-detector collects the light scattered (in our apparatus the collector made an angle of 173° with the laser). Because the light emitted by the laser is coherent the light scattered is also coherent. At the detector the light scattered by the different particles undergo constructive or destructive interferences depending on the distance between the particles. Since the particles in solution are subject to Brownian motion the interferences changes and intensity recorded by the captor vary with time. The Brownian motion is a function of the size of the particles therefore it is possible to recover the size and distribution of the particles from the variation of scattered intensity. The data treatment is usually done using an auto-correlation function that measures the similarity of the curve to itself as function of the time lag considered. The slower the intensity variations are (large particles) the longer the curve stays similar to itself. (Figure 54)
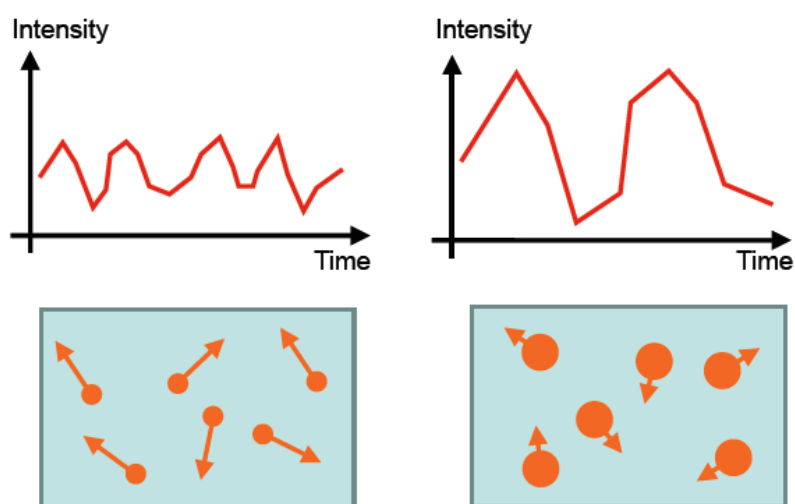
Figure 54. Schematic representation of the variation of scattered intensity with time for small particles (left) and big particles (right).

DLS is used to measure the size of sub-micrometer particles. The intensity of light scattered in the elastic regime is proportional to the hydrodynamic radius at the power six therefore the intensity of light diffused by big particles is much higher than the light diffused by small particles. In consequence it is difficult to estimate the size distribution of polydisperse samples and in most cases the fraction of small particles is underestimated. The size calculated by DLS is based on the Stokes-Einstein equation, which suppose spherical particles. When DLS is used to measure non spherical particles (such as clay platelets) the size recorded corresponds to the equivalent hydrodynamic radius of the particles which is neither the platelet thickness nor their diameter. The hydrodynamic radius nevertheless increases with the size of the platelets (and their aggregation). DLS is an effective way to estimate the size of the biggest particles of a solution even if in our case it is not quantitative. All the measurements have been performed on a Zetasizer Nano-ZS device (Malvern Instrument, Ltd., UK) at a scattering angle of 173º and a wavelength of 632.8 nm (He/Ne Laser) and at 25 ºC. Each sample has been measured three times; the size and polydisperisty reported corresponded to the average value of these measurements. We used standard disposable cuvettes (Malvern Instruments, Ltd., UK) that were rinsed with Milli-Q water prior to the introduction of solution.

3.6.2   X-ray photoelectron spectroscopy (XPS)

X-ray photoelectron spectroscopy (XPS) is a technique based on the measurement of the kinetic energy of electrons emitted by a sample under X-ray irradiation.[192, 193] Upon irradiation with photons (light) of sufficient energy any material emits electrons called photoelectrons. Since the energy levels of electrons of an atom are quantified, the kinetic energy of the photoelectrons emitted upon irradiation with monochromatic light (in our case X-ray) is also quantified. Each atom emits a set of photoelectrons with specific energies (the kinetic energy of the electron is equal to the energy of the photon received minus the energy of the orbital). Each element has, therefore, a defined XPS spectrum. XPS looks at the core electrons of the elements (because of the high energy of X-rays). The energy of the photoelectrons emitted is therefore primarily defined by the nature of the element (large difference between the peaks of different elements). The chemical

environment of the element also influences the position of the peak but the variations are small and often lead to convoluted peaks. While elemental analysis using XPS is straightforward the identification of the different environments asks more practice. To summarize XPS is a quantitative analysis technique that gives information about the composition, chemical state and electronic state of the elements at the surface of a material.

The experimental set-up of the analysis is presented in Figure 55. Typically a X-ray source shines monochromatic X-rays on a sample placed in ultra high vacuum. The photoelectrons emitted by the sample are collected, passed through an electron energy analyzer and detected. An energy scan of the analyzer provides via the electron detector an XPS spectrum.
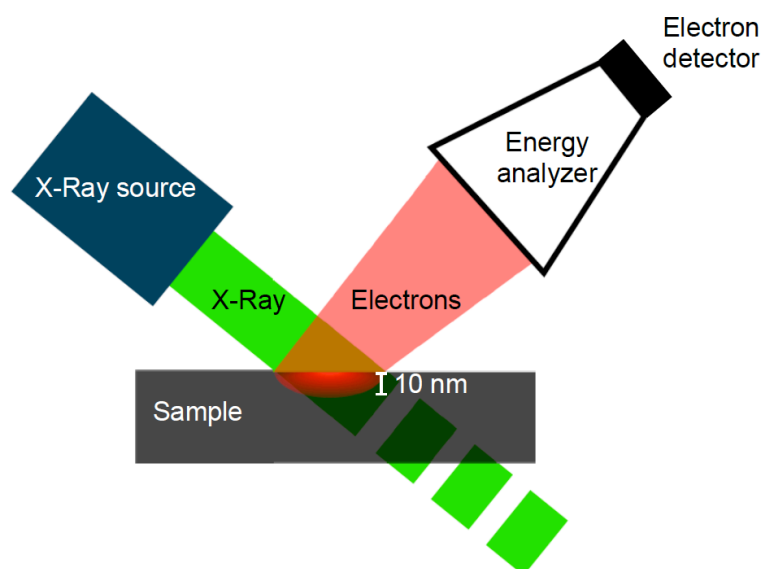
Figure 55. Schematic representation of an XPS set-up. An X-ray beam (green) is focused on the surface of the sample (grey) and the photoelectrons emitted by the surface of the sample (red) are analysed.

While X-ray can easily go through the material, the photoelectrons emitted are quickly diffracted and adsorbed by the material. Most of the electrons at the surface of the sample reach the detector while at 10 nm of depth the electrons do not escape the material and cannot be analyzed (at 3 nm depth the detection is already limited). XPS is therefore only sensitive and quantitative to the surface of the sample. In layered materials the composition of the surface layer is over-

represented compared to the other layers. Rough or porous surfaces are also difficult to analyze because the electrons in the holes may not reach the detector.

Experimentally the photoemission spectra of the films were recorded from multilayers deposited on silicon wafers. The measurements were performed on a Multilab 2000 (Thermo) spectrometer equipped with Al Kα anode (hν = 1486.6 eV). The nitrogen to carbon ratio have been calculated using the sensitivity factors, as determined by Scofield[194] directly on the nitrogen and carbon peaks respectively at 399.7 eV and 285.2 eV. While the peaks comported several contribution from different chemical environments we considered them as single peaks and did not perform deconvolution.

4 Clay-containing hybrid multilayers

Following the work reported by Kotov et al.,[5] the objective of this work is to build "elasto-rigid" LbL-films mimicking the structure of nacre or bones. Our strategy is to combine clay, a hard nano-reinforcing element, with polydimethylsiloxane, a soft "elastomeric" matrix, in order to distribute the stress among the hard platelets and maximize the strength of the films. A first investigation on the influence of the preparation on their assembly sets the basis of our work. We have then investigated the impact of the deposition condition (nature of the polyelectrolyte, pH, drying step) on the growth of clay-containing multilayers before looking at their combination with polydimethylsiloxane derivatives. The mechanical properties of the resulting nacre-inspired multilayers will be discussed at the end of this chapter.

4.1 Clay suspensions and their assembly in films

The mechanical properties of clay-containing multilayers depend on the chemical nature of the clay, their degree of exfoliation and their polydispersity. Therefore we realized the following study in collaboration with Süd-Cemie (now Clariant).

4.1.1 Purification of clay suspensions

Simple agitation of a clay powder in deionized water for a couple of days leads to turbid suspension (Figure 56 Left). This suspension consists of well-exfoliated clay sheets, clay aggregates and some impurities. We purified this solution in order to understand and optimize the deposition of clays. Several techniques can be used

to separate the constituents of the suspension. Sedimentation is the simplest, the solution is left to rest without agitation before extracting the supernatant. While sedimentation for one day allowed removing some big aggregates the supernatant was still turbid revealing the presence of small aggregates. In order to separate them from well-exfoliated platelets we used centrifugation. In this technique a tube containing the suspension rotates around an axis, the resulting centripetal force accelerates significantly the sedimentation of the particles. Our centrifuge was able to reach 10000 g at 16000 rpm. At this speed one hour is sufficient to remove a large part of the small aggregates and to produce a quite transparent solution (Figure 56 Right). Sedimentation has also been used to separate large and small exfoliated clay platlets.[195]
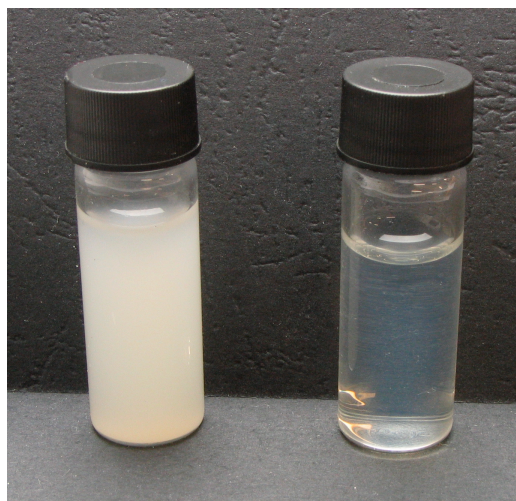
Figure 56. Optical image of EXM2039 suspension at 5 g/L in water after agitation for three days in water (left) and of the supernatant recovered after centrifugation at 1000 g for 1 hour (right).

Within our collaboration with Clariant® we received five different samples of clays. The three first samples were similar in composition but were produced through different treatments; they all have a cation exchange capacity of 113 meq/g:

EXM 1289 is a natural montmorillonite with sodium and calcium ions;

EXM 1246 is a sodium-activated montmorillonite with mostly sodium counterions;

EXM 2039 is a phosphonate-activated montmorillonite with phosphonate and sodium counterions.

The two last samples had different origins and were provided without specific treatment:

EXM 0242 is a natural montmorillonite with a cation exchange capacity of 99meq/g;

EXM 1743 is a natural montmorillonite with a cation exchange capacity of 66meq/g.

We prepared dispersions of each clay sample at 5 mg/mL in water and stirred them for three days in order to exfoliate them. Then we looked at the quantity (solid mass remaining after solvent evaporation) and size of the particles present in the supernatant after each consecutive purification step.
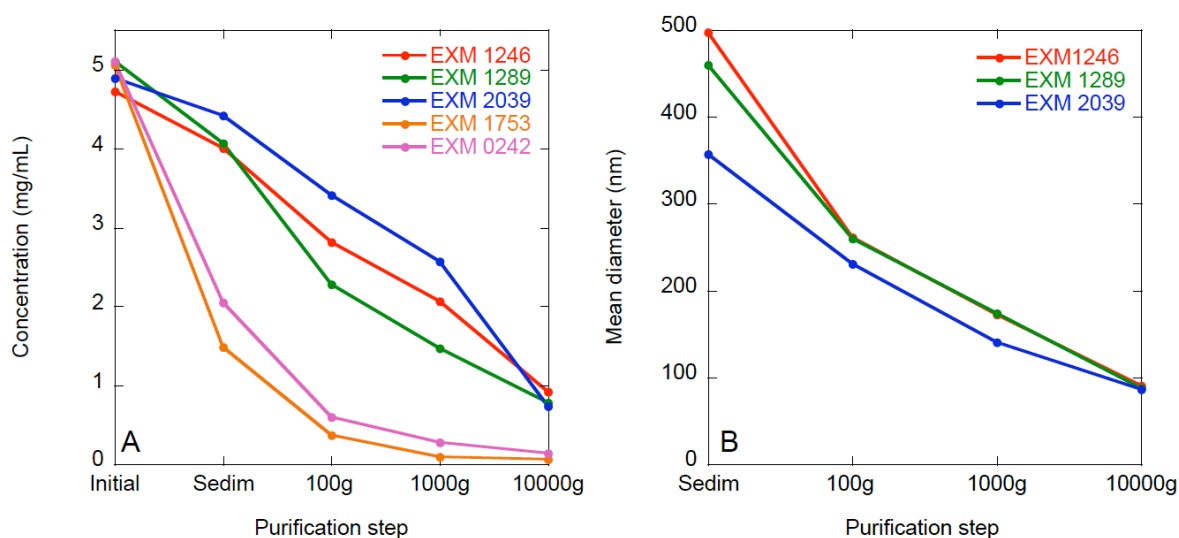
Figure 57. (A) Concentration of clays in the supernatant after sedimentation for one day, then centrifugation for one hour at 100, 1000 and 10000 g. (B) Mean diameter of the particles measured by DLS (weighed in intensity) in the supernatant of the solution after each purification step.

It appears clearly (Figure 57A) that the two samples with low charge density (EXM 1743 and EXM 0242) did not disperse properly. Most of the material was removed after sedimentation. Due to their large polydispersity and their low concentration in the supernatant, these particles were difficult to characterize and to use for multilayer build-up. Therefore, we did not work further with these two samples.

The exchange of calcium for sodium counterions improves the dispersion of the clays. As we can see in Figure 57A, the concentration of particles in the supernatant decrease less at each purification step for EXM 1246 than for EXM 1289. Similarly the activation of clays with phosphonates (EXM 2039) increases the amount of exfoliated particles in the supernatant obtained below 10000 g. The solid residue collected after sedimentation or centrifugation at 100 and 1000 g was

tubid while at 10000 g a clear gel was obtained. The turbidity of the solutions or solid residue is indicative of the presence of clay stacks that diffuse light. Well-exfoliated particles do not diffuse visible-light and lead to transparent solutions and gels. As solutions were transparent at 1000 g (Figure 56 left) they probably already contained mainly exfoliated particles. The centrifugation step at 10000 g starts to remove large exfoliated clay particles while small ones stay in solution. This explains the sedimentation of a clear gel at 10000 g. The amount of sediments collected after centrifugation at 10000 g is higher for phosphonate activated than for sodium-activated montmorillonite, which is itself higher than the one obtained for natural calcium-sodium montmorillonite. The different activation steps seem to increase the amount of large exfoliated clays in the supernatant obtained after centrifugation at 1000 g. After centrifugation at 10000 g concentration and size of the particles in the supernatant is the similar in all cases.

We observed by Dynamic Light Scattering (DLS) that the size of the particles in the supernatant decreases during purification (Figure 57B). However, the size determined is a relative value because the model for evaluating DLS data is based on spherical particles and the sensitivity of the measurement is function of the size of the objects. We can still observe that the size of the biggest particles decreases with the speed of centrifugation. Up to 1000 g EXM2039 gives smaller particles than EXM1289 and EXM1246 probably because the amount of aggregates is lower. After centrifugation at 10000g the supernatant solutions contain clay particles of similar size and concentration independently of the clay pretreatment.

Centrifugation has a significant effect on size and concentration of the clay particles in the supernatant. We will now see how clay purity affects the growth and aspect of layer-by-layer assembled films.

4.1.2 Influence of the purity of clay solution on the film growth and morphology

The influence of clay purity was studied by building clay-based multilayer films from clay solution obtained after sedimentation and after centrifugation at 10000 g by dipping. As expected, we can observe in Figure 58A that all films show a linear growth but films built with the supernatant from sedimentation are thicker than films

built with the supernatant after centrifugation at 10000 g. The presence of larger non-exfoliated clay stacks in the supernatant after sedimentation explains the faster growth for theses systems. The stacks are bigger than exfoliated clays and their adsorption on the film causes a larger thickness increase. We observed that EXM2039 gives the thinnest films after sedimentation because it contains more exfoliated particles. Natural EXM1289 gives thinner film than EXM1246. The difference is in agreement with the DLS results where sodium activated suspensions presented slightly larger particles than the natural one after sedimentation (Figure 57B). The large error bars for the thickness of the films built from sedimented supernatant compared to centrifuged ones are caused by the poor homogeneity of these solutions (Figure 58A). For clay solutions recovered after centrifugation at 10000 g, all the films grow almost at the same speed but the thickness increment for clay is lower than for clay solutions after sedimentation. Film homogeneity is higher (smaller error bars) with centrifuged solutions than with sedimented ones. From another experiment not represented here it appeared that two films built from the clear gel residue or the supernatant after centrifugation at 10000 g had the same film growth increment (around 1.7 nm per layer pair). The construction of films with well-exfoliated platelets, i.e. after centrifugation at 1000 g or higher, leads to a steady growth and homogeneous films. It is independent of the pre-treatment and of additional centrifugation steps.

The photographs (Figure 58B and C) show the macroscopic aspect of clay-based LbL films prepared with sedimented and centrifuged clay solution respectively. The light diffusion (inhomogeneous white patterns) visible on the film built from sedimented solutions reveals the presence of bigger aggregates. The white patterns visible on the surface prepared from sedimented solution are the macroscopic manifestation of the thickness inhomogeneity reported before. Films built from supernatant recovered after centrifugation at 10000 g did not diffuse light.
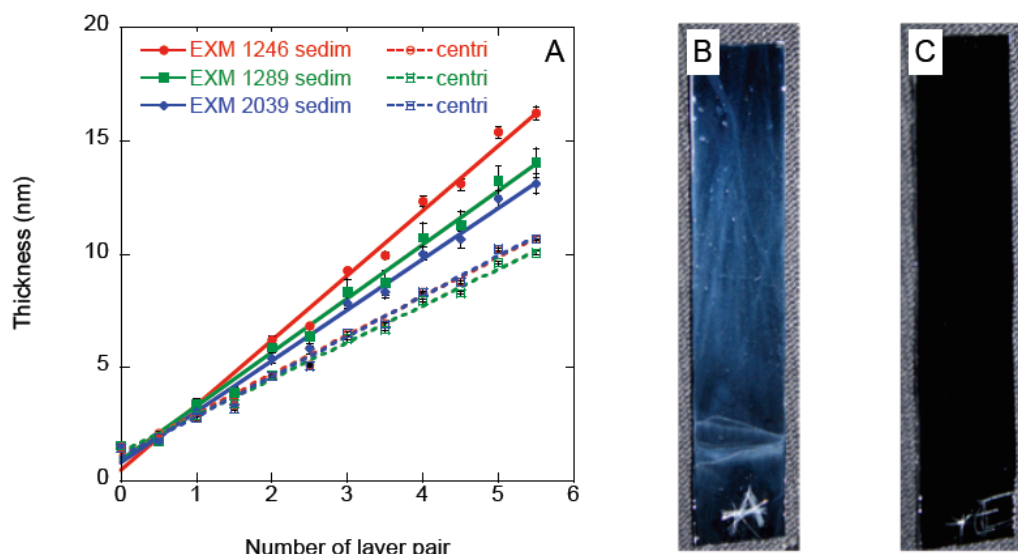
Figure 58. (A) Variation of the thickness of clay-based films as a function of the number of layer pairs followed by ellipsometry. Films were prepared on silicon wafers pre-coated with poly(ethylene imine) (PEI) with a poly(diallyldimethylammonium chloride) (PDDA) solution (1mg/mL) and montmorillonite solutions (EXM1246, EXM1289 and EXM2039) purified either by sedimentation (plain lines) or by centrifugation at 10 000 g (dotted lines). (B) Optical photograph (light diffusion) of a non homogeneous PEI[EXM1289/PDDA]$_5$ film prepared with a clay solution purified by sedimentation. (C) Optical photograph (light diffusion) of a homogeneous PEI[EXM1289/PDDA]$_5$ film prepared with a clay solution centrifuged at 10000 rpm.

This observation confirms results observed by ellipsometry where lower error bars were obtained for films built from centrifuged clay solutions. In order to obtain homogeneous films that do not diffuse light, ie transparent films, the clay solutions need to be transparent which require a centrifugation step at 1000 g, at least. We will now see how the pretreatment and the centrifugation steps change the microscopic morphology of the film.

4.1.3 Microscopic characterization of the different clays

Morphology of the clays and of the clay-based LbL films was determined using atomic force microscopy (AFM). The AFM images of films built with EXM1246, EXM1289 and EXM2039 are fairly similar (Figure 59). The film built with EXM2039 (Figure 59C) appears a little bit smoother but since this image was performed on a different day than the two others with a different tip, that could be an artifact. The pretreatment of the clays did not appear to dramatically modify the morphology of

the multilayers. Since the build-up speed and the morphology of the films were independent of the clay pretreatment we decided to use mainly EXM2039. We have seen previously that the phosphonate pretreatment increases the amount of particles dispersed (at 1000 g) leading to solutions with a higher amount of dispersed material. The large roughness of such multilayers, however, prevented us to determine precisely the size and the shape of individual clay platelets.
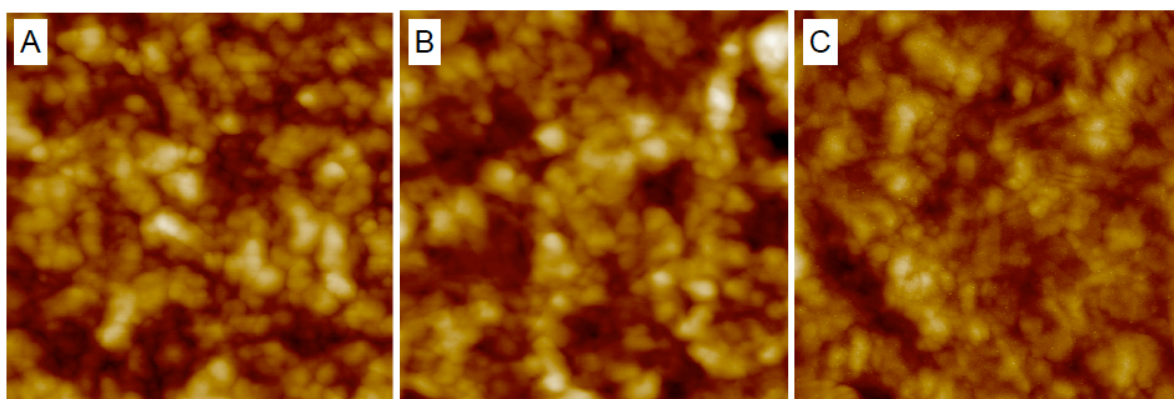
Figure 59. AFM height images of PEI[Clay/PDDA]₅ films where Clay corresponds to EXM1246 (A), EXM1289 (B) or EXM 2039 (C). The clay suspension was purified by centrifugation at 1000g. Vertical scale bar is 30 nm. Images are 1x1 μm.

The shape of clay platelets is more visible on a single layer pairs because the particles stand out on the low roughness of the silicon substrate. We deposited a single layer of EXM2039 on a PEI coated silicon wafer. As expected the centrifugation step has an impact on the size of the adsorbed platelets. Centrifugation at 10000 g allows separation of big particles (Figure 60B) from smaller particles (Figure 60A). We can still see some small particles among the big ones in Figure 60B. They were probably close to the bottom of the tube during centrifugation and got trapped in the gel. It is also possible to see some aggregated particles in the gel obtained after centrifugation (Figure 60C). it is probable that a longer beforehand centrifugation at 1000 g would have allowed to get rid of them. Similarly a longer centrifugation time at 10000 g would probably have lowered the size of the particles in the supernatant. This study opened a way to control the size of the clay particles before their incorporation in the multilayers.
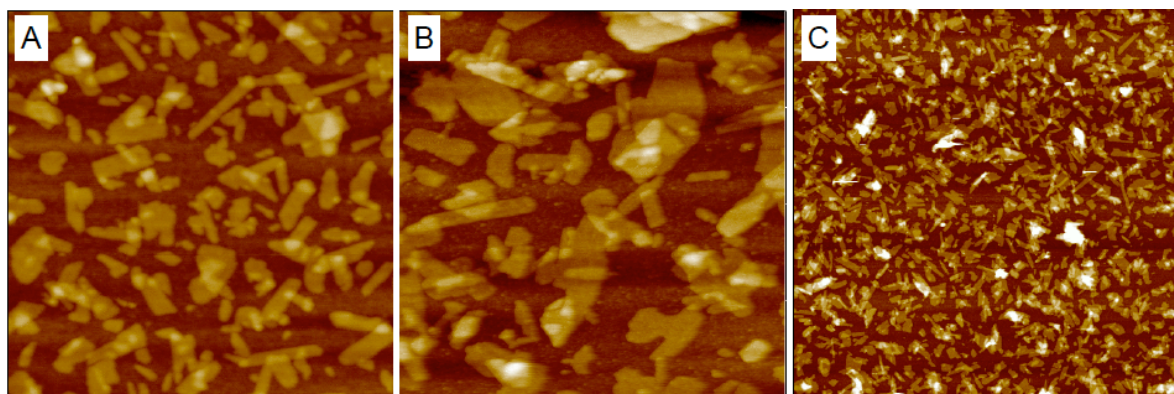
Figure 60. AFM images of EXM2039 solutions deposited on PEI coated silicon wafer as a function of their purification: (A) Supernatant after centrifugation at 10000 g for two hours. Size 1x1 μm; (B) Re-dispersed transparent gel obtained after centrifugation at 10000 g of a solution previously centrifuged at 1000 g. Size 1x1 μm. (C) Lower magnification of (B). Size 5 x 5 μm. Vertical scale bars are 10 nm.

This work, carried out in collaboration with Clariant®, sets the basis for the construction of clay-containing multilayer with focus on the impact of the clay solution on the film growth. We have seen that some clays are easier to disperse than others and that clay suspensions free of aggregates are necessary to build films of good quality. The pretreatment of the clays has an impact on the quantity of clay dispersed in solution, but does not appear to change the construction and the morphology of the film obtained. Centrifugation can be used to remove big aggregates and choose the size of the particles that will be deposited. We will now look at the influence of polyelectrolyte choice and construction parameters on the build-up of clay-based multilayers.

4.2   Controlling the build-up of LbL assembled clay films.

Many parameters have been used to modify the structure of layer-by-layer assembled films.[89, 95, 116] The objective of this project is to measure the mechanical properties of freestanding films. This requires films with thickness in the micron range to support manipulation and characterization. In this chapter we studied the impact of some assembly parameters such as the nature of the polyelectrolyte and the pH of deposition on the film growth. The objective was to find parameters that would allow the fast production of high quality films.

4.2.1 Nature of the polyelectrolyte and degree of ionisation.

As clays are negatively charged, two positively charged polyelectrolytes were selected for the buil-up of multilayer films: poly(diallyldimethylammonium chloride) (PDDA) and poly(vinyl amine) (PVAm). PDDA is a strong polyelectrolyte bearing quaternary ammonium groups (Figure 61B). Therefore its degree of ionization does not change with the pH. As such it was an interesting polyelectrolyte to study the influence of clay treatment on the growth but the possibilities of control over the construction are limited since its degree of ionization is constant. In order to later combine clays with poly(dimethylsiloxane) derivatives we needed a polymer bearing primary amine groups that can react covalently. We choose poly(vinyl amine) (PVAm) because of its high density of primary amine groups. Poly(vinyl amine) is a weak polyelectrolyte and its degree of ionization varies with the pH. Primary amine such as isopropylamine have a pKa of 10.5. However, as the amine groups are densely packed along the chain in PVAm, its degree of ionization at pH 8 is close to 0.3 and it decreases to 0 at pH 12 (see Figure 81A).[196]
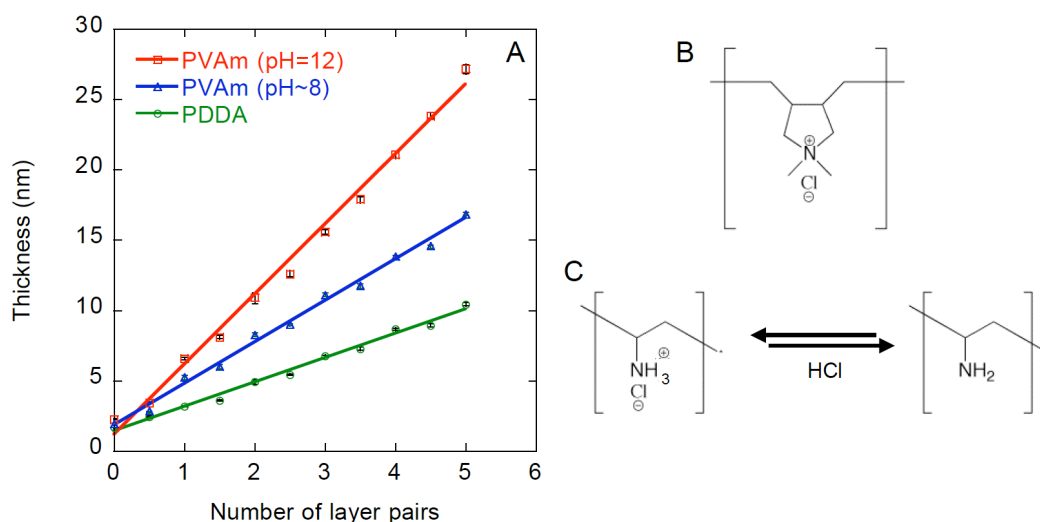
Figure 61. (A) Variation of thickness for multilayers composed of EXM1246 and either PDDA a strong polyelectrolyte or PVAm a weak polyelectrolyte as a function of the number of layer pairs. The pH of the PVAm solution was left as unmodified (pH~8) or adjusted with NaOH above to pH=12. (B) Chemical structure of PDDA. (C) Chemical structures of PVAm as a function of the pH.

The effect of the degree of ionization of the polyelectrolyte on the construction of the film appears clearly on Figure 61. Films built with PDDA (1.7 nm/layer pair) grow slower than films built with poly(vinyl amine) at pH=8 (2.9 nm/layer pair). Decreasing the degree of ionization of the poly(vinyl amine) also increases the thickness increment per layer. At pH=12 the thickness increment per layer pair reaches 4.9 nm/layer pair. Charge stoichiometry in the film can explain[93] the increase in thickness increment with decreasing degree of ionization. The amount of polymer needed to compensate the charge of the clay layer increases when the charge of the polymer decreases. The actual explanation for the increase of build-up with pH increase might involve more complex arguments such as changes of the polyelectrolyte conformation. It is actually surprising that there is a construction at pH 12 since the degree of ionization of poly(vinyl amine) is close to zero.[196] In this case electrostatic interactions are probably replaced by hydrogen bonding and it is also possible that proximity of the clay platelets promotes the apparition of charges on the polymer chains. We tried to answer some of these questions by following the kinetics of adsorption using quartz crystal microbalance (QCM).

Following the growth using QCM leads to the same observations than ellipsometry, the film built at pH=12 grows faster than the film built at pH=8 (Figure 62 and Figure 63). As expected the amount of poly(vinyl amine) adsorbed from the solution at pH=12 is higher than the amount adsorbed from the solution at pH=8 (Figure 62). The amount of adsorbed clays also increases when the pH of the PVAm solution increases, even if the pH of the clay solution remains equal to 10. The large amount of PVAm adsorbed on the film at high pH certainly promotes the adsorbtion of a large amount of clay. Nevertheless, the ratio clay/poly(vinyl amine) in the film decreases when the pH of the PVAm increases. This confirms that the increase of layer thickness increment is promoted by an increase of polymer content in the multilayer in order to compensate the charge of the clay layer.

The adsorption times of PVAm and clays are also higher at high pH. This is certainly due to the higher amount of material deposited. The lower charge density in the film at pH 12 makes them softer[95] and allows more rearrangements on the surface and therefore longer adsorption times. We will see in the next part that there is also certainly some diffusion of the polymer in the film at high pH.
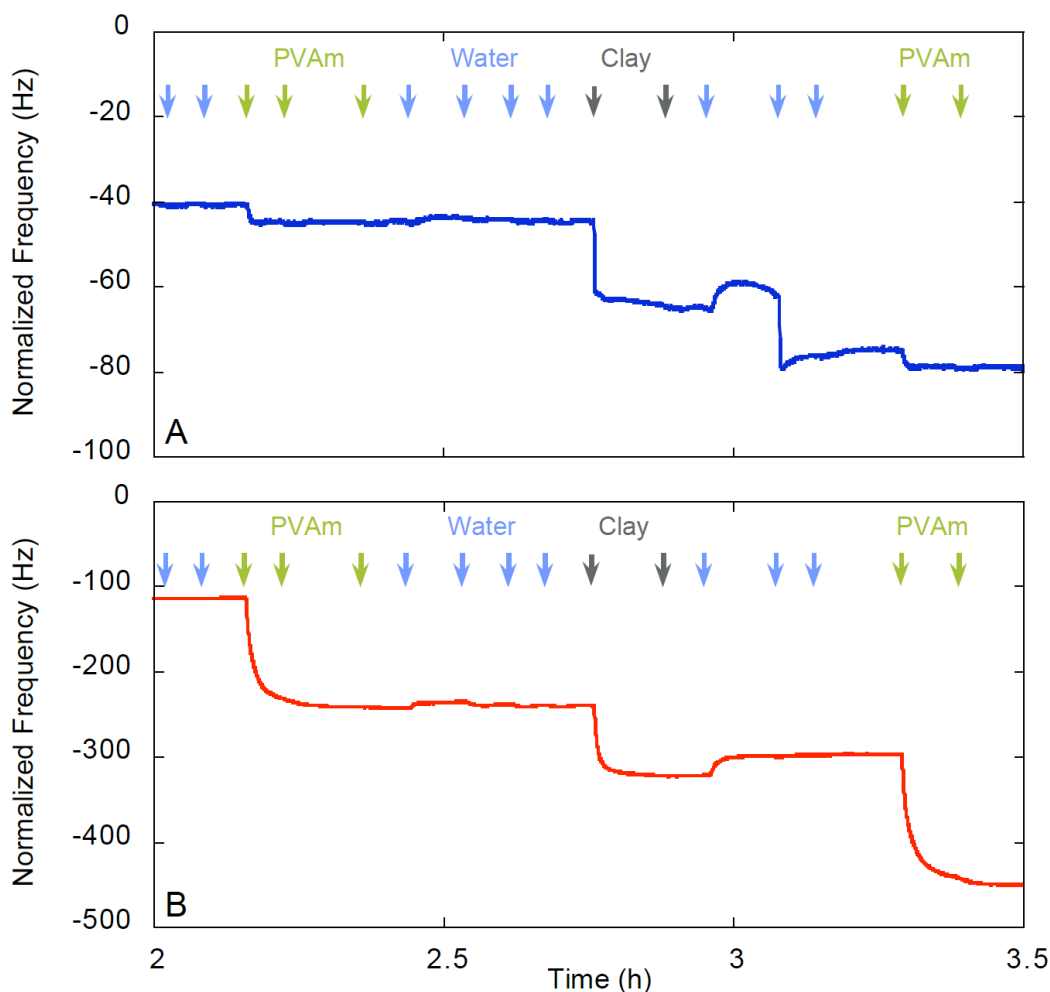
Figure 62. Frequency variationof the fifth harmonic as a function of time observed by QCM for the construction of EXM2039 and PVAm. Both curves start from the 3rd layer of PVAm. (A) PVAm solution at pH~8. (B) PVAm solution at pH 12. The arrows on the top of the curves indicate the injection of the different solutions.

We see in Figure 62A a surprising shift in the frequency during the second rinsing after deposition of clay. What appears as an adsorption of material (mass increase) is probably due to a swelling of the film in Milli-Q water. A simultaneous increase of the dissipation (not shown here) confirms this hypothesis. When the film swells, the apparent mass increases because water molecules enter in the film. At the same time the film becomes softer which causes the increase in dissipation.

We have shown that it was possible to build clay-based LbL films with poly(vinyl amine) and that these films were growing faster than with poly(diallyldimethylamonium chloride). We also observed that increasing the pH of the PVAm solution allowed to reduce the construction time of thick multilayers. Surprisingly the film did not show similar build-up behavior (linear versus

superlinear) when the growth was followed by QCM or ellipsometry (Figure 61 and Figure 63A). We tried to understand this phenomenon by studying a major difference between experiments carried out by ellipsometry and QCM: the drying.

4.2.2   Effect of drying during build-up by dipping

If the density of the film is constant, the thickness of the film is proportional to the mass of material adsorbed. In consequence the frequency shift observed by QCM, which is proportional to the mass of the film (for rigid films), should be proportional to the thickness measured by ellipsometry. Surprisingly we observed for (clay/PVAm)$_n$ films built at similar conditions linear growth using ellipsometry (Figure 61) and super-linear growth using QCM (Figure 63B).
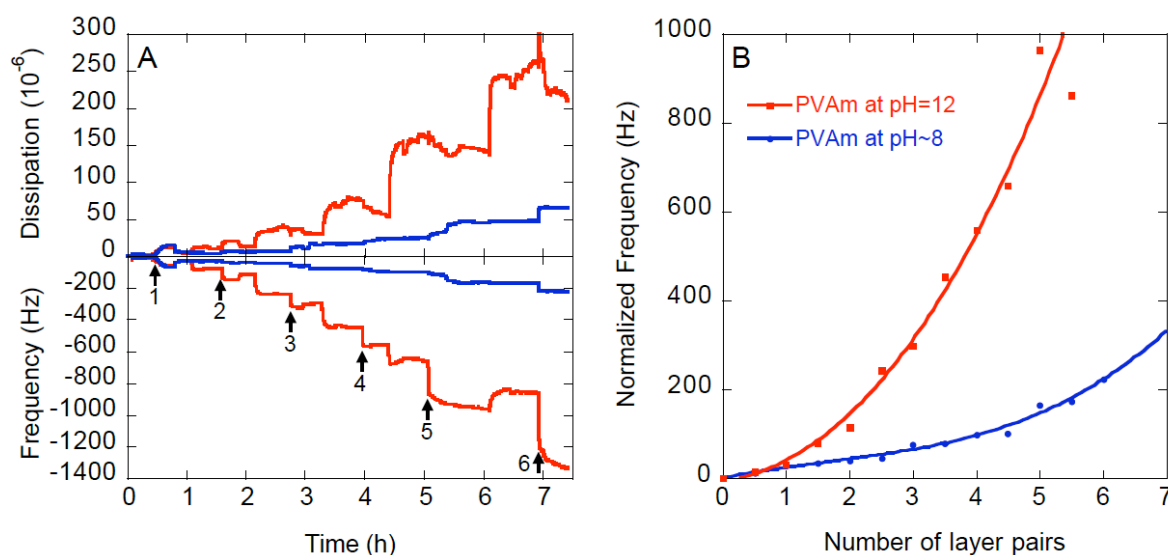
Figure 63. Monitoring the construction of [EXM2039/PVAm]$_n$ films with PVAm at pH~8 and pH=12 by QCM at the fifth harmonic. (A) Normalized frequency and dissipation curves. The numbers correspond to the adsorption of clays and to the number of layer pair. (B) Frequency variation observed after deposition of each layer.

We can see in Figure 63A and B that the amount of material adsorbed at each step increases with the thickness of the film. It appears more clearly with the PVAm solution at pH=12 than at pH=8. The superlinear increase at pH=8 becomes more visible for the fifth and sixth layer pairs. The high dissipation values observed for both films makes analysis of the amount of adsorbed material only qualitative (out of the range of application of the Sauerbrey equation). However the shape of the build-up curves shown in Figure 63B is correct. The apparent desorption for the 5th

and a half layer pair at pH=12 in Figure 63B corresponds to a film thickness higher than the penetration depth of the fifth harmonic of the QCM,[98] therefore it should not be considered. This desorption was not visible on the first harmonic of the crystal which has a larger penetration depth.
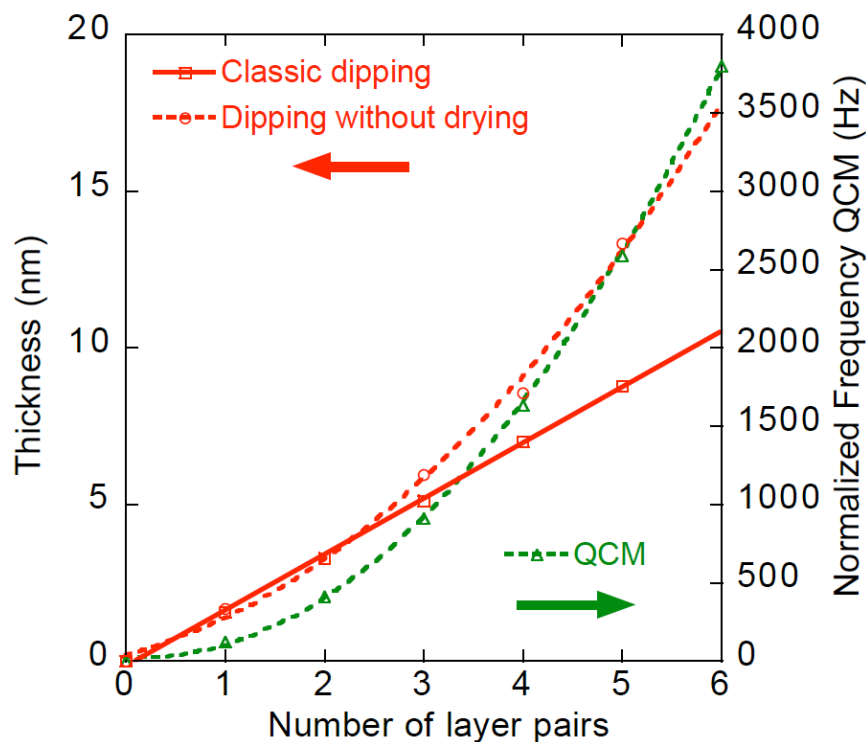
Figure 64. Construction of [EXM1246/PDDA]$_n$ films (n = 1, 2, 3, 4 or 5) in different assembly conditions followed either by ellipsometry or QCM: Classic dipping with drying and ellipsometry measurement after each layer (plain red line); Dipping without drying, each sample was dried and measured only after deposition of 1, 2, 3, 4 or 5 layer pairs (dotted red line); Frequency shift of the first harmonic as observed by QCM during build-up without drying (dotted green line).

The high dissipation values observed are caused by the presence of water in the film, which plastifies the multilayers.[178] Since the dissipation was exceptionally high compared to other reports on polyelectrolyte multilayers,[98, 154] we assumed that the hydration of the multilayers could be linked to the superlinear growth. The major difference between ellipsometry and QCM-D experiments is that the first one measures the film growth in the dry state while the second one measures it in the wet state. In order to see if the superlinear growth was linked to the abscence of drying steps during the build-up, we designed complementary experiments. We used PDDA as polyelectrolyte to work with a constant degree of ionization. We built (clay/PDDA)$_n$ films having one to five layer pairs (n = 1, 2, 3, 4 or 5) without

intermediate drying steps and we measured their thickness by ellipsometry only at the end, after a single drying step. We compared the results with classic dipping where the sample is dried at each layer and QCM experiments where the sample is never dried during acquisition.

We can see in Figure 64 that while the growth of (clay/PDDA)$_n$ film is linear when the film is dried after each layer, it becomes superlinear if the intermediate drying steps are removed. The resulting exponential growth is somewhat similar to what is observed during QCM experiments. The slight shift between the two curves is caused by the hydration state of the film during the measurement by ellipsometry (dry state) and by QCM (wet state).
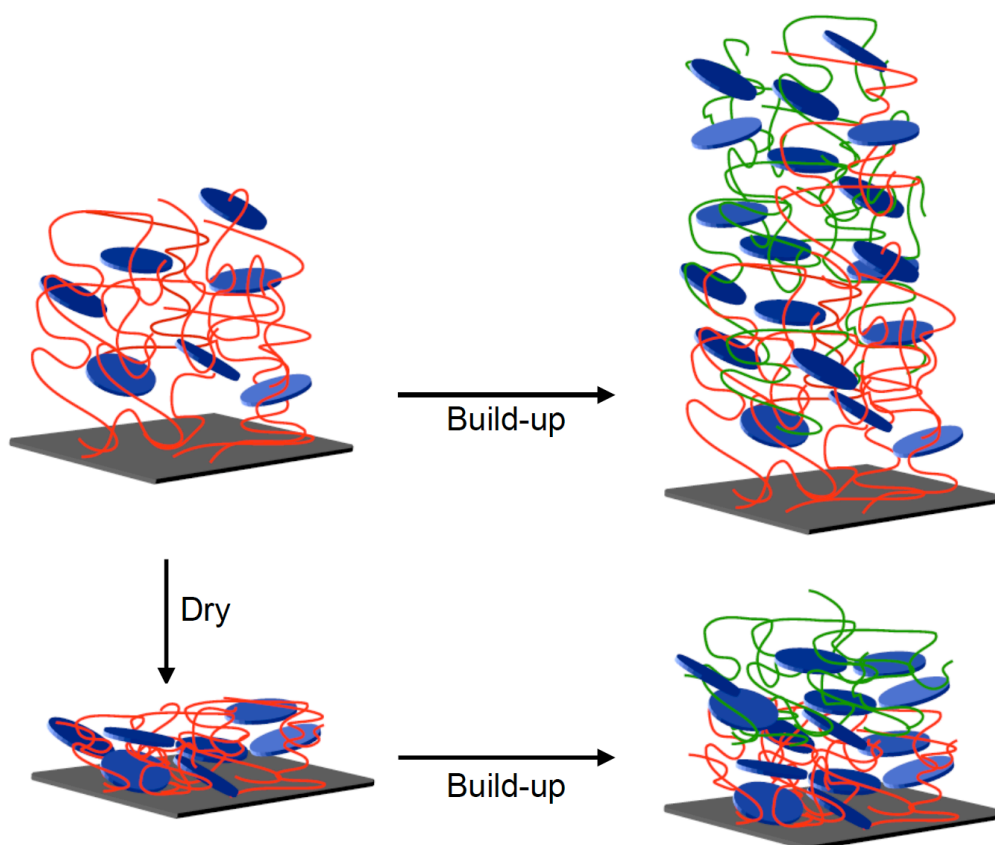
Figure 65. Schematic representation of the effect of drying on the growth of clay-containing multilayers. Blue discs represent clay platelets. Red lines are polyelectrolytes adsorbed in the previous step. Green lines represent polyelectrolytes adsorbed as last layer. The open structure in the absence of drying allows diffusion of the polymer chains and a superlinear growth. Drying steps during film build-up leads to a tight network where diffusion of polymer chains is prevented.

We believe that the transition from linear to superlinear growth when the intermediate drying steps are skipped is related to a hydration hysteresis of the film (Figure 65). When the film is dried there are rearrangements in the film leading to the formation of new polymer/clay bonds that form a tight network that cannot rehydrate easily. In consequence clays or polyelectrolytes sequentially adsorb at the surface of the film because the tight network prevents any diffusion. In contrary, as long as the film has never been dried it forms a loose hydrated network which allows for diffusion of the polyelectrolytes. The multilayer can then act as a reservoir and lead to a superlinear growth.[97] This suggested mechanism is depicted in Figure 65 where two different colors were used for the polyelectrolytes already present in the film and newly deposited in order to visualize the diffusion.

It had already been reported for polyelectrolyte multilayers that the intermediate drying steps could change the morphology and build-up regime of multilayers.[197] Other groups have built clay-containing films without drying and reported superlinear growth,[125] but to our knowledge this effect has never been studied. In this part we unambiguously showed that skipping intermediate drying steps lead to superlinear growth for polyelectrolyte-clay film that otherwise grow linearly.

As the construction of thick films using dipping is time consuming, we also tried to study spray-assisted deposition of clays in order to assemble more rapidly micron thick clay-based films.

4.2.3   Spraying of clay-based films

Spray-assisted deposition can be considered an important improvement of the LbL technique with respect to accelerating and scaling-up of the process.[113] We therefore studied the spray assembly of polyelectrolytes and clays. Preliminary experiments showed that it was possible to build films using PDDA but not with poly(ethylene imine) (PEI). This weak polyelectrolyte commonly used in layer-by-layer assembly as adhesion promoting agent was leading to an exponential growth followed by the destruction of the film after few layer pairs. We noticed that decreasing the pH of the PEI solution prior to deposition led to a slow but steady growth. As PEI is a branched polymer containing primary, secondary and tertiary amines it is therefore not a good model to understand the build-up behavior. Therefore, we decided to study the growth of multilayers consisting of clays and

poly(vinyl amine) at different pH. As we already discussed poly(vinyl amine) only contains primary amino groups, which make the ionization phenomenon less complex.
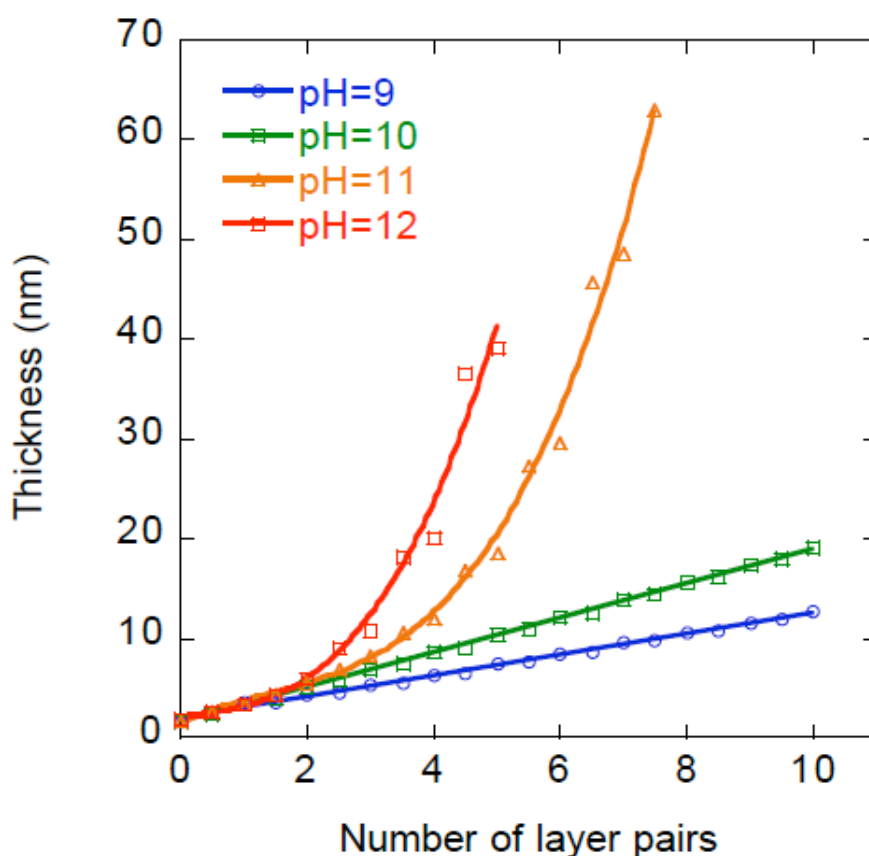
Figure 66. Spray assisted assembly of EXM 2039 and PVAm followed by ellipsometry. The pH of the PVAm solution was adjusted from 9 to 12 using a 0.5 M sodium hydroxide solution.

As we can see in Figure 66 the pH of the PVAm solution strongly influences the build-up of the multilayer. As long as the pH of the solution is below 10, the film growth is linear. Above pH 10 the film assembly becomes superlinear and lead to the destruction of the multilayer after few layer pairs. The multilayers break after 7,5 layer pairs at pH 11 and 5 layer pairs (or lower) at pH 12. Beside the transition from linear to superlinear we notice that the layers thicknesses are increasing with the pH as it was already reported for dipping. One can also observe that the largest thickness increases during superlinear build-up corresponds to the adsorption of PVAm while the thickness increases related to clay adsorption remain relatively small. When monitoring the build-up by QCM-D (Figure 62) we observed similarities in the growth regime. The relative proportion of poly(vinyl amine) and

clays increases when the pH increases. During spray-assisted assembly we observed a superlinear growth despite drying after each layer. It is already known that the assembly technique has an influence on the structure of the LbL films.[116] In our case it appears to change the growth regime. We believe that the large amount of poly(vinyl amine) adsorbed at high pH for sprayed films compared to dipped films allows film hydration and superlinear growth. For dipped films it has been reported that some polyelectrolyte couples lead to superlinear growth even in the presence of clay platelets.[198] The large content of poly(vinyl amine) and water in the multilayer probably weakens its structure and leads to its rupture under the shear flow created by the spray of droplets. In consequence the higher the pH, the higher the poly(vinyl amine) content and the sooner the films break.

The addition of salt in the polymer solution had for effect to make the growth linear. We tried to prepare thick films in this way but they had poor mechanical resistance and were diffusing light (probably linked to a poor nano-organisation of the film). After theses trials we stopped to study the spray assembly of clay-containing films. As hydration is one of the key parameters controlling the build-up of clay-containing multilayers, we investigated this phenomenon in more detail.

4.2.4   Hydration phenomenon

In a traditional dipping experiment, after deposition of one component and rinsing the sample is dried, its thickness is for example measured by ellipsometry and dipped in the solution of the next component. This implies that the deposition of each component happens during the hydration of the film. In order to separate the step of hydration and the step of adsorption during dipping, we performed an experiment where the film was pre-hydrated before deposition of the next component. We dipped the film in Milli-Q water after each ellipsometry measurement, in this way when the film is introduced in the PVAm or clay solution, it is already hydrated (Figure 67).
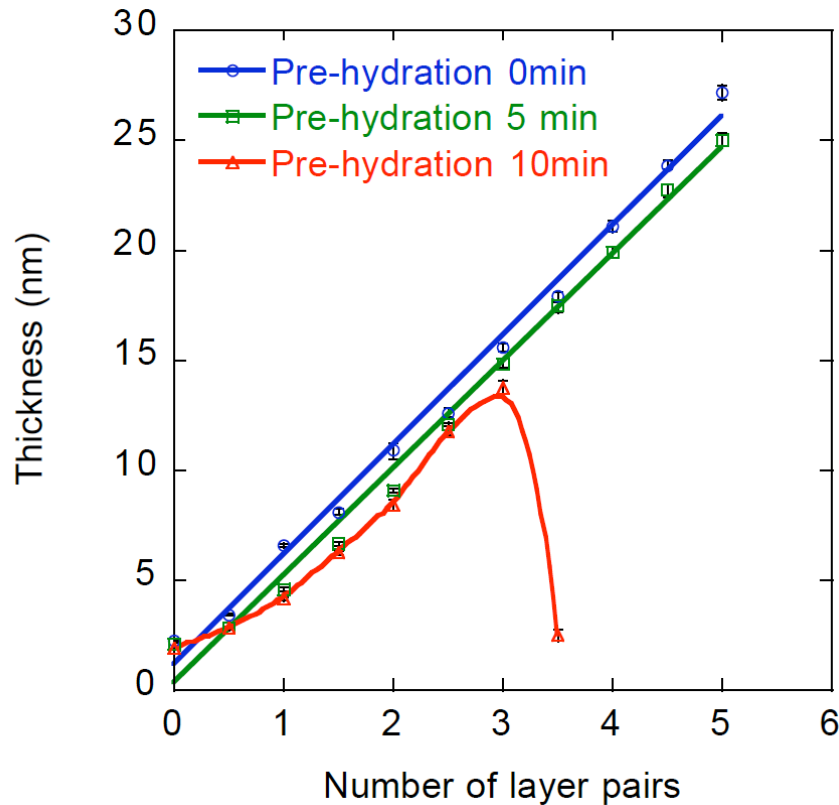
Figure 67. Effect of the film pre-hydration time on the construction of (EXM2039/PVAm)$_n$ films by dipping followed by ellipsometry. Films are built with PVAm solution at pH 12. Pre-hydration was done by dipping the film in Milli-Q water for 5 or 10 min after each ellipsometry measurement and before the deposition of the next layer.

A pre-hydration time of five minutes did not significantly modify the build-up of the film. However if we look closely we can see an inflexion of the curve at the beginning of the construction compared to the film built without pre-hydration. We tried to build a film with a hydration time of ten minutes but we observed the deconstruction of the film already after three layer pairs. Note that pre-hydration is not equivalent to film construction without drying because we didn't see a superlinear build-up. But the deconstruction of the film is similar to the one observed during spray assisted assembly. This study confirms that superlinear growth is limited to never dried films in dip-assisted assembly. It indicates that the deconstruction during spray-assisted assembly is not only induced by shear but also by some hydration phenomenon.

We also looked at the rehydration of the films by QCM. To do so we dried the film built on a QCM crystal (Figure 63), reintroduced the crystal in the QCM cell and then filled the cell with Milli-Q water. This experiment corresponds to the pre-

hydration step described above for ellipsometric measurements. We started recording the frequency shift immediately after the introduction of water.
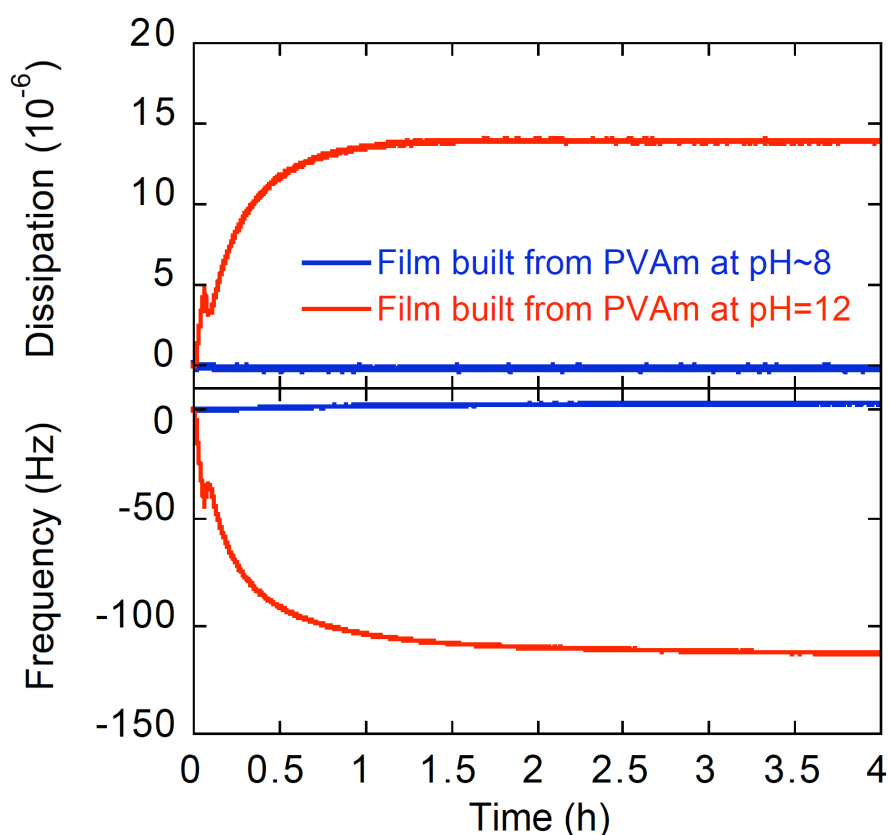
Figure 68. Variation of frequency and dissipation of the fifth harmonic as a function of time observed by QCM during re-hydration of (clay/PVAm)$_n$ films built previously with PVAm solutions at pH 8 and 12. Signal acquisition started immediately after introduction of water in the measurement cell containing the dried film deposited on the QCM crystal.

We can see in Figure 68 that films built from PVAm solution at pH=12 are strongly swelling while films built at pH=8 did not. As shown previously, the change of clay/PVAm stoichiometry in the film with the pH of construction is certainly responsible for this difference. In the film built from PVAm solution at pH 12 the large amount of deprotonated amine groups induce water adsorption in the film. In the film built at pH=8 most of the amine group are already protonated and interact with clay platelets. Therefore the water molecules have more difficultly to penetrate in the film. It is probable that there is some hydration of the film but the time-scale and amplitute of this phenomenon makes it difficult to visualize on this graph. A small bump, visible on the red curve few minutes after the beginning of the experiment, was caused by re-injection of water in the cell. It is only visible on the

film built from PVAm solution at pH 12 because its softness makes it more sensible to flow variation in the QCM cell.

The frequency shift obtained during rehydration of the film built at pH 12 represents 11% of the total frequency shift obtained during the construction of the film (water from rehydration)(Figure 63). The absolute frequency after rehydration (multilayer and water from rehydration) is only half that of the never-dried films (multilayer and water trapped during build-up). At pH=8 there is no visible rehydration and the final mass is only 35% of the mass of the original film. These values confirm that both films at pH=8 and pH=12 are hydrated. The film built from PVAm at pH=8 is actually more hydrated than the film built from PVAm at pH=12, probably because the higher the degree of ionization of the PVAm the more hygroscopic it is. However, after drying only the film built at pH=12 is rehydrated.

These results confirm the high hydration of the clay-based films built without drying which is responsible for their superlinear growth. The partial rehydration of the multilayer built from PVAm solution at pH=12 is certainly linked to their deconstruction during spray build-up, and pre-hydration experiment. While as there is no rehydration at pH=8 we do not observe either superlinear growth or destruction of the films.

In this part we have shown that decreasing the charge on the polyelectrolyte allowed to increase the growth of the film. We also showed that skipping the drying step during dipping led to highly hydrated films growing exponentially. For sprayed films the use of PVAm solution at high pH led to exponential growth and destruction of the films. This set of experiments clearly outlines the importance of hydration on the preparation of clay-based multilayers. These results open some perspectives for understanding and tailoring the gas-barrier and flame retardant properties of these multilayers. One should also keep in mind that humidity could impact the mechanical properties of clay-based multilayers. We will now focus on the preparation of films containing clay platlets and polydimethylsiloxane derivatives.

4.3 Hybrid films combining PDMS and Clays

In biological composites the combination of soft polymer glue with hard anisotropic particles is the key toward high strength and high toughness. The softest elastomers are made of polydimethylsiloxane (PDMS) and it would be interesting to combine them with clay. Layer-by-layer assembly was historically developed for charged species dispersed in water. Polydimethylsiloxanes are typically neutral and insoluble in water. In this part we will see how to assemble them using the layer-by-layer technique and how to combine them with clays.

4.3.1 PDMS multilayers

Recently, our group developed an approach allowing to make poly(dimethylsiloxane)-based multilayers.[199] It relies on the covalent assembly of amine terminated poly(dimethylsiloxane) (Figure 69A) and maleic anhydride-containing polymer (Figure 69B). While maleic anhydride has a limited reactivity toward water it reacts with amines at room temperature to form amide bonds. The end-point attachment of bi-functional polymers at an interface is problematic (Figure 69 C). If the two functional groups react on the surface then the chain can not react further and build a multilayer. Even when one of the functional group is still available, the conformation of the polymer can be such that the second end-group is hidden is the polymer coil preventing further reaction. Despite these problems the alternated deposition of bis-aminopropyl-PDMS and maleic anhydride-containing polymer led to steady buildup and smooth LbL films.

Originally these experiments were carried out using poly(ethylene-alt-maleic anhydride), but we couldn't reproduce the results because the commercial product was insoluble in tetrahydrofuran. The batch was apparently crosslinked and Sigma-Aldrich exchanged it upon request for poly(methyl vinyl ether-alt-maleic anhydride). This polymer readily dissolved in tetrahydrofuran as expected and since both polymers have a similar structure we did not expect major changes in their reactivity. We tried to reproduce some of the results previously published using poly(methyl vinyl ether-alt-maleic anhydride) (PMEMA) and bifunctional poly(dimethylsiloxane) (PDMS) of high and low molecular weights.
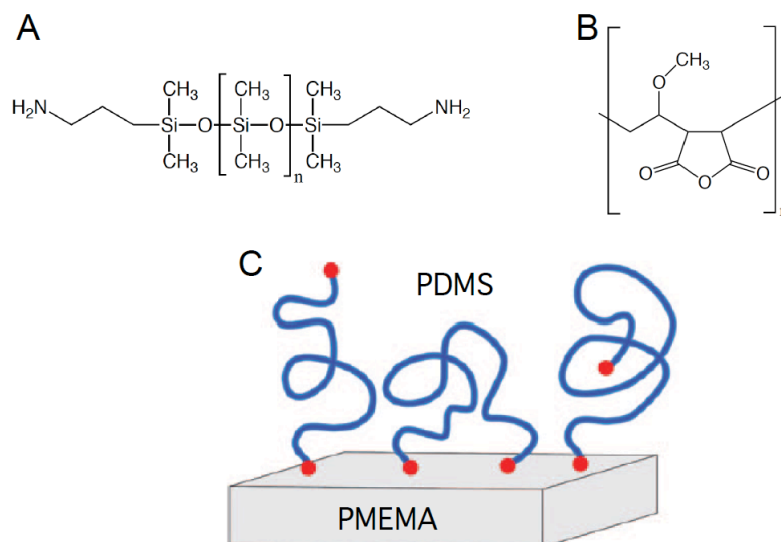
Figure 69. (A) Chemical structure of poly(dimethylsiloxane) bis(3-aminopropyl) terminated (PDMS). (B) Chemical structure of poly(methyl vinyl ether-alt-maleic anhydride) (PMEMA). (C) Schematic representation of possible conformations of end-fonctionalized chains on a substrate of PMEMA.[199]

Similarly to what was previously reported we observed an increase of the build-up speed with the concentration of the solutions (Figure 70). We also observed (Figure 70A) that all the multilayers are growing in a saw-teeth fashion. This previously described phenomenon is linked to conformational changes of the multilayer upon dipping in tetrahydrofuran and toluene.

The deposition time described in the article, for the adsorption of PMEMA and PDMS of 30 min and 50 min respectively, were not compatible with the preparation of thick multilayers that requires hundreds of deposition cycle (more than a week would be needed for a single film). Therefore, we tried to build films with lower deposition times, 5 minutes for each component, and concentrations of 5 g/L. The growths observed were 4.0 and 5.1 nm/layer pair respectively for the high and the low molecular weights PDMS. These values were similar to the ones found for longer deposition times (4.1 and 4.8 nm/layer pair). There might be some changes in the structure of the films even if the growths are similar, but since the films appeared homogeneous we decided to keep this deposition time. Later we used only solutions at 5 g/L in order to save expensive bi-functional PDMS and we also limited our studies to PDMS 2500 because PDMS 27000 produced inhomogeneous thick films.
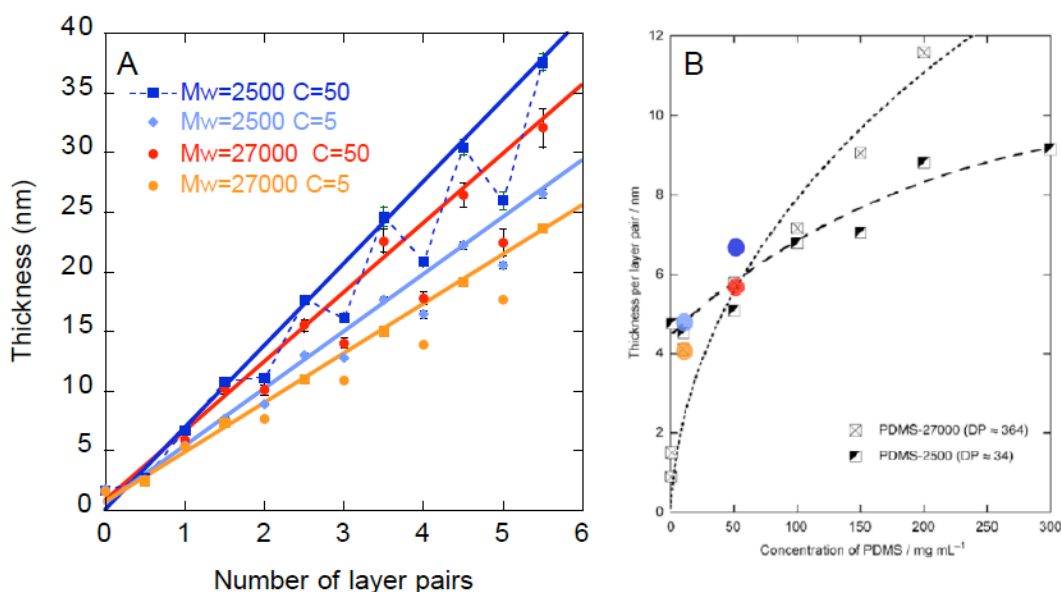
Figure 70. (A) Buildup of covalently assembled multilayers using poly(methyl vinyl ether-alt-maleic anhydride) dissolved in tetrahydrofuran and poly(dimethylsiloxane) bis(3-aminopropyl) terminated dissolved in toluene. The concentration C of both solutions was either 5 or 50 g/L. Two bi-functional PDMS with different molecular weights (Mw) were used: one had a molecular weight of 2500 g/mol and the other one a molecular weight of 27000 g/mol. The linear fit of the thickness increment after dipping in toluene are represented together with one actual thickness evolution in order to keep the graph readable. (B) Comparison of the thickness increase per layer pair (corresponding colored dots) with previously published results.[199]

Based on the previous investigations, we studied the construction of thick films consisting only of PDMS and PMEMA. We used an automated dipping station and built [PVAl/Clay/PVAm][PMEMA/PDMS$_{2500}$]$_{80}$ films. The first layer consisting of poly(vinyl alcohol), clays and poly(vinyl amine) offers an homogeneous amine covered surface for the deposition of the first layer of PMEMA, which did not adsorbed well directly on hydrophobic silicon wafer. After deposition of 80 layer pairs the film was 410 nm thick and the refractive index measured by the spectroscopic ellipsometry was 1.42. Surprisingly one month later the film thickness was only 254 nm and the refractive index measured was 1.47. This is certainly due to conformational changes similar to the one observed during alternative dipping in THF and Toluene and causing the saw teeth growth (Figure 70).[199]
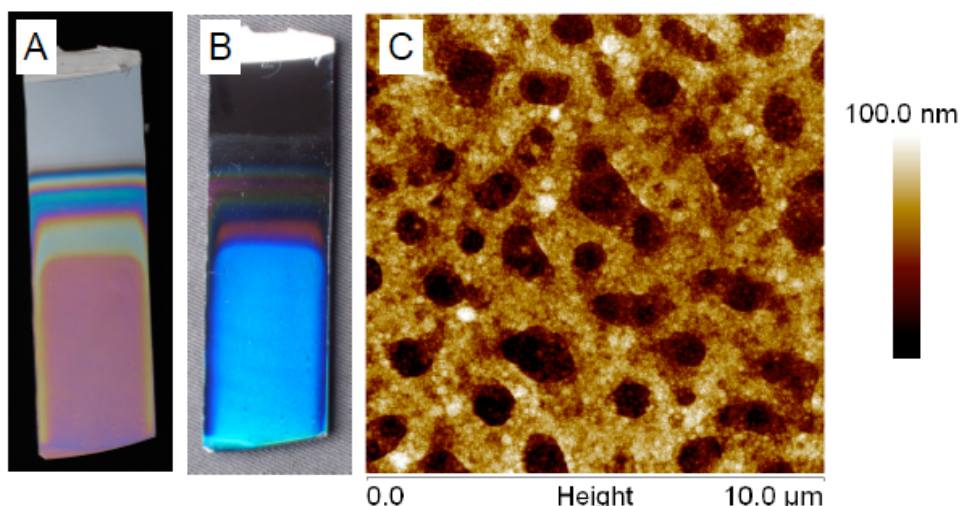
Figure 71. [PVAl/Clay/PVAm][PMEMA/PDMS$_{2500}$]$_{80}$ film built on hydrophobic silicon wafer. (A) Optical photograph showing interference colors on the sample (direct illumination and white background). (B) Optical photograph showing the light diffused by the sample (side illumination and dark background) . (C) AFM image of the sample in the light diffusing region.

This film showed a good overall homogeneity but diffused blue light under side illumination (Figure 71A and B) which we never observed on other films. We imaged the film using AFM in tapping mode and we observed fairly regular pores with micron range diameters (Figure 71C). These pores are responsible for light diffusion. We believe that the pores were created by the thickness variation during construction. If the film swells too much its structure can break and lead to the formation of pores that will grow with the film. The preparation and analysis of such structures was not the topic of this thesis it nevertheless opens interesting perspectives for future projects.

4.3.2   Combining clays and PDMS

We have seen that it was possible to reproduce the construction of PDMS-containing films, and that even with a shorter deposition time the films were homogeneous and reasonably thick. In the previous chapter we saw that it was possible to build films with clays and poly(vinyl amine). Based on the results, we will now study their combination in order to form multilayers containing clays and PDMS.

Poly(vinyl amine) contains primary amine groups that can react with PMEMA (containing maleic anhydride groups), therefore it is possible to link clay platelets

and PDMS in a single film using PVAm and PMEMA as bridge. The construction of a multilayer of PMEMA and poly(vinyl amine) led to a steady linear growth with a slope of 4.9 nm/layer pair. We have shown that it is possible to alternate the deposition of clay suspension and poly(vinyl amine) solution in water, of PMEMA solution in THF and PDMS solution in toluene, and finally Poly(vinyl amine) solution in water and PMEMA solution in THF. We could then combine them in a four-components multilayer.
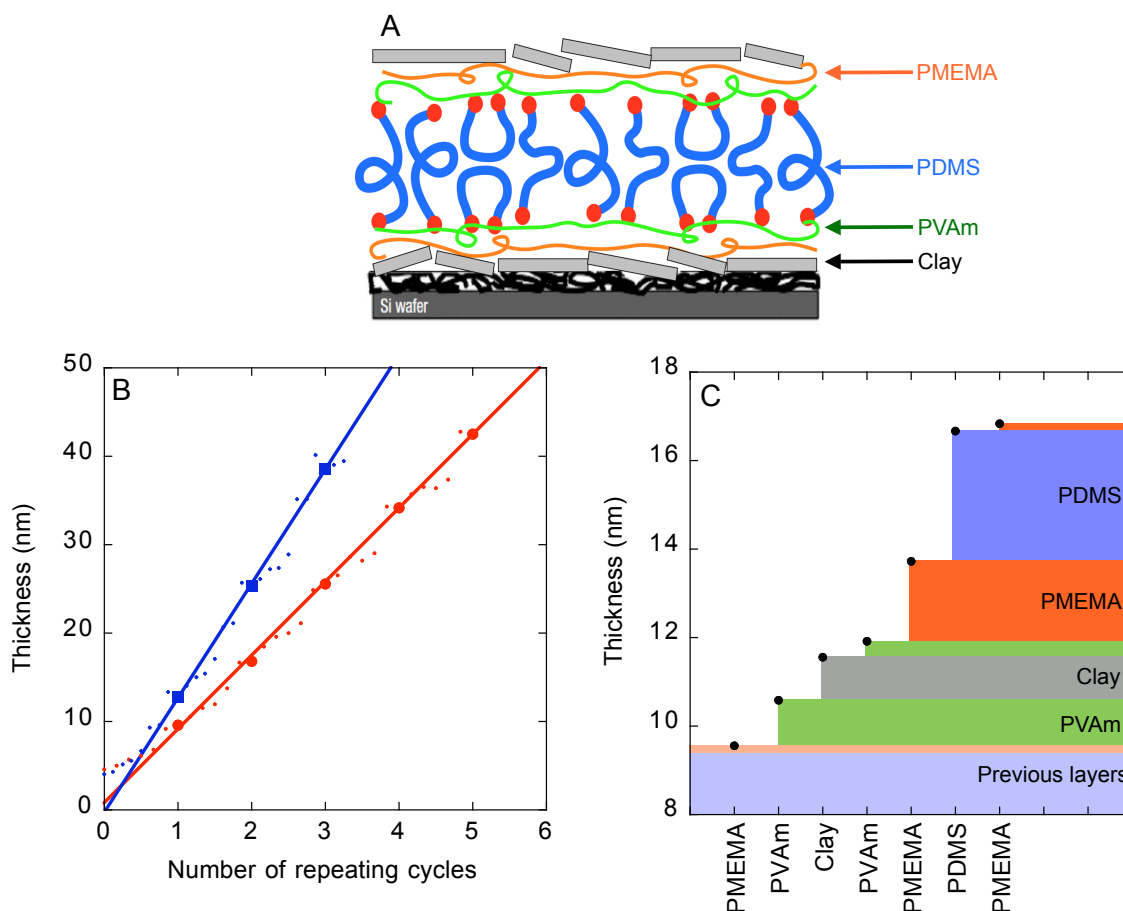
Figure 72. (A) Schematic representation of the architecture of a film combining clays and PDMS. (B) Thickness variation as a function of the number repeating cycles for the construction of [PVAm/Clay/PVAm/PMEMA/PDMS$_{2500}$/PMEMA]$_5$ (red) and [PVAm/Clay/PVAm/PMEMA/PDMS$_{2500}$/PMEMA/PDMS$_{2500}$/ PMEMA]$_3$ (blue) films followed by ellipsometry. Both films were built on octadecyltrichlorosilane treated silicon wafers. (C) Close up on the thickness evolution of the film for the second repeating cycle of the blue curve. Each color represents one component.

Figure 72A shows that it is possible to build films combining clay and PDMS with intermediate layers of PMEMA and poly(vinyl amine). Each component contributes

to the growth of the film (Figure 72B). After the first deposition cycle, the thickness increases regularly with each repeating cycle. One of the objectives is to study the influence of the amount of clays and PDMS in the multilayer on the mechanical properties of the film. Therefore we studied the construction of films with one layer of PDMS for each layer of clays and two layers of PDMS for each layer of clays.In both cases the thickness of the clay layer has a similar thickness (around 1.1 nm) while the total thickness of the repeating cycle goes from 8.3 nm with one layer of PDMS to 12.9 nm with two layers. These values are only indicative because the refractive index of each layer is different and can be subject to modification along the deposition as we have seen for PDMS/PMEMA films (paragraph 4.3.1). It gives, however, a good approximation of the amount of clays in each material: from about 13% with one layer of PDMS to about 8.5% with two layers. In comparison alternate deposition of clays and poly(vinyl amine) without pH modification led to composites with a clay content of nearly 75%.
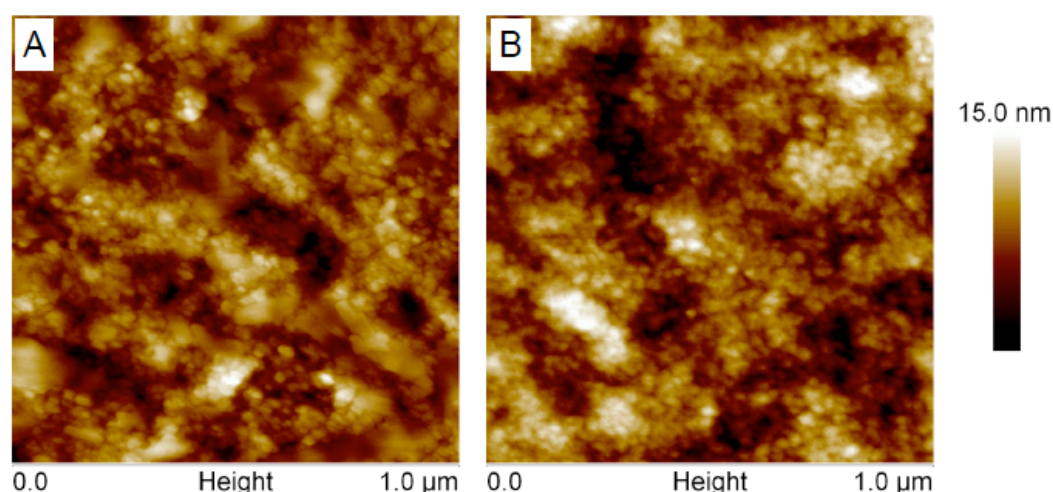
Figure 73. AFM images of [PVAm/Clay/PVAm/PMEMA/PDMS$_{2500}$/ PMEMA]$_4$PVAm/Clay (A) and [PVAm/Clay/PVAm/PMEMA/PDMS$_{2500}$/ PMEMA]$_5$ (B) films.

We took AFM images after the deposition of a clay layer (Figure 73A) and after deposition of PDMS layer on top of it (Figure 73B). Clay platelets are only visible on the first image and do not appear on the second. This confirms the complete coverage of clays by polymers during each cycle. These images also show that clay particles are laying flat on the surface, since their height varies by less than 15 nm over distances of hundreds of nanometers. The surface does not seem completely covered with clays since the globular structure is still visible between

clay platelets. This is surprising given the fact that the 1.1 nm thickness increase during clays deposition corresponds to the thickness of clay platelets, but the disposition and density of clay particles appears similar to what was observed directly on activated silicon wafer (Figure 60B).

We have seen here that it was possible to build PDMS-containing multilayers and to combine them with clays and poly(vinyl amine). We have studied their growth and provided a way to control the amount of clays and PDMS in the material. We will now look at the structure and mechanical properties of these architectures.

4.4 Thick multilayers and their mechanical properties

The structure and composition of nacre-like multilayers defines their mechanical properties. In order to characterize the mechanical properties of nacre-inspired multilayers it is necessary to prepare freestanding micron-thick films.

4.4.1 Freestanding multilayers

The production of freestanding multilayers is challenging. The first examples were only reported ten years after the discovery of the LbL technique.[169] For our system, a suitable sacrificial layer needs to be insoluble in water, terahydrofuran, and toluene to resist to the film construction but should be processable as thin film and soluble in at least one solvent to release the film. We did not find polymers fitting these requirements and our trials on reversible crosslinking using disulfide bonds were not satisfactory. The use of hydrofluoridric acid as already reported in the literature[5] could damage the clays and the PDMS besides the fact that it is extremely toxic. Therefore, we decided to modify the surface of silicon wafers in order to render it hydrophobic and reduce the adhesion of the multilayer on the substrate.[6, 200] We used octadecyltrichlorosilane that covalently attachs to OH groups at the surface of activated silicon wafers to form a hydrophobic coating (Figure 74A).
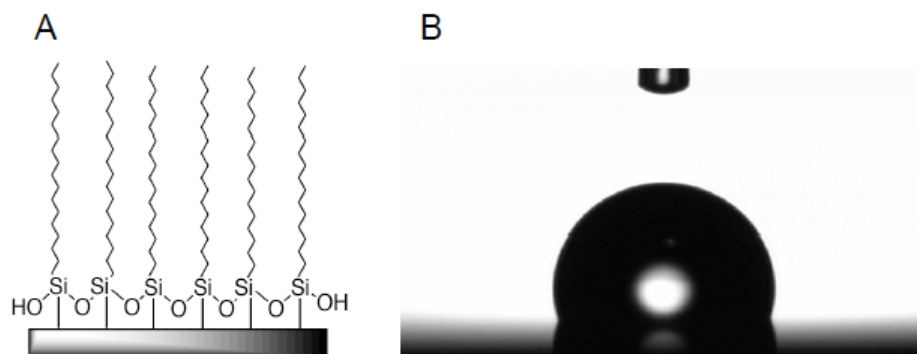
Figure 74. (A) Schematic representation of an octadecyltrichlorosilane coated silicon wafer. (B) Contact angle observed after surface modification (105º).

Before surface modification activated silicon wafers have typically a silicon oxide layer of 1.8 nm at their surface. After treatment with octadecyltrichlorosilane the thickness of the surface layer measured by ellipsometry reached 4.5 nm. Rinsing, rubbing with fabric or sticking tape on the surface did not change this value (as long as the substrate was clean). We also measured the contact angles of native and modified substrates. Contact angle increases from ~5º after plasma activation of the silicon wafer to about 105º after surface modification with octadecyltrichlorosilane (Figure 74B).

We have demonstrated that we could build films on hydrophobic silicon wafers in the same way as on plasma activated ones and the growth on both surfaces were similar (Figure 72A). We observed a slower growth for the first two or three layers, but the difference becomes negligible afterwards. The main advantage of such a hydrophobic silicon wafer is that the LbL-film only poorly adhere on the surface. A multilayer built on it can be easily removed from the support using adhesive tape. One only needs to grab a corner of a multilayer to detach it entirely if the film is resistant enough, weak films break before detaching. If a multilayer does not tolerate detachment from the support it means that it is also too weak for mechanical characterization and its thickness should be increased.

Using a dipping robot we were able to produce thick films combining clays and PDMS on hydrophobic silicon wafers.
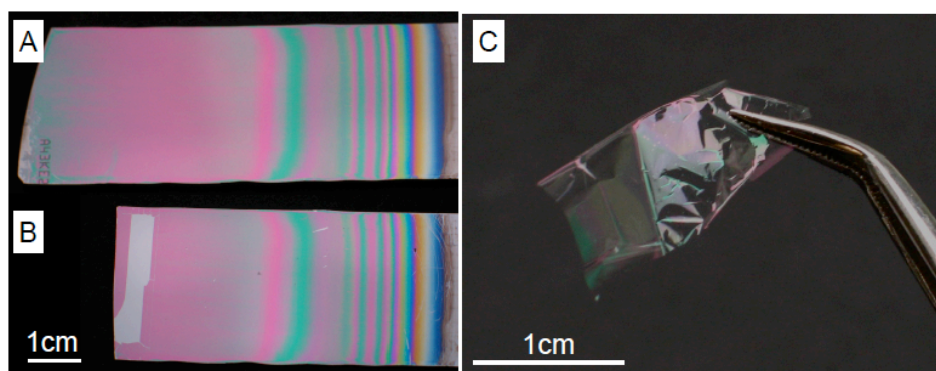
Figure 75. (A) Reflection photograph of a [PVAm/Clay/PVAm/PMEMA/ PDMS$_{2500}$/PMEMA]$_{100}$ film showing homogeneous Fabry-perrot interference colors. The rainbow on the right is due to the evaporation of the solution during assembly. (B) Same multilayer as in (A) where the bottom was cut without damaging the film to carry out AFM measurements and thin stripes of film were cut and detached on the left for mechanical tests. (C) Freestanding piece of the same film showing high transparency and interference colors. Due to static electricity the film folded in two on itself.

As we can see in Figure 75 the film completely covers the substrate without cracks. The rainbow visible on the top of the sample corresponds to a gradient of thickness, due to the evaporation of the dipping solutions during deposition. The colors observed are due to interference between the light reflected on the surface of the silicon substrate and the light reflected on the surface of the film. These Fabry-Perot fringes are directly related to the thickness and homogeneity of the film.[201] The nearly uniform pink color on the left part of the substrate indicates good homogeneity of the film. When measured by spectroscopic ellipsometry with a constant refractive index of 1.55 for the film, its thickness was 770 ± 20 nm all over the pink region and slightly thicker in the blue-green region on the left (up to 835nm).

We can see in Figure 75B that the films can be peeled from a hydrophobic surface. The film still adheres enough to stay on the modified silicon wafer without self-detaching which makes storage and manipulation easy. The substrate could even be cut without damaging the film. The detachment of the film from the substrate could be done using tape (Figure 75C). The freestanding film is transparent and displays the similar pink and green interference colors. Freestanding multilayers tend to stick to themselves or to the tape after detachment and their flexibility and large surface makes them extremely sensitive to air flows, the preparation of intact

film samples for mechanical testing had therefore a poor success rate. We were, nevertheless, able to build micron thick multilayers on hydrophobic silicon wafers and to detach them from the substrate. The actual structure of such thick films is especially interesting, to be mechanically resistant the film needs to be homogeneous and the clay platelets need to be aligned in the plane of the film.

4.4.2   Structure of the films

In order to calculate the stress applied on the material during tensile testing it is important to know the thickness of the sample. Ellipsometry is a fast and easy way to measure the thickness of films deposited on silicon wafers but the quantitative interpretation of ellipsometric data can be difficult. Our thickness measurements were done using a spectroscopic ellipsometer that allows measuring simultaneously the refractive index of the film and its thickness. We found an average refractive index close to 1.55 this value was fixed as a constant for all measurements in order to have comparable results (Surface roughness or small defects can create artifacts when measuring both the refractive index and the thickness).
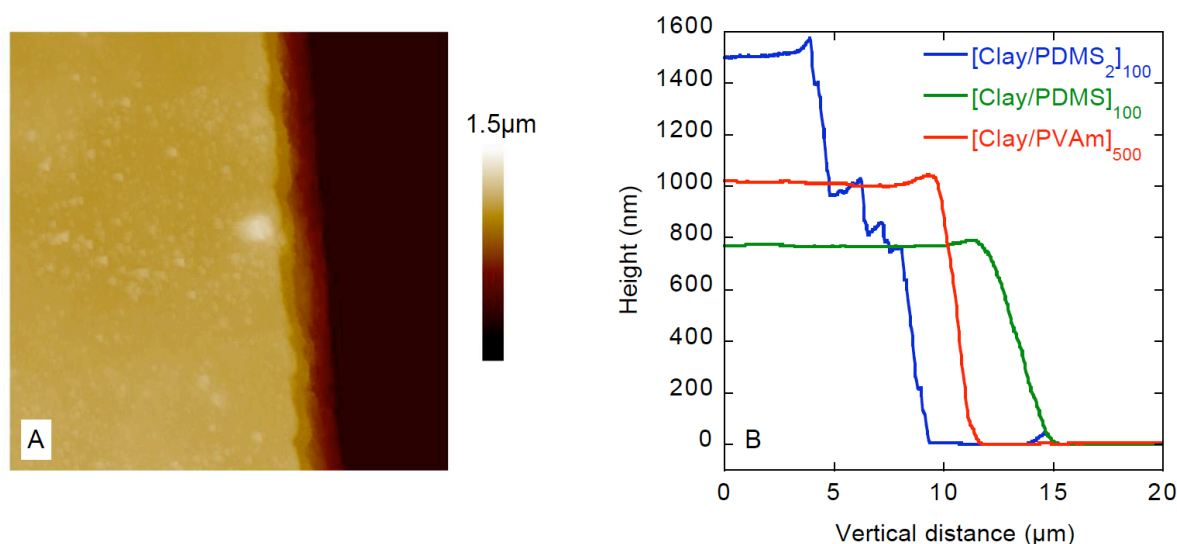
Figure 76. (A) AFM image of the edge of a [PVAm/Clay/PVAm/PMEMA/PDMS$_{2500}$/PMEMA]$_{100}$ film on a silicon wafer. The size of the image is 20 x 20 μm and the vertical scale is 1.5 μm. (B) Edge profiles of several films measured by AFM: [PVAm/Clay/PVAm/PMEMA/PDMS$_{2500}$/PMEMA/ PDMS$_{2500}$/PMEMA]$_{100}$ (blue), [PVAm/Clay]$_{500}$ (red) and [PVAm/Clay/PVAm/PMEMA/ PDMS$_{2500}$/PMEMA]$_{100}$ (green).

In order to confirm the thickness obtained by ellipsometry, we imaged by AFM the edges of multilayers resting on a silicon substrate (Figure 76A) and measured the profiles of the steps (Figure 76B). For all the films characterized we obtained similar thickness values with both AFM and spectroscopic ellipsometry (Table 1). Thus, the refractive index of 1.55 appears realistic and can be used for the thickness characterization of these films even with single wavelength ellipsometers. An accurate film thickness is required for the mechanical measurement described in chapter 4.4.3.

Multilayer architectures	Ellipsometry	AFM
[PVAm/Clay]$_{500}$	1030±50 nm	1020 nm
[Clay/PDMS]$_{100}$	770±20 nm	770 nm
[Clay/PDMS/PDMS]$_{100}$	1450±50 nm	1500 nm

Table 1. Thicknesses measured by spectroscopic ellipsometry and AFM for [PVAm/Clay/PVAm/PMEMA/PDMS$_{2500}$/PMEMA]$_{100}$ (simplified by [Clay/PDMS]$_{100}$), [PVAm/Clay/PVAm/PMEMA/PDMS$_{2500}$/PMEMA/PDMS$_{2500}$/ PMEMA]$_{100}$ (simplified by [Clay/PDMS/PDMS]$_{100}$) and [PVAm/Clay]$_{500}$ films.

The thickness of [Clay/PDMS]$_{100}$ (770 nm) is below the value expected from the first experiments Figure 72 with an increment per cycle of 8.3 nm. For the first experiments the films thicknesses were measured with a single wavelength ellipsometer assuming a refractive index of 1.46 (refractive index of SiO_2). As the actual refractive of the film index is closer to 1.55, the thickness measured were slightly overestimated. This systematic error does not impact the clay content estimation. However, the film with two layers of PDMS is thicker than expected (1290 nm) because the concentration of the PMEMA solution was 5 times higher (5 g/L) than in the initial experiment (1 g/L). The same film built from a PMEMA solution at 1g/L was 1010 ± 10 nm thick but such film contained many defects and only few mechanical tests could be performed (increasing the concentration of the PMEMA solution improved the quality of the film). It is probable that the actual clay content in the film containing two PDMS layers is slightly lower than the 8.5% expected.

AFM images show that the surface is smooth despite the presence of some small particles. The stratified structure of the multilayer is visible on Figure 76A, were the

edge of the film presents small steps corresponding to clay layers. But it is on the SEM images that the layered structure is the most visible.
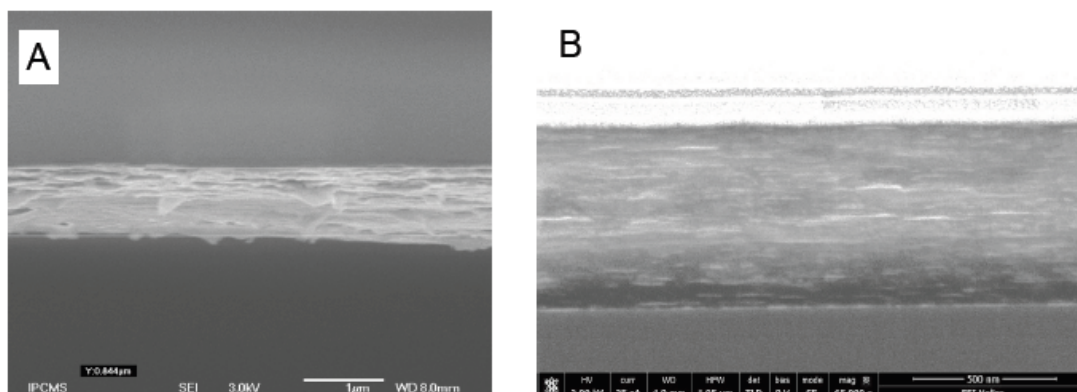
Figure 77. (A) SEM image of the edge of [PVAm/Clay/PVAm/PMEMA/PDMS$_{2500}$/PMEMA]$_{100}$ film. (B) Same film imaged after ion milling allowing a clean cut of the sample. This experiment was run by FEI, on a Helios Nanolab 660.

We can observe in Figure 77A some clay platelets edging out of the multilayer. They all lay parallel to the plane of the film. A similar structure was observed for films consisting only of clays and poly(vinyl amine) but the sample containing two layers of PDMS for each layer of clays displayed a smoother edge. It is probable that the lower content of clays in the material changed the way the multilayer broke.

The organization of the platelets in the multilayer is even more visible in Figure 77B (courtesy FEI) Ion milling consists on firing argon ions on a sample partially protected by a layer of platinum. At the edge of the platinum protection the sample is cut precisely without mechanical stress. We can observe structural homogeneities without topographic effect coming from the mechanical stress during sample preparation.

The clay particles and the matrix respond differently to the electron beam. Clay platelets appear as white stripes while the polymeric matrix is grey and uniform. We see clearly the parallel layers of exfoliated clay particles embedded in the polymer matrix. This stratified structure resembles that of nacre[1] with smaller inorganic platelets.

We also measured the thickness of hybrid LbL films using SEM but the precision of such measurement was poor. The limited access to SEM equipments did not allow us to optimize the sample preparation in order to obtain reliable thickness

measurements. However, the average thicknesses measured were consistent with results obtained from ellipsometry and AFM, despite their high standard deviation.

All the film prepared present a layered structure similar to that of nacre with in plane alignment of the reinforcing clay platelets. Their thickness is precisely known. Their mechanical properties can therefore be discussed with respect to their architecture and composition.

4.4.3 Influence of the amount of PDMS on the mechanical properties

We successfully prepared freestanding multilayers with various clay content, measured their thickness and proved that they had a nacre-like structure. The next step was to study the influence of film composition and architecture on their mechanical properties.

The films prepared had strength and Young's modulus in the upper range of LbL-assembled nano-composites,[51, 134] in dry condition [Clay/PVAm]$_{500}$ even surpass non cross-linked poly(vinyl alcohol)/clay nano-composites.[5] Indeed the mechanical properties of such multilayer surpass those of composites assembled by drying or vacuum filtration.[202] We observed that the Young's modulus of the film decreases with a decreasing content of clays. The modulus of lamellar macro and micro-composites can be calculated using the rule of mixture.[17]

$$E_c = V_p \times E_p + V_m \times E_m$$

Equation 7

With V and E representing respectively the volumic fraction of a component in the composite and the Young's Modulus of this component. Subscripts indicate if the characteristics refer to the entire composite (c), the particles (p) or the matrix (m). In our case the matrix being much softer (E_m<1 GPa) than the clay particles (E_p~220 GPa)[130] the Young's modulus of the composite should be proportional to the content of clays. We previously estimated the clay content in the multilayer at 13% with one layers of PDMS and 8.5% with two layers Figure 72. Rough estimation of the theoretical modulus using the rule of mixture gives 29 GPa for the film with one layer of PDMS and 19 GPa with two layers of PDMS. The modulus measured respectively of 22 GPa and 10 GPa are slightly lower but follow the same trend. In the multilayer without PDMS the clay content estimated by

ellipsometry was nearly of 75% and the Young's Modulus expected in this case was over 150 GPa. We assume that the lower value reported here (45 GPa) is due to a lower reinforcing efficiency of the nano-platelets. There is probably not enough polymers around the clay particles to efficiently transfer the stress from one particle to another. In consequence some fraction of the particles don't participate to the reinforcement of the composite and the modulus increase is lower than expected.
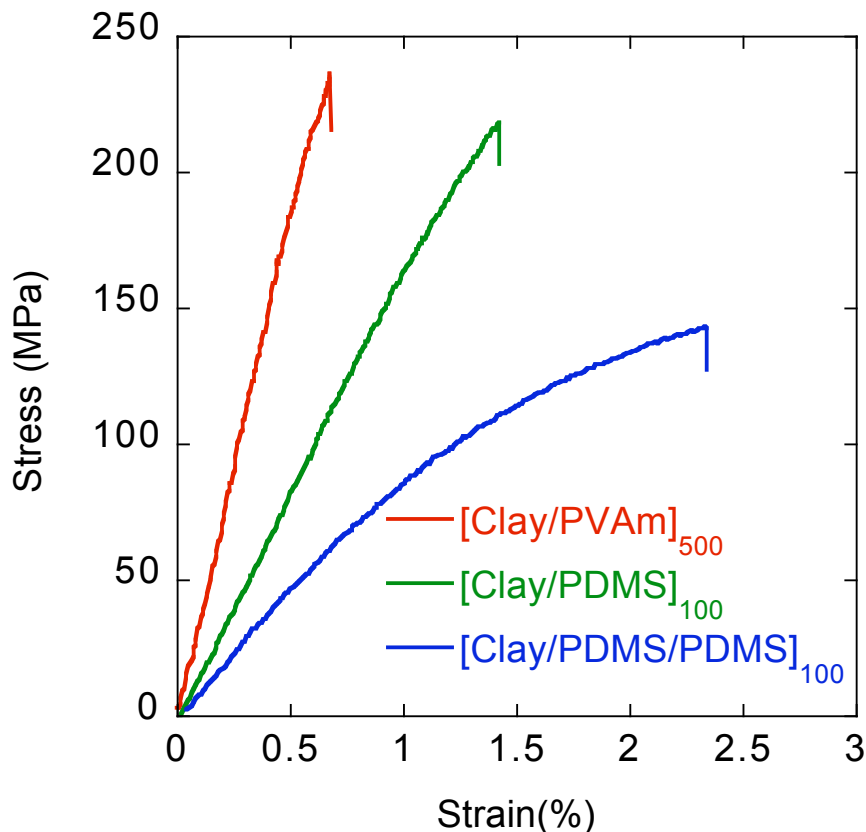
Figure 78. Typical stress-strain curves obtained for [Clay/PVAm]$_{500}$ (red), [PVAm/Clay/PVAm/PMEMA/PDMS$_{2500}$/PMEMA]$_{100}$ (green) and [PVAm/Clay/PVAm/PMEMA/PDMS$_{2500}$/PMEMA/PDMS$_{2500}$/PMEMA]$_{100}$ (blue) in dry humidity conditions (RH<5%).

The stress at break also decreases with the content of clays in the film while the strain at break increases. The incorporation of one layer of PDMS only causes a small decrease of the tensile strength, which also suggests efficient reinforcement when clay particles are combined with PDMS. The film with one or no layer of PDMS in their structure presents a purely elastic deformation while the film containing two layers of PDMS has a curved shape that could be associated with some plastic deformation and rupture. Further incorporation of PDMS in the

multilayers could increase the plastic deformation and the toughness of the film but the Young's modulus would dramatically decrease.

Multilayer	Young's Modulus (GPa)	Stress at break (MPa)	Strain at break (%)
[Clay/PVAm]$_{500}$	45±5	251±14	0.60±0.1
[Clay/PDMS]$_{100}$	22±3	215±2.2	1.2±0.1
[Clay/PDMS/PDMS]$_{100}$	10.0±0.5	140±5	2.3±0.3

Table 2. Mechanical characteristics of (Clay/PVAm)$_{500}$ (red), [PVAm/Clay/PVAm/PMEMA/PDMS$_{2500}$/PMEMA]$_{100}$ (green) and [PVAm/Clay/PVAm/PMEMA/PDMS$_{2500}$/PMEMA/PDMS$_{2500}$/PMEMA]$_{100}$ (blue) obtained in dry conditions (RH<5%). Each result corresponds to the average of four tensile tests and the standard errors are reported.

[Clay/PVAm]$_{500}$ [Clay/PDMS]$_{100}$ [Clay/PDMS /PDMS]$_{100}$
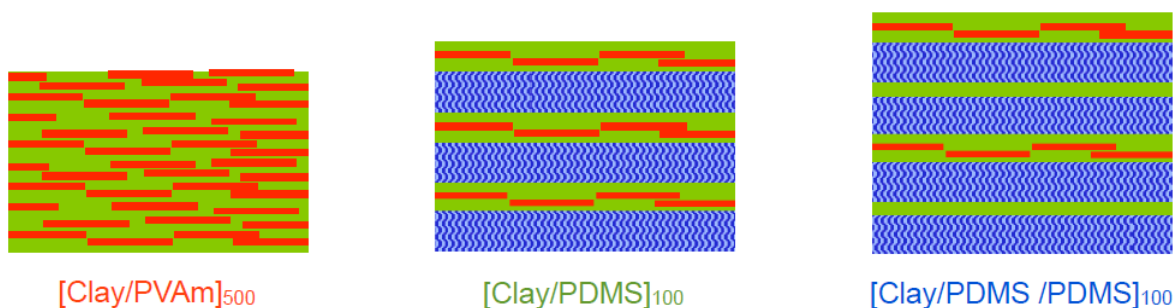
Figure 79. Schematic representation of the structure of the films prepared. With in red the clay platlets, in blue the PDMS layer and in green the adhesive layer (poly(vinyl amine) and/or PMEMA). The relative thicknesses are not on scale.

Tensile tests were performed in dry conditions because water appeared to modify the mechanical properties of the films. Initially most of the measurements were performed in ambient conditions with relative humidity between 20 % and 40 % and led to the results presented in Figure 80 and Table 3.

We observed that humidity strongly decreases the stress at break of the film especially for the film with high clay content. The Young's Modulus on the other hand is only weakly affected. As explained before, the Young's modulus depends on the content and modulus of the clay platelets. As none of them changes with humidity the composite modulus remains constant. The decrease of stress at break suggests that some bonds are weakening when humidity increases. It is know that water can weakens electrostatic interaction and act as plasticizer for polyelectrolyte complexes.[178] We believe that water weakens the clay-PVAm interface and softens

the PVAm itself leading to the premature rupture of the film. According to the shear lag model developed for microcomposites[42] a failure of the matrix or platelet/matrix interface leads to a ductile rupture of the material because the platelets slide against each-others. Surprisingly in our films the weak point appears to be the PVAm but the material is brittle. Such kind of rupture is typically associated with a rupture of the platelets. Given the crystalline structure of clays it is improbable that their strength dramatically decreases with humidity and other clay-containing composites did not present any humidity dependent strength.[5]
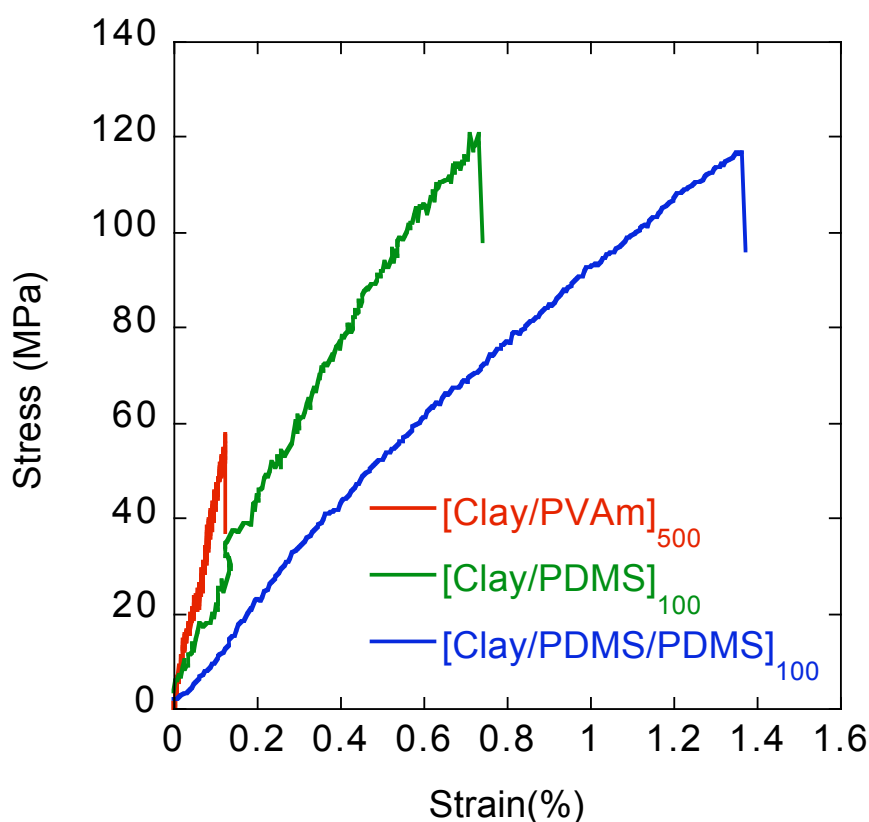
Figure 80. Stress-strain curves obtained for [Clay/PVAm]$_{500}$ (red), [PVAm/Clay/PVAm/PMEMA/PDMS$_{2500}$/PMEMA]$_{100}$ (green) and [PVAm/Clay/PVAm/PMEMA/PDMS$_{2500}$/PMEMA/PDMS$_{2500}$/PMEMA]$_{100}$ (blue) at ambient humidity conditions (RH~30%).

We believe that models developed for macro- and micro-composites cannot be applied because of the nanometric scale of the interactions between clay platelets. Other LbL assembled nano-composites also present surprising behavior compare to micro composites. For example an 8-fold increase of the Young's modulus was reported for clays/poly(vinyl alcohol) composites upon cross-linking[5] which is

contradictory with the rule of mixture since neither the content or the modulus of the nano-reinforcing component are modified. The films containing clays and PDMS have a lower sensitivity to humidity. We assume that the hydrophobic properties of the PDMS reduce the humidity uptake of the film. The crosslinking of poly(vinyl amine) with PMEMA also probably reduces its sensibility to water.

Multilayer	Young's Modulus (GPa)	Stress at break (MPa)	Strain at break (%)
[Clay/PVAm]$_{500}$*	53±11	60±5	0.11±0.1
[Clay/PDMS]$_{100}$	18±0.3	121±6	0.8±0.1
[Clay/PDMS/PDMS]$_{100}$*	8.4±0.5	126±10	1.6±0.3

Table 3. Mechanical characteristics of (Clay/PVAm)$_{500}$ (red), [PVAm/Clay/PVAm/PMEMA/PDMS$_{2500}$/PMEMA]$_{100}$ (green) and [PVAm/Clay/PVAm/PMEMA/PDMS$_{2500}$/PMEMA/PDMS$_{2500}$/PMEMA]$_{100}$ (blue) in ambient humidity conditions (RH~30%). For films marked with * only two curves were exploitable while for the other one the value and standard error corresponds to four measurements.

Note that the film containing two layers of PDMS was in this case only 1 μm thick which corresponds to the construction with a solution of PMEMA at 1 g/L. As we can see (Table 2 and Table 3) the Young's modulus of the two films are comparables.

In this project we prepared successfully nacre-like materials by combining clays, poly(vinyl amine) and PDMS. The mechanical properties of [clay/PVAm] films surpass those of most non crosslinked layer-by-layer assembled films[5, 51] but their strength is sensitive to humidity. We showed that it was possible to tune the Young's modulus of these materials by controlling the content of soft PDMS between the clay layers. The combination of clays with PDMS also reduced the sensitivity of the films to humidity.

These results open perspectives for many further experiments. It would, for example, be interesting prepare multilayers incorporating platelets with smaller aspect ratio. Smaller Clay platelets small enough could allow plastic deformation and improve toughness of the films.[131] On the other hand the incorporation of thicker inorganic platelets or shorter PDMS segments could lead to films with a higher Young's modulus.

Nacre and bones combine strength and toughness, but their maximal deformation and flexibility are limited. Wood on the other hand can be either flexible to handle bending (young trees) or stiff and strong (old trees) to support the weight of the leaves and branches. The variation of mechanical properties of wood structures are controlled by the organization of the cellulose fibers in the cell wall.[8] In the following chapter the preparation of multilayers containing cellulose is described and their properties are discussed in regard with the content and organization of the fibers in the film.

5 Fibrilar wood-inspired nano-composites

Wood and more generally the cell walls of plants combine flexibility, strength and lightweight. These materials are polymer/polymer composites, they consist of ordered strong cellulose fibrils embedded in a soft matrix. The concentration of the cellulose fibers and their organization in the material define the flexibility and the resistance of the entire structure.[8] In the present work, we produced films with similar architectures using layer-by-layer technique. The multilayers obtained consist of fibrils randomly oriented in the plane of the material and bound by a polymeric matrix. We varied the composition of the film by changing the pH of construction and studied its effect on the properties of the film. Using spin-assisted layer-by-layer assembly we also prepared oriented multilayers. The strength of these wood-inspired structures reaches record values along the direction of orientation while the transverse strength decreases compared to random films.

5.1 Dip-assisted assembly of MFC-containing multilayer.

Poly(vinyl amine) is known to improve the mechanical properties of paper.[203] We assembled anionic microfibrillated cellulose (MFC) with poly(vinyl amine) (PVAm) using dip-assisted layer-by-layer assembly. Poly(vinyl amine) is a weak polyelectrolyte and we reported in the previous chapter that its interaction behavior

changes with the pH of deposition. Typically as the pH of the poly(vinyl amine) solution increases film build-up speed increases. In this part we will look at the influence of the pH on the build-up and composition of the film. We will also study the microstructure of films containing microfibrillated cellulose and characterize the optical and mechanical properties of the obtained freestanding multilayers.

5.1.1   Effect of the pH on the construction

We first investigated the influence of the charge density of the poly(vinyl amine) on the construction of the multilayer. The degree of ionization of poly(vinyl amine) (weak polyelectrolyte) changes with the pH (Figure 81A). As the pH increases less and less amine groups are protonated and the charge of the poly(vinyl amine) chains decreases. The most significant behavior changes take place when the degree of ionization tend to zero. Therefore we built multilayers from poly(vinyl amine) solutions with a pH varied from 8 to 11 (Figure 81B). The pH of the MFC suspension and rinsing solutions were kept constant at pH = 6.0 ± 0.5.
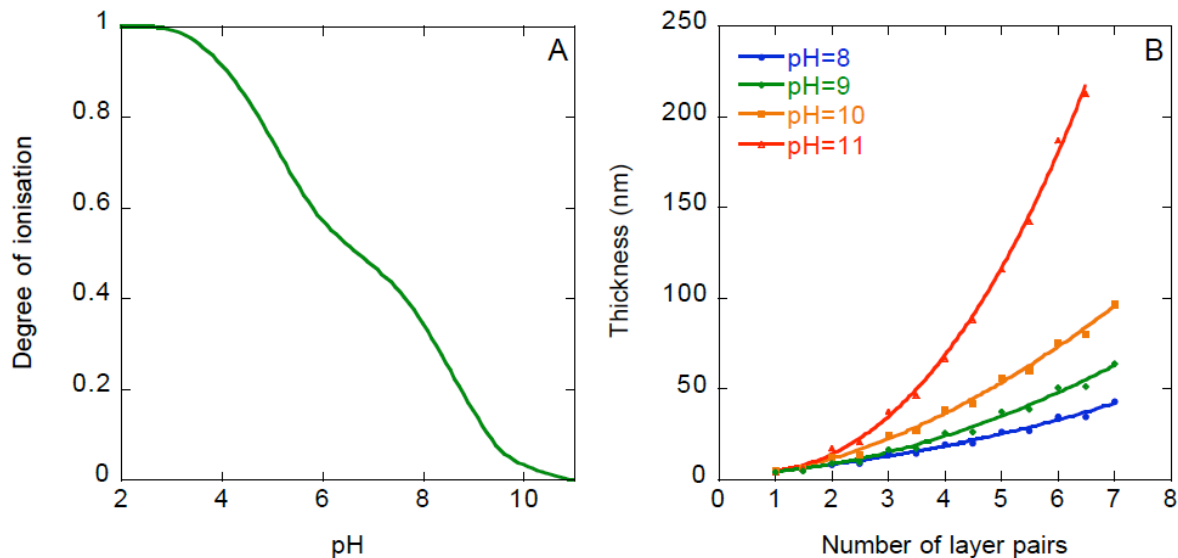
Figure 81. (A) Evolution of the degree of ionization of the PVAm with the pH in the absence of salt.[204] (B) Dip-assisted assembly of poly(vinyl amine) and microfibrillated cellulose as a function of the pH of the PVAm solution followed by ellipsometry.

As the charge density on the PVAm is reduced with higher pH the build-up speed increases: a 6 layer pair film built at pH 8 was 35 ± 1 nm thick while a 6 layer pair film built at pH 11 was 187 ± 10 nm. Simultaneously the growth regime of the film changes from (nearly) linear to super linear. This phenomenon, reported for other

polyelectrolyte couples,[93, 205] is related to the decrease of the charge of the PVAm with the pH (Figure 81A), while the MFCs bearing carboxylic groups (pKa around 4.5) do not see their degree of ionization modified[204] in the studied pH range. It has been reported that as the charge on the PVAm chains decreases the amount of PVAm adsorbing on reference cellulose surfaces increases.[206] At the same time the mobility of the PVAm in the film increases, and the film growth becomes superlinear. In all experiments, we rinsed with pure water (pH = 6.0) to prevent salt crystallization during drying. The solutions of MFC were also kept at a pH of 6 to prevent colloidal destabilization. Under these experimental conditions, we observed a clear effect of the pH on the construction of the films, the superlinear behavior may have been amplified by the alternation of high and low pH.[207] At low pH we observed a step-growth with higher thickness increase for the MFC than for the PVAm. At high pH this difference is much less pronounced. We quantified this effect by ellipsometry and X-ray photoelectron spectroscopy (XPS) (Figure 82B).
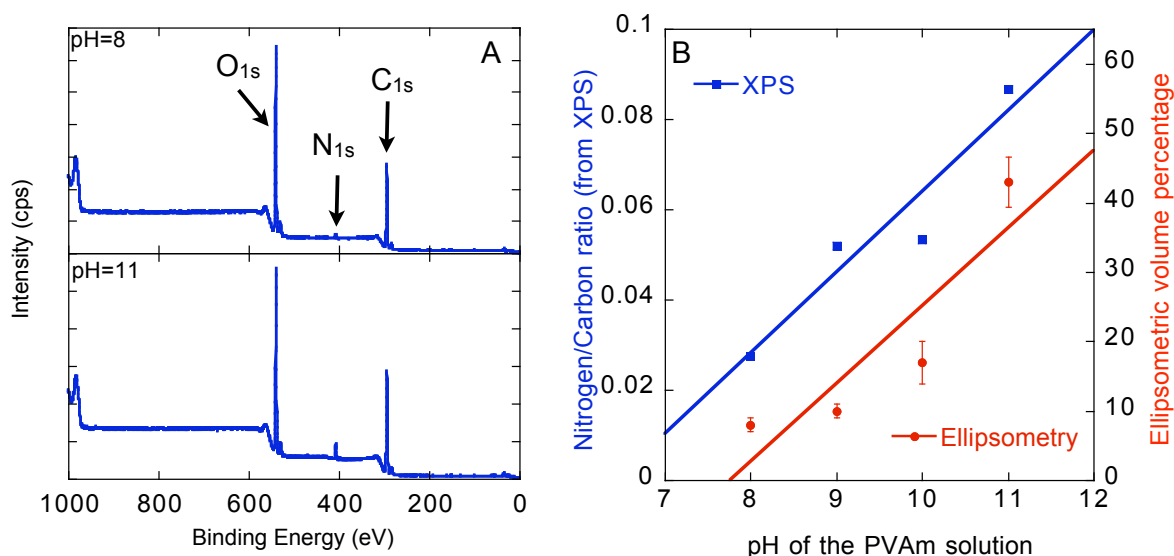
Figure 82. (A) Example of two XPS curves from samples built at pH 8 (top) and 11 (down). (B) Content of PVAm in the films built at different pH values. (in blue) Ratio of the integral under the N1s and C1s peaks in the XPS spectra of micron thick films with MFC as last layer. (in red) Percentage of the ellipsometric thickness increase for the PVAm layer. Solid lines have no physical meaning and are just guide for the eyes.

We measured the thickness of the films by ellipsometry after the deposition of each layer of either PVAm or MFC. The ratio of components in the film corresponds to

the ratio of their thicknesses. Despite some errors in both measurements (Figure 82B), XPS corroborates compositional data obtained from ellipsometric thickness determinations and confirms that the amount of PVAm adsorbed in the film during build-up increases with the pH this is also consistent with previously reported results on other films.[94] Simple explanation of this effect is that as the charge density of the PVAm decreases, more and more PVAm molecules are needed to compensate the charge of the MFC (constant) and to produce a film with stoichiometric charge balance. The XPS spectra of micron thick films prepared by dipping with MFCs as last layer show a similar trend (Figure 82A and B). By increasing the pH of the PVAm solution, the area under the peak of the 1s orbital of nitrogen increases as compared to the area under the peak of the 1s orbital of carbon, revealing that the content of nitrogen on the surface is multiplied by a factor of about 3 as the pH is raised from 8 to 11. Since the last layer is composed of MFC an increase of the nitrogen/carbon on the surface correspond to an increase of the PVAm in the film. The effect of this controlled variation of the film composition with respect to PVAm (soft matrix) and MFC (nano-reinforcing component) on mechanical properties of such films will be studied later. We will now look at the microstructure of the film containing microfibrillated cellulose.

5.1.2   Microstructure of MFC layers

Microfibrillated cellulose form fibrils with a diameter of a couple of nanometers and micrometer length. They can be imaged using AFM after assembly on a silicon substrate and drying. Typical AFM images of $(PVAm/MFC)_8$ films built at pH 8 and 11 by dipping are shown in Figure 83.

We see that the films are continuous and display random in plane orientation of the MFC fibrils. Similar films built on hydrophobically modified silicon wafers were similar. One can notice that films built at pH 8 have a lower surface roughness (RMS = 4.9 nm) than those built at pH 11 (RMS = 8.9 nm). This difference is likely due to the higher thickness of the films built at pH 11, the roughness to thickness ratio actually decreases from pH=8 to pH=11. In any case it was already observed for other film forming components that multilayers with superlinear growth have rougher surfaces than their counterparts growing linearly.[205]
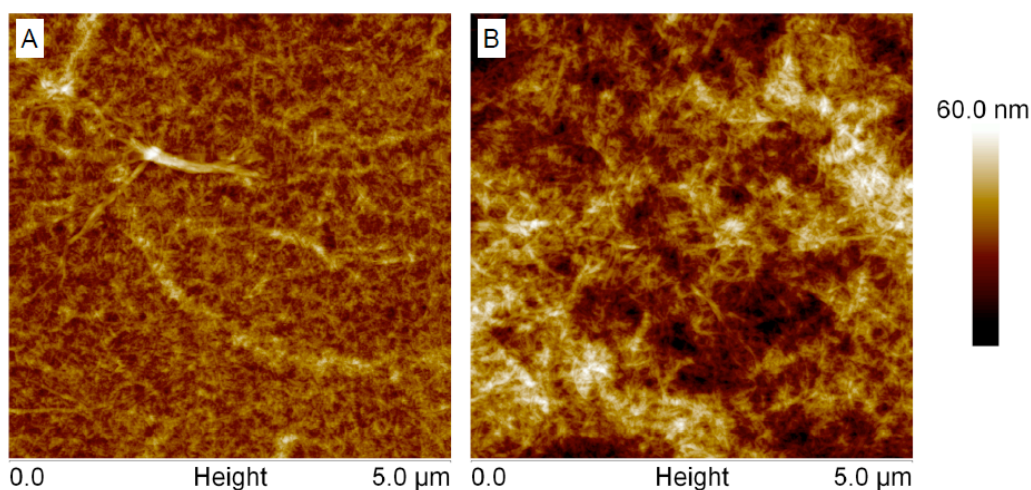
Figure 83. AFM images of (PVAm/MFC)$_8$ films built on silicon wafer from a PVAm solution at pH 8 (A) and at pH 11(B). The respective film thicknesses are 58 ± 1 nm and 320 ± 9 nm from ellipsometry.

In general the morphologies observed in the present work are very similar to those observed by other groups for LbL films containing MFCs.[6, 148] These structures have a similar organization as the external layer of plant cell wall with in plane randomly oriented fibers embedded in a matrix. While the ultimate film strength would require parallel orientation of the fibers, this organization leads to isotropic mechanical properties. We will now see how to prepare thick freestanding multilayers and characterize their tensile properties.

5.1.3 Thick freestanding films

In order to produce freestanding micron thick films we used octadecyltrichlorosilane coated silicon wafer. As explained in the previous chapter a film built on such substrate can be peeled easily. It has been reported that MFC-containing film could be built on similar supports.[6] In our case, however, the construction of thick film on modified substrates led to the formation of crack patterns on the surface of the film (Figure 84A). At pH = 8 the first cracks appeared for a film thickness of about 600 nm making the mechanical tests impossible. The apparition of cracks is probably due to the shrinking of the film upon drying in combination with poor adhesion on the silicon substrate. We noticed that the cracking of the film was pH sensitive; increasing the pH lowered significantly the number of cracks. Apparently, as the amount of polymer in the film increases, the

stress generated by drying decreases. This probably also explains why previously reported films containing about 20 % of poly(ethylene imine) did not crack.[6]

The construction of multilayers directly on hydrophobic silicon wafer has already been reported for LbL-films composed of clays and poly(vinyl alcohol) (PVAl).[131] Thus we used one layer pair of this clay-based system to enhance the adhesion of our film on the hydrophobic substrate. AFM imaging of the first layer pair shows that the fibrils are adsorbing on the substrate with (Figure 84C) and without (Figure 84B) pre-deposited poly(vinyl alcohol)/clay layer. But after deposition of this adhesion layer it became possible to build micron thick films without macro-cracks (Figure 84D). As the film is transparent (no light diffusion) we assumed that there was no micro cracks either, this was later confirmed by AFM. Because of its neutrality poly(vinyl alcohol) has more affinity to the hydrophobic substrate than poly(vinyl amine) therefore it adheres better on the substrate. Clays adhere on PVAl through hydrogen bonding and provide a silicon-oxide surface similar to the one of activated silicon wafer traditionally used in LbL deposition. This ensures the correct subsequent deposition of $(MFC/PVAm)_n$ films. Such a procedure only improved the adhesion enough to build micron thick films. The construction of thicker films at low pH eventually generates enough internal stress to induce cracks. Films deposited on top of theses substrates can still be easily removed using tape or tweezers.
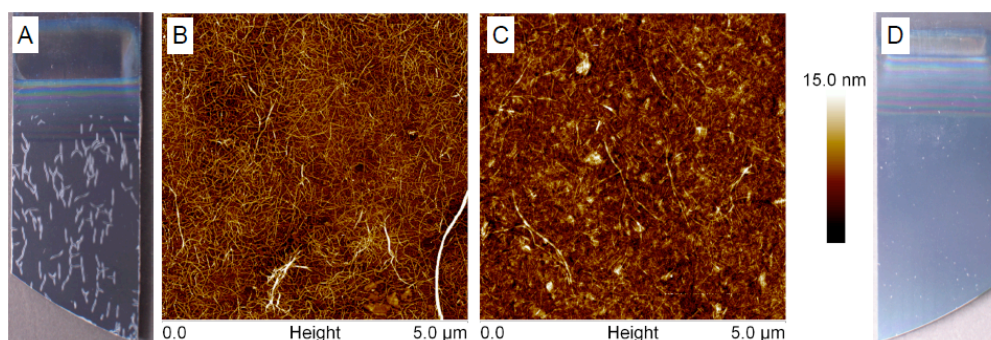
Figure 84. (A) **Optical photograph of the light diffused by $(PVAm/MFC)_{160}$ film built from a PVAm solution at pH=8. (B) AFM image of $(PVAm/MFC)_1$ built on a hydrophobic silicon wafer from a PVAm solution at pH 8. (C) AFM image of $(PVAl/clay/PVAm/MFC)_1$ built on a hydrophobic silicon wafer from a PVAm solution at pH 8. (D) Optical photograph of the light diffused by $(PVAl/clay)_1(PVAm/MFC)_{150}$ film built from a PVAm solution at pH=8.**

The characterization of the thickness of the film using spectroscopic ellipsometry is fast but the quantitative analysis of the ellipsometric data can be difficult. In order

to confirm the thickness values obtained by ellipsometry using a constant refractive index of 1.55 we imaged the edge of some samples by scanning electron microscopy and atomic force microscopy (Figure 85).
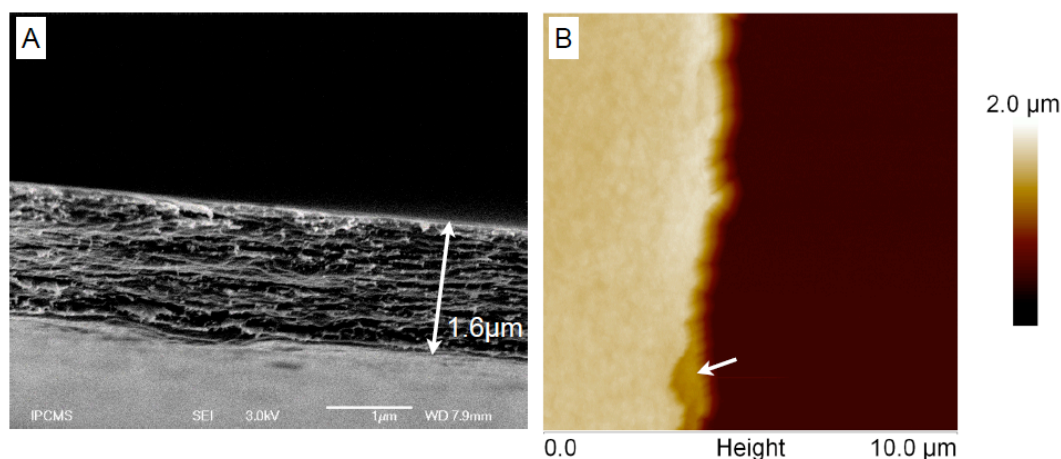
Figure 85. (A) **Cross section SEM image of a (PVAm/MFC)$_{30}$ film built from a PVAm solution at pH 11. The thickness measured is 1.6 μm. (B) AFM image of the edge of a (PVAm/MFC)$_{70}$ film built from a PVAm solution at pH 9 resting on a silicon wafer. The white arrow points at a step created during the rupture of the film. The profile reports a film thickness of 1.1 μm.**

The thickness of the film built at pH 11 measured by SEM was 1.6 μm which corresponds to the thickness obtained by spectroscopic ellipsometry (1.6 ± 0.1 μm). Similarly the thickness of the film built at pH 9 measured by AFM (1.1 μm) corresponds to the one obtained by spectroscopic ellipsometry (1.1 ± 0.1 μm). The model used in ellipsometry with a constant refractive index equal to 1.55 leads to accurate values both at high and low construction pH. The in-plane orientation of cellulose micro-fibrils in the film is visible on the SEM image. Both AFM and SEM confirm that films prepared are uniformly thick, homogeneous and rather smooth. In order to obtain smooth edges for microscopy the film were notched and carefully torn. The use of a scalpel gave rough edges that prevented accurate thickness measurements. One can observe on the edge at the bottom of the AFM image an intermediate step on the edge of the film (Figure 85B), which is typical of layered materials.

The homogeneity of the film and the precise assembly of microfibrillated cellulose and poly(vinyl amine) at the nano-scale make these films transparent (Figure 86A).

The presence of micro inhomogeneities or micro-scale phase separation would reduce transparency substantially.
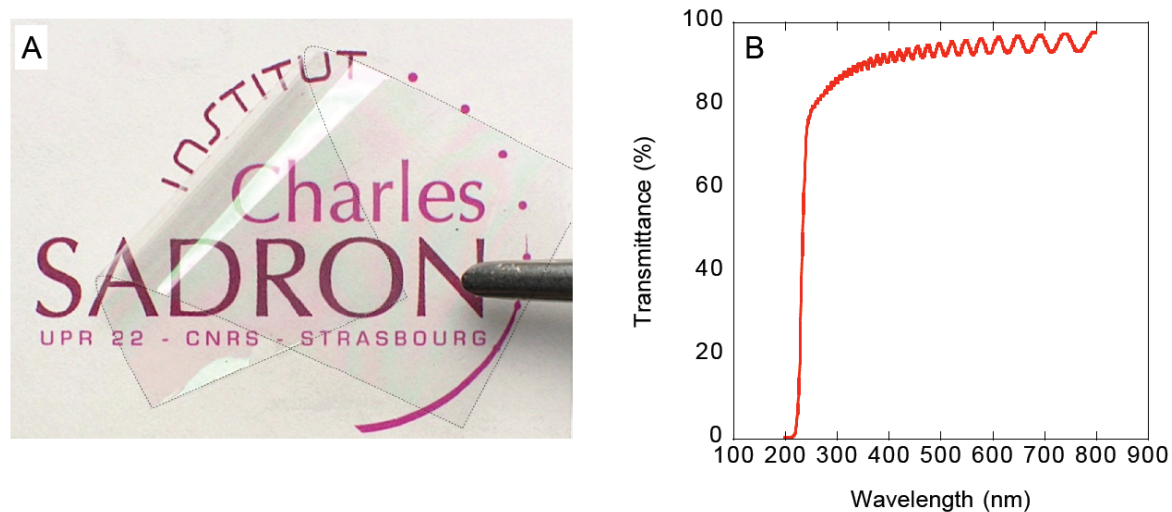
Figure 86. (A) **Optical photograph of a (PVAm/MFC)$_{60}$ film built from a PVAm solution at pH=10.5. The film thickness measured by spectroscopic ellipsometry is 3.8 ± 0.1 μm. The edges of the film are marked with a dotted line to facilitate the visualisation of film edges.** (B) **UV-Vis spectrum of a freestanding (PVAm/MFC)$_{75}$ film built from a PVAm solution at pH=10. The film thickness obtained by spectroscopic ellipsometry is 3.4 ± 0.1 μm.**

We recorded the UV-visible transmittance of a (PVAm/MFC)$_{75}$ freestanding film between 200 and 800 nm (Figure 86B). The film shows a high transparency over the entire visible spectrum with over 85% transmittance, while it strongly absorbs UV below 250 nm which is common for cellulosic material. Contrary to films prepared by vacuum filtration[55] this film do not require any polishing step to be transparent because their surface is flat after preparation. The UV-visible spectrum also displays typical Fabry-Perrot fringes which confirms the homogeneity of thickness and refractive index of the film.[201] The periodicity of the fringes can also be used to calculate the thickness of the film. Assuming a refractive index of 1.55 we estimated a thickness of 3.3 μm from this curve. Indeed this value is in good agreement with what was found by ellipsometry (3.4 μm). One can also distinguish shades of green and pink on the optical photography (Figure 86A), these colors come from interferences and are typically observed for thin films with uniform thickness and refractive index.

These films can be manipulated and folded without breaking. Their large surface and low thickness make them sensitive to air flows such as breathing or moving an

object, which makes the storage and sample preparation difficult. Such films were usually left on their support and the stripes of films needed for tensile tests were directly cut on the silicon wafer using a scalpel. After lifting off each sample was placed in a homemade sample holder (see material and method) before mechanical characterization.

5.2 Mechanical properties of MFC multilayers assembled by dipping

We could produce transparent nano-composites combining microfibrillated cellulose and poly(vinyl amine) using layer-by-layer assembly. The freestanding films produced are homogeneous, display a random in plane orientation of the cellulose fibers and their cellulose content is controlled by the pH of deposition of the poly(vinyl amine). We will now see how this impact the mechanical properties of the films with a specific focus on the influence of relative humidity (RH).

5.2.1 Influence of the pH of assembly on the mechanical properties of the films

The mechanical properties of the (PVAm/MFC)$_n$ films built from different PVAm solutions were systematically studied. In order to get comparable behavior for the different films the number of layer pairs was adjusted to have a similar total thickness for all the films (from 1.0 to 1.6 microns). The typical shape of the stress-strain curves is presented Figure 87 and the mechanical characteristics of the films are summarized in Table 4.
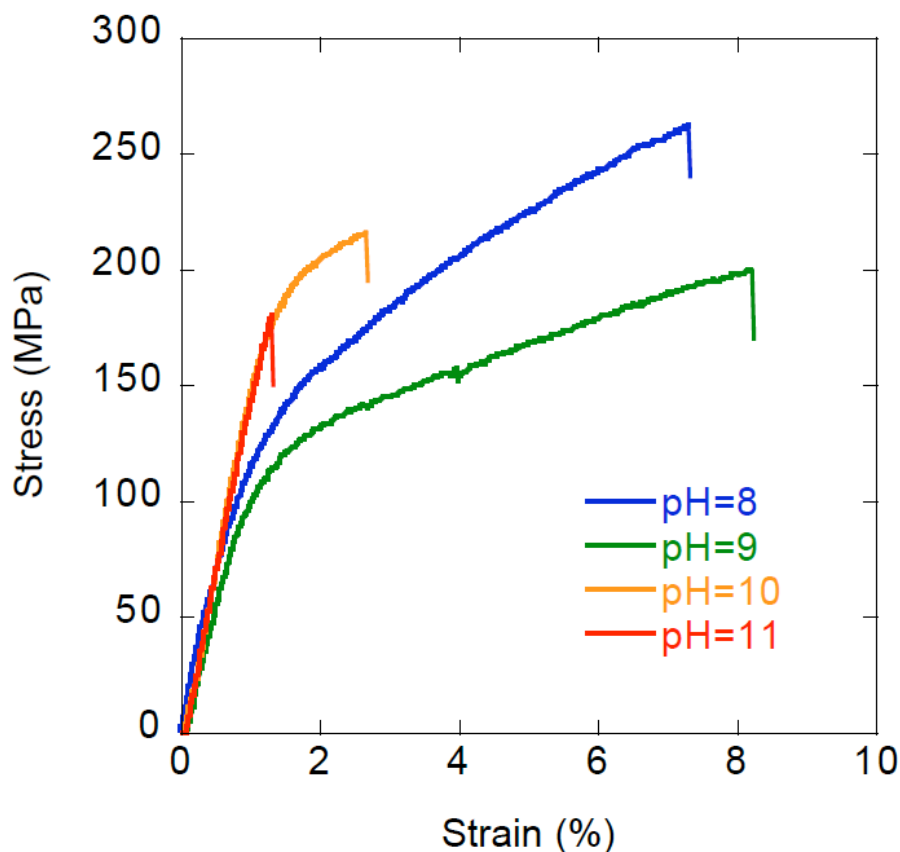
Figure 87. Typical stress strain curves obtained for micron thick (PVAm/MFC)$_n$ films built from PVAm solutions at pH ranging from 8 to 11 and tested at ambient humidity condition (RH~50%).

The mechanical characteristics obtained for these multilayers (with strength up to 290 MPa in some cases) are in the range of the best MFC-based material[7, 55] and are approaching the strongest LbL based materials (400 MPa).[5] We found that the Young's modulus of the film was sensitive to the pH of film construction: at pH 8 and 9 the modulus was around 12 GPa while at pH 10 and 11 we found a modulus around 17 GPa. We attributed this increase to a better reinforcing efficiency of the embedded MFCs as the content of PVAm increases. Similarly films built at pH 8 and 9 had a lower yield strength than the film built at pH 10, and the film built at pH 11 always broke before yielding (Figure 87). When the content in PVAm increases there are less weak fiber/fiber interactions and more strong fiber/PVAm interactions, therefore the Young's modulus and the yield strength increases. At pH 10 an optimum composition seems to be reached with a high Young's modulus, high strength and fast growth. However the best values in terms of strength (290 or 235 MPa) were obtained for films built at low pH probably due to higher content of MFC and higher toughness. The relatively large standard deviation obtained for

these measurements are due to the difficulty to obtain perfectly smooth edges during sample preparation leading to a premature breaking of the film (i.e. some abnormally low mechanical properties were due to the sample preparation and not to the sample itself). In all cases, the shape of the tensile curves was characteristic of the pH of construction. We also built multilayers containing cationic microfibrillated cellulose and poly(acrylic acid) deposited at pH 3. Their build-up and mechanical properties were similar with strength reaching 250 MPa but due to limited supply of these cationic fibrils we stopped these measurements. To summarize, the amount of polymer in the film increases with the pH of construction. With a pH increase the strength and toughness of the film decrease because the amount of reinforcing components decrease. At the same time the Young's modulus and yield point increase because the reinforcing efficiency of each fibers increase as the amount of soft glue (PVAm) increases.

pH	Number of layer pairs	Thickness (µm)	Young's Modulus (GPa)	Stress at break (MPa)	Strain at break (%)
8	150	1.35 (±0.01)	12.1 (±1.8)	206 (±66)	4.7 (±3.1)
9	70	1.12 (±0.05)	11.9 (±1.1)	209 (±19)	8.9 (±2.6)
10	30	1.02 (±0.03)	17.7 (±0.6)	197 (±27)	2.5 (±1.8)
11	30	1.65 (±0.07)	16.5 (±1.5)	141 (±43)	0.9 (±0.4)

Table 4. Mechanical characteristics of micron thick films built from PVAm solutions at pH ranging from 8 to 11 and tested at ambient humidity condition (RH~50%). At least four samples (same film) were tested for each films and the number in brackets indicates the standard deviation.

Wågberg *et al.* recorded modulus of 9.3 GPa and strength of 80 MPa for (PEI/MFC)$_n$ layer-by-layer assembled films.[6] Their measurement were performed in moisture free conditions as water is known to plasticize polyelectrolyte multilayers.[178] The large difference in mechanical properties could be attributed to variation of humidity or to the nature of the polyelectrolytes. In order to answer this question we decided to investigate the influence of humidity on the mechanical properties of the films.

5.2.2   Plasticizing effect of water

We studied the effect of relative humidity (RH) on the mechanical properties of a film built at pH=10. We used a thicker film in order to facilitate the manipulation and to ensure sufficient strength in wet conditions. The measurements in dry conditions (equilibration for 24 hours) were done under a flux of dried compressed air in a closed box, while the measurements in wet conditions were performed after deposition of a drop of water on the surface of the films. The presence of a drop of water on the film during measurement was assumed to be similar to the thin layer of water present at the surface of a sample in an atmosphere saturated with humidity (RH=100%).
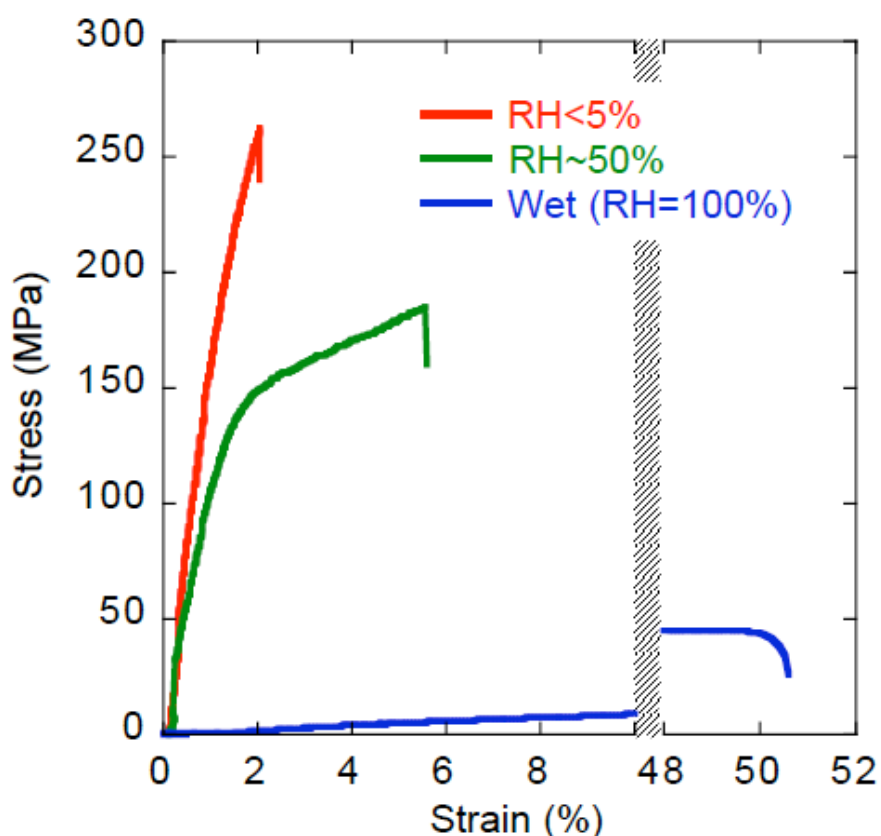
Figure 88. Typical stress strain curves obtained for (PVAm/MFC)$_{75}$ thick films (3.4 ± 0.1 µm) built from PVAm solution at pH=10 in various humidity conditions. Note the x-axis break between 10 and 48%.

The general effect of humidity can be clearly seen on the stress-strain curves. As humidity increases, strength and Young's modulus of the film decrease while the

strain at break increases (Figure 88). This effect can be mostly attributed to the nature of the interactions in the material (Figure 89).

Humidity	Young's Modulus (GPa)	Stress at break (MPa)	Strain at break (%)
< 5 %	16 (±3)	237(±31)	1.7 (±0.4)
~ 50 %	12 (±2)	174 (±20)	3.3 (±2.2)
Wet (100%)	0.12 (±0.01)	46 (±11)	49 (±8)

Table 5. Mechanical characteristics of thick (PVAm/MFC)$_{75}$ films (3.4 ± 0.1 μm) built from PVAm solution at pH=10 in various humidity conditions. At least three measurements (same film) were done in each conditions and the number in brackets indicates the standard deviation.

At low RH, there is very little water in the film, the electrostatic interactions between the fibers and the PVAm are strong, and the PVAm is rigid. This leads to a very strong composite, reaching the strengths of the best MFC-based materials with low maximal strain and no plastic deformation. Compared to previously reported poly(ethylene imine)/MFC LbL films[6] these films have higher Young's modulus and strength. Since the humidity conditions are similar we attributed this to the strong binding of PVAm with cellulose.[208] In this context it is also interesting that linear polymers are known to reach higher strengths than comparable highly branched dendrimers which is tought to be due to more entangled conformations for similar molar mass.[17] The humidities at which we performed the mechanical tests are also slightly higher (~3%) than those used by Wägberg and coworkers (~0%).

At ambient conditions (RH~50%), the film absorbs some water. As a consequence the electrostatic interactions and the hydrogen bonding between MFC and PVAm decrease and the poly(vinyl amine) is partially plastified. Surprisingly the Young's modulus is weakly affected (Table 5). This is in agreement with theories for macro-composites with high aspect ratio fibers[17] but recent buckling experiments on cellulose-containing LbL films suggested that hydration could also decrease the modulus of the film by a factor 10.[157, 209] This difference could be explained by the nature of the polycation used. The poly(vinyl amine) used for the present work, is known to bring wet strength to paper formulation,[208] while polyethyleneimine might be more sensitive to humidity. Another explanation for the observed differences

could arise from the techniques used, as buckling mechanics and tensile experiments might lead to different results when applied to lamellar composites.[174]

At ambient humidity conditions the films yield around 150 MPa and reach strains up to 6%. The plastic deformation can be explained according to the shear-lag theorie[17, 42] which considers sliding at the interface between the fibers and the PVAm or plastic deformation of the PVAm. Both phenomena would be promoted by the increase of humidity as water can either plastify PVAm or screen the electrostatic interactions between the fiber and the polymer matrix.
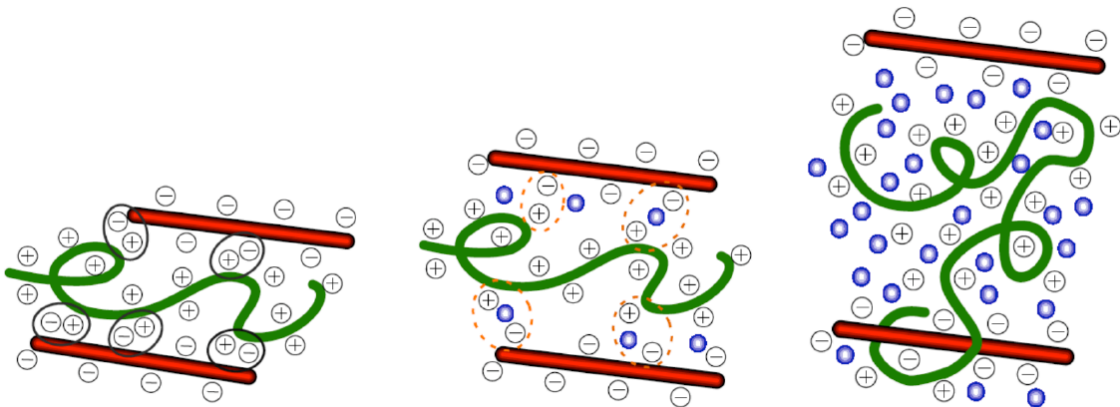
Figure 89. Simplified molecular sketch of the effect of hydration on the interactions between MFC and PVAm. The green lines represent PVAm, the red sticks correspond to MFC and the blue dots represent the water molecules in the film, + and - symbols are representing respectively pending ammonium and carboxylate groups (counter ions have been omitted for clarity).

In wet conditions (RH=100%), the films swell and the electrostatic interactions and hydrogen bonds between the 2 components are greatly decreasing in strength allowing rearrangements and diffusion in the film. Consequently the Young's modulus decreases to 120 MPa and the maximal stress decreases to a quarter of its value at ambient conditions (RH=50%). On the other hand the maximal strain increase to 50%. As the interactions holding the material together are screened the figers and polymer chains can move and rearrange to withstand the deformation without breaking. The elastic modulus and maximal strain are calculated using the dry thickness; this makes the comparison with other cellulose hydrogels difficult.[210, 211]

158

Interestingly heating the films for 12 hours at 120°C before mechanical tests doubled the strength and Young's modulus in wet conditions but didn't impact significantly the properties at other humidities. The thermal treatment creates covalent amide bonds between the carboxylic groups at the surface of the fibrils and the amine groups of the PVAm.[212] In the wet state the hydrogen and electrostatic interaction are screened while covalent bonds stay unmodified. Therefore the Young's Modulus and strength are improved by the creation of amide bonds. In the dry states the electrostatic and hydrogen interaction are probably sufficient to reach high strength and some extra covalent bonds do not impact the overall mechanical properties.

Note the lower strength and Young's modulus for this 3.4 µm film than for the 1.0 µm thick film built at pH 10 (Table 4 and Table 5). It appears that there was a decrease of the pH of the solution of PVAm during deposition. After 30 layer pairs the pH of the PVAm solution was 9.8 while after 75 layer it reached 9.3. This explains why the mechanical properties of thicker films are located between the properties of the film built at pH 10 and at pH 9 when the pH of the deposition solution is not regularly adjusted during deposition. Based on this observation, the conclusions on the changes of mechanical properties with humidity remain valid.

We also measured the mechanical properties of the film previously measured at ambient humidity in the dry state. The typical shape of the stress-strain curves is presented Figure 90 and the mechanical characteristics of the films are summarized in Table 6.
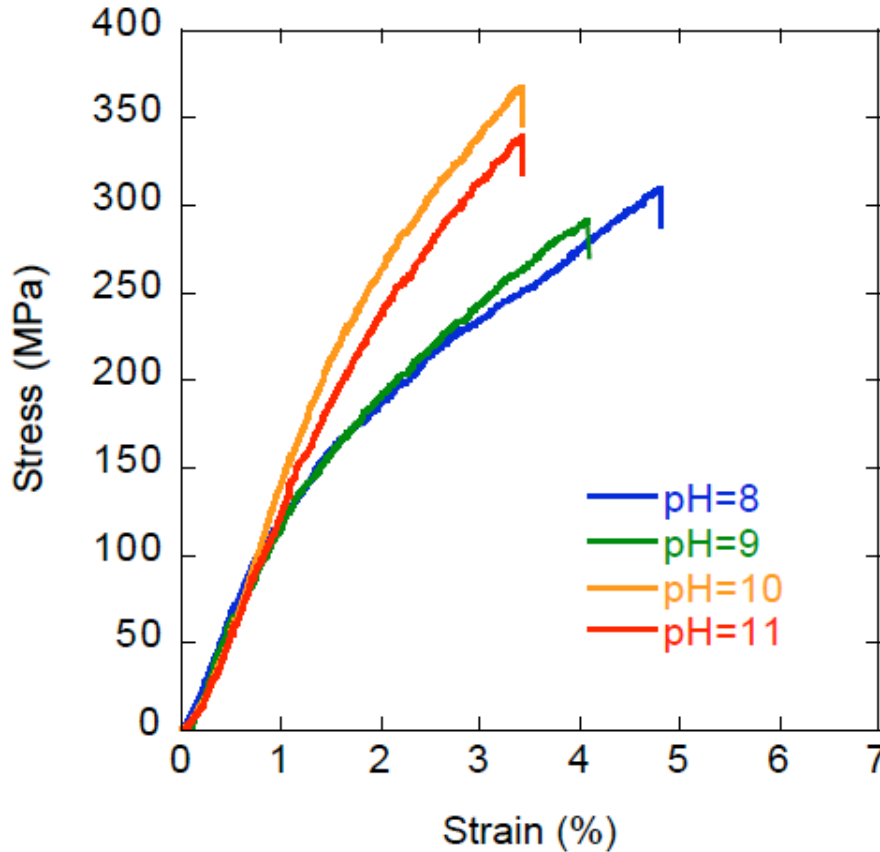
Figure 90. Typical stress strain curves obtained for micron thick (PVAm/MFC)ₙ films built from PVAm solutions at pH ranging from 8 to 11 and tested in dry conditions (RH<5%).

Data in Figure 90 are from individual experiments whereas the data in Table 6 are average values. Average values are too low because films with more defects systematically break prematurely. The optimization of the sample preparation with respect to a reduction of defects leads to mechanical properties closer to the bulk values. The standard deviation obtained for these measurements are higher than the values obtained in ambient conditions. The brittleness of the dry films added to their low thickness made it difficult to obtain reproducible results.

Measured in dry conditions the films had a lower stress at break and reached higher strength than at room humidity conditions. We also noticed that films built at pH 10 and 11 are more sensitive to humidity than films built at pH 8 or 9. The first films contain larger amounts of poly(vinyl amine) than the later ones. A stronger impact of hydration on their mechanical properties is actually to be expected since water mostly plasticizes poly(vinyl amine). In all cases the plastic deformation disappears in dry conditions. Here again we observe that a variation of humidity between 50% and 5% had a low impact on the Young's modulus (Table 4).

pH of buildup	Number of layer pair	Thickness (µm)	Young's Modulus (GPa)	Stress at break (MPa)	Strain at break (%)
8	150	1.35 (±0.01)	13.3 (±1.1)	215 (±93)	3.0 (±2.0)
9	70	1.12 (±0.05)	12.2 (±0.5)	237 (±55)	3.0 (±1.9)
10	30	1.02 (±0.03)	15.4 (±0.6)	235 (±76)	2.2 (±1.8)
11	30	1.65 (±0.07)	14.1 (±0.2)	251 (±112)	2.2 (±1.2)

Table 6. Mechanical characteristics of micron thick films built from PVAm solutions at pH ranging from 8 to 11 and tested in dry conditions (RH<5%). At least three measurements were done for each films and the number in brackets indicates the standard deviation.

Hydration has a strong influence on the mechanical properties of these layer-by-layer assembled films. Water makes the poly(vinyl amine) phase softer which allows plastic deformation and increases the toughness of the film. But water also reduces the adhesion between the matrix and the microfibrilated cellulose and therefore the strength of the films. In dry conditions several samples reached a stress at break over 300 MPa a value surpassing most microfibrillated cellulose based composites.[145] In wet conditions the films are soft because the electrostatic interactions holding the material together are mostly screened. The mobility of the poly(vinyl amine) chains could be an advantage to allow self-repaire of damaged materials.

5.2.3   Self-repairing

During our investigations on the effect of hydration, we observed that films had the tendency to stick to themselves after immersion in water. Since some LbL materials growing superlinearly were reported to posses self-repairing capabilities,[213] this was further investigated. The films built from poly(vinyl amine) solution at pH=11 presented the most pronounced superlinear behavior (Figure 81) and were also the most sticky when wet. MFC-based films were less and less self-adhesive as the pH of construction decreased. All the self-repairing experiments reported hereafter were conducted with films built from a poly(vinyl amine) solution at pH=11.
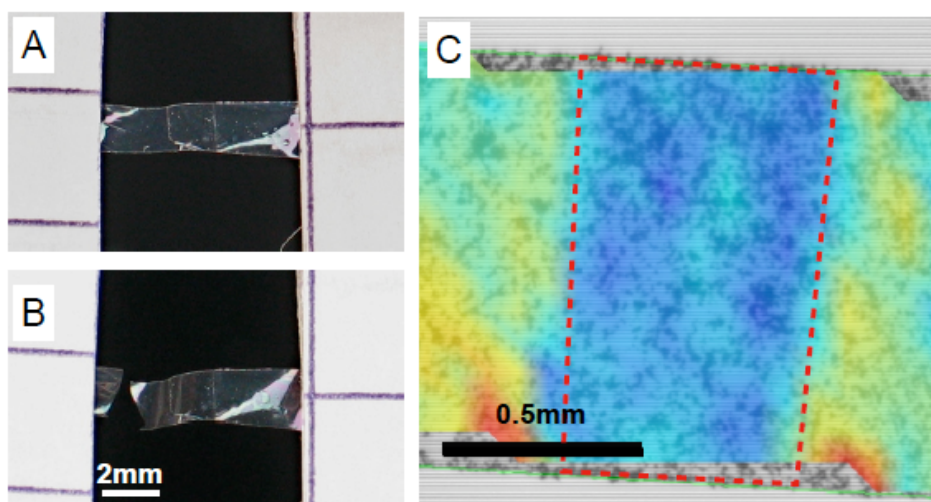
Figure 91. Optical images of a self-repaired film before (A) **and after** (B) **pulling on it.** (C) **Visualization of the deformation of a repaired film by image correlation. The image extracted from the video (grey scale) displays the film with black patterns coming from printer toner deposited on it. The colors added by the correlation software show in blue low deformation regions, and in orange high deformations. The overlap region is outlined in dashed red.**

A simple self-repairing experiment is performed by superposing the edges of two wet films with an overlap of 0.5 to 2 mm. The procedure typically implied to dispose one part of a film on a hydrophobic substrate, wet it and then place the second film piece (still dry) on it. After wetting completely both of them, the water was removed with a gentle blow of compressed air, which led to the production of a self-standing film. Then, we carried out tensile tests on the repaired films and surprisingly all the samples broke outside of the repaired region (Figure 91B). The stress at break obtained for repaired films was 157 ± 33 MPa, a value comparable to the 174 ± 20 MPa obtained for virgin films. By deformation mapping obtained from digital image correlation (Figure 91C) it was shown that the overlap area between both films deforms much less than the rest of the film. The lower deformation in this region reveals a proper healing: the film behaves as if it was a continuous film with a region twice as thick in the middle. A film twice as thick has a cross section twice as big and is therefore subject to a twice lower stress, which implies a lower deformation. We did not observe regions of high and low deformation that would appear if the two pasted films were sliding or partially delaminating. The red parts at the bottom of the images come from artifacts in the calculation of deformation at the limits of the area of interest known as edge effects.

The self-repairing properties observed at wet conditions are probably enabled by the mobility of the polymer chains in the multilayer in the presence of water. Composite hydrogels showing somewhat similar behavior have been described.[214, 215] We also performed self-healing experiment on supported films. With a sharp razor blade we sliced the surface of a film resting on a silicon substrate and imaged the cut by AFM. We immersed the film in water for five minutes and re-imaged the same part of the cut after drying (Figure 92).
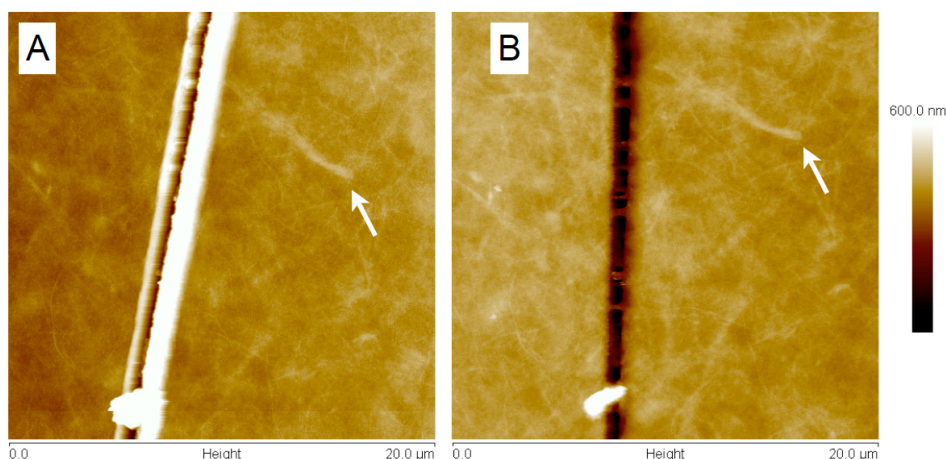
Figure 92. AFM images of the cut made in a (MFC/PVAm)$_{30}$ film (1.65 μm thick) before immersion in water (A) and after immersion in water for five minutes and drying (B). A random feature in the film, indicated by the white arrow, confirms that both images were taken at the same location.

Before immersion in water the cut presents rough elevated edges and pieces of film are present near the cut. After immersion in water the edges of the material are laying flat and links have been formed between the two edges of the material. It is also visible on the bottom of the cut that the piece of film initially resting on the top of the cut has been incorporated in the film and bridges the gap. We later tried to immerse the film in water for one hour, but there was no further healing of the cut. Looking more closely at the two images it seems that most of the bridges after immersion correspond to small particles present in the cut on the right image. The absence of contact between the edges of the film prevents a full healing of the cut, but the film is soft enough to allow particles in contact with the two edges of the material to fuse and to stitch the cut. This is more visible on the particle at the bottom of the image that partially merges with the film upon hydration. This experiment confirms that the films built at pH=11 can self-heal in the presence of water. A more tangible proof of the self-repairing abilities of these films at the

micro-scale would require contact between the two edges, which may be an interesting perspective for future work.

Layer-by-layer can be used to prepare strong microfibril-based films in combination with poly(vinyl amine). The mechanical properties of the films depend on the composition of the film that can be controlled by the construction parameters. The humidity conditions during measurements also strongly impact the mechanical properties of the films. We have seen that once they are fully hydrated the film with the highest amount of poly(vinyl amine) can self-heal but only if the two parts to be repaired are put in contact.

The structure of these films with random in plane orientation of the fibrils mimic the primary layer of plant cell wall. But it is the secondary plant cell walls with oriented fibers that controls the mechanical properties of wood.[2] In order to prepare stronger films we prepared oriented structures.

5.3 Spin-assisted orientation of the microfibrils

Spin coating has been used to orient collagen fibrils[216] in thin films and to produce carbon nanotube-based transistor[164] with exceptionally high on/off ratio. The strength of fiber reinforced composites depends on the orientation of the fibers in the material.[17] In this part we will discuss the construction of cellulose-containing multilayer using spin-assisted layer-by-layer deposition. We will then evaluate the orientation of the micro-fibrils in the film and the resulting mechanical properties.

5.3.1 Spin assisted build-up of MFC containing films

Spin-assisted LbL-assembly allows to build thick multilayers more rapidly than dipping.[114] The film produced in this way are also typically smoother (at the microscale) than dipped films.[115] We built films by spin-assisted LbL using anionic microfibrillated cellulose at pH=6 and poly(vinyl amine) at pH=8. The LbL-films were built directly on hydrophobic silicon wafers using two different rotation speeds. Surprisingly we did not have adhesion problems with spin-assisted deposition. The film growth followed by ellipsometry is reported in Figure 93 together with optical photograph showing interference colors at different stages of the build-up.
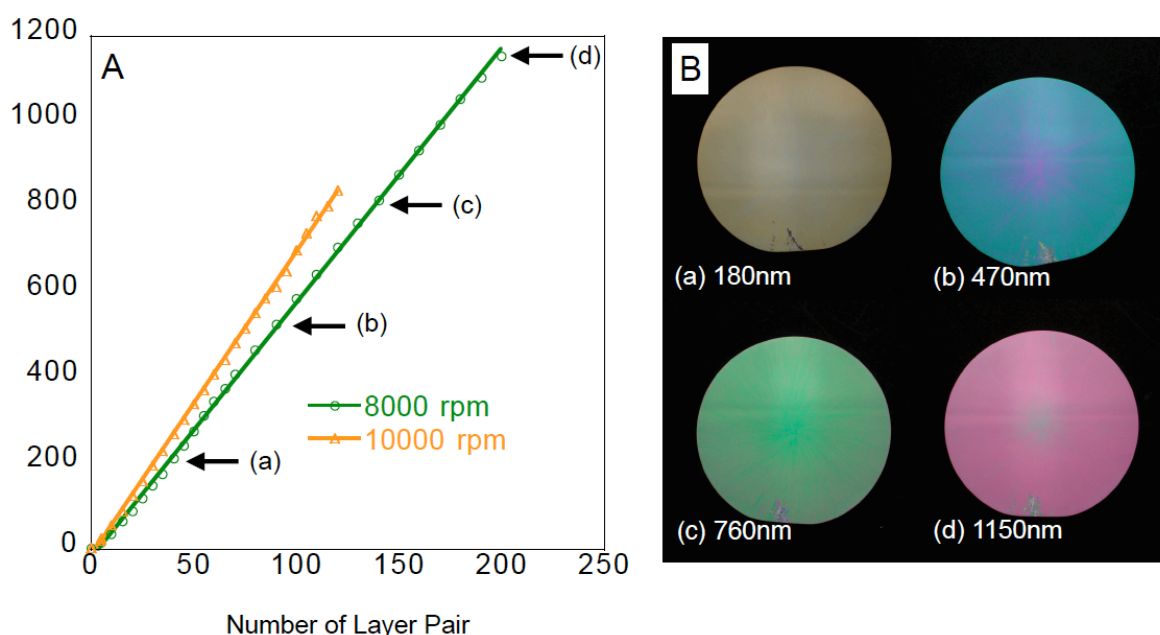
Figure 93: (A) Build-up of (PVAm/MFC)$_n$ using spin-assisted assembly with rotation speed of 8000 and 10000 rpm followed by ellipsometry. Film thickness was measured every five (or ten) layer-pairs using spectroscopic ellipsometry assuming a constant refractive index of 1.55. Letters in brackets correspond to the pictures (B). (B) Reflection pictures showing the interference colors of the film at different thicknesses (indicated below each sample).

The growth of the multilayer is linear both at 8000 and 10000 rpm. We measured build-up speeds of 5.9 and 7.1 nm/layer-pair respectively. The slightly faster growth at 10000 rpm is surprising since for pure polyelectrolyte films it was reported that the growth speed decreased with an increase rotation speed.[114] We also measured lower thickness at the center of the sample, visible on some reflection pictures (Figure 93B), which is the inverse of what Wang and coworkers reported. It seems that for our system the higher the shear the thicker the film. A better alignment of the fibers in the film with increasing shear may cause the faster growth. Such an effect cannot be observed with polyelectrolytes or spherical particles. The thickness increase is also more important for dipping than for spin-assisted deposition. With similar solutions a 150 layer pair film assembled by dipping was 1.35 µm thick while it was only 0.88 µm by spin-assisted deposition at 8000 rpm. However the time necessary to assemble one layer pair was below one minute by spin-assisted LbL against more than fifteen minutes for dipping, which makes spin-assisted assembly ten times faster than dipping to produce a film of a given thickness. The reflection images of the sample display uniform colors except at the

center of the sample, which confirms the thickness homogeneity measured by ellipsometry. These multilayers are also transparent as we can observe interference colors up to micron thicknesses. The presence of defects or inhomogeneities would make the film hazy or opaque. We tried to build films with poly(vinyl amine) solution at pH=10 and pH=11 in order to accelerate the deposition time. The films obtained where non-homogeneous and partially detached from the substrate during deposition. We did not investigate this effect further.
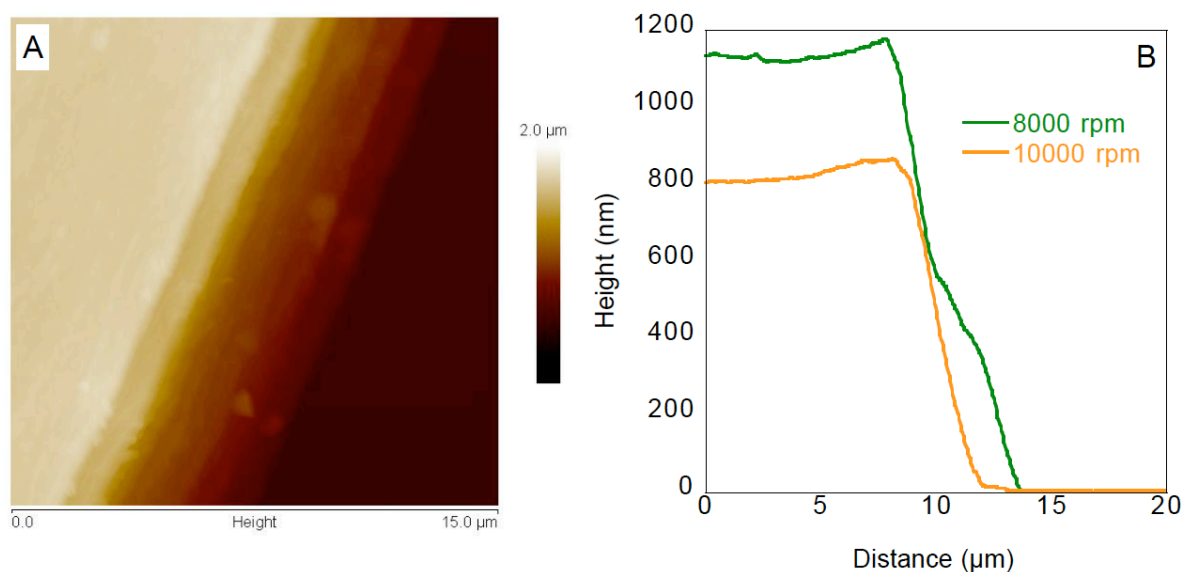
Figure 94. (A) AFM image of the edge of a (PVAm/MFC)$_{200}$ film assembled by spin-assisted LbL with a rotation speed of 8000rpm resting on a silicon wafer. (B) Profiles measured on the AFM images for (PVAm/MFC)$_{200}$ assembled with a rotation speed of 8000 rpm, and (PVAm/MFC)$_{120}$ assembled with a rotation speed of 10000 rpm.

As for previous multilayers, it was necessary to confirm the thickness. Ellipsometry proved to be difficult since the refractive index of oriented films are known to vary with the orientation.[217] We therefore measured the profile of the edge of the films on silicon wafer by AFM (Figure 94). The thickness measured by AFM for the films assembled at 8000 rpm and 10000 rpm were 1.13 μm and 0.81 μm respectively. These values are in good agreement with the values found by spectroscopic ellipsometry 1.15 μm ± 0.01 and 0.84 μm ± 0.01 respectively where we assumed a refractive index of 1.55. These ellipsometric values are the averages of measurements done parallel and perpendicular to the direction of orientation of the fibers. The layered organization of the film, its low roughness and its thickness

homogeneity are visible in Figure 94A. A small bump is visible on the AFM profiles near the edge of the film that was certainly created during the cut of the material (Figure 94). The thickness of the film was measured between the surface of the silicon wafer and the surface of the film away from the edge.

We have seen that it was possible to build transparent, thick and homogeneous MFC-based films using spin-assisted layer-by-layer assembly. The film thickness was measured by AFM and ellipsometry. Now, we will try to visualize and quantify the orientation of the cellulose fibers in the film.

5.3.2   Macroscopic visualization of the orientation

Microfibrillated cellulose is a partially crystalline material. The cellulose crystals in the fibers have different optical properties perpendicular and parallel to the direction of the fibers.[145] When they are randomly oriented in a film or solution the material is isotropic because on average the properties are the same in all directions. If for some reasons there is a preferential direction of orientation for the fibers the material obtained is birefringent.[217] We visualized these phenomenon using optical photography and microscopy between cross polarizers.

The optical image taken at low angle (about 70º to the normal) displays different interference colors in the light reflected along the diameter pointing to the camera or across the diameter perpendicular to it (Figure 95A). This shows that the fibers are aligned radially on the substrate. In one case the light propagates through the film along the fiber axis (diameter pointing toward the camera) and in the other case perpendicular to the fiber axis. Since the refractive indexes are different along and across the fiber axis, the optical pathways are different and the interferences colors observed changes. This is not visible on images taken perpendicularly to the surface (Figure 93B) because the propagation of the light is always perpendicular to the fiber axis. The orientation of the fibers is also visible on the micrographs taken between cross polarizes (Figure 95B). When the fibers are in the direction of one of the polarizers there is no light transmitted (i.e. at 0 and 90°). When they are oriented at 45° to each polarizer the light transmitted is maximum. We observe that the maximum transmission is obtained when the edge makes an angle of 45° with the cross polarizers. This confirms that the fibers are oriented parallel to the edge

of the film which corresponds to a radial orientation during spin-assisted LbL. This was previously reported for films containing cellulose nanocrystals.[217]
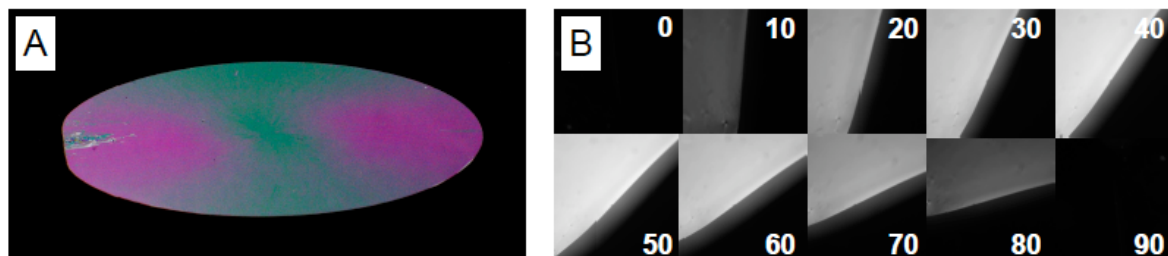
Figure 95. Optical characterization of a (PVAm/MFC)$_{200}$ film built at 8000 rpm. (A) Optical photograph taken with an angle of about 70° to the normal of the film. The contrast was enhanced to improve color visibility. (B) Optical micrographs of an edge of the film taken every ten degrees from 0 to 90° (left to right and up to down) between cross polarizers. The cut corresponds to a radius of the circular support.

These optical characterizations unequivocally show that there is an orientation of the fibrils in the plane of the film. It is, however, difficult to quantify the orientation with these optical techniques. In order to evaluate the influence of the rotation speed and distance from the center on the degree of orientation we performed AFM imaging of several samples.

5.3.3 Microscopic semi-quantitative characterization of orientation.

AFM imaging allows seeing individual fibers deposited on a substrate. We use AFM to confirm and quantify the orientation observed by cross polarized microscopy.

It is easier to image a film consisting of few layer pairs because individual cellulose fibers stand out on substrates with low roughness. We first imaged fibers directly deposited on hydrophobically modified silicon wafers (Figure 96A). We observed a micro-structuration of the film with "holes" in addition to the orientation. Such features have already been reported for spin-assisted LbL films on hydrophobic silicon wafers[218] and were attributed to partial de-wetting of the film during build-up. These pores disappear when the film is thicker. The influence of the hydrophobic substrate disappears after few layers, therefore the majority of the cellulose fibers

adsorb on an hydrophilic poly(vinyl amine) covered substrate. A better representation of the orientation of the fibers in the material is obtained using hydrophilic silicon wafers. The rest of the experiments were carried out on a single layer pair of (PVAm/MFC) deposited on hydrophilic silicon wafers.
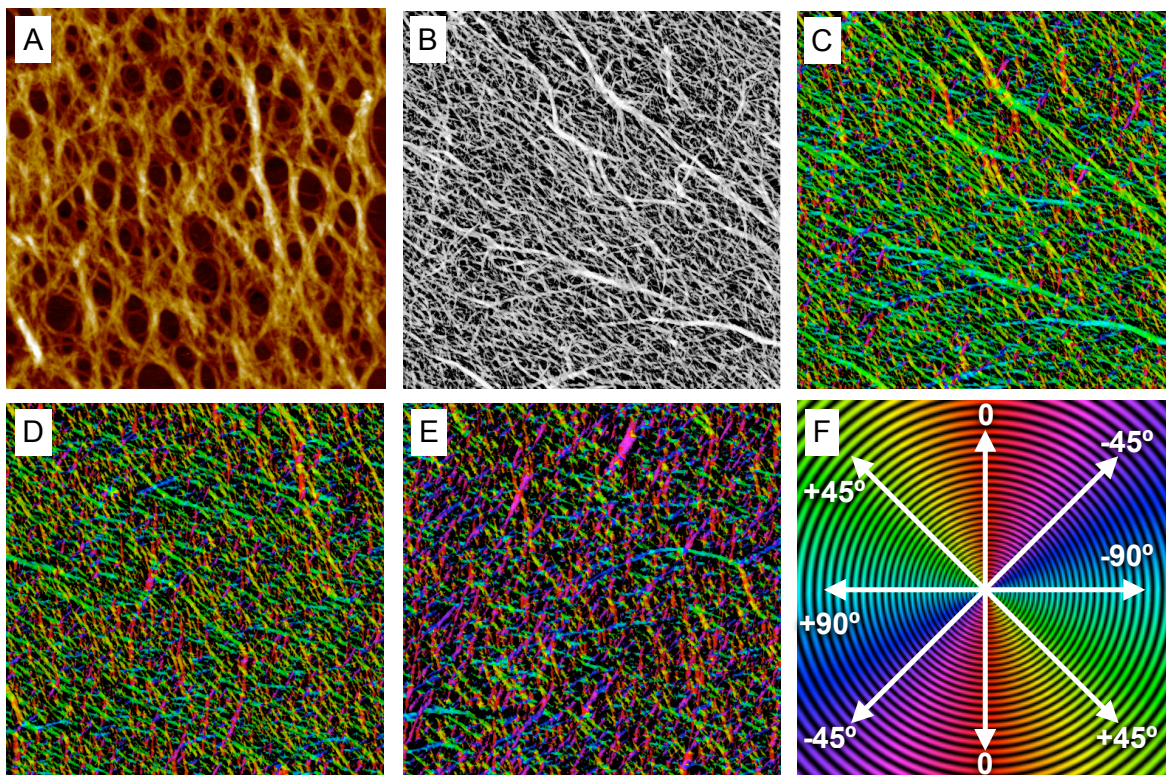
Figure 96. (A) AFM image of (PVAm/MFC)$_3$ assembled by spin-assisted LbL at 8000 rpm on hydrophobic substrate. (B) AFM image of (PVAm/MFC)$_1$ assembled by spin-assisted LbL at 8000 rpm on hydrophilic substrate. The image was taken at 20 mm from the center. (C) Image (B) after orientation analysis and visual representation. (D) Visual representation of the orientation from AFM images of the same sample in (C) but imaged at 10 mm from the center. (E) Identical sample and treatment as for (C) and (D) but taken near the center of the sample. (F) Scale giving the color/orientation relation. All the AFM images are 3*3 μm. The vertical scale is 37 nm for (A) and between 14 and 15 nm for (B), (C), (D), and (E).

After coating a 5 cm wide sample we carefully cut it and imaged the surface at specific distances from the center. We used specific tape for microscopy to glue the piece of sample in the AFM in order to avoid contamination with cyanoacrylate glue or drift with office double sided tape. We regularly imaged samples twice (scan up and scan down) to make sure of the absence of drift. A displacement during imaging would lead to artifacts in the orientation analysis. The vertical scale of the AFM images was set in order to obtain black and white images with a

maximum of fibers visible and sharp contrast (Figure 96B). We then analyzed the images with Orientation-J, a program (package for the software ImageJ) developed by the Biomedical Imaging Group in the EPFL which allows to visualize and quantify the degree of orientation of each pixel of an image (it only works with black and white images).[183] After orientation analysis using Orientation-J we obtained an image (Figure 96C) where the color of each pixel is defined by the local orientation (Figure 96F). This allows visualizing the general direction of orientation (main color) and the degree of orientation of the image (intensity of the color). For example we observed that the degree of orientation is higher at 20 mm (Figure 96C) from the center than at 10 mm (Figure 96D) while at the center of the sample it is hard to distinguish any orientation (Figure 96E).
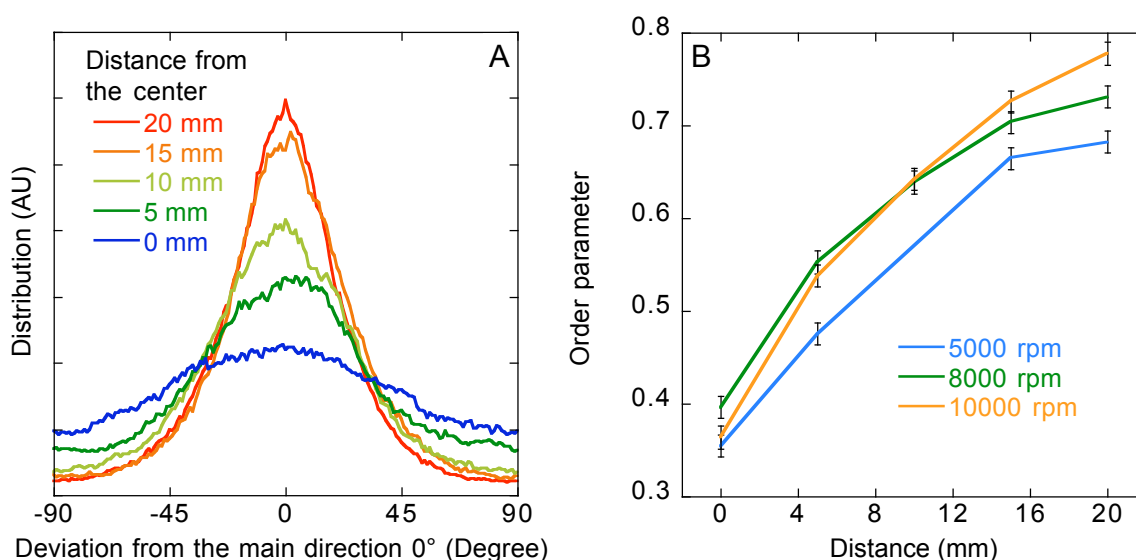
Figure 97. (A) Distribution of orientation obtained after analysis with Orientation-J of AFM images taken at various distance from the center. The sample was (PVAm/MFC)$_1$ assembled at 8000 rpm. The curves have been centered on zero by translation. (B) Evolution of the order parameter as a function of the distance from the center and the rotation speed during assembly. At least two AFM images of (PVAm/MFC)$_1$ were analysed for each point. The error bars are indicative and represent the average standard deviation for all the measurements.

We represented in Figure 97A the distribution of orientation obtained at different distances from the center of the sample (PVAm/MFC)$_1$ assembled at 8000 rpm by spin-assisted assembly. These curves confirm that the degree of orientation of the fibers increases with the distance from the center. The driving force for the fiber orientation is the shear created by spinning during assembly. Further away from

170

the center the shear increases as does the degree of orientation. Even near the center of the sample we observe some orientation. The random shear created by the fall of the drop during assembly and the millimeter accurate positioning of the AFM tip during imaging are probably responsible for this slight orientation. Further from the center a small position inaccuracy have a smaller impact on the distribution of orientation.

For liquid crystals it is usual to characterize the degree of orientation of the nematic phase using an order parameter.[219] In the case of aligned particles the order parameter (S) corresponds to the average of the second Legendre polynomial.

$$S = \left\langle \frac{3\cos^2(\theta) - 1}{2} \right\rangle$$

Equation 8

Where θ is the angle between an element and the main direction of orientation of the sample. The average is weighed by the intensity measured at each angle. This parameter defines with a single number the degree of orientation of a sample. The value obtained is 0 for non-oriented and 1 for perfectly oriented samples. We used this order parameter to quantify the orientation because it is robust and commonly used.

As expected we observe in Figure 97B that the order parameter increases with the distance from the center. The shear applied during assembly also increases with the rotation speed. We also observed that the order parameter was generally increasing with the rotation speed. The effect appears stronger between 5000 and 8000 rpm than between 8000 and 10000 rpm where it barely exceeds the error bars. The order parameter is sensitive to small degree of orientation. This explains the relatively high order parameter measured close to the center when nearly no orientation was visible on the AFM images (Figure 96E). The variation of degree of orientation observed with the distance and the rotation speed are significant. At two centimeters from the border an order parameter close to 0.7 corresponds to what was measured by X-ray diffraction on the best cold drawn cellulose films.[58]

We have built oriented (PVAm/MFC) multilayers by spin-assisted assembly, and estimated the degree of orientation in these samples. We will now look at the mechanical properties of these films.

5.3.4 Oriented films with record mechanical properties.

Stripes of spin-assembled multilayers were cut parallel and perpendicular to the direction of orientation of the fibers (Figure 98A) and characterized by tensile testing. All the samples have been cut at more than one centimeter from the center to limit the variations of orientation and the tests were performed in dry conditions (RH < 5%). The typical shapes of the curves are reported Figure 98B and mechanical characteristics of the films are summarized in Table 7.
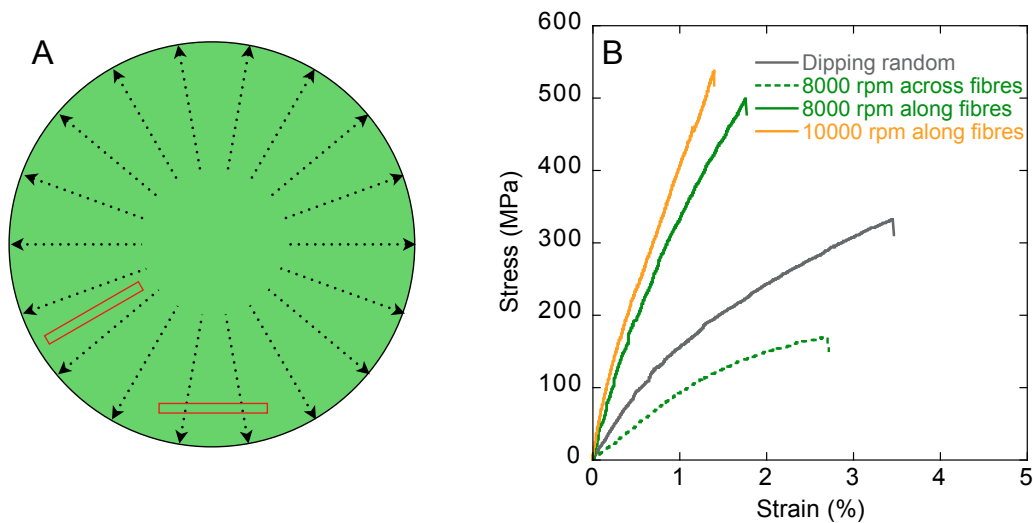
Figure 98. (A) Shematic representation of the sample preparation for the mechanical tests. The arrows indicate the directions of orientation of the fibers and the red lines the edges of the samples (parallel and perpendicular to the direction of orientation). (B) Typical stress strain curves obtained for (PVAm/MFC) films prepared by dipping (not oriented) and spin-assisted assembly (oriented). The rotation speed during spin-assisted assembly is reported together with the direction of solicitation.

The orientation of the fibers in the film is defining the Young's modulus of the film. While oriented films loaded along the direction of orientation have a modulus close to 33 GPa, it drops to 9 GPa when the load is applied across the direction of orientation. We compared the results with films prepared by dipping that display random in plane orientation. Their Young's modulus (14 GPa) falls between that of oriented films loaded along and across the fiber direction. In theory, it is possible to calculate the modulus of composites with in plane random oriented fibers (E_{2D}), from the longitudinal (E_L) and transverse (E_t) moduli of oriented composites with similar composition.[17] Using the equation:

$$E_{2D} = \frac{3}{8}E_L + \frac{5}{8}E_T \qquad \text{Equation 9}$$

The modulus of the random-oriented films should be close to 18 GPa. This is significantly higher than the value measured (14 GPa) but given that the two methods of deposition are different it is possible that the composition or organization of the films changes slightly.[115]

Sample	Young's Modulus (GPa)	Stress at break (MPa)	Strain at break (%)
Dipping	14.2 (±1.0)	286 (±47)	3.2 (±0.8)
Spin 8 krpm across fibers	9.3 (±0.5)	145 (±17)	2.14 (±0.3)
Spin 8 krpm along fibers	32.8 (±1.7)	491 (±19)	2.0 (±0.1)
Spin 10 krpm along fibers	33.1 (±2.0)	473 (±28)	1.7 (±0.7)

Table 7. Mechanical characteristics of (PVAm/MFC) films prepared by dipping (no oriented) and spin-assisted assembly (oriented). The speed of rotation during spin-assisted assembly is reported together with the direction of solicitation. At least four measurements were carried out for each film and the numbers in brackets indicate the standard deviation.

The strength of the films increases from oriented films loaded across the fiber direction, to random-oriented films and reaches its maximum for oriented films loaded in the direction of orientation (490 Mpa). For similar degrees of orientation the films consisting of pure microfibrillated cellulose and our composite presented similar Young's moduli.[58] Note that the strength of our oriented multilayers surpassed that of the best films prepared by cold drawing.[58, 220] We attribute this to synergetic strengthening effect from poly(vinyl amine)[203] and high degree of orientation of the fibers in the material. In comparison composite films consisting of MFC and hydroxyethylcellulose with a MFC content of 68% showed strength of 355 MPa and a modulus of 13 GPa. The limited effect of an increase of rotation speed on the mechanical properties supports the limited effect observed on the order parameter. Some tests not reported here were carried in ambient humidity conditions. Oriented films loaded along the fiber reached 300 MPa but maintained a Young's modulus close to 30 GPa. Across the fiber direction the modulus was halved to about 5 GPa while the maximal stress barely reached 100 MPa. In the first case the load is borne by the cellulose fibers that are not plasticized by water, therefore humidity has a low effect on the Young's modulus. In the second case it

is the poly(vinyl amine) that bears the load and as it is strongly plasticized by water the modulus decreases with humidity. The strength generally decreases with humidity as the interaction holding the material together are screened by the water incorporated in the film.

To conclude we have successfully prepared and characterized oriented microfibrillated cellulose composites. The strength of these films in the direction of orientation surpasses those of the best cellulose containing films[58, 145] and many layer-by-layer assembled films with record strength.[5, 141, 145, 159, 221] As for natural material the exceptional strength of these materials emerge from the combination of strong building blocks, efficient binding with a softer matrix and alignment of the reinforcing building blocks in the direction of orientation. Compared to cold drawing this technique provides a way to control the orientation on supported films without post-assembly treatments, which opens the path for future projects. The combination of spin-assisted and dip-assisted LbL could lead to the production of bi layered with different orientations. The difference of swelling upon hydration in the two layers could induce reversible motion very similar to what is found in nature.[44]

Conclusion and perspectives

The goal of this work was to use layer-by-layer assembly to produce bio-inspired nano-composites with interesting structures and mechanical properties. Two types of biological structures were taken as source of inspiration. Nacre a highly mineralized structure protecting mollusks against their predator and wood a purely organic composite that gives to trees their structure and resistance. The same primary principle is at the origin of their mechanical performances. They consist of strong reinforcing particles bounded together by a softer matrix. Such composites exhibit high Young's Modulus and high strength because they contain large amounts of reinforcing particles but also toughness and flaw resistance because the soft matrix can deform and dissipate energy. The mechanical property of such composites depends on the nature of the components, their relative proportion and on their adherence with each other. These biological composites nevertheless differ with respect to their structure. Nacre, on one hand, consists in a stack of inorganic platelets (> 95 %) bound together by a proteinaceous glue. The efficiency of such structures rely on the in-plane alignment of the platelets. Wood, on the other hand, consists of a cellular structure made of cellulose fibrils (~50 %) connected together by softer biopolymers. The strength and modulus of such composites are governed by the orientation of the fibrils.

In this thesis we successfully implemented some of the key principles identified in biological composites into layer-by-layer assembled films. We prepared nacre-inspired multilayers containing clay nanoplatelets and poly(dimethylsiloxane) derivatives on one hand and wood-inspired multilayers consisting of microfibrillated cellulose and poly(vinyl amine) on the other hand. The films prepared presented in plane orientation of the nano-reinforcing components similar to the one found in nacre and wood cell wall. Due to the nano-scale dimension and homogeneous dispersion of the colloids the film prepared were transparent. The sequential assembly also maximize the contact area between the nano-particles and the matrix which ensures an efficient stress transfer. Due to the electrostatic nature of the interactions in the materials, humidity had a strong impact on the mechanical properties of the films. The multilayers prepared have a strength and a Young's

modulus in the upper range of layer-by-layer assembled films and match those of their biological counterparts (Figure 99).
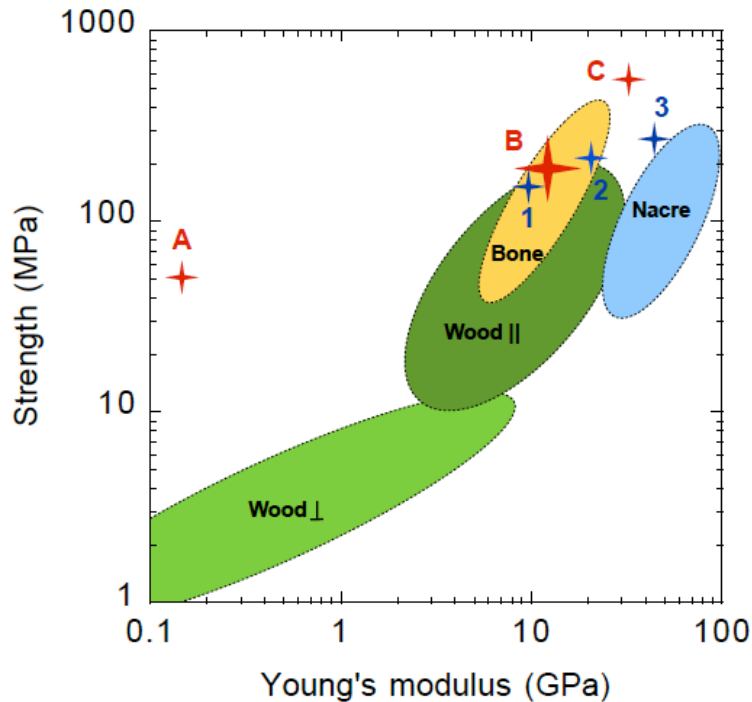
Figure 99. Young's Modulus plotted against the maximal strength. The biological composites from which the films are inspired are represented : wood, nacre and bones. Nacre-inspired multilayers : (1) [Clay/PDMS/PDMS], (2) [Clay/PDMS] and (3) [Clay/PVAm]. Wood-inspired multilayers : (A) wet film, (B) Different films built from solutions at pH 8 to 11 in dry or ambient humidity conditions with random in plane orientation of the fibrils and (C) oriented films loaded along the direction of the fibers.[8, 222]

Nacre-inspired multilayers based on clay and poly(vinyl amine) have the highest strength (250 MPa) and Young's modulus (45 GPa) reported for non cross-linked clay-containing multilayers due to the large amount of clay particles in the films. However the strength of the films dramatically decreased with an humidity increase. The incorporation of a soft poly(dimethylsiloxane) derivative (PDMS) between the clay layers allowed to tune the Young's modulus of these films at will. One layer of PDMS between each layer of clays decreased the modulus to 22 GPa and two layers brought it down to 10 GPa. In addition the PDMS acts as hydrophobic crosslinker for the poly(vinyl amine) which stabilized the mechanical properties with respect to humidity. Note the reinforcing efficiency of these architectures; a 20 fold increase of the PDMS modulus (typically below 1 GPa) is brought about by the introduction of less than 20 % of clays. To the best of our

knowledge this is the first demonstration of the possibility to tune the tensile properties of LbL-assembled films with a variation of the film architecture. Our in-depth investigation of the influence of the clay preparation (centrifugation speed) and conditions of assembly (pH of the solutions, drying step, pre-hydration) on the structure of the multilayers can likely be used for engineering further material properties such as gaz barrier and flame-retardancy. These results also open the door for further experiments; it would, for example, be interesting to adjust the size of the clay particles in order to reach higher toughness.

Wood-inspired multilayers based on microfibrillated cellulose and poly(vinyl amine) possess multiple interesting properties. In addition to their transparency and partial biodegradability these multilayers are very strong for polymer-based films. With a Young's modulus around 13 Gpa and strength reaching over 250 MPa in ambient humidity conditions (RH~50%) these composites have mechanical properties similar to the one of the best nano-papers made of pure microfibrillated cellulose (strength around 220 MPa and modulus of 13 GPa).[7, 55] Note that the films have a strength above that of the wood of origin, spruce, that fails below 100 Mpa along the grain direction.[8] Interestingly by varying humidity one can switch between the different mechanical behavior of these multilayers. In dry conditions the films are strong (up to 300 Mpa for some samples) and brittle, their strength diminish in ambient humidity conditions (between 170 and 220 MPa) but a plastic deformation appears that increases their toughness, once they are wet the films become soft and ductile (Young's modulus around 120 MPa and strength of 50 MPa). In addition, the mobility of the soft polymer phase, in the wet state, enabled self-healing. While some LbL-assembled multilayers have been reported to self-repair,[213] to our knowledge it is the first mechanically resistant multilayer with this property. At last we used spin-assisted layer-by-layer assembly to produce composites with unidirectional in-plane orientation of the fibers (where dip-assisted assembly produces composites with random in-plane orientation). As for wood structures the mechanical properties of the films changed dramatically with the direction of orientation of the fibers. Films loaded along the fiber direction presented record strength (with some hits above 500 MPa) compared to oriented MFC nano-papers and composites,[58, 223] reaching strength of 400 MPa and 350 MPa respectively. The direct assembly of oriented structures by spin-assisted

layer-by-layer assembly could be used to produce carbon nanotube-based composites with outstanding mechanical and electrical properties.[164, 221]

This work also opens the possibility to prepare multilayers made of clays and microfibrillated cellulose. The level of control brought by the layer-by-layer assembly technique could lead to further improvements with respect to mechanical properties, flame retardancy and gas barrier of these already promising hybrid structures.[61, 224, 225]

Bibliography

1.   Dunlop, J. W. C.; Fratzl, P., Biological Composites. In *Annual Review of Materials Research, Vol 40*, Clarke, D. R.; Ruhle, M.; Zok, F., Eds. Annual Reviews: Palo Alto, 2010; Vol. 40, pp 1-24.

2.   Lichtenegger, H.; Reiterer, A.; Stanzl-Tschegg, S. E.; Fratzl, P., Variation of cellulose microfibril angles in softwoods and hardwoods - A possible strategy of mechanical optimization. *Journal of Structural Biology* **1999,** *128* (3), 257-269.

3.   Meyers, M. A.; McKittrick, J.; Chen, P.-Y., Structural Biological Materials: Critical Mechanics-Materials Connections. *Science* **2013,** *339* (6121), 773-779.

4.   Decher, G., Fuzzy nanoassemblies: Toward layered polymeric multicomposites. *Science* **1997,** *277* (5330), 1232-1237.

5.   Podsiadlo, P.; Kaushik, A. K.; Arruda, E. M.; Waas, A. M.; Shim, B. S.; Xu, J.; Nandivada, H.; Pumplin, B. G.; Lahann, J.; Ramamoorthy, A.; Kotov, N. A., Ultrastrong and stiff layered polymer nanocomposites. *Science* **2007,** *318* (5847), 80-83.

6.   Karabulut, E.; Wagberg, L., Design and characterization of cellulose nanofibril-based freestanding films prepared by layer-by-layer deposition technique. *Soft Matter* **2011,** *7* (7), 3467-3474.

7.   Henriksson, M.; Berglund, L. A.; Isaksson, P.; Lindstrom, T.; Nishino, T., Cellulose nanopaper structures of high toughness. *Biomacromolecules* **2008,** *9* (6), 1579-1585.

8.   Gibson, L. J., The hierarchical structure and mechanics of plant materials. *Journal of the Royal Society Interface* **2012,** *9* (76), 2749-2766.

9.   Keten, S.; Xu, Z.; Ihle, B.; Buehler, M. J., Nanoconfinement controls stiffness, strength and mechanical toughness of [beta]-sheet crystals in silk. *Nat Mater* **2010,** *9* (4), 359-367.

10.   Vallee, R. B.; Hook, P., Molecular motors: A magnificent machine. *Nature* **2003,** *421* (6924), 701-702.

11.   Soldati, T.; Schliwa, M., Powering membrane traffic in endocytosis and recycling. *Nat Rev Mol Cell Biol* **2006,** *7* (12), 897-908.

12.   Vukusic, P.; Sambles, J. R., Photonic structures in biology. *Nature* **2003,** *424* (6950), 852-855.

13.   Frankel, R. B.; Blakemore, R. P.; Wolfe, R. S., Magnetite in freshwater magnetotactic bacteria. *Science* **1979,** *203* (4387), 1355-1356.

14.   Aldersey-Williams, H., Towards biomimetic architecture. *Nat Mater* **2004,** *3* (5), 277-279.

15.   Aizenberg, J.; Weaver, J. C.; Thanawala, M. S.; Sundar, V. C.; Morse, D. E.; Fratzl, P., Skeleton of Euplectella sp.: Structural hierarchy from the nanoscale to the macroscale. *Science* **2005,** *309* (5732), 275-278.

16.   Bhushan, B., Biomimetics: lessons from nature-an overview. *Philosophical Transactions of the Royal Society A: Mathematical, Physical and Engineering Sciences* **2009,** *367* (1893), 1445-1486.

17.   Landel, R. F.; Nielsen, L. E., *Mechanical Properties of Polymers and Composites, Second Edition*. Taylor & Francis: 1993.

18.   Ashby, M. F., *Materials Selection in Mechanical Design*. Elsevier Science: 2004.

19.   Dupeux, M., *Aide-mémoire de science des materiaux Ed. 3*. Dunod: 2013.

20.   Zhou, M., Exceptional Properties by Design. *Science* **2013,** *339* (6124), 1161-1162.

21.   Miserez, A.; Weaver, J. C.; Thurner, P. J.; Aizenberg, J.; Dauphin, Y.; Fratzl, P.; Morse, D. E.; Zok, F. W., Effects of laminate architecture on fracture resistance of sponge biosilica: Lessons from nature. *Adv. Funct. Mater.* **2008,** *18* (8), 1241-1248.

22.   Yang, W.; Chao, C.; McKittrick, J., Axial compression of a hollow cylinder filled with foam: A study of porcupine quills. *Acta Biomaterialia* **2013,** *9* (2), 5297-5304.

23.   Weaver, J. C.; Milliron, G. W.; Miserez, A.; Evans-Lutterodt, K.; Herrera, S.; Gallana, I.; Mershon, W. J.; Swanson, B.; Zavattieri, P.; DiMasi, E.; Kisailus, D., The Stomatopod Dactyl Club: A Formidable Damage-Tolerant Biological Hammer. *Science* **2012,** *336* (6086), 1275-1280.

24.   Yang, W.; McKittrick, J., Separating the influence of the cortex and foam on the mechanical properties of porcupine quills. *Acta Biomaterialia* **2013,** *9* (11), 9065-9074.

25.   Bekah, S.; Rabiei, R.; Barthelat, F., The Micromechanics of Biological and Biomimetic Staggered Composites. *Journal of Bionic Engineering* **2012,** *9* (4), 446-456.

26.   Meyers, M. A.; McKittrick, J.; Chen, P. Y., Structural Biological Materials: Critical Mechanics-Materials Connections. *Science* **2013,** *339* (6121), 773-779.

27.   Fratzl, P.; Weinkamer, R., Nature's hierarchical materials. *Prog. Mater Sci.* **2007,** *52* (8), 1263-1334.

28.   Nikolov, S.; Petrov, M.; Lymperakis, L.; Friak, M.; Sachs, C.; Fabritius, H. O.; Raabe, D.; Neugebauer, J., Revealing the Design Principles of High-Performance Biological Composites Using Ab initio and Multiscale Simulations: The Example of Lobster Cuticle. *Adv. Mater.* **2010,** *22* (4), 519-+.

29.   Sun, J.; Bhushan, B., Hierarchical structure and mechanical properties of nacre: a review. *Rsc Advances* **2012,** *2* (20), 7617-7632.

30.   Currey, J. D., The structure and mechanics of bone. *Journal of Materials Science* **2012,** *47* (1), 41-54.

31.   Meyers, M. A.; Chen, P.-Y.; Lin, A. Y.-M.; Seki, Y., Biological materials: Structure and mechanical properties. *Prog. Mater Sci.* **2008,** *53* (1), 1-206.

32.   Li, X. D.; Chang, W. C.; Chao, Y. J.; Wang, R. Z.; Chang, M., Nanoscale structural and mechanical characterization of a natural nanocomposite material: The shell of red abalone. *Nano Lett.* **2004,** *4* (4), 613-617.

33.   Meyers, M. A.; Chen, P. Y.; Lopez, M. I.; Seki, Y.; Lin, A. Y. M., Biological materials: A materials science approach. *Journal of the Mechanical Behavior of Biomedical Materials* **2011,** *4* (5), 626-657.

34.   Fratzl, P., A Composite Matter of Alignment. *Science* **2012,** *335* (6065), 177-178.

35.   Gao, H. J.; Ji, B. H.; Jager, I. L.; Arzt, E.; Fratzl, P., Materials become insensitive to flaws at nanoscale: Lessons from nature. *Proceedings of the National Academy of Sciences of the United States of America* **2003,** *100* (10), 5597-5600.

36.   Peterlik, H.; Roschger, P.; Klaushofer, K.; Fratzl, P., From brittle to ductile fracture of bone. *Nature Materials* **2006,** *5* (1), 52-55.

37.   Nalla, R. K.; Kinney, J. H.; Ritchie, R. O., Mechanistic fracture criteria for the failure of human cortical bone. *Nature Materials* **2003,** *2* (3), 164-168.

38.   Fernandes, A. N.; Thomas, L. H.; Altaner, C. M.; Callow, P.; Forsyth, V. T.; Apperley, D. C.; Kennedy, C. J.; Jarvis, M. C., Nanostructure of cellulose microfibrils in spruce wood. *Proceedings of the National Academy of Sciences of the United States of America* **2011,** *108* (47), E1195-E1203.

39.   Lichtenegger, H.; Muller, M.; Paris, O.; Riekel, C.; Fratzl, P., Imaging of the helical arrangement of cellulose fibrils in wood by synchrotron X-ray microdiffraction. *J. Appl. Crystallogr.* **1999,** *32*, 1127-1133.

40.   Beall, G. W. P. C. E. Fundamentals of polymer-clay nanocomposites.

41.   Munch, E.; Launey, M. E.; Alsem, D. H.; Saiz, E.; Tomsia, A. P.; Ritchie, R. O., Tough, Bio-Inspired Hybrid Materials. *Science* **2008,** *322* (5907), 1516-1520.

42.   Bonderer, L. J.; Studart, A. R.; Gauckler, L. J., Bioinspired design and assembly of platelet reinforced polymer films. *Science* **2008,** *319* (5866), 1069-1073.

43.   Erb, R. M.; Libanori, R.; Rothfuchs, N.; Studart, A. R., Composites Reinforced in Three Dimensions by Using Low Magnetic Fields. *Science* **2012,** *335* (6065), 199-204.

44.   Erb, R. M.; Sander, J. S.; Grisch, R.; Studart, A. R., Self-shaping composites with programmable bioinspired microstructures. *Nat Commun* **2013,** *4*, 1712.

45.   Jalili, R.; Aboutalebi, S. H.; Esrafilzadeh, D.; Konstantinov, K.; Moulton, S. E.; Razal, J. M.; Wallace, G. G., Organic Solvent-Based Graphene Oxide Liquid Crystals: A Facile Route toward the

Next Generation of Self-Assembled Layer-by-Layer Multifunctional 3D Architectures. *Acs Nano* **2013,** *7* (5), 3981-90.

46.   Cheng, Q.; Wu, M.; Li, M.; Jiang, L.; Tang, Z., Ultratough Artificial Nacre Based on Conjugated Cross-linked Graphene Oxide. *Angewandte Chemie-International Edition* **2013,** *52* (13), 3750-3755.

47.   An, Z.; Compton, O. C.; Putz, K. W.; Brinson, L. C.; Nguyen, S. T., Bio-Inspired Borate Cross-Linking in Ultra-Stiff Graphene Oxide Thin Films. *Adv. Mater.* **2011,** *23* (33), 3842-+.

48.   Walther, A.; Bjurhager, I.; Malho, J.-M.; Pere, J.; Ruokolainen, J.; Berglund, L. A.; Ikkala, O., Large-Area, Lightweight and Thick Biomimetic Composites with Superior Material Properties via Fast, Economic, and Green Pathways. *Nano Lett.* **2010,** *10* (8), 2742-2748.

49.   Yao, H.-B.; Fang, H.-Y.; Tan, Z.-H.; Wu, L.-H.; Yu, S.-H., Biologically Inspired, Strong, Transparent, and Functional Layered Organic-Inorganic Hybrid Films. *Angewandte Chemie-International Edition* **2010,** *49* (12), 2140-2145.

50.   Huang, L.; Li, C.; Yuan, W.; Shi, G., Strong composite films with layered structures prepared by casting silk fibroin-graphene oxide hydrogels. *Nanoscale* **2013,** *5* (9), 3780-3786.

51.   Tang, Z. Y.; Kotov, N. A.; Magonov, S.; Ozturk, B., Nanostructured artificial nacre. *Nature Materials* **2003,** *2* (6), 413-U8.

52.   Svagan, A. J.; Samir, M. A. S. A.; Berglund, L. A., Biomimetic Foams of High Mechanical Performance Based on Nanostructured Cell Walls Reinforced by Native Cellulose Nanofibrils. *Adv. Mater.* **2008,** *20* (7), 1263-1269.

53.   Olsson, R. T.; Samir, M.; Salazar-Alvarez, G.; Belova, L.; Strom, V.; Berglund, L. A.; Ikkala, O.; Nogues, J.; Gedde, U. W., Making flexible magnetic aerogels and stiff magnetic nanopaper using cellulose nanofibrils as templates. *Nature Nanotechnology* **2010,** *5* (8), 584-588.

54.   Agarwal, M.; Lvov, Y.; Varahramyan, K., Conductive wood microfibres for smart paper through layer-by-layer nanocoating. *Nanotechnology* **2006,** *17* (21), 5319-5325.

55.   Nogi, M.; Iwamoto, S.; Nakagaito, A. N.; Yano, H., Optically Transparent Nanofiber Paper. *Adv. Mater.* **2009,** *21* (16), 1595.

56.   Sehaqui, H.; Zhou, Q.; Berglund, L. A., Nanostructured biocomposites of high toughness-a wood cellulose nanofiber network in ductile hydroxyethylcellulose matrix. *Soft Matter* **2011,** *7* (16), 7342-7350.

57.   Svagan, A. J.; Samir, M.; Berglund, L. A., Biomimetic polysaccharide nanocomposites of high cellulose content and high toughness. *Biomacromolecules* **2007,** *8* (8), 2556-2563.

58.   Sehaqui, H.; Mushi, N. E.; Morimune, S.; Salajkova, M.; Nishino, T.; Berglund, L. A., Cellulose Nanofiber Orientation in Nanopaper and Nanocomposites by Cold Drawing. *Acs Applied Materials & Interfaces* **2012,** *4* (2), 1043-1049.

59.   Das, P.; Schipmann, S.; Malho, J.-M.; Zhu, B.; Klemradt, U.; Walther, A., Facile Access to Large-Scale, Self-Assembled, Nacre-Inspired, High-Performance Materials with Tunable Nanoscale Periodicities. *Acs Applied Materials & Interfaces* **2013,** *5* (9), 3738-3747.

60.   Sehaqui, H.; Kochumalayil, J.; Liu, A.; Zimmermann, T.; Berglund, L. A., Multifunctional Nanoclay Hybrids of High Toughness, Thermal, and Barrier Performances. *Acs Applied Materials & Interfaces* **2013,** *5* (15), 7613-7620.

61.   Wu, C.-N.; Saito, T.; Fujisawa, S.; Fukuzumi, H.; Isogai, A., Ultrastrong and High Gas-Barrier Nanocellulose/Clay-Layered Composites. *Biomacromolecules* **2012,** *13* (6), 1927-1932.

62.   Kis, A.; Csanyi, G.; Salvetat, J. P.; Lee, T.-N.; Couteau, E.; Kulik, A. J.; Benoit, W.; Brugger, J.; Forro, L., Reinforcement of single-walled carbon nanotube bundles by intertube bridging. *Nat Mater* **2004,** *3* (3), 153-157.

63.   Coleman, J. N.; Khan, U.; Gun'ko, Y. K., Mechanical reinforcement of polymers using carbon nanotubes. *Adv. Mater.* **2006,** *18* (6), 689-706.

64.   Neudeck, G. W.; Pierret, R. F., Introduction to Microelectronic Fabrication. *Modular Series on Solid State Devices* **2002,** *5*.

65.   Melngailis, J., Focused ion-beam technology and applications. *Journal of Vacuum Science & Technology B* **1987,** *5* (2), 469-495.

66.   Piner, R. D.; Zhu, J.; Xu, F.; Hong, S. H.; Mirkin, C. A., "Dip-pen" nanolithography. *Science* **1999,** *283* (5402), 661-663.

67.   Xia, Y. N.; Whitesides, G. M., Soft lithography. *Annu. Rev. Mater. Sci.* **1998,** *28*, 153-184.

68.   Sun, H. B.; Kawata, S., Two-photon photopolymerization and 3D lithographic microfabrication. *Nmr - 3d Analysis - Photopolymerization* **2004,** *170*, 169-273.

69.   Gates, B.; Qin, D.; Xia, Y. N., Assembly of nanoparticles into opaline structures over large areas. *Adv. Mater.* **1999,** *11* (6), 466-+.

70.   Campbell, M.; Sharp, D. N.; Harrison, M. T.; Denning, R. G.; Turberfield, A. J., Fabrication of photonic crystals for the visible spectrum by holographic lithography. *Nature* **2000,** *404* (6773), 53-56.

71.   Beck, J. S.; Vartuli, J. C.; Roth, W. J.; Leonowicz, M. E.; Kresge, C. T.; Schmitt, K. D.; Chu, C. T. W.; Olson, D. H.; Sheppard, E. W.; McCullen, S. B.; Higgins, J. B.; Schlenker, J. L., A new family of mesoporous molecular-sieves prepared with liquid-crystal templates. *JACS* **1992,** *114* (27), 10834-10843.

72.   Zhao, D. Y.; Huo, Q. S.; Feng, J. L.; Chmelka, B. F.; Stucky, G. D., Nonionic triblock and star diblock copolymer and oligomeric surfactant syntheses of highly ordered, hydrothermally stable, mesoporous silica structures. *JACS* **1998,** *120* (24), 6024-6036.

73.   Zhao, D. Y.; Feng, J. L.; Huo, Q. S.; Melosh, N.; Fredrickson, G. H.; Chmelka, B. F.; Stucky, G. D., Triblock copolymer syntheses of mesoporous silica with periodic 50 to 300 angstrom pores. *Science* **1998,** *279* (5350), 548-552.

74.   Xia, Y. N.; Gates, B.; Yin, Y. D.; Lu, Y., Monodispersed colloidal spheres: Old materials with new applications. *Adv. Mater.* **2000,** *12* (10), 693-713.

75.   Simmel, F. C., Three-Dimensional Nanoconstruction with DNA. *Angew. Chem. Int. Ed.* **2008,** *47* (32), 5884-5887.

76.   Winfree, E.; Liu, F. R.; Wenzler, L. A.; Seeman, N. C., Design and self-assembly of two-dimensional DNA crystals. *Nature* **1998,** *394* (6693), 539-544.

77.   Seeman, N. C., DNA in a material world. *Nature* **2003,** *421* (6921), 427-431.

78.   Aida, T.; Meijer, E. W.; Stupp, S. I., Functional Supramolecular Polymers. *Science* **2012,** *335* (6070), 813-817.

79.   Lehn, J. M., *Supramolecular Chemistry*. Wiley: 1995.

80.   George, S. M., Atomic Layer Deposition: An Overview. *Chem. Rev.* **2010,** *110* (1), 111-131.

81.   Ahonen, M.; Pessa, M.; Suntola, T., Study of ZnTe films grown on glass substrates using an atomic layer evaporation method. *Thin Solid Films* **1980,** *65* (3), 301-307.

82.   Roberts, G. G., An applied science perspective of Langmuir-Blodgett films. *Advances in Physics* **1985,** *34* (4), 475-512.

83.   Langmuir, I., The constitution and fundamental properties of solids and liquids. II. Liquids. 1. *JACS* **1917,** *39* (9), 1848-1906.

84.   Blodgett, K. B., Monomolecular films of fatty acids on glass. *JACS* **1934,** *56* (2), 495-495.

85.   Peterson, I. R., Langmuir-Blodgett films. *J. Phys. D: Appl. Phys.* **1990,** *23* (4), 379.

86.   Decher, G.; Hong, J. D., Buildup of ultrathin multilayer films by a self-assembly process .3. Consecutive alternating adsorbtion of anionic and cationic bipolar amphiphiles and polylectrolytes on charged surfaces *Berichte Der Bunsen-Gesellschaft-Physical Chemistry Chemical Physics* **1991,** *95* (11), 1430-1434.

87.   Decher, G., Layer-by-Layer Assembly (Putting Molecules to Work). In *Multilayer Thin Films*, Wiley-VCH Verlag GmbH & Co. KGaA: 2012; pp 1-21.

88.   Iler, R. K., Multilayers of colloidal particles. *J. Colloid Interface Sci.* **1966,** *21* (6), 569-594.

89.   Dubas, S. T.; Schlenoff, J. B., Factors Controlling the Growth of Polyelectrolyte Multilayers. *Macromolecules* **1999,** *32* (24), 8153-8160.

90.   McAloney, R. A.; Sinyor, M.; Dudnik, V.; Goh, M. C., Atomic Force Microscopy Studies of Salt Effects on Polyelectrolyte Multilayer Film Morphology. *Langmuir* **2001,** *17* (21), 6655-6663.

91.   Adamczyk, Z.; Bratek, A.; Jachimska, B.; Jasinski, T.; Warszynski, P., Structure of poly(acrylic acid) in electrolyte solutions determined from simulations and viscosity measurements. *J. Phys. Chem. B* **2006,** *110* (45), 22426-22435.

92.   Shiratori, S. S.; Rubner, M. F., pH-dependent thickness behavior of sequentially adsorbed layers of weak polyelectrolytes. *Macromolecules* **2000,** *33* (11), 4213-4219.

93.   Choi, J.; Rubner, M. F., Influence of the degree of ionization on weak polyelectrolyte multilayer assembly. *Macromolecules* **2005,** *38* (1), 116-124.

94.   Yoo, D.; Shiratori, S. S.; Rubner, M. F., Controlling bilayer composition and surface wettability of sequentially adsorbed multilayers of weak polyelectrolytes. *Macromolecules* **1998,** *31* (13), 4309-4318.

95.   Bieker, P.; Schönhoff, M., Linear and Exponential Growth Regimes of Multilayers of Weak Polyelectrolytes in Dependence on pH. *Macromolecules* **2010,** *43* (11), 5052-5059.

96.   Elbert, D. L.; Herbert, C. B.; Hubbell, J. A., Thin Polymer Layers Formed by Polyelectrolyte Multilayer Techniques on Biological Surfaces. *Langmuir* **1999,** *15* (16), 5355-5362.

97.   Porcel, C.; Lavalle, P.; Decher, G.; Senger, B.; Voegel, J. C.; Schaaf, P., Influence of the polyelectrolyte molecular weight on exponentially growing multilayer films in the linear regime. *Langmuir* **2007,** *23* (4), 1898-1904.

98.   Picart, C.; Lavalle, P.; Hubert, P.; Cuisinier, F. J. G.; Decher, G.; Schaaf, P.; Voegel, J. C., Buildup Mechanism for Poly(l-lysine)/Hyaluronic Acid Films onto a Solid Surface. *Langmuir* **2001,** *17* (23), 7414-7424.

99.   Salomäki, M.; Vinokurov, I. A.; Kankare, J., Effect of Temperature on the Buildup of Polyelectrolyte Multilayers. *Langmuir* **2005,** *21* (24), 11232-11240.

100.   Hubsch, E.; Ball, V.; Senger, B.; Decher, G.; Voegel, J. C.; Schaaf, P., Controlling the growth regime of polyelectrolyte multilayer films: Changing from exponential to linear growth by adjusting the composition of polyelectrolyte mixtures. *Langmuir* **2004,** *20* (5), 1980-1985.

101.   Kleinfeld, E. R.; Ferguson, G. S., Stepwise formation of multilayered nanostructural films from macromolecular precursors. *Science* **1994,** *265* (5170), 370-373.

102.   Kotov, N. A.; Dekany, I.; Fendler, J. H., Layer-by-layer self-assembly of polyelectrolyte-semiconductor nanoparicle composite films. *J. Phys. Chem.* **1995,** *99* (35), 13065-13069.

103.   Schmitt, J.; Decher, G.; Dressick, W. J.; Brandow, S. L.; Geer, R. E.; Shashidhar, R.; Calvert, J. M., Metal nanoparticle/polymer superlattice films: Fabrication and control of layer structure. *Adv. Mater.* **1997,** *9* (1), 61-&.

104.   Decher, G.; Lehr, B.; Lowack, K.; Lvov, Y.; Schmitt, J., New nanocomposite films for biosensors-Layer-by-layer adsorbed films of polyelectrolytes, proteines or DNA. *Biosensors & Bioelectronics* **1994,** *9* (9-10), 677-684.

105.   Lvov, Y.; Haas, H.; Decher, G.; Mohwald, H.; Mikhailov, A.; Mtchedlishvily, B.; Morgunova, E.; Vainshtein, B., Successive deposition of alternate layers of polyelectrolytes and a charged virus. *Langmuir* **1994,** *10* (11), 4232-4236.

106.   Kurt, P.; Banerjee, D.; Cohen, R. E.; Rubner, M. F., Structural color via layer-by-layer deposition: layered nanoparticle arrays with near-UV and visible reflectivity bands. *J. Mater. Chem.* **2009,** *19* (47), 8920-8927.

107.   Onda, M.; Lvov, Y.; Ariga, K.; Kunitake, T., Sequential reaction and product separation on molecular films of glucoamylase and glucose oxidase assembled on an ultrafilter. *J. Ferment. Bioeng.* **1996,** *82* (5), 502-506.

108.   Ladam, G.; Schaad, P.; Voegel, J. C.; Schaaf, P.; Decher, G.; Cuisinier, F., In situ determination of the structural properties of initially deposited polyelectrolyte multilayers. *Langmuir* **2000,** *16* (3), 1249-1255.

109.   Li, Y.-C.; Schulz, J.; Mannen, S.; Delhom, C.; Condon, B.; Chang, S.; Zammarano, M.; Grunlan, J. C., Flame Retardant Behavior of Polyelectrolyte-Clay Thin Film Assemblies on Cotton Fabric. *Acs Nano* **2010,** *4* (6), 3325-3337.

110.   Schneider, G.; Decher, G., From functional core/shell nanoparticles prepared via layer-by-layer deposition to empty nanospheres. *Nano Lett.* **2004,** *4* (10), 1833-1839.

111.   DeRocher, J. P.; Mao, P.; Han, J.; Rubner, M. F.; Cohen, R. E., Layer-by-Layer Assembly of Polyelectrolytes in Nanofluidic Devices. *Macromolecules* **2010,** *43* (5), 2430-2437.

112.   Caruso, F.; Caruso, R. A.; M√∂hwald, H., Nanoengineering of Inorganic and Hybrid Hollow Spheres by Colloidal Templating. *Science* **1998,** *282* (5391), 1111-1114.

113.   Schlenoff, J. B.; Dubas, S. T.; Farhat, T., Sprayed polyelectrolyte multilayers. *Langmuir* **2000,** *16* (26), 9968-9969.

114.   Chiarelli, P. A.; Johal, M. S.; Casson, J. L.; Roberts, J. B.; Robinson, J. M.; Wang, H. L., Controlled fabrication of polyelectrolyte multilayer thin films using spin-assembly. *Adv. Mater.* **2001,** *13* (15), 1167-+.

115.   Cho, J.; Char, K.; Hong, J. D.; Lee, K. B., Fabrication of highly ordered multilayer films using a spin self-assembly method. *Adv. Mater.* **2001,** *13* (14), 1076-+.

116.   Izquierdo, A.; Ono, S. S.; Voegel, J. C.; Schaaf, P.; Decher, G., Dipping versus spraying: Exploring the deposition conditions for speeding up layer-by-layer assembly. *Langmuir* **2005,** *21* (16), 7558-7567.

117.   Cini, N.; Tulun, T.; Decher, G.; Ball, V., Step-by-Step Assembly of Self-Patterning Polyelectrolyte Films Violating (Almost) All Rules of Layer-by-Layer Deposition. *JACS* **2010,** *132* (24), 8264-+.

118.   Krogman, K. C.; Cohen, R. E.; Hammond, P. T.; Rubner, M. F.; Wang, B. N., Industrial-scale spray layer-by-layer assembly for production of biomimetic photonic systems. *Bioinspiration & Biomimetics* **2013,** *8* (4).

119.   Bergaya, F.; Theng, B. K. G.; Gerhard, L., *Handbook of Clay Science*. first
 ed.; Elsevier: 2006; p 1224.

120.   Ray, S. S.; Okamoto, M., Polymer/layered silicate nanocomposites: a review from preparation to processing. *Prog. Polym. Sci.* **2003,** *28* (11), 1539-1641.

121.   Kotov, N. A.; Haraszti, T.; Turi, L.; Zavala, G.; Geer, R. E.; Dekany, I.; Fendler, J. H., Mechanism of and defect formation in the self-assembly of polymeric polycation-montmorillonite ultrathin films. *JACS* **1997,** *119* (29), 6821-6832.

122.   Priolo, M. A.; Holder, K. M.; Gamboa, D.; Grunlan, J. C., Influence of Clay Concentration on the Gas Barrier of Clay-Polymer Nanobrick Wall Thin Film Assemblies. *Langmuir* **2011,** *27* (19), 12106-12114.

123.   Kotov, N. A.; Magonov, S.; Tropsha, E., Layer-by-layer self-assembly of alumosilicate-polyelectrolyte composites: Mechanism of deposition, crack resistance, and perspectives for novel membrane materials. *Chem. Mater.* **1998,** *10* (3), 886-895.

124.   Yang, Y.-H.; Malek, F. A.; Grunlan, J. C., Influence of Deposition Time on Layer-by-Layer Growth of Clay-Based Thin Films. *Industrial & Engineering Chemistry Research* **2010,** *49* (18), 8501-8509.

125.   Laachachi, A.; Ball, V.; Apaydin, K.; Toniazzo, V.; Ruch, D., Diffusion of Polyphosphates into (Poly(allylamine)-montmorillonite) Multilayer Films: Flame Retardant-Intumescent Films with Improved Oxygen Barrier. *Langmuir* **2011,** *27* (22), 13879-13887.

126.   Priolo, M. A.; Gamboa, D.; Holder, K. M.; Grunlan, J. C., Super Gas Barrier of Transparent Polymer‚àíClay Multilayer Ultrathin Films. *Nano Lett.* **2010,** *10* (12), 4970-4974.

127.   Holder, K. M.; Priolo, M. A.; Secrist, K. E.; Greenlee, S. M.; Nolte, A. J.; Grunlan, J. C., Humidity-Responsive Gas Barrier of Hydrogen-Bonded Polymer-Clay Multilayer Thin Films. *Journal of Physical Chemistry C* **2012,** *116* (37), 19851-19856.

128.   Priolo, M. A.; Holder, K. M.; Greenlee, S. M.; Grunlan, J. C., Transparency, Gas Barrier, and Moisture Resistance of Large-Aspect-Ratio Vermiculite Nanobrick Wall Thin Films. *Acs Applied Materials & Interfaces* **2012,** *4* (10), 5529-5533.

129.   Podsiadlo, P.; Kotov, N. A.; Ieee, *Nanoscale Design of Ultrastrong Materials by LBL Assembly*. Ieee: New York, 2008; p 341-344.

130.   Manevitch, O. L.; Rutledge, G. C., Elastic properties of a single lamella of montmorillonite by molecular dynamics simulation. *J. Phys. Chem. B* **2004,** *108* (4), 1428-1435.

131.   Patro, T. U.; Wagner, H. D., Layer-by-layer assembled PVA/Laponite multilayer free-standing films and their mechanical and thermal properties. *Nanotechnology* **2011,** *22* (45).

132.   Podsiadlo, P.; Michel, M.; Lee, J.; Verploegen, E.; Kam, N. W. S.; Ball, V.; Lee, J.; Qi, Y.; Hart, A. J.; Hammond, P. T.; Kotov, N. A., Exponential growth of LBL films with incorporated inorganic sheets. *Nano Lett.* **2008,** *8* (6), 1762-1770.

133.   Podsiadlo, P.; Michel, M.; Critchley, K.; Srivastava, S.; Qin, M.; Lee, J. W.; Verploegen, E.; Hart, A. J.; Qi, Y.; Kotov, N. A., Diffusional Self-Organization in Exponential Layer-By-Layer Films with Micro- and Nanoscale Periodicity. *Angewandte Chemie-International Edition* **2009,** *48* (38), 7073-7077.

134.   Podsiadlo, P.; Liu, Z.; Paterson, D.; Messersmith, P. B.; Kotov, N. A., Fusion of seashell nacre and marine bioadhesive analogs: High-strength nanocompoisite by layer-by-layer assembly of clay and L-3,4-dihydroxyphenylaianine polymer. *Adv. Mater.* **2007,** *19* (7), 949-+.

135.   Harrington, M. J.; Masic, A.; Holten-Andersen, N.; Waite, J. H.; Fratzl, P., Iron-Clad Fibers: A Metal-Based Biological Strategy for Hard Flexible Coatings. *Science* **2010,** *328* (5975), 216-220.

136.   Zhang, H.; Zou, K.; Sun, H.; Duan, X., A magnetic organic‚Äìinorganic composite: Synthesis and characterization of magnetic 5-aminosalicylic acid intercalated layered double hydroxides. *J. Solid State Chem.* **2005,** *178* (11), 3485-3493.

137.   Liu, Z. P.; Ma, R. Z.; Osada, M.; Iyi, N.; Ebina, Y.; Takada, K.; Sasaki, T., Synthesis, anion exchange, and delamination of Co-Al layered double hydroxide: Assembly of the exfoliated nanosheet/polyanion composite films and magneto-optical studies. *JACS* **2006,** *128* (14), 4872-4880.

138.   Huang, S.; Cen, X.; Peng, H.; Guo, S.; Wang, W.; Liu, T., Heterogeneous Ultrathin Films of Poly(vinyl alcohol)/Layered Double Hydroxide and Montmorillonite Nanosheets via Layer-by-Layer Assembly. *J. Phys. Chem. B* **2009,** *113* (46), 15225-15230.

139.   Zhao, X.; Zhang, Q. H.; Hao, Y. P.; Li, Y. Z.; Fang, Y.; Chen, D. J., Alternate Multilayer Films of Poly(vinyl alcohol) and Exfoliated Graphene Oxide Fabricated via a Facial Layer-by-Layer Assembly. *Macromolecules* **2010,** *43* (22), 9411-9416.

140.   Compton, O. C.; Nguyen, S. T., Graphene Oxide, Highly Reduced Graphene Oxide, and Graphene: Versatile Building Blocks for Carbon-Based Materials. *Small* **2010,** *6* (6), 711-723.

141.   Hu, K.; Gupta, M. K.; Kulkarni, D. D.; Tsukruk, V. V., Ultra-Robust Graphene Oxide-Silk Fibroin Nanocomposite Membranes. *Adv. Mater.* **2013,** *25* (16), 2301-2307.

142.   Huang, G.; Yang, J.; Gao, J.; Wang, X., Thin Films of Intumescent Flame Retardant-Polyacrylamide and Exfoliated Graphene Oxide Fabricated via Layer-by-Layer Assembly for Improving Flame Retardant Properties of Cotton Fabric. *Industrial & Engineering Chemistry Research* **2012,** *51* (38), 12355-12366.

143.   Chen, J. T.; Fu, Y. J.; An, Q. F.; Lo, S. C.; Huang, S. H.; Hung, W. S.; Hu, C. C.; Lee, K. R.; Lai, J. Y., Tuning nanostructure of graphene oxide/polyelectrolyte LbL assemblies by controlling pH of GO suspension to fabricate transparent and super gas barrier films. *Nanoscale* **2013,** *5* (19), 9081-9088.

144.   Yang, M.; Hou, Y.; Kotov, N. A., Graphene-based multilayers: Critical evaluation of materials assembly techniques. *Nano Today* **2012,** *7* (5), 430-447.

145.   Klemm, D.; Kramer, F.; Moritz, S.; Lindstrom, T.; Ankerfors, M.; Gray, D.; Dorris, A., Nanocelluloses: A New Family of Nature-Based Materials. *Angew. Chem. Int. Ed.* **2011,** *50* (24), 5438-5466.

146.   Lavoine, N.; Desloges, I.; Dufresne, A.; Bras, J., Microfibrillated cellulose - Its barrier properties and applications in cellulosic materials: A review. *Carbohydr. Polym.* **2012,** *90* (2), 735-764.

147.   Eichhorn, S. J.; Dufresne, A.; Aranguren, M.; Marcovich, N. E.; Capadona, J. R.; Rowan, S. J.; Weder, C.; Thielemans, W.; Roman, M.; Renneckar, S.; Gindl, W.; Veigel, S.; Keckes, J.; Yano, H.; Abe, K.; Nogi, M.; Nakagaito, A. N.; Mangalam, A.; Simonsen, J.; Benight, A. S.; Bismarck, A.; Berglund, L. A.; Peijs, T., Review: current international research into cellulose nanofibres and nanocomposites. *Journal of Materials Science* **2010,** *45* (1), 1-33.

148.   Wagberg, L.; Decher, G.; Norgren, M.; Lindstroem, T.; Ankerfors, M.; Axnaes, K., The build-up of polyelectrolyte multilayers of microfibrillated cellulose and cationic polyelectrolytes. *Langmuir* **2008,** *24* (3), 784-795.

149.   Fall, A. B.; Lindstrom, S. B.; Sundman, O.; Odberg, L.; Wagberg, L., Colloidal Stability of Aqueous Nanofibrillated Cellulose Dispersions. *Langmuir* **2011,** *27* (18), 11332-11338.

150.   Aulin, C.; Varga, I.; Claessont, P. M.; Wagberg, L.; Lindstrom, T., Buildup of polyelectrolyte multilayers of polyethyleneimine and microfibrillated cellulose studied by in situ dual-polarization interferometry and quartz crystal microbalance with dissipation. *Langmuir* **2008,** *24* (6), 2509-2518.

151.   Aulin, C.; Johansson, E.; Wagberg, L.; Lindstrom, T., Self-Organized Films from Cellulose I Nanofibrils Using the Layer-by-Layer Technique. *Biomacromolecules* **2010,** *11* (4), 872-882.

152.   Utsel, S.; Malmstrom, E. E.; Carlmark, A.; Wagberg, L., Thermoresponsive nanocomposites from multilayers of nanofibrillated cellulose and specially designed N-isopropylacrylamide based polymers. *Soft Matter* **2010,** *6* (2), 342-352.

153.   Eriksson, M.; Notley, S. M.; Wagberg, L., The influence on paper strength properties when building multilayers of weak polyelectrolytes onto wood fibres. *J. Colloid Interface Sci.* **2005,** *292* (1), 38-45.

154.   Notley, S. M.; Eriksson, M.; Wagberg, L., Visco-elastic and adhesive properties of adsorbed polyelectrolyte multilayers determined in situ with QCM-D and AFM measurements. *J. Colloid Interface Sci.* **2005,** *292* (1), 29-37.

155.   Karabulut, E.; Pettersson, T.; Ankerfors, M.; Wagberg, L., Adhesive Layer-by-Layer Films of Carboxymethylated Cellulose Nanofibril Dopamine Covalent Bioconjugates Inspired by Marine Mussel Threads. *Acs Nano* **2012,** *6* (6), 4731-4739.

156.   Aulin, C.; Karabulut, E.; Amy, T.; Wagberg, L.; Lindstrom, T., Transparent Nanocellulosic Multilayer Thin Films on Polylactic Acid with Tunable Gas Barrier Properties. *Acs Applied Materials & Interfaces* **2013,** *5* (15), 7352-7359.

157.   Cranston, E. D.; Eita, M.; Johansson, E.; Netrval, J.; Salajkova, M.; Arwin, H.; Wagberg, L., Determination of Young's Modulus for Nanofibrillated Cellulose Multilayer Thin Films Using Buckling Mechanics. *Biomacromolecules* **2011,** *12* (4), 961-969.

158.   Eita, M.; Arwin, H.; Granberg, H.; Wagberg, L., Addition of silica nanoparticles to tailor the mechanical properties of nanofibrillated cellulose thin films. *J. Colloid Interface Sci.* **2011,** *363* (2), 566-572.

159.   Mamedov, A. A.; Kotov, N. A.; Prato, M.; Guldi, D. M.; Wicksted, J. P.; Hirsch, A., Molecular design of strong single-wall carbon nanotube/polyelectrolyte multilayer composites. *Nature Materials* **2002,** *1* (3), 190-194.

160.   Podsiadlo, P.; Shim, B. S.; Kotov, N. A., Polymer/clay and polymer/carbon nanotube hybrid organic-inorganic multilayered composites made by sequential layering of nanometer scale films. *Coord. Chem. Rev.* **2009,** *253* (23-24), 2835-2851.

161.   Ma, R.; Sasaki, T.; Bando, Y., Layer-by-Layer Assembled Multilayer Films of Titanate Nanotubes, Ag- or Au-Loaded Nanotubes, and Nanotubes/Nanosheets with Polycations. *JACS* **2004,** *126* (33), 10382-10388.

162.   Cao, K.; Siepermann, C. P.; Yang, M.; Waas, A. M.; Kotov, N. A.; Thouless, M. D.; Arruda, E. M., Reactive Aramid Nanostructures as High-Performance Polymeric Building Blocks for Advanced Composites. *Adv. Funct. Mater.* **2013,** *23* (16), 2072-2080.

163.   Nakashima, T.; Zhu, J.; Qin, M.; Ho, S.; Kotov, N. A., Polyelectrolyte and carbon nanotube multilayers made from ionic liquid solutions. *Nanoscale* **2010,** *2* (10), 2084-2090.

164.   LeMieux, M. C.; Roberts, M.; Barman, S.; Jin, Y. W.; Kim, J. M.; Bao, Z., Self-Sorted, Aligned Nanotube Networks for Thin-Film Transistors. *Science* **2008,** *321* (5885), 101-104.

165.   Shim, B. S.; Kotov, N. A., Single-walled carbon nanotube combing during layer-by-layer assembly: From random adsorption to aligned composites. *Langmuir* **2005,** *21* (21), 9381-9385.

166.   Huang, Y.; Duan, X. F.; Wei, Q. Q.; Lieber, C. M., Directed assembly of one-dimensional nanostructures into functional networks. *Science* **2001,** *291* (5504), 630-633.

167.   Lynch, M. D.; Patrick, D. L., Organizing carbon nanotubes with liquid crystals. *Nano Lett.* **2002,** *2* (11), 1197-1201.

168.   Correa-Duarte, M. A.; Grzelczak, M.; Salgueirino-Maceira, V.; Giersig, M.; Liz-Marzan, L. M.; Farle, M.; Sierazdki, K.; Diaz, R., Alignment of carbon nanotubes under low magnetic fields through attachment of magnetic nanoparticles. *J. Phys. Chem. B* **2005,** *109* (41), 19060-19063.

169.   Mamedov, A. A.; Kotov, N. A., Free-standing layer-by-layer assembled films of magnetite nanoparticles. *Langmuir* **2000,** *16* (13), 5530-5533.

170.   Jiang, C. Y.; Tsukruk, V. V., Freestanding nanostructures via layer-by-layer assembly. *Adv. Mater.* **2006,** *18* (7), 829-840.

171.   Ono, S. S.; Decher, G., Preparation of ultrathin self-standing polyelectrolyte multilayer membranes at physiological conditions using pH-responsive film segments as sacrificial layers. *Nano Lett.* **2006,** *6* (4), 592-598.

172.   Mallwitz, F.; Laschewsky, A., Direct Access to Stable, Freestanding Polymer Membranes by Layer-by-Layer Assembly of Polyelectrolytes. *Adv. Mater.* **2005,** *17* (10), 1296-1299.

173.   Zhuk, A.; Mirza, R.; Sukhishvili, S., Multiresponsive Clay-Containing Layer-by-Layer Films. *Acs Nano* **2011,** *5* (11), 8790-8799.

174.   Chung, J. Y.; Nolte, A. J.; Stafford, C. M., Surface Wrinkling: A Versatile Platform for Measuring Thin-Film Properties. *Adv. Mater.* **2011,** *23* (3), 349-368.

175.   Nolte, A. J.; Treat, N. D.; Cohen, R. E.; Rubner, M. F., Effect of relative humidity on the Young's modulus of polyelectrolyte multilayer films and related nonionic polymers. *Macromolecules* **2008,** *41* (15), 5793-5798.

176.   Jia, F.; Cao, Y.-P.; Liu, T.-S.; Jiang, Y.; Feng, X.-Q.; Yu, S.-W., Wrinkling of a bilayer resting on a soft substrate under in-plane compression. *Philosophical Magazine* **2012,** *92* (12), 1554-1568.

177.   Saha, R.; Nix, W. D., Effects of the substrate on the determination of thin film mechanical properties by nanoindentation. *Acta Mater.* **2002,** *50* (1), 23-38.

178.   Hariri, H. H.; Lehaf, A. M.; Schlenoff, J. B., Mechanical Properties of Osmotically Stressed Polyelectrolyte Complexes and Multilayers: Water as a Plasticizer. *Macromolecules* **2012,** *45* (23), 9364-9372.

179.   Mermut, O.; Lefebvre, J.; Gray, D. G.; Barrett, C. J., Structural and mechanical properties of polyelectrolyte multilayer films studied by AFM. *Macromolecules* **2003,** *36* (23), 8819-8824.

180.   Binnig, G.; Quate, C. F.; Gerber, C., Atomic Force Microscope. *Phys. Rev. Lett.* **1986,** *56* (9), 930-933.

181.   Rivoal, J.-C.; Frétigny, C., Microscopie à force atomique (AFM). *Techniques de l'ingenieur Mesures tridimensionnelles et etats de surface* **2005,** *base documentaire : TIB409DUO* (ref. article : r1394).

182.   Ruste, J., Microscopie électronique à balayage Principe et équipement. *Techniques de l'ingénieur Techniques d'analyse par imagerie* **2013,** *base documentaire : TIB387DUO* (ref. article : p865).

183.   Rezakhaniha, R.; Agianniotis, A.; Schrauwen, J.; Griffa, A.; Sage, D.; Bouten, C.; van de Vosse, F.; Unser, M.; Stergiopulos, N., Experimental investigation of collagen waviness and orientation in the arterial adventitia using confocal laser scanning microscopy. *Biomechanics and Modeling in Mechanobiology* **2011**, 1-13.

184.   Chu, T. C.; Ranson, W. F.; Sutton, M. A.; Peters, W. H., Application of Digital-Image-Corelation Technique to Experimental Mechanics. *Experimental Mechanics* **1985,** *25* (3), 232-244.

185.   Hild, F.; Roux, S., Digital image correlation: from displacement measurement to identification of elastic properties - a review. *Strain* **2006,** *42* (2), 69-80.

186.   Christophe, D.; Jean-Philippe, P.; Frank, B.; Pierre, B.; Jean-Louis, S.; Jean-Hervé, L.; Bernard, C., Ellipsométrie Théorie. *Techniques de l'ingénieur Métrologie optique et photonique* **2003,** *base documentaire : TIB143DUO* (ref. article : r6490).

187.   Lincot, D.; Pauporté, T., Microbalance à cristal de quartz. *Techniques de l'ingénieur Méthodes Electrochimiques* **2006,** *base documentaire : TIB388DUO* (ref. article : p2220).

188.   Marx, K. A., Quartz crystal microbalance: A useful tool for studying thin polymer films and complex biomolecular systems at the solution-surface interface. *Biomacromolecules* **2003,** *4* (5), 1099-1120.

189.   O'Sullivan, C. K.; Guilbault, G. G., Commercial quartz crystal microbalances - theory and applications. *Biosensors & Bioelectronics* **1999,** *14* (8-9), 663-670.

190.   Sauerbrey, G., Verwendung von Schwingquarzen zur Wägung dünner Schichten und zur Mikrowügung. *Zeitschrift für Physik* **1959,** *155* (2), 206-222.

191.   Berne, B. J.; Pecora, R., *Dynamic Light Scattering: With Applications to Chemistry, Biology, and Physics*. Dover Publications: 2000.

192.   Hollander, J. M.; Jolly, W. L., X-ray photoelectron spectroscopy. *Acc. Chem. Res.* **1970,** *3* (6), 193-200.

193.   Siegbahn, K.; Edvarson, K., X-Ray spectroscopy in the precision range of 0.00001. *Nuclear Physics* **1956,** *1* (8), 137-159.

194.   Scofield, J. H., Hartree-Slater subshell photoionization cross-sections at 1254 and 1487 eV. *J. Electron. Spectrosc. Relat. Phenom.* **1976,** *8* (2), 129-137.

195.   Ploehn, H. J.; Liu, C., Quantitative analysis of montmorillonite platelet size by atomic force microscopy. *Industrial & Engineering Chemistry Research* **2006,** *45* (21), 7025-7034.

196.   Feng, X.; Pelton, R., Carboxymethyl cellulose: Polyvinylamine complex hydrogel swelling. *Macromolecules* **2007,** *40* (5), 1624-1630.

197. Lvov, Y.; Ariga, K.; Onda, M.; Ichinose, I.; Kunitake, T., A careful examination of the adsorption step in the alternate layer-by-layer assembly of linear polyanion and polycation. *Colloids and Surfaces a-Physicochemical and Engineering Aspects* **1999,** *146* (1-3), 337-346.

198. Srivastava, S.; Ball, V.; Podsiadlo, P.; Lee, J.; Ho, P.; Kotovlt, N. A., Reversible loading and unloading of nanoparticles in "Exponentially" growing polyelectrolyte LBL films. *JACS* **2008,** *130* (12), 3748-+.

199. Gill, R.; Mazhar, M.; Felix, O.; Decher, G., Covalent Layer-by-Layer Assembly and Solvent Memory of Multilayer Films from Homobifunctional Poly(dimethylsiloxane). *Angewandte Chemie-International Edition* **2010,** *49* (35), 6116-6119.

200. Lutkenhaus, J. L.; Hrabak, K. D.; McEnnis, K.; Hammond, P. T., Elastomeric flexible free-standing hydrogen-bonded nanoscale assemblies. *JACS* **2005,** *127* (49), 17228-17234.

201. Guan, Y.; Yang, S.; Zhang, Y.; Xu, J.; Han, C. C.; Kotov, N. A., Fabry-Perot Fringes and Their Application To Study the Film Growth, Chain Rearrangement, and Erosion of Hydrogen-Bonded PVPON/PAA Films. *The Journal of Physical Chemistry B* **2006,** *110* (27), 13484-13490.

202. Yao, H.-B.; Tan, Z.-H.; Fang, H.-Y.; Yu, S.-H., Artificial Nacre-like Bionanocomposite Films from the Self-Assembly of Chitosan-Montmorillonite Hybrid Building Blocks. *Angewandte Chemie-International Edition* **2010,** *49* (52), 10127-10131.

203. Lorencak, P.; Stange, A.; Niessner, M.; Esser, A., Polyvinylamine-A new polymer for increasing paper strength. *Wochenblatt Fur Papierfabrikation* **2000,** *128* (1-2), 14-18.

204. Feng, X.; Pelton, R.; Leduc, M.; Champ, S., Colloidal complexes from poly(vinyl amine) and carboxymethyl cellulose mixtures. *Langmuir* **2007,** *23* (6), 2970-2976.

205. Fu, J. H.; Ji, J.; Shen, L. Y.; Kueller, A.; Rosenhahn, A.; Shen, J. C.; Grunze, M., pH-Amplified Exponential Growth Multilayers: A Facile Method to Develop Hierarchical Micro- and Nanostructured Surfaces. *Langmuir* **2009,** *25* (2), 672-675.

206. Geffroy, C.; Labeau, M. P.; Wong, K.; Cabane, B.; Stuart, M. A. C., Kinetics of adsorption of polyvinylamine onto cellulose. *Colloids and Surfaces a-Physicochemical and Engineering Aspects* **2000,** *172* (1-3), 47-56.

207. Peng, C. Q.; Thio, Y. S.; Gerhardt, R. A.; Ambaye, H.; Lauter, V., pH-Promoted Exponential Layer-by-Layer Assembly of Bicomponent Polyelectrolyte/Nanoparticle Multilayers. *Chem. Mater.* **2011,** *23* (20), 4548-4556.

208. Feng, X.; Pouw, K.; Leung, V.; Pelton, R., Adhesion of colloidal polyelectrolyte complexes to wet cellulose. *Biomacromolecules* **2007,** *8* (7), 2161-2166.

209. Johansson, E.; Wagberg, L., Tailoring the mechanical properties of starch-containing layer-by-layer films. *Colloids and Surfaces a-Physicochemical and Engineering Aspects* **2012,** *394*, 14-22.

210. Abe, K.; Yano, H., Cellulose nanofiber-based hydrogels with high mechanical strength. *Cellulose* **2012,** *19* (6), 1907-1912.

211. Way, A. E.; Hsu, L.; Shanmuganathan, K.; Weder, C.; Rowan, S. J., pH-Responsive Cellulose Nanocrystal Gels and Nanocomposites. *Acs Macro Letters* **2012,** *1* (8), 1001-1006.

212. Rydzek, G.; Schaaf, P.; Voegel, J.-C.; Jierry, L.; Boulmedais, F., Strategies for covalently reticulated polymer multilayers. *Soft Matter* **2012,** *8* (38), 9738-9755.

213. Wang, X.; Liu, F.; Zheng, X.; Sun, J., Water-Enabled Self-Healing of Polyelectrolyte Multilayer Coatings. *Angewandte Chemie-International Edition* **2011,** *50* (48), 11378-11381.

214. Haraguchi, K.; Uyama, K.; Tanimoto, H., Self-healing in Nanocomposite Hydrogels. *Macromol. Rapid Commun.* **2011,** *32* (16), 1253-1258.

215. Wang, Q.; Mynar, J. L.; Yoshida, M.; Lee, E.; Lee, M.; Okuro, K.; Kinbara, K.; Aida, T., High-water-content mouldable hydrogels by mixing clay and a dendritic molecular binder. *Nature* **2010,** *463* (7279), 339-343.

216. Saeidi, N.; Sander, E. A.; Zareian, R.; Ruberti, J. W., Production of highly aligned collagen lamellae by combining shear force and thin film confinement. *Acta Biomaterialia* **2011,** *7* (6), 2437-2447.

217. Cranston, E. D.; Gray, D. G., Birefringence in spin-coated films containing cellulose nanocrystals. *Colloids and Surfaces a-Physicochemical and Engineering Aspects* **2008,** *325* (1-2), 44-51.

218.   Zimnitsky, D.; Shevchenko, V. V.; Tsukruk, V. V., Perforated, freely suspended layer-by-layer nanoscale membranes. *Langmuir* **2008,** *24* (12), 5996-6006.

219.   Priestley, E. B.; Wojtowicz, P. J.; Sheng, P., *Introduction to Liquid Crystals*. Plenum Press: 1975.

220.   Gindl, W.; Martinschitz, K. J.; Boesecke, P.; Keckes, J., Changes in the molecular orientation and tensile properties of uniaxially drawn cellulose films. *Biomacromolecules* **2006,** *7* (11), 3146-3150.

221.   Shim, B. S.; Zhu, J.; Jan, E.; Critchley, K.; Ho, S. S.; Podsiadlo, P.; Sun, K.; Kotov, N. A., Multiparameter Structural Optimization of Single-Walled Carbon Nanotube Composites: Toward Record Strength, Stiffness, and Toughness. *Acs Nano* **2009,** *3* (7), 1711-1722.

222.   Wegst, U. G. K.; Ashby, M. F., The mechanical efficiency of natural materials. *Philosophical Magazine* **2004,** *84* (21), 2167-2181.

223.   Gindl, W.; Keckes, J., Drawing of self-reinforced cellulose films. *J. Appl. Polym. Sci.* **2007,** *103* (4), 2703-2708.

224.   Sehaqui, H.; Liu, A.; Zhou, Q.; Berglund, L. A., Fast Preparation Procedure for Large, Flat Cellulose and Cellulose/Inorganic Nanopaper Structures. *Biomacromolecules* **2010,** *11* (9), 2195-2198.

225.   Das, P.; Schipmann, S.; Malho, J.-M.; Zhu, B.; Klemradt, U.; Walther, A., Facile access to large-scale, self-assembled, nacre-inspired, high-performance materials with tunable nanoscale periodicities. *Acs Applied Materials & Interfaces* **2013,** *5* (9), 3738-47.

Abstract

Natural materials such as nacre or wood gain their exceptional mechanical performances from the precise organisation of rigid and soft components at the nano-scale. Layer-by-layer assembly allows the preparation of films with a nano-scale control over their organisation and composition. This work describes the assembly and properties of new nano-composites containing 1-D (cellulose nano-fibrils) and 2-D (clay nano-platelets) reinforcing elements. The clay platelets were combined with an extremely soft matrix (poly(dimethylsiloxane)) to mimic the lamellar architecture of nacre. Cellulose based composites with a random in plane orientation of the fibrils were studied first, later we aligned the fibrils in a single direction to mimic further the cell wall of wood. The mechanical properties of these bio-inspired composites match or surpass those of their natural counterparts, while being transparent and in one case self-repairing.

Résumé

Les performances exceptionnelles des composites naturels comme la nacre ou le bois émergent de l'arrangement précis d'éléments souples et rigides à l'échelle nanométrique. L'assemblage couche-par-couche permet la fabrication de films avec un contrôle nanométrique de l'organisation et de la composition. Ce travail décrit l'assemblage et les propriétés de nouveaux nano-composites contenant des nano-renforts 1-D (fibrilles de cellulose) et 2-D (plaquettes d'argile). Nous avons combiné les argiles avec une matrice extrêmement souple de poly(diméthylsiloxane) dans une architecture lamellaire imitant celle de la nacre. Nous avons étudié des composites à base de fibrilles de cellulose aléatoirement orientées dans le plan, puis alignées dans une direction pour mieux imiter les parois cellulaires du bois. Les propriétés mécaniques de ces composites bio-inspirés égalent ou surpassent celles de leurs homologues naturels, tout en étant transparents et dans certains cas auto-réparants.

Rémi Mérindol
Layer-by-Layer assembly of strong bio-inspired nanocomposites

Résumé

Les performances exceptionnelles des composites naturels comme la nacre ou le bois émergent de l'arrangement précis d'éléments souples et rigides à l'échelle nanométrique. L'assemblage couche-par-couche permet la fabrication de films avec un contrôle nanométrique de l'organisation et de la composition. Ce travail décrit l'assemblage et les propriétés de nouveaux nano-composites contenant des nano-renforts 1-D (fibrilles de cellulose) et 2-D (plaquettes d'argile). Nous avons combiné les argiles avec une matrice extrêmement souple de poly(diméthylsiloxane) dans une architecture lamellaire imitant celle de la nacre. Nous avons étudié des composites à base de fibrilles de cellulose aléatoirement orientées dans le plan, puis alignées dans une direction pour mieux imiter les parois cellulaires du bois. Les propriétés mécaniques de ces composites bio-inspirés égalent ou surpassent celles de leurs homologues naturels, tout en étant transparents et dans certains cas auto-réparants.

Mots Clés : Multicouches de polyelectrolytes, bio-mimétique, matériaux hiérarchiques, propriétés mécaniques, films ultrafins, auto-réparant, microfibrilles de cellulose, architectures multimateriaux.

Abstract

Natural materials such as nacre or wood gain their exceptional mechanical performances from the precise organisation of rigid and soft components at the nano-scale. Layer-by-layer assembly allows the preparation of films with a nano-scale control over their organisation and composition. This work describes the assembly and properties of new nano-composites containing 1-D (cellulose nano-fibrils) and 2-D (clay nano-platelets) reinforcing elements. The clay platelets were combined with an extremely soft matrix (poly(dimethylsiloxane)) to mimic the lamellar architecture of nacre. Cellulose based composites with a random in plane orientation of the fibrils were studied first, later we aligned the fibrils in a single direction to mimic further the cell wall of wood. The mechanical properties of these bio-inspired composites match or surpass those of their natural counterparts, while being transparent and in one case self-repairing.

Key words : Polyelectrolyte multilayers, bio-mimicry, hierarchical materials, mechanical properties, ultrathin films, self-healing, microfibrillated cellulose, multimaterial architectures.